School of Chemical and Petroleum Engineering

Department of Petroleum Engineering

Shale Gas Potential Evaluation of Goldwyer and Laurel Formations, Canning Basin, WA.

Muftah Muammer El Khalgi

This thesis is presented for the Degree of

Doctor of Philosophy of

Curtin University

Jan 2018

DECLARATION

To the best of my knowledge and belief, this thesis contains no material previously published by any other persons except where due acknowledgment has been made. This thesis contains no material which has been accepted for the award of any other degree or diploma in any university.

Signature: …………...……………………...

Date: ……… 31/01/2018 ………….

Summary

The Middle Ordovician Goldwyer Formation is composed of fine-grained shallow to deep marine sediments deposited during a regional sea level rise in the Canning Basin. The presence of very rich organic content facies, high thickness and the depth of burial render the Goldwyer Formation to be the most prospective target for future gas shale development in most of the southern regions of the basin. A re-evaluation of the available geochemical data proves the Upper and Lower Goldwyer shales to be organic rich in most of the Broome Platform and the Northern Barbwire Terrace. The correlation and mapping of the total organic content (TOC) and remaining hydrocarbon potential (S2) data showed good to very good hydrocarbon generation potential and higher levels of thermal maturity in the south-eastern and eastern regions of the Broome Platform and the Northern Barbwire Terrace. The rich organic facies (2.5 - 5.0 wt% TOC) of the Lower Goldwyer shale were deposited in calm anoxic marine conditions during a significant sea level rise over most of the southern parts of the Canning Basin. Moreover, the Goldwyer shales showed a strong correlation between the organic content and porosity and resistivity well-log data. An estimation and modelling of the total organic content calculated from the resistivity and density logs allowed for the identification and mapping of the favourable regions for future exploration plans, where measured geochemical data is absent. A similar distribution of the estimated organic facies to those attained from the measured geochemical data has been achieved. The Goldwyer Formation has mainly Type II oil-prone kerogen in the upper shale facies and Type II/ III oil and gas-prone kerogen in the lower shale facies.

A laboratory examination of different sample types revealed the variations of the adsorption potential due to the effect of the composition and total organic content. Pure organic samples have the highest adsorption capacity compared to non-organic and rich clay samples. However, the montmorillonite type of clay still has high adsorption potential, when compared to some rich-organic shales. This could be related to the higher surface area of this type of clay, which allows it to host more gas molecules.

The petrophysical study of the selected core samples depicted the compositional, textural and geomechanical properties of the Goldwyer shales. The range of clay content of the lower mudstone facies is found to be 40 - 60%, with less various amounts of quartz and carbonate. This resulted in the brittleness property to be of low to moderate quality. However, major vertical to sub-vertical natural fractures were identified in some continuous intervals from the visual core observations and scanning electron microscopy (SEM) images. As such, this improves the future plans for hydraulic fracturing. A correlation of the measured compressional (DTp) and shear (DTs) sonic transit times revealed a new valid equation to estimate DTs from DTp, which helped to estimate the geomechanical properties of the Goldwyer shales in the absence of measured well-log data. The total organic content, as well as fluid and matrix density were considered as rolling factors in the total porosity estimation from the logs. The average total porosity of the Lower Goldwyer shale is up to 6% in the Broome Platform and Northern Barbwire Terrace. Moreover, the vertical section correlation and 3D model revealed an increase of the total porosity of the rich clay facies due to the increase of the organic content in the Lower Goldwyer shale.

A detailed observation of over 400 metres of thick core, petrographic, geochemical and petrophysical study of the Goldwyer Formation in the Theia-1 well has led to the identification of seven main lithofacies. The sequence stratigraphic framework and depositional settings of these intervals were identified and correlated across the Broome Platform and the Northern Barbwire Terrace. Vertical parasequence variation and depositional cycles have been defined using gamma ray parasequence (GRP) and lithological variations. 23 depositional cycles have been identified in the Goldwyer Formation including: the upward increased GRP or retrogradational depositional parasequence (caused by the upward increase of the water depth and clay and organic content), the upward decreased GRP or progradational depositional parasequence (caused by the upward decrease of the water depth and increase of quartz and calcareous content), as well as the upward constant GRP or aggradational depositional parasequence (where there is no distinctive change of the sea level and mineral composition).

Parasequence sets of the Goldwyer Formation were interpreted to have six stratigraphic intervals in the Lower Goldwyer shale, and three stratigraphic intervals in each of the Middle Goldwyer carbonate and the Upper Goldwyer shale units. The

sequence boundaries and sea level changes within these intervals are defined based on the gamma ray parasequences and the compositional variations, integrated with the vertical systematic trends of the organic facies and relative hydrocarbon potential index (RHP). The established stratigraphic framework defined the lowstand system tract (LST), highstand system tract (HST), condensed sections (CS), maximum flooding surfaces (MSF) and the sequence boundaries (SB) of the Goldwyer Formation.

A lateral correlation of these intervals disclosed the interplay of tectonic and accommodation space that constructed and modified the Goldwyer Formation during and after the time of deposition. A 2D seismic interpretation and fault modelling have confirmed the dominant extensional tectonism in the Central Canning Basin and its effect on the thickness trends and depth of the Goldwyer Formation. This increased the quality of the 3D models and the later distribution analysis of the formation in the area. The stratigraphic intervals of the Lower and Upper Goldwyer shales showed an increased thickness and depth of burial towards the southwestern and eastern regions of the Broome Platform, due to the extensional movement and thick-skinned normal faulting. The wide spread coverage of the thick fine-grained organic-rich mud facies indicated the increased accommodation space due to the sea level rise during the time of deposition. Therefore, the Goldwyer Formation is interpreted to be deposited in a restricted deep marine environment in the Broome Platform that shallows up towards the Barbwire Terrace.

This dissertation identifies the favourable stratigraphic intervals of the Goldwyer shales for the purpose of future petroleum exploration and shale gas development, based on the integrated study of the key geological, geochemical and petrophysical characteristics. The most potential sweet spots in the Canning Basin are defined using the generated 3D geological and petrophysical modelling, correlated with 2D maps and stratigraphic cross sections.

Dedication

I would like to dedicate my thesis to my father, Muammer El Khalgi, who has always instilled in me, that "great achievements need hard work and big sacrifices". To my mother, Ajeliya Abolkhair, my wife, Lubna Almutawah, my daughters, Enas and Raghad El Khalgi, and my brother, Mohamed El Khalgi. Also, to my parents-in-law, Mr. Ali Almutawah and Mrs. Zainab Ramadan.

Acknowledgment

In The Name of Allah, The Most Gracious, The Most Merciful

I owe a heartfelt gratitude to Allah for all his bounties and for giving me the opportunity and ability to study my PhD.

First of all, I would like to express my thanks and appreciation to my honourable supervisor, Professor Reza Rezaee. I am very grateful for his continual support and guidance, as well as his valuable knowledge and experience, which have inspired and motivated me to attain an outstanding achievement during my PhD study, not only academically, but also through my personal life.

I would like to extend my great thanks to the Department of Mines and Petroleum (now the Department of Mines, Industry Regulation and Safety) of Western Australia for providing the authorisations G32403, G32825 and N00413 to view and sample the cores from the wells in the Canning Basin, and for providing the data base used in this study. I would like also to highly thank Finder Exploration for providing the access to the core and database of the Theia 1 well. My sincere appreciation goes to Mr Aaron Bond for his cooperation and time.

 I would like also to thank my panel committee members, Professor Brian Evans (chair) and Dr. Ali Saeedi for their support and comments that helped me to refine the content of this project. I want to also thank the other research staff in the Petroleum Engineering Department. Special thanks to the Head of Department, Dr. Mofazzal Hossain, for his guidance and support during the hard times. Also, my previous colleagues and office-mates: Dr. Yazeed, Dr. Abu Al Kasim, Dr. Adnan Alhinai Dr, Omar Imbarek and Mr, Abdurrahim Elkaseh for their friendship, advice and support.

My sincere thanks and gratitude go to my father and mother for their love, prayers and encouragement that helped me a lot throughout my entire life and brought me to where I am today. I would like to thank my brother, Mohammed, for his priceless support and unwavering efforts. Special thanks also to my father-in-law, Ali Almutawah, and mother-in-law, Zainab Ramadan, for their precious support and patience.

Great thanks to Dr. Salem Aboglila, Khaled Aun, Abdulhadi Almgherbi, Mr Omar Imbarek and Mr Abdulhafied Elkhalgi for their continued support during my academic journey. Special thanks go to Mr Paul England for his continued support and friendship.

The final acknowledgement must be given to my beloved wife, Lubna Almutawah, for her long-suffering patience while I was working on this project; without her help and forbearance, looking after me and my daughters, this project would have not been possible.

CONTENTS

FIGURES

TABLES

1. Chapter 1: Introduction

1.1 Shale Gas Plays Overview

Gas Shales are traditional shales that contain thermally mature organic matter and other geological and petrophysical properties, which make them the source and reservoir at the same time (Rezaee 2015). In shale plays, gas is produced from sedimentary rocks characterized by very low permeability, due to their fine-grained texture. The depositional environment is the primary controller of the potentiality of the organic-rich play. It controls the lithology, petrophysical characteristics (porosity, permeability and fracibility) and organic geochemistry of the rock. The set quantity of the total organic content (TOC) for the potential shale play varies from one researcher to another. Although TOC is an important indicator of shale gas potentiality, Shuangfang et al. (2012) pointed out that thermal maturity levels play a significant role in determining if a gas has been generated. Generally, the average vitrinite reflectance (Ro) to enter the gas generation maturity ranges from 0.7% for Type III kerogen to 1.1% for Types I and II kerogens. However, it can be noted that 1.1 - 1.4% Ro is the accurate value (Staff 2010). Type III kerogen can produce gas at early maturation levels. At a shallow burial depth, the generated hydrocarbon will be only biogenic gas, which may undergo leakage and diffusion, that results in a low efficiency shale gas window (Shuangfang et al. 2012).

The study of shale gas should, therefore, start with the rock itself. A detailed study of core description in terms of sedimentary structures, textures and stratification provide the preliminary bases of the mineralogical characterisation of the shale reservoir (Slatt and Abousleiman 2011). Mineral composition has a direct effect on shale gas fracability. Shales with higher quartz and carbonate content provide better fracking results than clay-rich shale plays. In addition, brittle minerals help to preserve fractures and uphold a shale from collapse. The average required amount of brittle minerals for shale gas plays is 50 to 60% (Shuangfang et al. 2012; Zou et al. 2010). According to Shuangfang et al. (2012), if the percentage of brittle to non-brittle minerals of a particular shale play exceeds 50%, then that shale play is considered a favourable horizontal drilling target. Interbedding or interlamination by silty to sandy layers within shale units can also enhance the connectivity of production pathways. Moreover, the minimum required thickness for commercial shale gas production is 30 meters (Jinchuan et al. 2004; Martineau 2007).

1.2 Definitions and Classification

1.2.1   Shale

Shales are fine-grained, clay-rich and laminated sedimentary rocks. They can also be rich in organic content. The mud particles are less than 0.0625mm in size (Tourtelot 1960). The origin of the mud could be terrigenous or biogenic. Skeletal and organic matters make up biogenic muds, which are usually composed of silica and calcareous materials. Detrital muds are mainly siliclastics, which are created by the reworking process of erosion and weathering of the pre-existing materials. The term, "black shale", describes organic rich shales that can be equivalent to other sedimentary rocks rich in organic materials rather than mud (Rezaee 2015). The very fine grain, size makes it very difficult and uncertain to study a hand specimen of shale. Hence, a microscopic study of a thin section is a necessity (Sorby 1908). The heterogeneity of black shale is very high on both vertical and lateral scales (Ghadeer and Macquaker 2012; Lobza and Schieber 1999; Macquaker et al. 2007; O'Brien 1996; Schieber 1994; Schieber and Riciputi 2004; Schieber et al. 2010). Also, the mechanism of deposition and lithification of black shales determine the texture, composition, nature and organic content.

1.2.2   Total Organic Content (TOC)

The organic content of a fine-grained sedimentary rock is referred to as total organic carbon in weight percentage (wt.%) (Jarvie 1991). Total organic carbon of shales can be potentially converted to oil or gas. Total organic content forms only a small portion of the total volume of the rock. However, bituminous type of coal generally contains greater than 50 wt% and 70% by volume of TOC (Rice 1993).

Carbon is the primary component of kerogen that can be transformed to oil and gas. However, hydrogen deficiency may cause the carbon to be a residual kerogen component, where it does not have the potential to generate hydrocarbons (Jarvie 1991). A TOC percentage comprises three carbon components: extractible organic matter carbon (EOM carbon), convertible carbon and a portion of residual carbon (Jarvie 1991). The EOM carbon consists of extractable hydrocarbons trapped in rock pore spaces. It is formed as a result of thermal cracking of kerogen and biological markers that are directly incorporated into the EOM carbon. The term, "enrichment shale gas window", is used to describe shales with TOC and thermal maturity that can produce gas (Shuangfang et al. 2012). Rezaee (2015) highlighted that the

minimum required TOC for commercial gas production is 2 wt.%. However, this value would be subjected to the gas prices. According to Zhang et al. (2012), marine shale gas plays can be classified based on TOC contentment to: prospective zones that present 0.3 to 1.5 wt.% TOC, favourable zones that present 1.5 to 2.0 wt.% TOC and target zones of higher than 2.0 wt.% TOC.

1.2.3   Gas Shales

Gas shales refer to fine-grained sedimentary rocks that have the capacity to produce gas. They are organic-rich gas prone rocks (Lakatos and Lakatos-Szabo 2009). The term, "unconventional" however, describes the type of resource which has extremely low permeability that requires reservoir stimulation for commercial production of gas. The similarity between conventional and unconventional hydrocarbon systems is that they are both characterized by complex geological and petrophysical characteristics, as well as heterogeneities at different scales. The difference between them lies in the fact that unconventional gas reservoirs have very fine-grained rock textures, nano-scale pore throat sizes distributions. The organic and clay content that are commonly found in such systems adsorb gases onto their surfaces. It is this clay and organic matter that give shales an anisotropic fabric, which affects both mechanical and transport properties. According to Bustin et al. (2008), the ratio of adsorbed and free gases depends on the amount of organic matter, pore size distribution, mineralogy, diagenesis, rock texture and reservoir pressure and temperature.

1.2.4   Potential Shale Gas Play (Sweet Spots)

Shale gas sweet spots are defined as those plays that show the unique characteristics of commercially valuable gas in place. Prospective shale reservoirs are those with maximum access to the well section and with easier fracing connectivity. However, the heterogeneity of the shale makes it difficult to obtain such characteristics. The crucial elements of sweet spot identification are total organic content (TOC) and porosity. The other key characteristic of shale play sweet spots is brittleness. Better shale plays would represent less swelling clay minerals and higher silica content, which will help to uphold natural fractures and support the permeability of the rock. (Zou et al. 2015) defined two sweet spots types, structural and continuous. Across a limited area, the structural sweet spots type is usually surrounded by the structure

margins with a stable interior and well-developed fractures. The continuous type on the other hand, covers large areas of slope zones and depression points.

1.3 Canning Basin

1.3.1 Overview

1.3.1.1 Structural Evolution and General Stratigraphy of the Canning Basin

The Canning Basin is a predominantly onshore sedimentary basin that covers an area of about 595000 square km. The basin preserves a long and complex multiphase depositional history, ranging from the Early Ordovician to Cenozoic. Indeed, the onshore part of the basin can be subdivided into two main provinces, the northern and southern, which are separated by thinner successions of the Broome (north-western) and Crossland (south-eastern) platforms on the contiguous mid-basin highs (Haines 2012). Two major north-westerly trending depocentres are contained in the basin: the Gregory Sub-basin and Fitzroy Trough; estimations showed up to 15 km of sediments of Devonian to younger rock are to be found in both sub-basins (Figure 1.1). An early transgression deposited the Ordovician sediments upon the Precambrian basement over most of the Canning Basin, with an approximate 1000 meters thickness (Brown et al. 1984). During the Middle to Late Aregian, the carbonate platform of the Willara Formation was developed and spread widely upon the basement highs.

Gradually, to the mid-Ordovician time period, the sea level rise restricted the mid-epeiric sea (Forman et al. 1981), resulting in the deposition of finer size clastics and carbonate sediments in shallow marine conditions (the Goldwyer Formation), and the dolomitized carbonate platforms (the Nita Formation). The Kidson Sub-basin down-warp non-deposition period followed across the entire Canning Basin, from the Late Ordovician to Early Silurian. This non-deposition period was fore-fronted by marine regression during the Late Lianyimian. From the Silurian to Mid-Devonian, the Fitzroy Trough and Broome Platform became areas of major tectonic activities in the basin. This resulted in restricted marine conditions caused by sea transgressions, which covered most of the basin area. Thick evaporate successions of the Caribuddy Formation were deposited across the Kidson Sub-basin and possibly the Fitzroy Trough (Brown et al. 1984).
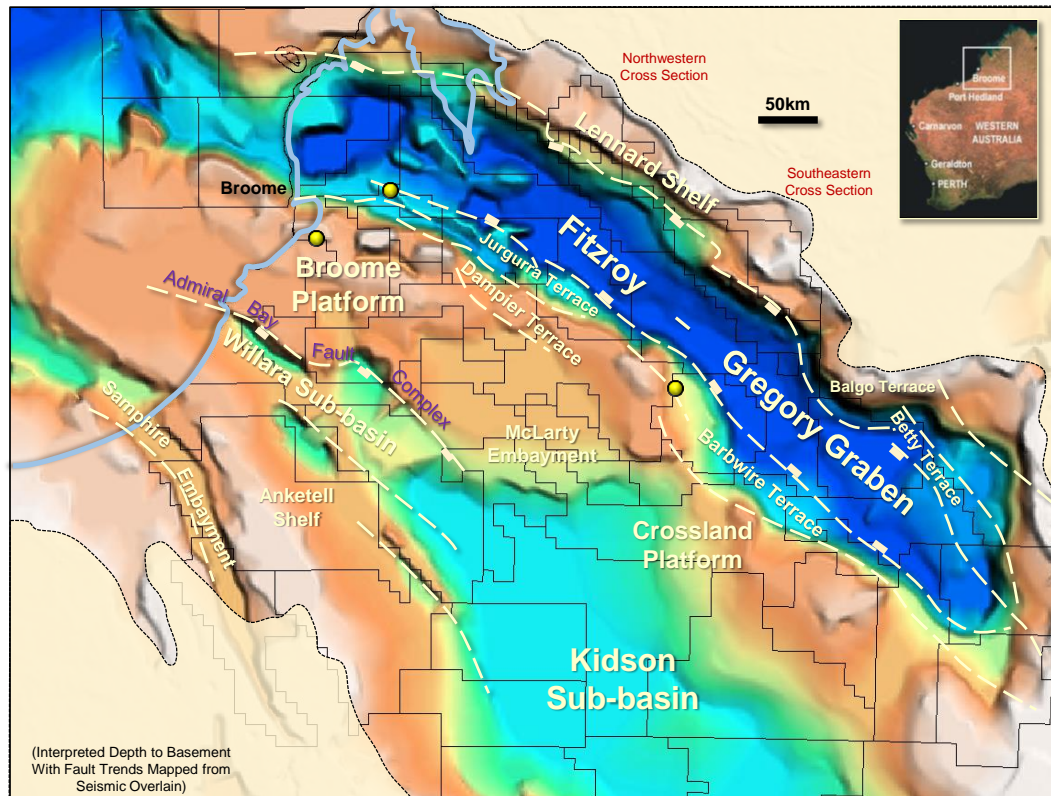
Figure 1.1 The base map highlights the major NW-SE depo-centers and tectonic subdivisions of the Canning Basin in Western Australia (modified from Buru Energy report 2010).

Some recent studies pointed out that the Carribudy Formation might be mainly deposited during the Ordovician era. An emergence of the Southern Sub-basin in the Early Devonian resulted in the widespread deposition of the red bed unit of the Tandalgoo Sandstone, above the entire southern regions of the Canning Basin. The Upper Tandalgoo is thought to be the marine clastics equivalent in the Fitzroy Trough. The Fitzroy Trough was established to be the main rifting depocentre in the Canning Basin during the Late Devonian. Both the shallow epiric sea and the deep fault bounded trough were connected. The Pillara Formation predominately covers the block-faulted shallow marine shelves over the trough. Moving on to the basin ward, fine-grained Gogoclastics were deposited. From the early Famennian to the late Carboniferous, deposition of the thin carbonates sequence (Mellinjerien Limestone) had covered the Tandalgoo sandstone in the Kidson Sub-basin. Later on, the Napier-Virgin Hills Formation was produced by an erosion in the northern margins. Deep in the Fitzroy Trough, the deposition of the Clanmeyer Shales took place, and due to the graben in-fill, the Luluigui shallow shelf carbonates and clastic sediments were also deposited. The second cycle of reef-building, that occurred in the Late Famennian, deposited the Nullara limestone. Subsequently, to the late

Devonian, carbonate build-ups, shallow marine carbonate and clastic Fairfield group (including the Laurel Formation) were deposited in a part of the Lennard Shelf, specifically the Barbwire and Jurgurra Terraces (Druce and Radke 1979). The shallow marine carbonates and deltaic sediments of the Laurel Formation, which were deposited in the Early Carboniferous over the northern parts of the Canning Basin, were known to have good source rock potential, reservoirs and seal. Due to the regression and subsidence carbonates, continental and marine clastics of the Anderson Formation had been rapidly filled in the graben early in the Carboniferous period, followed by the late Carboniferous erosional unconformity. Consequently, in the Stephanian to Sakmarian (Late Carboniferous), limited faulting growth facilitated resumed subsidence in the Fitzroy Trough (Yeates et al. 1984). According to Passmore (1991), a series of horsts and fault blocks were formed by the Late Carboniferous faulting offshore in the graben. The Bedout high might also have been formed at the same period. The widespread marine Grant Formation was deposited subsequently by the Early Permian transgression. Continently, the lateral equivalent of the Grant Formation (Paterson Formation) was deposited in the Southern Canning Basin. The transgression deposits are characterized by fine to coarse clastics of the base Grant Formation; however, in the middle Sakmarian, finer clastics were present. The Late Sakmarine regression is indicated by deltaic, rare marine and non-marine clastics from the Upper Grant Formation. During most of the Grant Formation deposition, a glacial environment continually demonstrated the surrounding areas of the cratonic highlands. Moreover, in the Fitzroy Trough, the Pool sandstone deposition was preceded by Late Sakmarian tectonics over most of the Canning Basin (Crowe et al. 1978). The sea level rise caused the deposition of the marine Noonkabah units above the Pool Sandstone. The main lithologies of these units are shale, siltstone and calcareous marine rocks. Consequently, marine regression followed the transgression in the Late Artinskian. This caused the sandy to silty Triwhite sandstone to be deposited in the Kidson Sub-basin. Figure 1.2 shows the stratigraphic sequence of the Central and Northern Canning Basin.
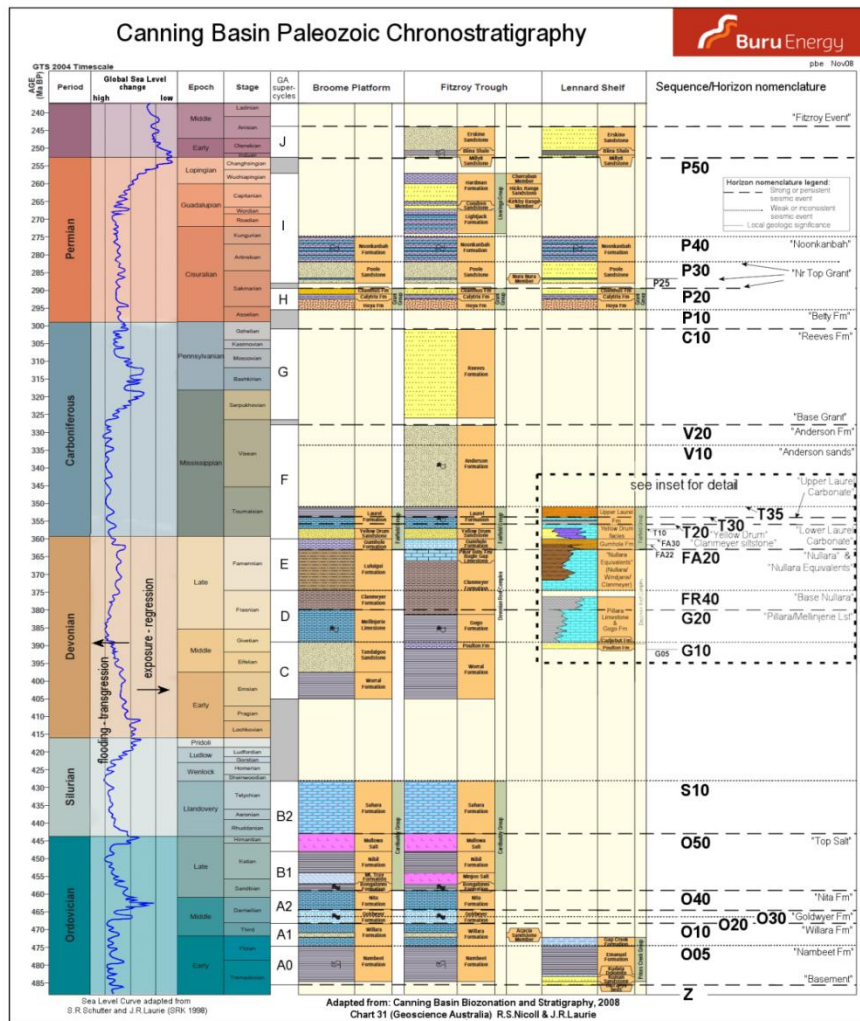
Figure 1.2 The stratigraphic column of the Central and Northern Canning Basin (Buru Energy report 2010).

Carey (1976) suggested that subsequently to the Late Permian rifting, which was associated with the Early Gondwana break-up, the low angle unconformity was established between the Early Triassic and Late Permian units in the Fitzroy Sub-basin. Earlier in the Triassic, the Blina Shale was deposited by the south-eastern transgression on the Fitzroy graben. Regression, represented by fine sandy to silty clastics of the Erska Sandstone, followed in the Late Acythian. Regional erosional unconformity between the Late Triassic and Early Jurassic resulted from the rifting in the Canning Basin. According to (Brown et al. 1984), initiated salt structures in the Kidson Sub-basin and en-echelon anticline in the graben might have been formed due to the later movement of the Fitzroy Trough along the bounding faults. Middle to Late Jurassic rifting occurred in the Canning Basin, which caused the deposition by the Late Jurassic. South-east transgressions resulted from the Australia and formerly adjoining continental mass rifting (Carey 1976; Powell 1976).

28

Consequently, from the Early Jurassic to Early Cretaceous, up to 700 and 4000 meters of sediments were deposited onshore and offshore (Forman et al. 1981). The oldest Jurassic sediments in the Canning Basin are represented by the Wallala Sandstone. It comprises a wide range of aeolian, fluvial, deltaic and marine clastics conditions. Tidal mudstone and sandstone of the Alexander Formation conformably overlay these deposits. On the other hand, the Alexander Formation is conformably overlain by the Kimmeridgian to the Earliest Cretaceous Jarlemia Siltstone that represents a transgression period. Along the northern margin of the sea, the Meda Formation and Barbwire Sandstone were deposited. Regressively, Broome Sandstone deposited over the Jarlemia Siltstone in the Early Cretaceous. The Canning Basin became almost a large plain after this regression.

1.3.2 Hydrocarbon Migration, Traps and Seals of the Canning Basin

Major petroleum systems found in the Canning Basin are of the Paleozoic age. They consist of five main petroleum systems: 1) The Vagrant or Mixed Source petroleum system that is sourced by the Devonian source rock, 2) the Gondwanan 1 petroleum system that is sourced by the Permian Noonkanbah source rock in the Cycas area, 3) the Larapintine 4 (L4) that is sourced from the Early Carboniferous Anderson formation in Lloyd and Boundary, 4) the Larapintine 3 (L3) that is sourced from the Early Carboniferous Laurel formation in West Kora, West Terrace, Sundown and Point Torment, as well as the Larapintine 3 that is sourced from the Late Devoninan Gogo formation in Blina, and finally, 5) the Larapintine 2 (L2) Petroleum system that is sourced from the Ordovician source rocks of the Bongabinni formation in Barbwire Terrace, and The Goldwyer Formation in the Mowla Terrace, Broome Platform and Willara Sub-basin.

Salt tectonism has divided the petroleum systems in the Canning Basin into pre and post salt. Source rocks aged from the Ordovician till Permian are the suppliers of active petroleum systems in the Canning Basin. These petroleum systems include the L2 sourced by the Goldwyer and Bongabinni source rocks, the L3 sourced by the Gogo Formation and the L4 petroleum system sourced by the Laurel Anderson and Grant Formation source rock (Edwards et al. 1997; Kennard 1994). Due to their characteristics, the Goldwyer and Laurel shales are currently potential targets for shale gas exploration. The first oil generation in the Canning Basin was assumed to be started in the late Devonian to the early Carboniferous (Kennard 1994). However,

recent studies suggested that the hydrocarbon generation in the Central Canning Basin could be as late as the Triassic age (Russell 1998). Structural traps in the basin were generated by two major tectonic events that took place prior to the hydrocarbon generation and migration, namely the Meda Compression and Fitzroy Transpression. Russell (1998) divided the hydrocarbon generation into three main events (main, sub and pre-salt). He firstly appointed the 326 Ma that occurred prior to the Meda Compressiono be the main oil expulsion event. Then, the 200 Ma lesser oil expulsion occurred between the Meda Compression and the Fitzroy Transpression that might be the preliminary associated with the area of higher heat flow. Lastly, secondary hydrocarbon migration took place during pre-salt tectonism. Hydrocarbons of this era are likely to be trapped within the structure of pre and post Meda Compression (Figure 1.3).
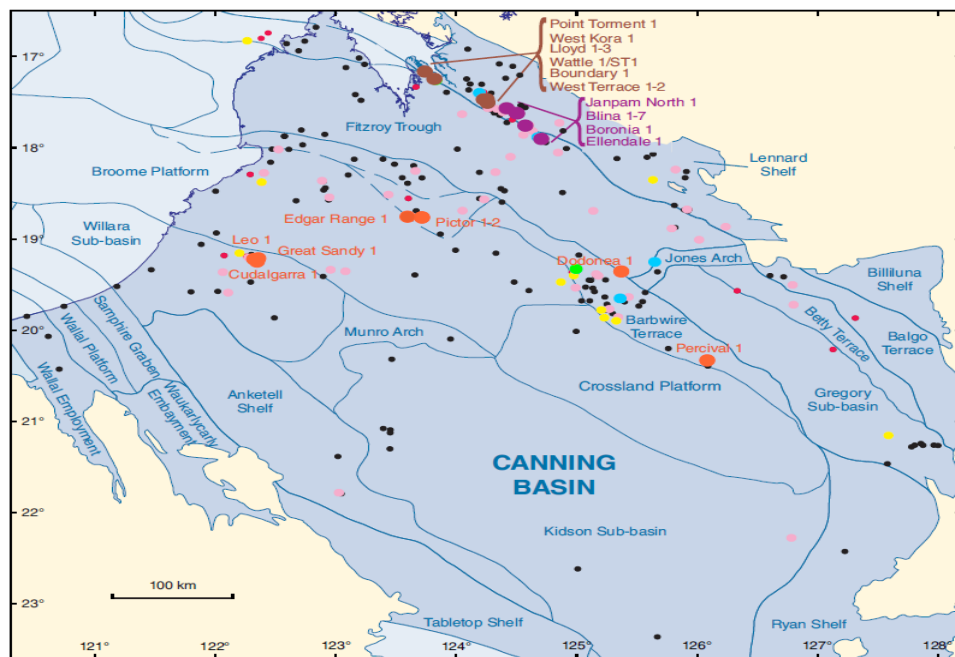
Figure 1.3 The Petroleum systems distribution of the Canning Basin (WAPIMS 2016).

(Kennard 1994; Russell 1998) stated that hydrocarbon maturity in the Canning Basin is affected by: the influence of local intrusions in the Gregory Sub-basin and Fitzroy Trough, the crystalline basement underlying the source rock, as well as the missing or eroded Late Permian deposits in the Western Broome Platform that caused the generated hydrocarbons to stay in the oil generation window.

1.3.3 Exploration, Discoveries and Prospectivity

The Canning Basin is lack of exploration for hydrocarbon prospect. Stratigraphic studies show that four petroleum systems are active in the basin. However, one of the least explored basins in the world is the Canning Basin. In comparison to the other petroleum basins, the Canning Basin has only 10 drilled wells per 10000 square metres, compared to 500 drilled wells per 10000 square meters in North America. Also, there has been limited structure analysis carried out on the basin to date (Carlsen and Ghori 2005). Thus, this would cause low data quality in most studied areas.

1.3.3.1 Exploration history

Oil shows in some water wells had initiated the interest of hydrocarbon exploration in the Canning Basin from the 1919s. The show was first seen in limestone rocks at the Princes Greek in the Pillara Range. The following year of the 1920s, asphaltic shows in water wells were encountered by the Freney Oil Company in the Lennard Shelf. The Associated Australian Oilfields also followed with some minor explorations in the area.

In the following 10 years, there were several events that boomed the exploration in the Canning Basin. It started with an increase of oil prices due to the events in Iraq and Iran during the 1979 - 1980s. Seismic reflection, as well as gravity and magnetic surveys conducted by the Bureau of Mineral Resources, enhanced exploration activities significantly. As such, exploration activities started to rise in the 1980s. A number of companies such as Amoco, Home Energy, Mobil, IEDC, BHP, WMC, amongst others started the search. The first oil discovery of the Blina#1 well in the Canning Basin was made above the edge of the Lennard Shelf by Home Energy. The hosting reservoir was the Fairfield Group. A discovery of five oil fields resulted from an extensive exploration process in the northern central part of the Canning Basin, including the Boundary, Blina, Sundown, West Terrace and Lloyd oilfields. However, the oil recovered by Shell from the Looma#1 well was the largest exploration in the basin as per 1996. The source of the area was proved to be from the Kidson Sub-basin in the Southern Canning Basin.

Since 2009, Buru Energy started its exploration activities in the Canning Basin. Their target was the Laurel Formation mainly for the purpose of the shale gas. The company conducted the first Bunda 3D seismic survey in the basin. A joining

exploration partner of Mitsubishi in 2010 enlarged Buru's activity in the area. The intersection of the light oil reservoir of the Laurel dolomitized limestone in the Ungani 1 well has renewed great hopes of oil exploration in the Canning Basin since the 1980s, although the target was the wet gas sand of the same formation. On the other hand, Buru discovered significant gas plays in their Valhalla and Yulleroo fields. The exploration took place between 2010 and 2013, followed by additional 3D seismic survey in 2013 called the "Ungani". Good permeability was counted in the sandstone layers above the Anderson formation in the Ungani Far West 1 well. The well was spudded in 2015 and oil samples of 41.5° API were recovered. Some strong gas shows were significant in the mud layers from the top Ungani Dolomite. In the last two years, Buru Energy's main focus had been on the Laurel tight sand play. They drilled about six more wells in their acreage and completed around 800 square meters of 3D seismic surveys. Although some oil fields in the Lennard shelf were depleted, others did produce from the clastic reservoirs of the Carboniferous to Permian age. The strata of the Upper Devonian Blina oil field have produced oil since 1983. Recently, in the late 2011s, major discoveries were found in the Laurel Formation (Lower Carboniferous) around the Fitzroy Trough's southern margins. Figure 1.4 shows the selected wells and sub-basins of the target Laurel Formation in this study of the Canning Basin shale gas evaluation. The reports from 2011 - 2013 by the Australian Council of Learned Academies and the US Energy Information Administration confirmed a total of 263 TCF (trillion cubic feet) of recoverable shale gas from the Goldwyer and Laurel Formations in the Canning Basin. Additional exploration wells emerged in other parts of the Canning Basin. Two exploration wells were drilled by New Standard Energy in the Northern Kidson Sub-basin (Named Nicolay#1 and Gibb-Maitland#1). A very successful well was also drilled by Finder Exploration in 2015 in the Central Broome Platform. The well intersected a very organic-rich Goldwyer Formation that produced oil and that proved overpressure. Figure 1.5 illustrates the selected wells for the targeted Goldwyer Formation in this shale gas evaluation study across the Canning Basin. The Department of Mines and Petroleum of Western Australia revealed that the Onshore Canning Basin has about 300 drilled wells and more than 90,000 square km 2D seismic lines. However, 3D seismic lines cover only 1200 square km of the giant basin.
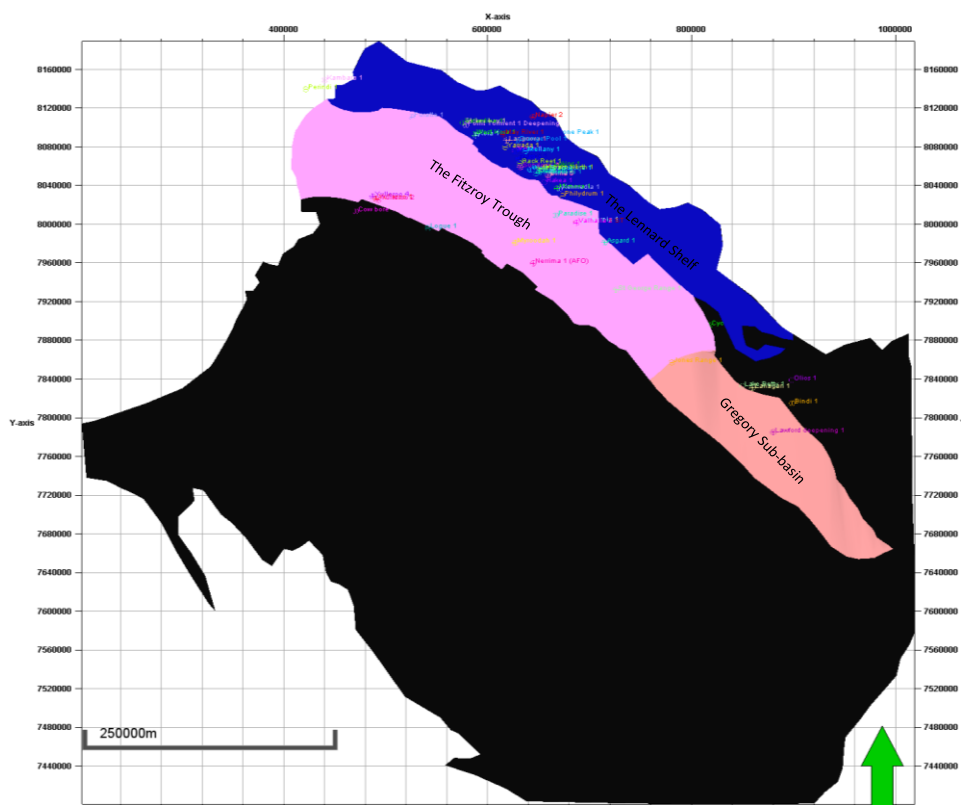
Figure 1.4 The base map showing the well locations and area of study for the Laurel Formation in the Canning Basin.
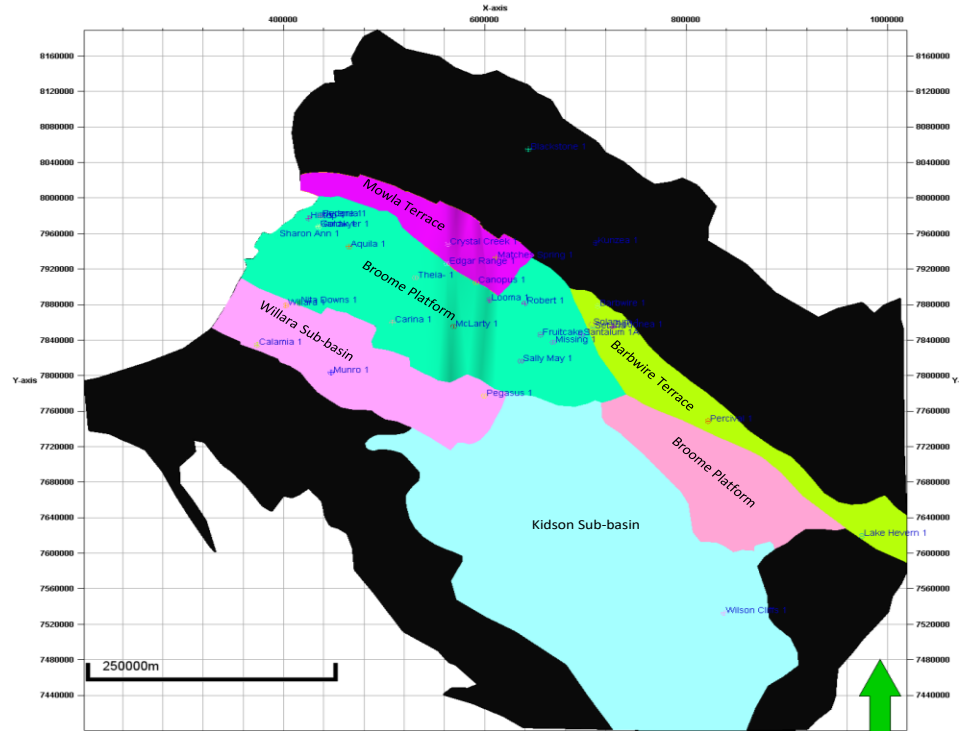
Figure 1.5 The base map showing the well locations and area of study for the Goldwyer Formation in the Canning Basin.

33

The Paleozoic organic-rich shales of the Canning Basin can be cross-correlated with those shale gas plays currently producing from the same era in the United States shale gas industry (Ghori 2013). A long depositional history and thick sedimentary successions have caused the Fitzroy Trough to be considered one of the highest prospective parts in the Canning Basin. The general features are carbonate build-ups and reefal developments along the structural development in the south and half graben hinge lines in the north (Jonasson 2001). A source rock evaluation in the Fitzroy Trough has been made based on regional observations. It is anticipated to be from the Devonian and Carboniferous Laurel and Anderson Formations, as well as the Lower Permian Grant Group. In most cases, it is believed that some units are now over-matured due to the great depth of burial across most of the trough. In the St George Range#1 well, the Laurel Formation carbonate section is found to have the best hydrocarbon shows of gas flows (2.9 mm^3/day). The Laurel Shale is inferred to be the potential source of the gas. Hydrocarbon shows demonstrate that generation and migration were active within the Fitzroy Trough. In addition, Buru Energy drilled Paradise 1 in 2010 to evaluate the shale gas potential of the Laurel Formation in the Northern Canning Basin.

The Ordovician Goldwyer Formation is known to be the richest organic shale in the Central Canning Basin (Ghori 2013). From this formation alone, the technically recoverable resource was estimated to be about 230 TCF. Previous studies of the Goldwyer source rock indicated significant oil and gas generation capacity in most of the central and southern parts of the basin (Administration and Kuuskraa 2011; Ghori 2004; Ghori 2013). In the Barbwire Terrace, the Upper G-Prisca rich shale itself was estimated to be capable of generating over 61 bbl of oil (Foster et al. 1986). Moreover, to the southern parts of the basin, this number is estimated to about 11079 MMbbl/km^2. These figures indicate high shale gas prospectivity for the Goldwyer Formation in most of the Canning Basin. The Goldwyer Formation is organic-rich marine shale with carbonate interbreeds representing homogenous thickness mainly in the Broome Platform, Barbwire Terrace and Mowla Terrace, while it becomes thicker and deeper in the Willara and Kidson Sub-basins. Moreover, it shows more carbonate abundance in the terraces. A few shale gas wells were recently drilled, targeting the rich Goldwyer shale such as the Nicolay#1 by

New Standard Energy in the northern margins of the Kindson Sub-basin and Thiea#1 by Finder Exploration in the Central Broome Platform. Although it is very organic-rich in the southern Canning Basin, the Bongabinni Formation has low thickness in the Broome Platform and Willara Sub-basin. However, it represents about 200 meters of thick strata in the Kidson Sub-basin (Haines and Ghori 2006). Out of the Permian organic successions, the Noonkanbah Shale is regarded the richest, but shale gas development is considered risky due to low maturity levels (Ghori 2013).

1.4 Geological Controls on Shale Gas Plays

1.4.1 Composition and Texture

Shale is defined as a fine-grained detrital sedimentary rock formed by the consolidation of clay, silt or mud (Slatt and Abousleiman 2011). The term, "shale", is highly descriptive and used to classify rocks with the smallest grain size in sedimentary geology. This term is not based on the mineralogy, but on a particle size finer than 0.004 mm. Shale is mainly composed of quartz, feldspar, carbonate particles, a variable mixture of clay minerals, organic matter and lesser amounts of other minerals (Forman et al. 1981).

In shale, the porosity ranges from 4.5 - 14%. Shales are known to have extremely low permeability (nano-darcy scale) and porosity. Pore size distribution is on the order of 0.3 to 0.6 nm, with a unimodal size distribution (Best and Katsube 1995). Due to these properties, shales form good seal rocks. The clay fabric orientation pattern, ratio of fine to coarse grain particles and a few other factors are the main driver controls on the petrophysical properties of the shale. The experimental study conducted by (Dewhurst et al. 1998) showed the responses of clay-rich and silt-rich samples to the effects of compaction. Silt-rich samples have a greater permeability than clay-rich samples, due to their greater range of pore throat size (Hildenbrand and Urai 2003) and the presence of bottle-shaped pores around the silt grains. According to Gipson (1966), from the statistical analysis of shales, there is a decrease in porosity with increasing depth, illite content and preferred clay mineral orientation. Also, the compaction pressure increases with depth, resulting in the gradual increases of both illite content and orientation of illite grains, which leads to the loss of porosity. This can be prevented by the presence of coarse quartz grains, as they are able to withstand high compaction pressures. Porosity in shales is related to its organic content as organic materials have larger pore throats (Krushin 1997). The

thermally mature Devonian and Jurassic gas shales of Western Canada were found to have greater micro-pore volumes associated with organic materials and hence, more gas adsorbed per wt% TOC (Best and Katsube 1995). Gas storage in gas shales may occur as free gas in natural fractures and in inter-granular porosities, as sorbet gas in kerogen and clay-particle surfaces, or as dissolved gas in bitumen (Curtis 2002).

1.4.2   Sedimentary Environment

In the continental environment, organic matter accumulates on river flanks as overbank deposits, as well as oxbow lakes deposits. Organic-rich shales from these sources account for about 20% of the total shale accumulations (Bohacs 2000). In lakes, the water depth is controlled by the accommodation space, which in turn is subjected to climate changes. The organic matter of such environments comes from reworked vegetation, phytoplankton and swamps. It is worth mentioning here that lakes include coastal, deep water and deltaic depositional environments (Rezaee 2015).

Nutrients derived from aeolian processes, oxygenation from the atmosphere and photosynthesis are the primary controllers of the organic enrichment of the lakes (Bohacs 2000; Talbot 1988). Rapid subsidence at basin rifts produces thick lake deposits. Lakes are commonly found as foreland basins, intramontane and rift settings. Up to 12% of organic content and up to 600 hydrogen index (HI) have been noticed in dysoxic deep lakes (below 100 metre depth) (Potter et al. 2005).

Coast morphology is primarily controlled by relative sea level changes, wave energy and tides (Dalrymple et al. 1992). Shales form a major sediment product of these transitional environments. They include lagoons, estuaries, tidal flats and deltas (Rezaee 2015).

Fine-grained sediments supplied by fluvial sources control mud abundance in paralic environments, while the sediment rework the mud. Organic matter distribution is variable and depends on the oxygen deficiency and speed of burial.

In restricted depositional environments, mud is mainly deposited behind the barriers that work as suspensors for the load (Eisma 1986; Newell 1988; Pryor 1975). Barriers also cause the accumulation of the dense organic section due to the filtration of larger inorganic particles. The climate controls the deposition in berried basins such as lagoons, estuaries and deltaic. Humid climates favor dark and organic-rich

muds. On the other hand, arid climates favor light and low to lean organic mud (Rezaee 2015).

The shallow marine environment is mud-dominated (Johnson and Baldwin 1996). Sediments from the seafloor are reworked on the continental shelf. They come mainly from river mouth bars and adjacent land deposits. Biogenic siliclastics are additional forms of shallow marine deposits. They are supplied by skeletal debris. A sea level rise causes vast widespread of shallow marine shales over large areas (Johnson and Baldwin 1996). The water depth of the shallow marine environment is less than 200 meters; hence they are in the photic zone. Shallow marine shales have strong evidence of terrigenous source deposits. It allows for the identification from deep marine shales (Rezaee 2015). Shelf seafloor sediments are three times more organic-rich than deep marine sediments (Dean et al. 1984; Degens et al. 1986). The rapid reach of the organic matter to the sea floor in the shallow marine environment abandons the oxidation effect. High sedimentation rates favor good organic matter preservation. In addition, dilution is minimized due to near-shore terrigenous sedimentation (Rezaee 2015). Intraplatform basins and ramp deposits are known to be in shallow depth environments. They therefore present anoxic to suboxic depositional conditions. There are few examples of organic-rich ram deposits (Burchette 1993; Droste 1990; Wright and Burchette 1996).

In deep marine sedimentary environments, the type of sediments changes laterally from the continental slope to the deep ocean. It starts with mixed terrigenous and biogenic sediments on the shelf margins. Moving towards the basin, the sediments become dominated by biogenic materials (Rezaee 2015). Organic matter enrichment is controlled by the type of depositional facies in the deep marine environment. Three main facies types are recognized by (Stow 1985) including the pelagites, turbidities and the contourites facies. Pelagic environments are characterized by high organic production rates. Turbidities are characterized by well-preservation and low oxygen conditions, due to the rapid runoff of slope deposits which buries the organic matter (Dean et al. 1984; Stow 1985). Deep sea water is characterized by low oxygen content and sea floor topography that favors organic enrichment. Thus, it supports high preservation rates (Savrda et al. 1984). The lack of deep water circulation caused by oceanic rises such as seamounts increases organic productivity (Boehlert

and Genin 1987). Several examples of high productivity of organic matters are documented in submarine topographic highs and oceanic plateaus (Waples 1983).

1.4.3 Vertical and Later Distribution of Shale Plays

The rise of sea level produces transgressive system shale deposits. Different thickness trends and facies distributions can be observed. The fast increase of sea level leads to the deposition of thin and discontinued shale facies. On the other hand, long and slow sea level rise creates thicker and well-stratified shale facies. Finning or coarsening upward successions are also indicators of certain depositional environments. Fining upward clay deposits of the Kimmeridge Formation were interpreted by Macquaker et al. (1998) as transgressive system tract successions.

Variations of organic content, geological and petrophysical properties can be observed within millimetres to thousands of meters scale within the rock unit (Bessereau et al. 1995; Bohacs et al. 2005; Passey et al. 2010). Systematic variations of rock properties occur on both vertical and horizontal scales (Guthrie and Bohacs 2009). The sedimentary environment is the primary control on these variations. Stratal stacking reflects the depositional process that makes up the rock. Mineralogy, organic content, thickness and lithology variations are usually preserved in the rock record and can be linked to the stacking and depositional conditions of a sedimentary environment (Passey et al. 2010).

Three marine settings are favourable for organic-rich shales: the continental slope, the constructional shelf margin and ramps (Bohacs 1998). In each depositional cycle, the organic content of the constructional margin deposits increases upwards till it reaches the maximum flooding point. A gradual decrease usually follows each stage. Thickness trends and sediment types follow accordingly to the same criteria. Organic content changes are almost negligible in ramp deposits, because it is usually homogenous throughout the facies (Passey et al. 2010). Organic deposition in the continental slope is derived by open ocean currents. Pelagic or hemiplegic, and sediment dispersal gravity are the dominant sources of the sediments (Bohacs 1993).

1.5 Geochemical and Petrophysical Properties of Shale Plays

The quantity of organic matter is controlled by the rate of production, destruction and dilution (Passey et al. 2010). Jarvie et al. (2007) stated that higher organic contents can be found if the production rate is maximized, destruction is minimized and dilution is optimized. In other words, a good preservation level of organic matter

requires a fast burial, reduced dilution by continental sediments and rapid development of anoxic benthic conditions (Singh 2008). Also, an increase in nitrate and phosphate concentration is proportional to the productivity (Selley 1985), such as during times of upwelling of deep water. Kerogen is formed by the evolution of organic matter post-burial. Kerogen is a complex hydrocarbon formed at low temperatures by biogenic decay and reactions of organic matter (Singh 2008). During diagenesis, methane, carbon dioxide and water are released. The evolution of organic matter with burial into kerogen and subsequently to oil and gas has been studied in detail (Tissot 1977; Tissot and Welte 1978). Gas is generated either as a biogenic or thermogenic gas. Biogenic gas is formed by anaerobic micro-organisms during the early diagenetic phase of burial or due to invasion of bacteria-laden meteoric water, whereas thermogenic gas is formed by the thermal breakdown of kerogen and hydrocarbons at greater depths and temperatures during the catagenesis phase. The amount of hydrocarbon generated is controlled by the type of kerogen present. Type III kerogens formed from terrestrial plant matter generally produce gas. These are the ones responsible for producing dry gas.

1.5.1 Total Organic Content

Geochemical analyses evaluate the accumulation, thermal maturation and potentiality of the organic matter. Good burial and preservation conditions allow for potential source rock accumulation. In shale, the quantity of the organic matter is controlled by the rate of production, destruction and erosion (Passey et al. 2010). Although organic productivity is high, some modern oceans are organic-lean because of the high oxidization rate (Demaison 1991; Rezaee 2015). The term, "destruction", is used to describe the mineralization of organic matter by organisms, as well as oxidation (Trabucho-Alexandre 2015). Minimized destruction and maximized production levels will produce organic-rich sediments. This is subjected to limited depositional conditions only. Suitable depositional environments would have low free oxygen biological activities that destroy organic matter. A lack of oxygenated water near the surface is a critical factor that promotes certain depositional environments such as seas, marshes and lakes to be valuable organic sources (Loucks and Ruppel 2007). The lack of free oxygen in the surface water will directly affect the amount of oxygen at the bottom of the basin to become an oxygen-free environment. High TOC content in shale gas plays is usually associated with high porosity and gas saturation.

1.5.2 Thermal Maturity and Kerogen Type

Thermal maturity is the decomposition of organic matter to oil or gas. Lack of permeability in source rocks and tight formations will cause the entrapment of the produced hydrocarbons inside the source to form unconventional reservoirs. The accumulated organic materials are buried during sedimentation. Subsidence and increased depth of burial will result in the stacking of the organic-rich sediments in such environments. Kerogen contains complex organic molecules that are produced by the removal of nitrogen, sulfur, oxygen and hydrogen. Increased pressures and temperatures, alongside the chemical reactions produced by pressure solvents, will deform the organic matter and produce insoluble kerogen. Kerogen has no chemical formula, thus it is classified based on the relative percentages of oxygen and hydrogen (Horsfield et al. 1994). Figure 1.6 highlights the stages of kerogen alteration and hydrocarbons production in the subsurface due to the increased maturation caused by pressure and temperature. At 60°C, hydrocarbons start to be generated. They would be mainly oil at this stage. At higher depths and thus temperatures above 100 °C, the organic source rock will be water free and contain oil/gas hydrocarbon with a lesser amount of kerogen. If overmaturation occurs, then only gas will be present. The hydrogen index and porosity will change accordingly to the aforementioned alterations.
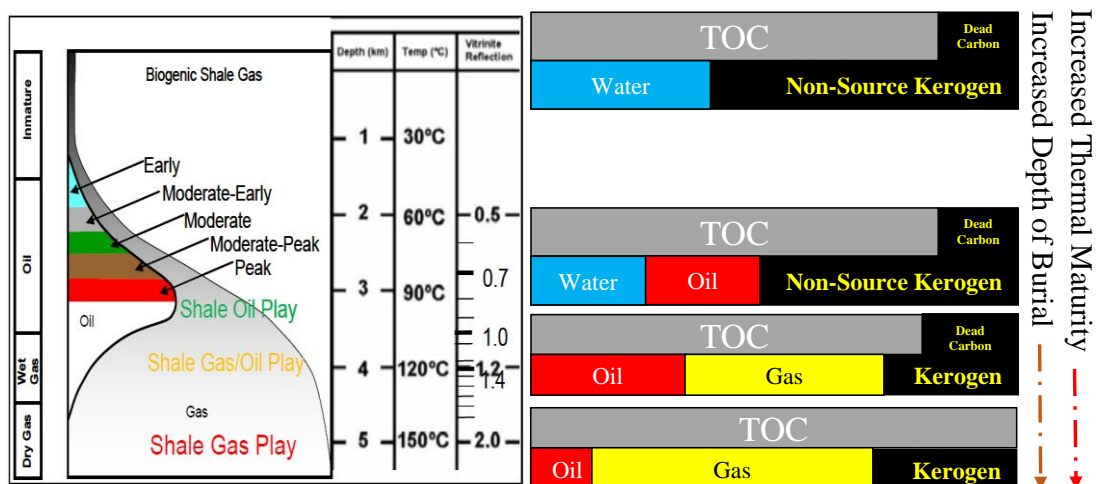
Figure 1.6 The thermal alteration and hydrocarbon generation of organic matter caused by burial (modified after (Forgotson 2007; Glorioso and Rattia 2012).

Four types of kerogen are recognised. Kerogen Type I has maximum hydrogen and minimum oxygen content. Continually, Type II kerogen comes from protein and lipid rich origins. Therefore, the hydrogen/oxygen ratio is lesser when compared to

Type I. Moreover, a smaller hydrogen to oxygen ratio is found in Type III kerogen, as it comes from land depositional environments that are rich in plants. Hence, this will produce mainly gas. The organic constituents of such types of kerogen are known to be oxygen-rich. However, the amount of hydrogen is very little. When pre-existing kerogen undergoes complete maturation, the remaining residue will form Type IV kerogen. Based on the aforementioned importance of the hydrogen and oxygen ratio, the Pseudo-Van Krevelen diagram is highly used in kerogen classification (Horsfield et al. 1994). Kerogen type identification is crucial to predict the possible hydrocarbon potentiality of the source rock.

Tmax is the maximum temperature where most of the hydrocarbon is produced during the Rock-Eval pyrolysis. According to most researchers, the oil generation window starts at 430°C. However, due to some errors of the Tmax analysis, it is recommended for other thermal maturity methods, such as the Hydrogen Index (HI), to be calibrated with the results. An analysis of the HI trend with depth would highlight the occurrence of the oil generation of the source rock. This would be seen as a rapid drop of HI with depth (Horsfield et al. 1994).

1.5.3 Vitrinite reflectance

Vitrinite is produced when lingo-cellulosic tissues are partially decomposed and thermally matured. The origin of these materials is land plants that first evolved in the Silurian era. Because it is absent in the Early Paleozoic, virtinite has been measured on graptolites, scolecodonts and chitinozoans particles, as well as some other organic constituents (Suárez-Ruiz et al. 2012). However, graptolites are the most commonly used in comparison to the others due to its greater abundance. For the shale gas exploration purpose, there is a crucial need to measure the vitrinite reflectance of the Ordovician source rocks. This is related to the vast spread of the organic-rich Cambrian to Silurian shales (Jarvie 2012; Pool et al. 2012). An increased depth of burial and temperature causes an increase of condensate aromatic structures of the lingo-cellulosic particles (which the vitrinite organic matter are formed from) (Carr and Williamson 1990). When this aromatic structure is more condensed, a fast increase is likely to occur for the vitrinite. Therefore, for a 1.56% graptolite reflectance, the corresponding vitrinite would be 1.3% Ro, which is the value for the gas window (Bustin et al. 1989; Schleicher et al. 1998). However, high

levels of thermal maturity resulting from high maximum temperatures and depths of burial may cause less defined vitrinite distributions (Goodarzi and Norford 1987).

Moreover, marine organic facies have limited phytoclastic content which causes a lack of vitrinite (Marshall 1998). Thus, an improper measurement of vitrinite reflectance may result in a significant evaluation mistake of the gas generation capacity of an organic matter (Strapoc et al. 2010). Kadkhodaie and Rezaee (2017) showed that vitrinite reflectance can be directly estimated from sonic and resistivity logs.

1.5.4 Remaining Hydrocarbon Potential (RHP)

The hydrogen content controls the amount of cracked oil to gas. The hydrogen/carbon atomic ratio is around 1.8 for oil. It is highly dependent on the composition (Jarvie et al. 2007). However, methane is about double this value (about 4 H/C). Therefore, cracking oil to gas leads to hydrogen deficiency and a reduction of gas generation capacity by time. Oxic and anoxic sedimentary environments are inferred from the correlation of residual hydrocarbon potential (RHP) data. Thus, RHP can be used to subdivide depositional sequences into high frequency successions (Slatt 2015) . The correlation with TOC and other lithology data provides higher resolution interpretations of sequence stratigraphy and sea level changes for the purpose of shale gas evaluation (Figure 1.7).
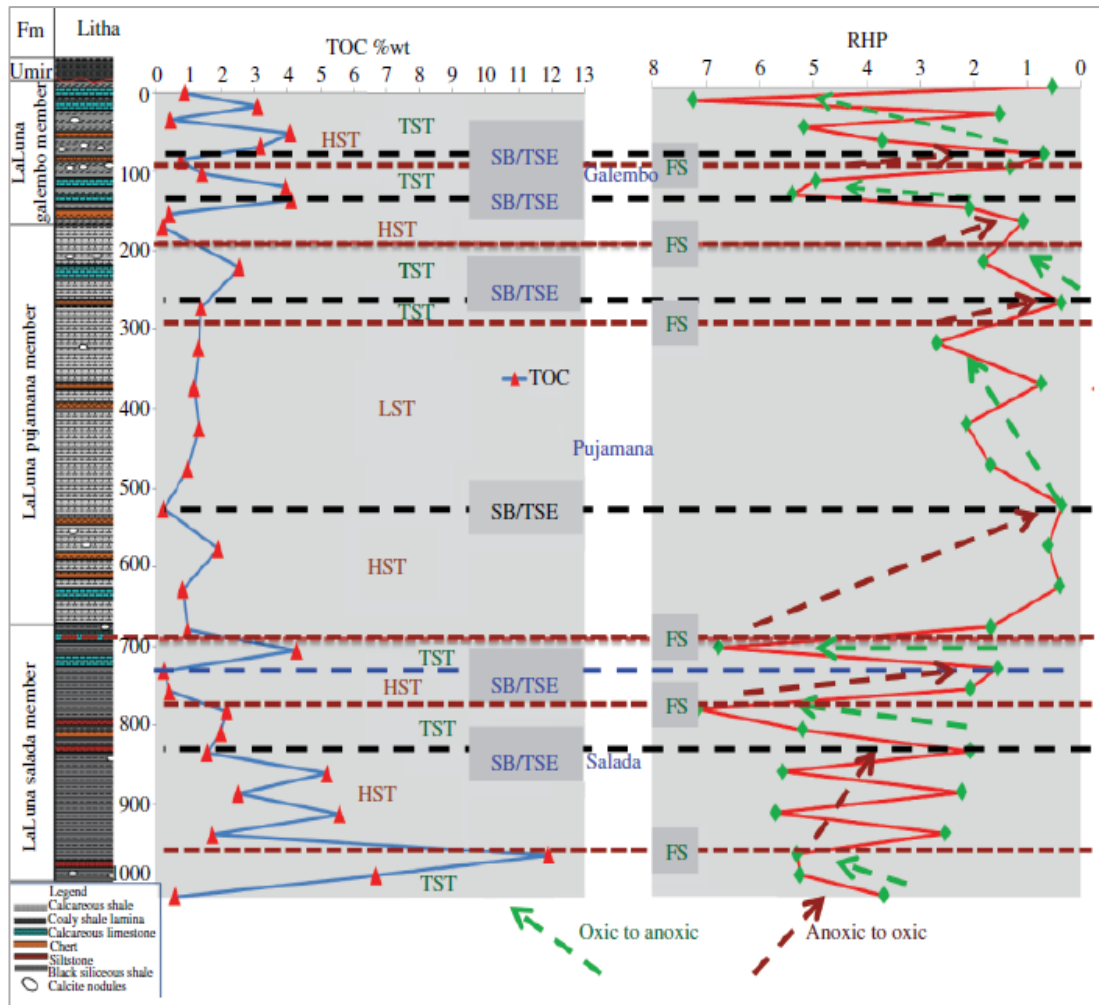
Figure 1.7 The sedimentary environment and sequence stratigraphy interpretation using the remaining hydrocarbon potential index from (Slatt 2015).

1.5.5 Porosity and Permeability

Pore throats' complexity and ultra-low permeability render the production of shale gas reservoirs as seriously challenging. Shale gas reservoirs are called "unconventional" because of the gas adsorption and very low permeability, which are not available in the conventional reservoirs. In shale gas is stored as a free compressed gas in the pore spaces, as adsorbed gas on the surface of clay and kerogen, and as a diffused gas within the solid organic matter (Curtis 2002). Organic pores will only develop when the maturity of the organic matter increases. However, over-maturation levels could destroy the physical properties of the shale (Caineng et al. 2015).

1.5.6 Saturation (Gas in Place and Water Saturation)

TOC is responsible for the gas generation and adsorption capacity of unconventional reservoirs. The expulsion efficiency of source rocks is directly related to sorption

capacity and saturation levels. Thus, sorption sites need to be filled prior to any gas expulsion (Pepper 1991). In their study of the New Albany shale, Strapoc et al. (2010) suggested that gas is mainly locally generated and has not migrated from other source strata. Therefore, although a lack of migration pathways is the case, high gas quantities can still be obtained from organic-rich shales. Furthermore, the porous structure of organic matter provides gas storage sites, as well as contributes to the total porosity of the rock. The surface area generated by either or both organic and mineral matters have a direct effect on the gas storage capacity. Thus, gas storage capacity can be directly related to the volume of microspores (Chalmers and Bustin 2007b; Ross and Bustin 2009). Figure 1.8 demonstrates the volumetric constituents of the shale gas matrix.
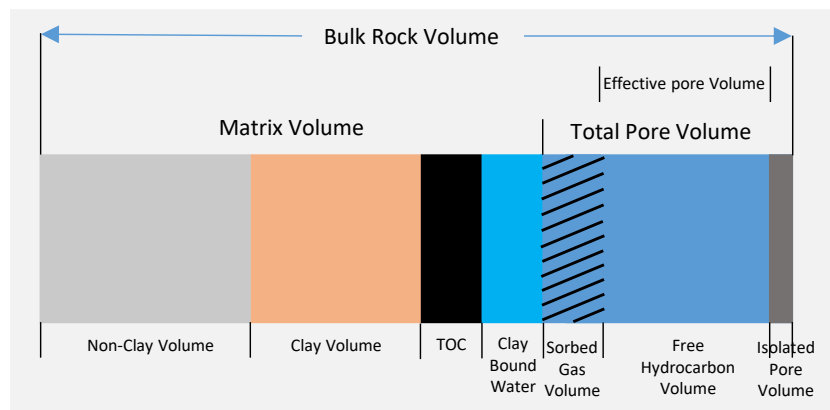
Figure 1.8 Volumetric constituents of the shale matrix (modified after (Ambrose et al. 2010).

Organic and inorganic components plus pore spaces are the build-up elements of shale gas rocks. Porosity can be classified as total pore volume representing sorbed, hydrocarbon and isolated pore volume, as well as effective pore volume (where it includes the connected pore spaces filled with gas).

1.6 Research Objectives

This study evaluates the shale gas prospectivity of the Goldwyer and Laurel formations in the Canning Basin. The main goal is to identify and map shale gas sweet spots of the highest potential targets for gas generation and production, using geological, geochemical, petrophysical and seismic approaches. The followings are the objectives of this study:

- Characterisation of geological and geochemical elements of the main shale beds in the Canning Basin.

- Evaluate the source rock potential of the Goldwyer and Laurel formations in the Canning Basin.

- Identify and 3D model the key parameters of the petrophysical properties such as TOC, fracability index and total porosity of the Goldwyer and Laurel formations.

- Discuss the various Lithofacies and sequence stratigraphy of the Goldwyer formation in the Central Canning Basin. Build the sequence concept and identify and map the vertical and lateral distribution of the lithofcies in the study area.

- Illustrate the sweet spots areas with the greatest gas potential in the Canning Basin.

2.   Chapter 2: Geochemical Analysis of the Goldwyer and Laurel Formations

2.1   Introduction

Organic matter is a key component of shale gas evaluation. The texture of shale, porosity, permeability and gas content is directly related to the organic content (Glorioso and Rattia 2012). Organic compounds (such as kerogen) that are present in shale gas are responsible for the generation and storage of hydrocarbons. The exposure to high temperatures causes different types of kerogen to produce crude oil, condensate or free gas. Thermogenic shale gas produces gas from either Type II or III kerogens at post-mature conditions (Glorioso and Rattia 2012). The determination of key organic parameters such as total organic content (TOC), thermal maturity and kerogen types is very important in the assessment of shale gas reservoirs. Organic materials develop and preserve in certain sedimentary environments. Deoxygenated and calm marine conditions are favorable places for the growth and preservation of organic materials. It is believed that maximum production, followed by minimum dilution and destruction of organic matter, will provide the best organic source for shale gas reservoirs. As it will be further explained in Chapter 6, large amounts of gas are adsorbed on organic matter, thus the total volume of TOC is necessary to estimate the total gas amount in place. Moreover, a low density of TOC has variable effects on shale matrix density. Therefore, density dependent calculations (such as shale gas porosity) involve the amount and density of the organic matter present in the rock (see Chapter 4 for more information). The source rock potential and thermal maturity of organic-rich rocks is usually assessed using the Rock Eval Analysis. One useful approach is to plot S2 versus TOC, which helps to establish the generation potential and kerogen type of the rock (Erik et al. 2006). On the other hand, the PI versus Tmax plot helps in identifying the thermal maturity of the organic-rich rock.

The vast and unexplored Canning Basin in the north-western region of Western Australia has proved to contain many potential organic-rich shales; these include the Laurel and Goldwyer shales (Figures 1.4 and 1.5). However, their potential is still poorly evaluated. In the basin, although conventional and tight gas discoveries have been made, they have not been well developed. The Tournaisian-Visean Laurel Formation is a deltaic to shallow marine deposit. The Upper Laurel section has relatively coarse terrigenous and occasional carbonate lithology, representing a

shallow marine to intertidal sub-tidal environment. However, the Lower Laurel is predominantly carbonates, except the areas adjacent to growing siliclastic provenances (Cadman et al. 1993). The Lower Carboniferous Laurel Shale is believed to be the source rock of the oil and gas reservoirs in the Lennard Shelf and Fitzroy Trough. Several recent studies of kerogen type, source rock potential and maturity have shown that the gas production from the Laurel Formation can be economically significant.

The Goldwyer Formation is mainly made up of mudstone and carbonates, whose ratios vary widely across the basin, as well as some local carbonate build-ups. Coarse siliciclastic rocks are rarely found as they are restricted only to minor fine-grained sandstones towards the south east of the basin. The average grain size in this formation is clay to siltstone. The sedimentary environment is generally chemically reduced, ranging in colours from grey-green to grey and black deposits. Also, pyrite is rarely present. The matrix is a weak to strong calcareous or dolomitic and contain millimetre-scale carbonate laminae in some places. Bioturbation, if present, ranges from discreet cylindrical and branching burrow systems to general churning of the sediments. These are absent in the black mudstone, presumably due to the presence of anoxic bottom conditions. The Upper Goldwyer Formation contains higher concentrations of Gloeocapsomorpha prisca compared to the Lower Goldwyer Formation (Foster et al. 1986). The source rocks in the Upper Goldwyer Formation are restricted to the Mowla and Western Barbwire Terraces. The Barbwire Terrace is known to have oil-prone source rocks (Edwards et al. 1997). The Lower Goldwyer Formation source rocks are also intersected in the same areas extending across the Northern Broome Platform (Edwards et al. 1997). The source rocks may extend to the adjacent Fitzroy Trough, but they have never been intersected by any of the wells, probably due to the high depth of the sediments. The source rocks in the Goldwyer Formation are commonly immature for hydrocarbon generation based on the conodont alteration indices (Nicoll 1993; Nicoll and Gorter 1984). The carbonate beds in the Goldwyer Formation were found to be tight and hence, the unit has not been considered to be a potential hydrocarbon reservoir (Haines 2004).

2.2   Rock Eval Pyrolysis

Rock Eval Pyrolysis was carried out on approximately 70 milligrams of pulverized shale samples. The samples were heated up to 600°C in an oxidation oven, and a programmed pyrolysis of up to 850°C at 25°C per minute. From this experimental procedure, an estimation of the free, already generated hydrocarbon in the sample was obtained (S1), as well as the hydrocarbon that could be generated from the thermal cracking of the remaining kerogen and high molecular weight free hydrocarbons that do not vaporise in the S1 peak (S2). S1 + S2 represent the total hydrocarbon genetic potential (Tissot 1984). Standard interpretative guidelines for the hydrocarbon generative potential is given as: S1 + S2 less than 2 mg HC/g rock corresponds to little or no oil potential and some potential for gas; S1 + S2 yield from 2 – 6 mg HC/g rock represents fair to moderate source rock potential, while S1 + S2 yield greater than 6 mg HC/g rock usually represents good to excellent source rock potential. In addition, the values for the organic carbon dioxide that evolved at low temperature pyrolysis (S3) were obtained. The residual organic carbon (S4) and Residual Carbon (RC) were also calculated. These values were then used to compute the Total Organic Carbon (TOC). The TOC provides a measure of the organic richness of the sample, expressed as a percentage of the weight of the dry rock (wt.%). Bissada (1982) described the organic content in rocks using the following scheme: 0 - 0.5 % weight TOC represents poor organic richness; 0.5 - 1.0 % weight TOC represent moderate richness; 1.0 - 2.0 % weight TOC represent a good source rock and 2.0 - 5.0 % weight TOC represent excellent source rocks.

Other ratios calculated from the Rock Eval data include the Hydrogen Index (HI), Oxygen Index (OI) and Production Index (PI), amongst others. The kerogen type and a generalised estimation of the source rock quality can be identified from the HI values (Tissot and Welte 1978). Type I, oil-prone kerogen is usually hydrogen rich and have HI values greater than 600 mg HC/g TOC. For the HI between 250 and 600 mg HC/g TOC, it represents Type II oil/oil and gas kerogen. Type III gas-prone kerogen is typified with HI between 50 and 250 mg HC/g TOC, while HI values of 0 - 50 mg HC/g TOC characterise Type IV kerogen, with a low capacity to generate hydrocarbons at appropriate levels of thermal maturity. Thermal maturity (Tmax) represents the temperature at the maximum hydrocarbon generation during the S2 cycle. Tmax values less than 425°C are considered immature, 435 - 440°C are in the early mature oil window, while values between 440 - 460°C are in the late mature oil

window. Moreover, values greater than 470ºC are considered overmature and would generate either a wet or dry gas for Type II kerogen (Espitalie et al. 1985).

2.3   Case Study

The results from the Rock Eval pyrolysis technique used in this study provide a fast method to identify the hydrocarbon source potential of the shale intervals. In this study, the Carboniferous Laurel shale and the Ordovician Goldwyer shales are studied across four Canning Basin's sub basins. The data for this study was obtained from the Western Australia Department of Mines open file records, combined with the data from the Rock Eval Pyrolysis experiments carried out on ten shale samples selected from various lithofacies of the Laurel and Goldwyer shales in the Canning Basin wells (Table 2.1).

Table 2.1 Rock-Eval Pyrolysis results of ten selected samples for shale gas evaluation in the Canning Basin.

Well Name	Depth from (m)	Tmax	S1	S2	S3	PI	TOC	HI	OI
Goldwyer Formation									
Goldwyer 1	981.15	441.00	0.35	2.21	0.35	0.14	0.96	230.92	36.57
McLartey 1	2003.76	430.00	2.44	4.20	0.61	0.37	2.89	145.08	21.07
Percival 1	2055.55	432.00	0.09	0.48	0.12	0.16	0.47	101.61	25.40
Solanum 1	396.00	436.00	0.43	2.59	0.27	0.14	0.97	266.18	27.75
Dodonea 1	1542.37	448.00	0.22	4.81	0.16	0.04	1.08	445.21	14.81
Laurel Formation									
Blina 1	1114.30	430.00	0.15	0.26	0.07	0.37	0.55	47.00	12.00
Blina 1	1118.50	430.00	0.08	0.16	0.16	0.35	0.41	38.00	38.00
Curringa 1	1869.00	430.00	0.10	3.50	1.54	0.03	2.89	121.00	53.00
Yarrada 1	1825.80	432.00	0.18	0.78	0.26	0.19	0.57	137.00	45.00
Yulleroo 1	3660.40	450.00	0.88	1.83	0.52	0.33	3.23	57.00	16.00

The comparison of measured TOC content against quantitative XRD minerology, which is shown in Figures 2.1 and 2.2, reveal a direct relationship between the organic and clay content of the shale samples. The higher the clay minerals, the deeper and more organic rich are the sedimentary environments found in both the Laurel and Goldwyer Formations.
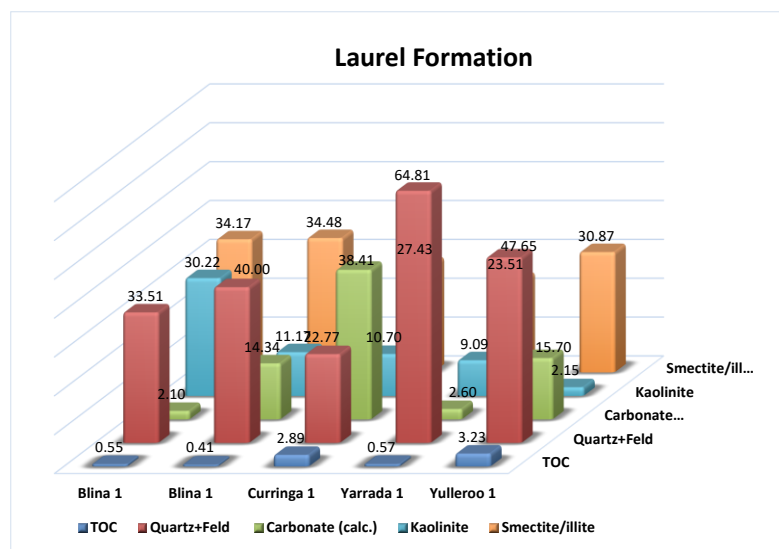
Figure 2.1 Comparison of measured TOC content and quantitative XRD minerology of five Laurel shale samples from the Canning Basin in Western Australia.
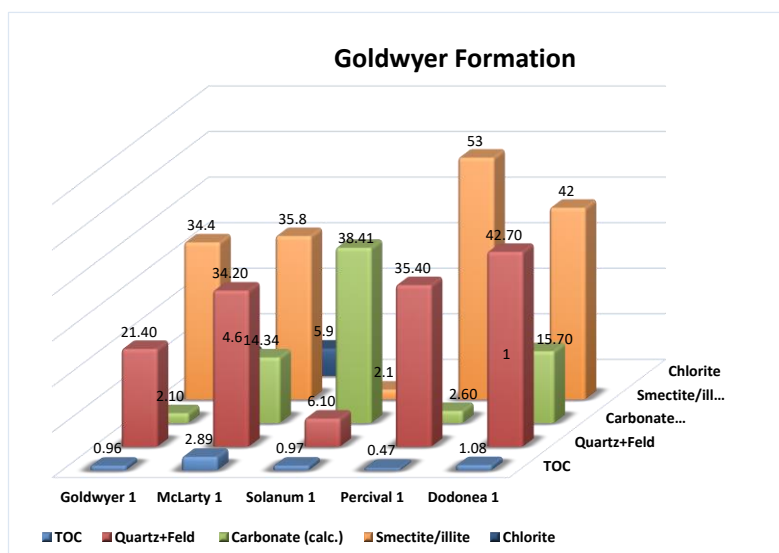
Figure 2.2 Comparison of measured TOC content and quantitative XRD minerology of five Goldwyer shale samples from the Canning Basin in Western Australia.

2.3.1   Carboniferous Laurel Formation

The shales from the Carboniferous Laurel Formation in the Canning Basin generally have TOC values between 0.2 - 6.0 wt.%, indicating fair to excellent organic richness. Also, the total hydrocarbon potential (S2) of about 20% of the samples is between 2 - 6 mg HC/g TOC. However, about 70% of the studied samples have S2 values between 0.2 – 2, indicating poor hydrocarbon generation potential. A plot of log TOC vs log S2 across the Laurel Formation indicates that majority of the

50

samples across the sub-basins have fair to good potential to generate hydrocarbons (Figure 2.3). Furthermore, the shales have mostly Type II/ III and Type III oil/gas-prone and gas-prone hydrocarbon generative potential, with a few samples in the dry gas zone (Figure 2.4).
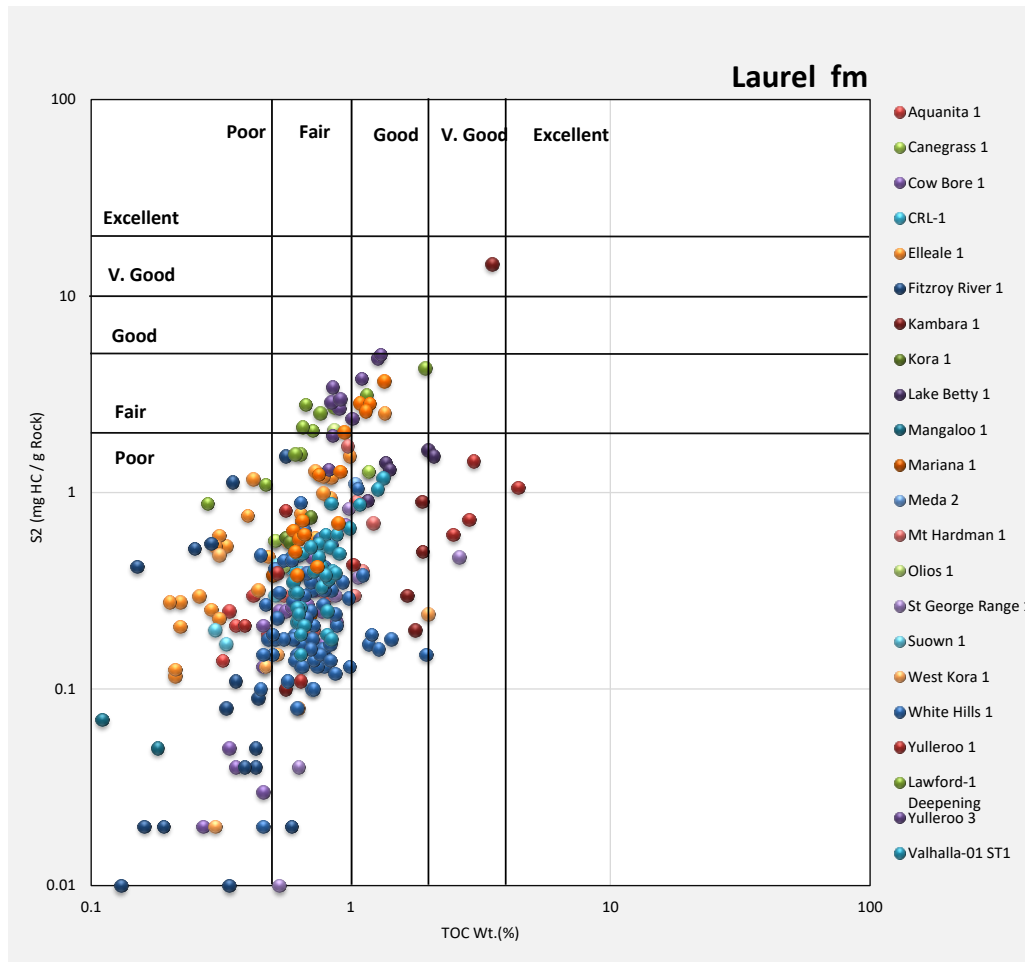
Figure 2.3 Log-log across plot of Rock-Eval Pyrolysis, S2 vs TOC, for Laurel shales in 21 wells across the Northern Canning Basin.

In terms of thermal maturity, the plot of vitrinite reflectance vs depth shows that most of the samples from this formation have immature to mature oil-prone kerogen, with values in the range of 0.5 - 2% Ro (Figure 2.5). However, in the absence of extensive Ro data, a plot of Production Index (PI) vs Tmax shows the maturity of the Laurel shale and the potential of the kerogen to convert to oil and gas. As indicated in the sparse Ro data, majority of the samples fall in the mature oil zone and condensate wet gas zone with PI values of 0.4 – 0.7, and about 70% of the sample interval fall in the immature and postmature dry gas zone respectively (Figure 2.6).

51

The conventional source rock investigation using the Rock Eval pyrolysis method for the Carboniferous Laurel Formation of the Canning Basin indicates a generally low to high amount of organic matter from a regional context.
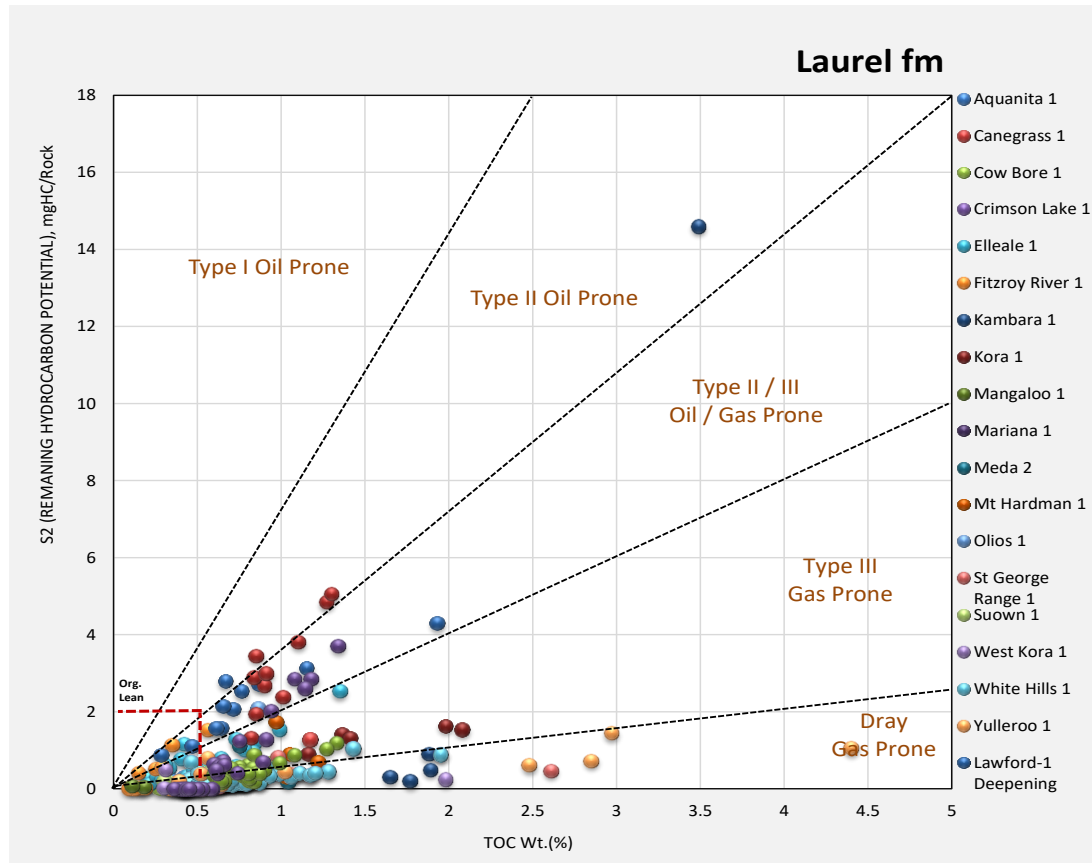
Figure 2.4 Linear across plot of Rock-Eval Pyrolysis, S2 vs TOC, for Laurel shales in 21 wells across the Northern Canning Basin.

It is observed that the dispersed organic matter in the source rock facies is composed mainly of Type II/ III oil/gas and gas-prone kerogen, indicating a mixture of both marine and terrestrial sources for the organic materials. Generally, the genetic potential (S1 + S2) of the source rocks is 3, thus indicative of terrestrial source material. This study further identifies the source rock potential in different Canning sub-basins, which is briefly discussed in the following sections.
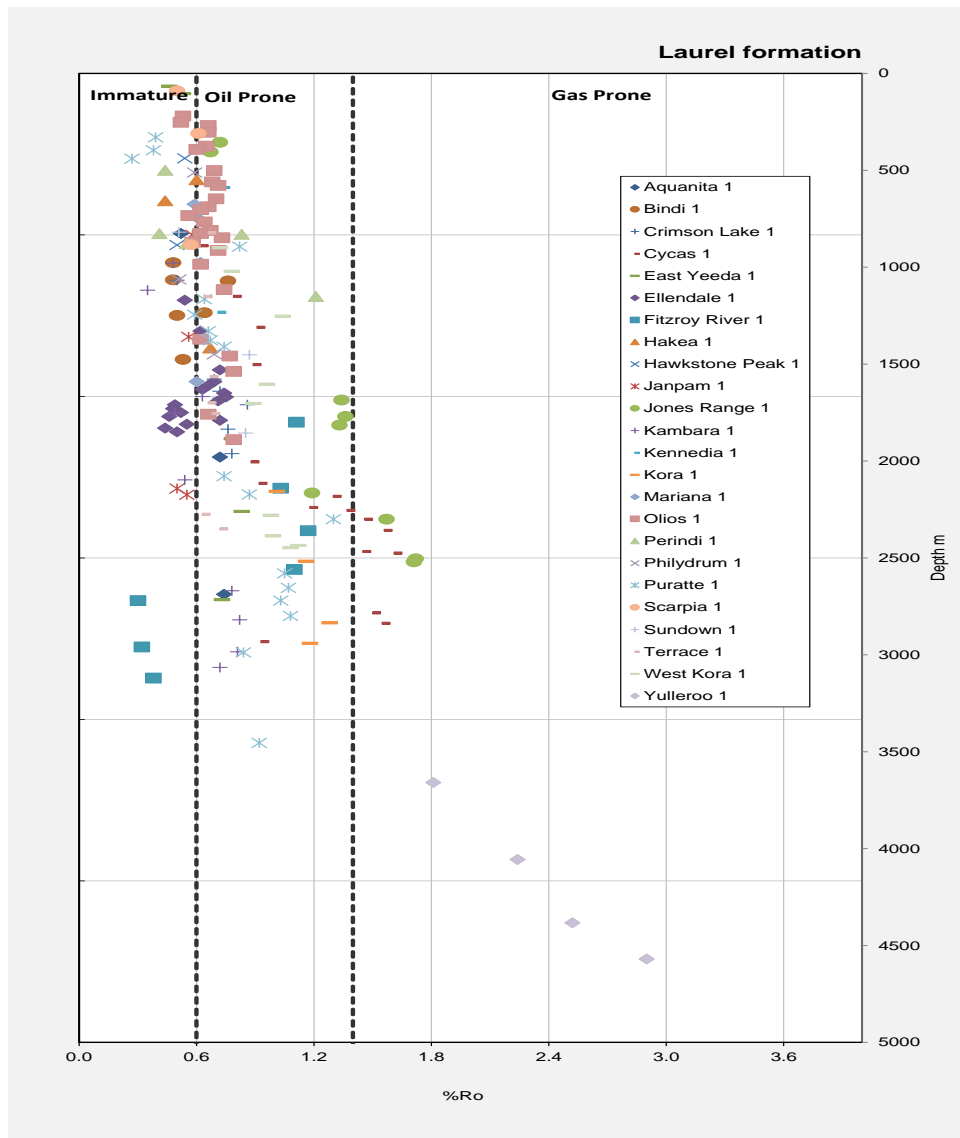
Figure 2.5 Plot of Vitrinite Reflectance (Ro) versus the depth of the Laurel Formation in the Canning Basin.
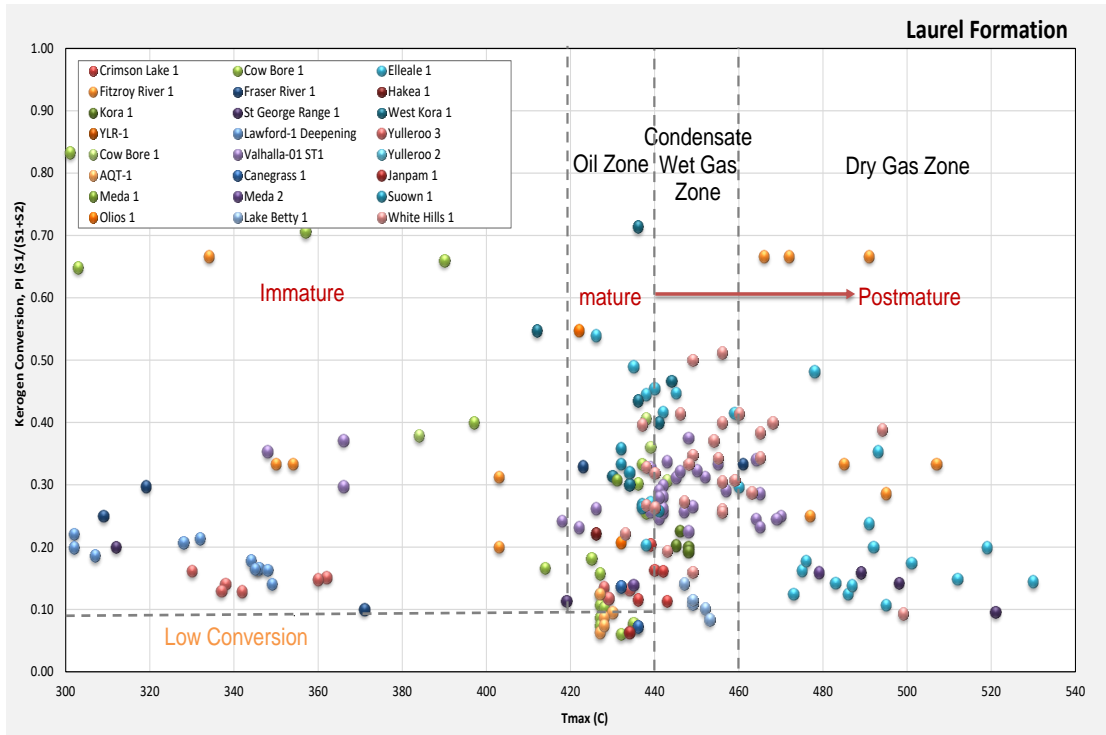
Figure 2.6 Linear cross plot of the Production Index (PI) vs Tmax for Laurel shales in 21 wells across the Northern Canning Basin.

2.3.1.1 Fitzroy Trough

The Fitzroy Trough is a deep Canning depocentre, with sediment thickness of up to 15 km. This has an implication for hydrocarbon generation within the Laurel formation. Total Organic Content in this sub-basin ranges between 0.5 - 4.4 wt%, with the plot of log S2 vs TOC (Figure 2.7) revealing poor to fair source potential, with Type II/ III and Type III oil/ gas and gas-prone kerogen (Figure 2.8).
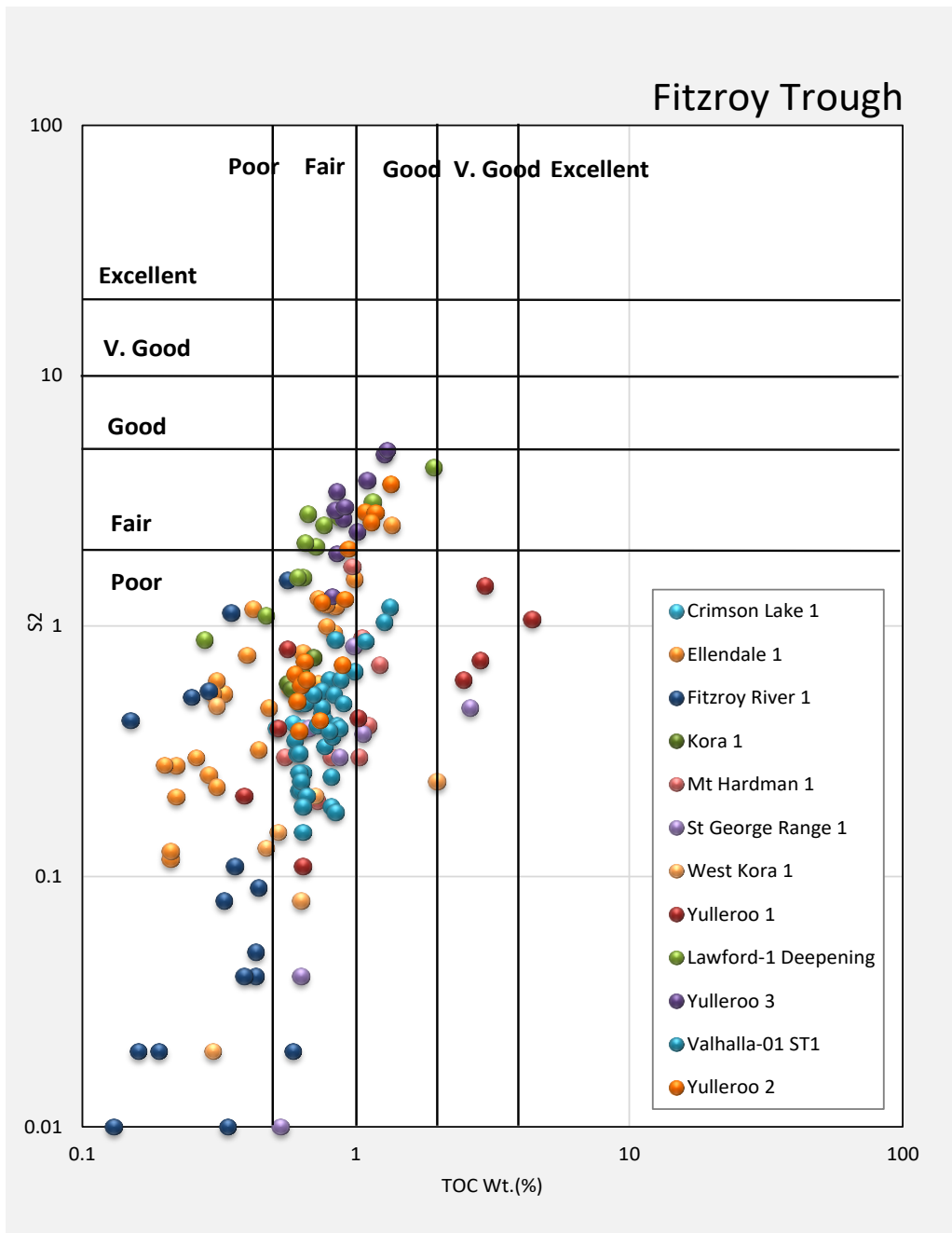
Figure 2.7 Log-log across plot of Rock-Eval Pyrolysis, S2 vs TOC, for the Laurel shales in the Fitzroy Trough.
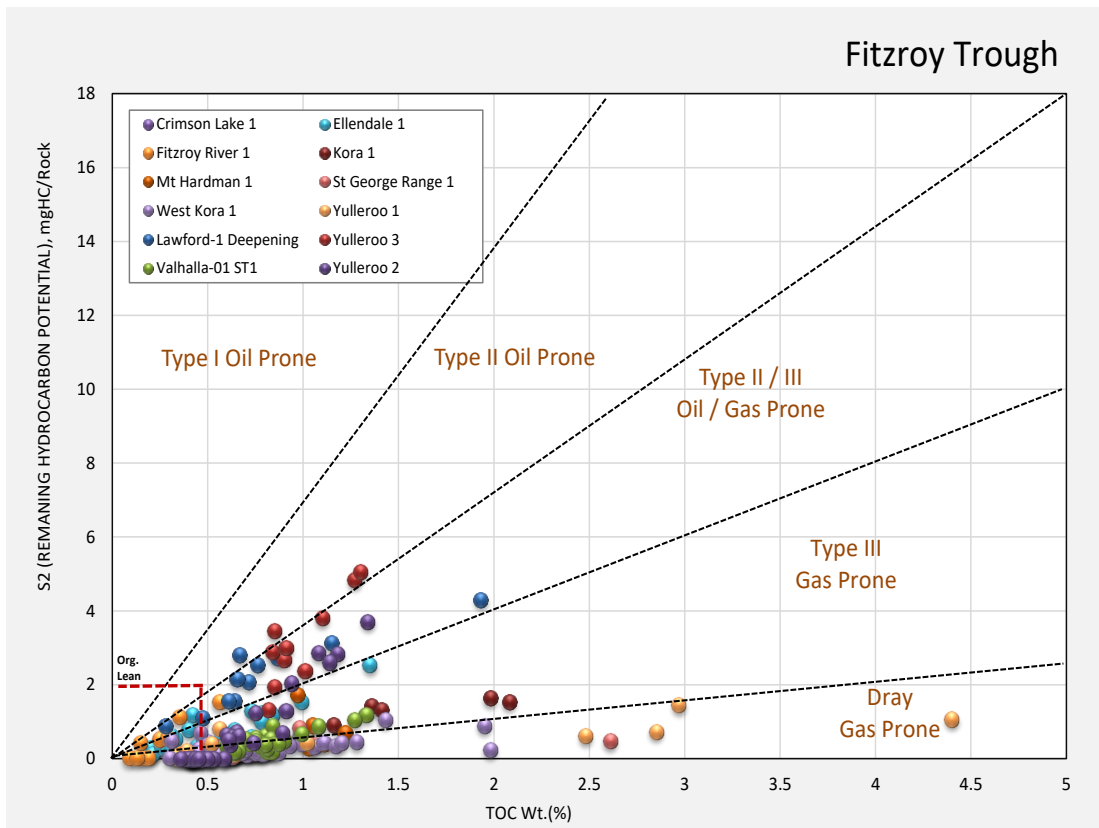
Figure 2.8 Linear cross plot of Rock-Eval Pyrolysis, S2 vs TOC, for the Laurel shales in the Fitzroy Trough.

Also, the thermal maturity of the Laurel shales in the Fitzroy Trough was evaluated from the vitrinite reflectance data. It revealed that the shales are mostly oil-prone in the margins and gas-prone in the centre. In addition, the Laurel source rock becomes mainly dry gas prone, with Ro values ranging between 0.2 - 2.8% towards the northern parts of the trough, (Figure 2.9). The Tmax data from the Laurel shale in the Fitzroy Trough indicates that this formation is mature to post-mature (435 to over $500^{O}C$), such as in the Valhalla#1 and Yulleroo#1 wells (Figure 2.10), which probably reflects the greater depth of burial of the Laurel Formation in this sub-basin. Ro seems to be greater in deeper samples that can be related to the deepening depth trend. This indicates tha tectonic movement has not moved the sediments upward so they did only undergone compaction.
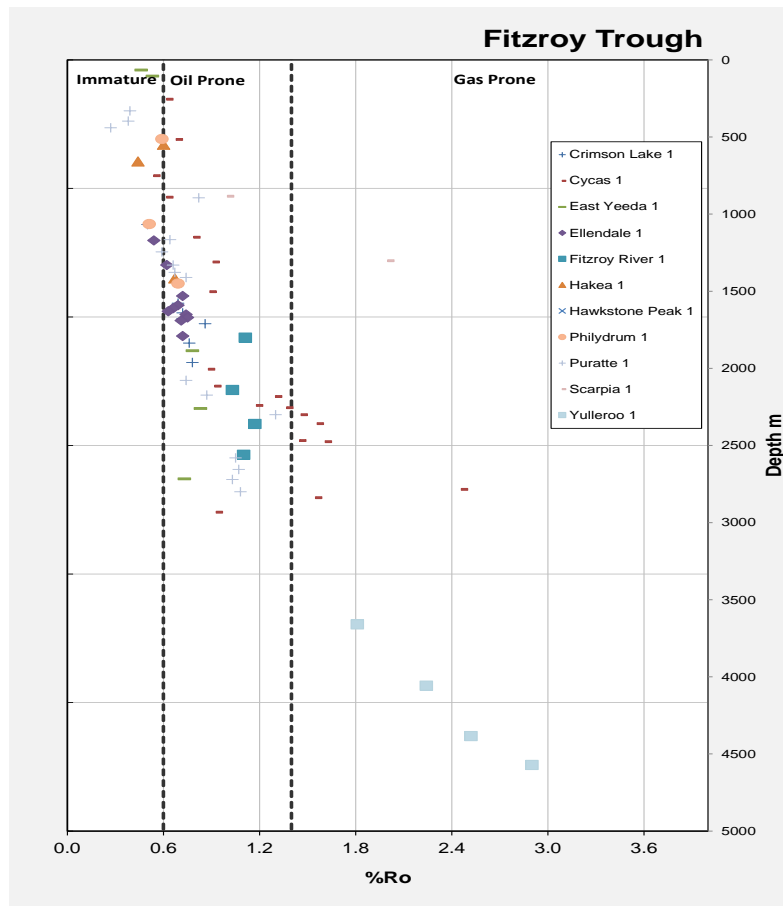
Figure 2.9 Plot of Vitrinite Reflectance (Ro) versus the depth of the Laurel Formation in the Fitzroy Trough.
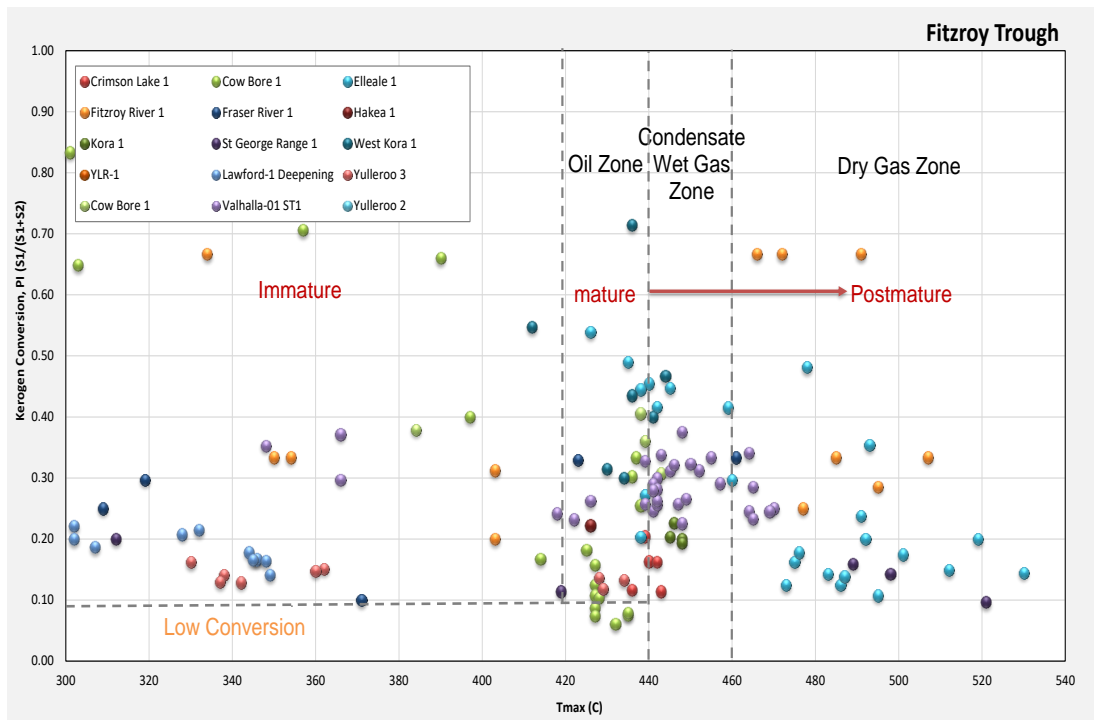
Figure 2.10 Linear cross plot of Production Index (PI) vs Tmax for the Laurel shales in the Fitzroy Trough.

57

2.3.1.2 Lennard Shelf

In the Lennard shelf, despite the long exploration history and high number of petroleum wells, fewer wells have been drilled to the Laurel shale. However, the results from the Rock Eval Pyrolysis indicate that majority of the shales studied have poor to fair source rock potential (Figure 2.11). The TOC values here range between 0.5 - 2.5 wt% in all the study wells. The plot of OI vs HI suggests the presence of Types III and IV gas-prone to inert kerogen due either to the poor organic matter preservation and/or overmaturity, where applicable (Figure 2.12). However, the linear cross plot of Tmax vs PI in the Lennard shelf indicates that the Laurel shale here is in the mature oil-wet zone, with low to moderate kerogen conversion potential (Figure 2.14).
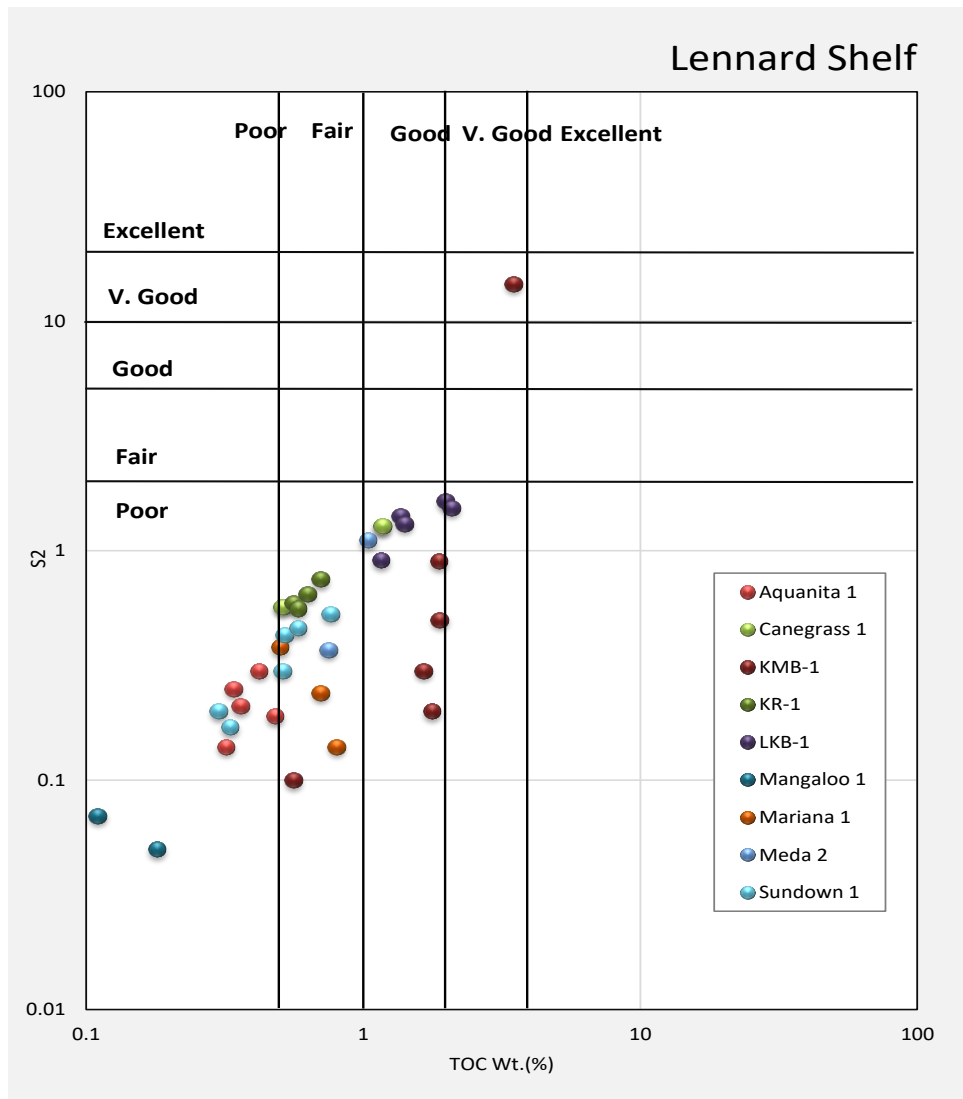
Figure 2.11 Log-log across plot of Rock-Eval Pyrolysis, S2 vs TOC, for the Laurel shales in the Lennard Shelf.
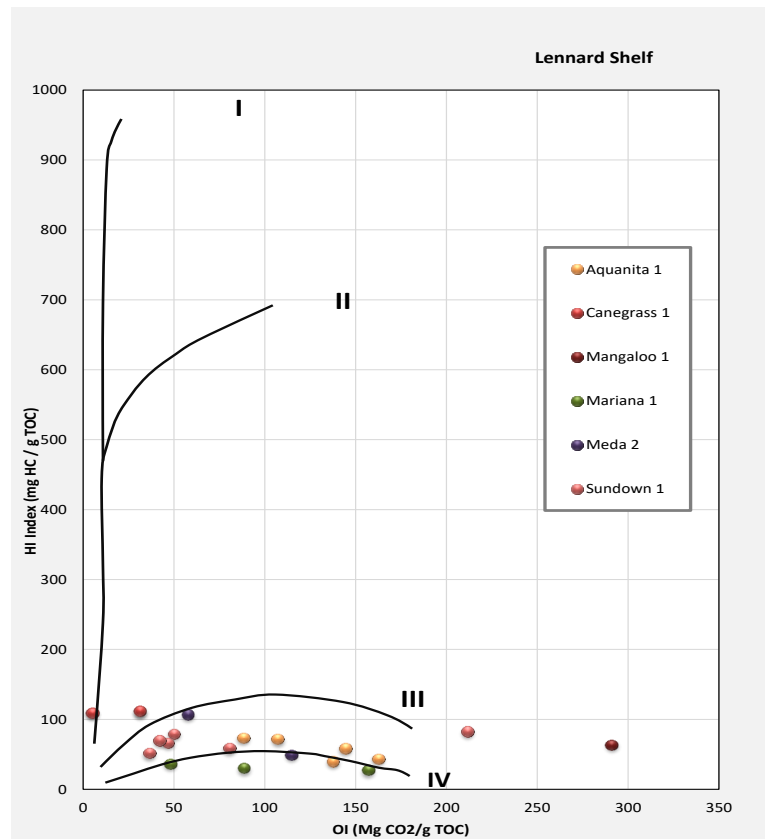
Figure 2.12 Pseudo Van-Krevelen plot of OI vs HI for five wells from the Laurel shales in the Lennard Sub-basin.

The vitrinite reflectance data plotted in Figure 2.13 confirms the same maturation levels with most of the Ro values between 0.6 and 1.3. This aligns with the analysis of the PI vs Tmax plot that indicates the mature oil window for the same samples. The exploration history of the Canning Basin also suggests a mature oil window of the Laurel shale in the Lennard Shelf, with most of the oil fields being discovered between 1980 and 1990.
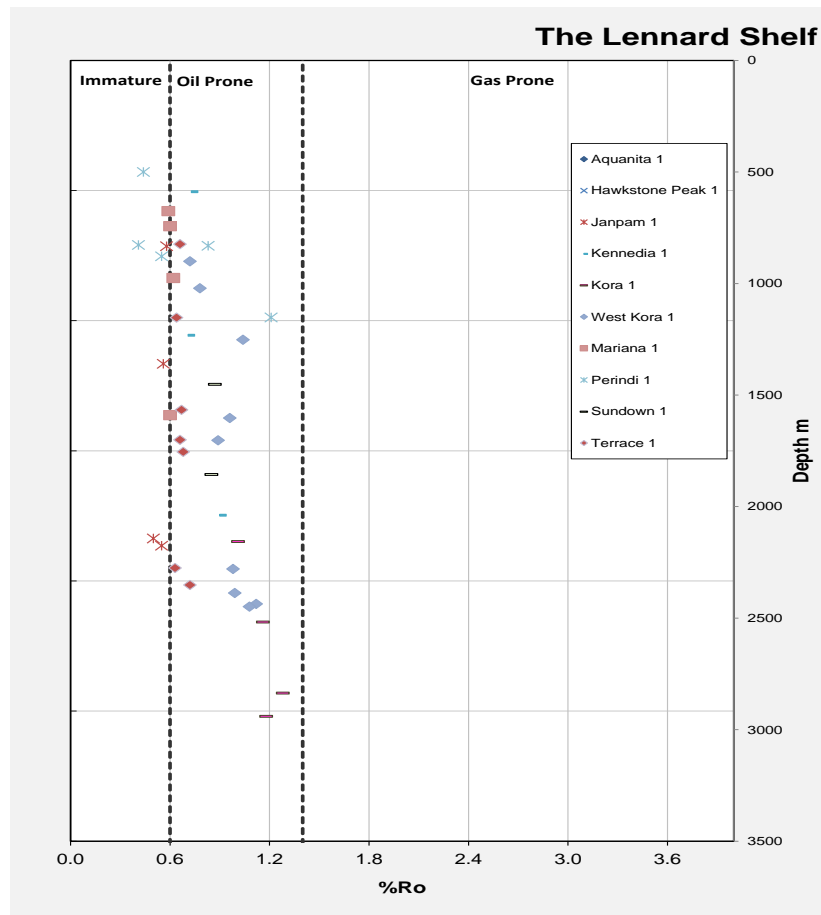
Figure 2.13 Plot of Ro versus depth of the Laurel Formation in the Lennard Shelf.
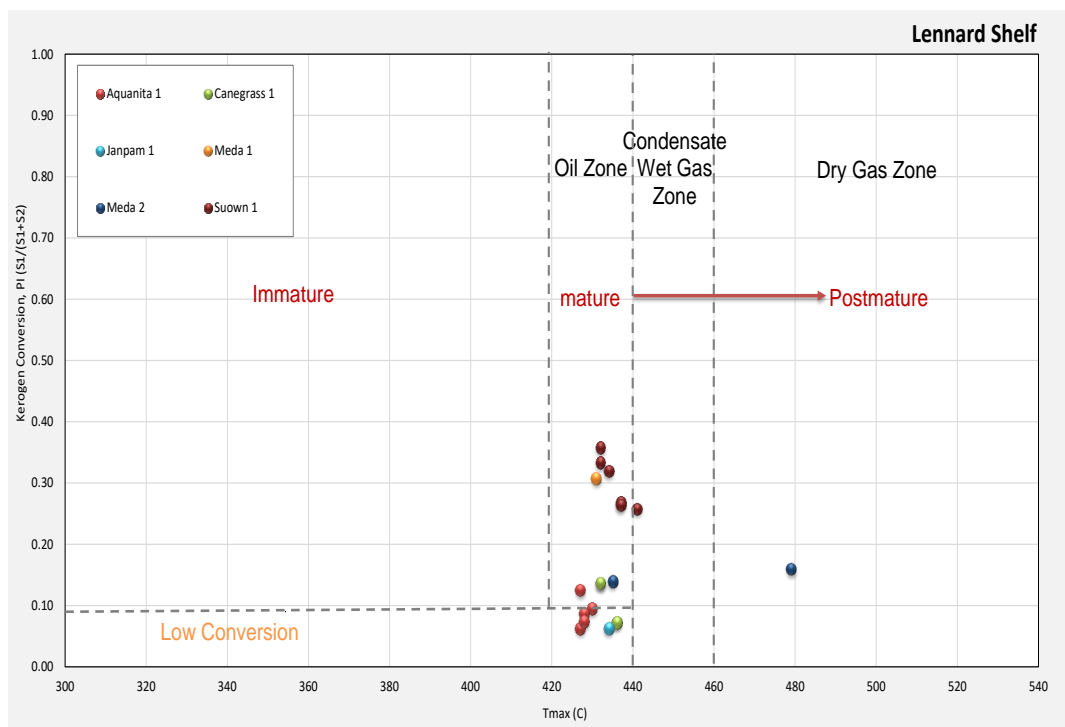
Figure 2.14 Linear cross plot of the Production Index (PI) vs Tmax for the Laurel shales in the Lennard Shelf.

60

In this sub-basin, the limited amounts or near absence of geochemical data or drill cores has made it difficult to evaluate the hydrocarbon potential of the Laurel shale. The only cored well in the Gregory sub-basin, the White Hills#1 well, has TOC values between 0.4 - 2.0 wt%. However, the plot of S2 vs TOC reveals that this shale is in the post-mature and dry gas generative window (Figure 2.15), which can be related to the higher depth of burial of the Laurel Formation in this sub-basin (over 2000 km). The Tmax data reveals the same maturity level from the aforementioned well (Figure 2.16).
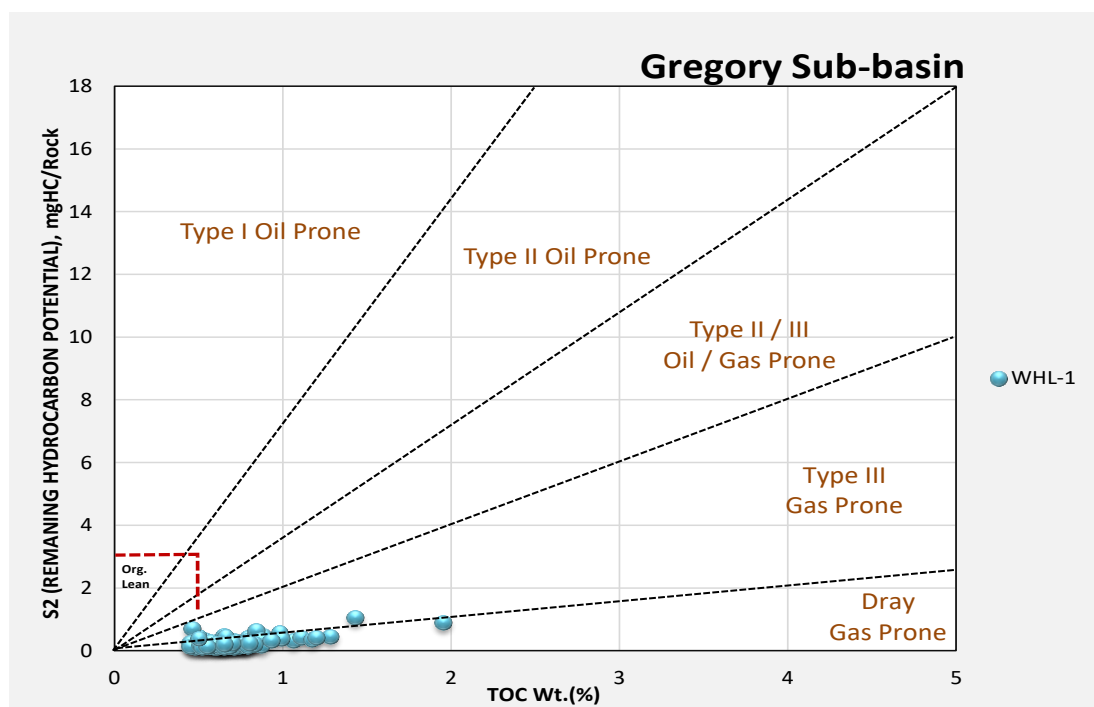
Figure 2.15 Linear across plot of Rock-Eval Pyrolysis, S2 vs TOC, for the Laurel shales in the Gregory Sub-basin.

61
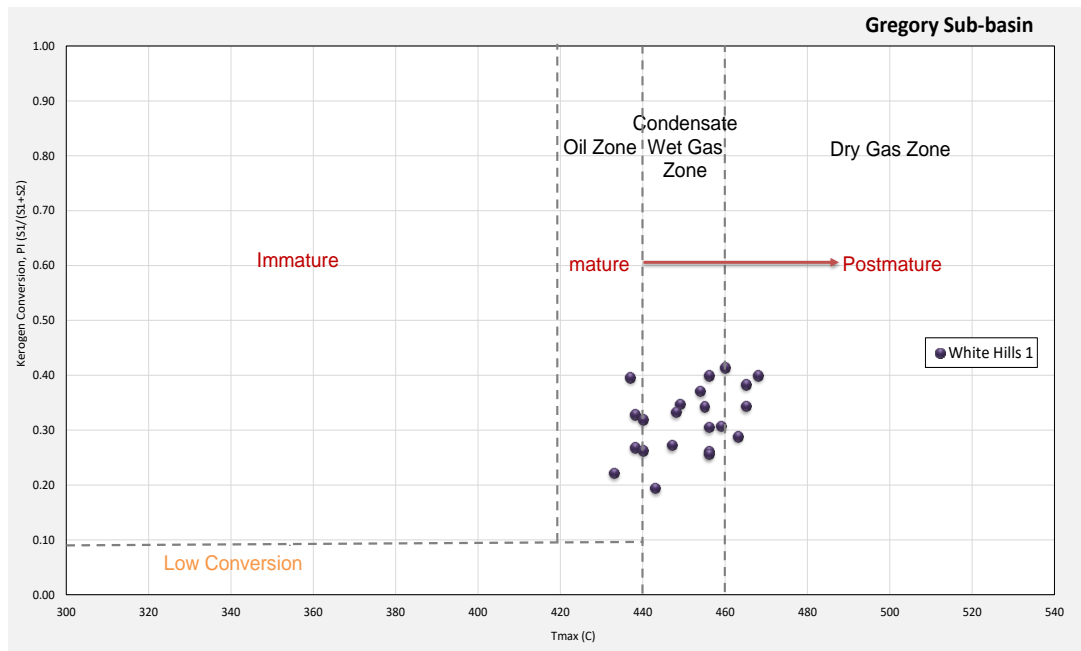
Figure 2.16 Linear cross plot of the Production Index (PI) vs Tmax for the Laurel shales in the Gregory Sub-basin.

2.3.2 Ordovician Goldwyer Formation

In the Ordovician Goldwyer Formation, the vitrinite reflectance (equivalent) data indicates that majority of the samples are mature with Ro > 0.7%, mostly in the oil generation window (Figure 2.17), with a few data points, or perhaps anomalies in the gas generating window, with Ro values up to 3.6%. Furthermore, the Tmax data is generally skewed 420 and 460°C, which indicates that the samples range from immature to peak mature oil generating window with condensate gas. The total organic content in the Goldwyer Formation varies between 0.2 - 3.5 wt%, reaching a maximum of 4.8 in the Kunzea#1 well, thus indicative of poor to very good potential source rock (Figure 2.18) and hydrocarbon potential (S1+S2) of up to 20 mgHC/gTOC. Majority of the hydrogen indices from the analysed samples are greater than 100 mgS2/g TOC. The logarithm plot of TOC vs S2 in Figure 2.18 shows that a fraction of the Goldwyer shale's (about 40%) data points have fair to good potential to generate hydrocarbon. The Pseudo VanKrevelen plot shows that the Goldwyer shale has mostly Type II oil-prone and Type II/ III oil and gas-prone kerogen (Figure 2.19). Figure 2.20 confirms the same kerogen type II/III and kerogen type III. In terms of kerogen conversion, about 30 - 40% of the sample

62

interval falls in the mature oil zone, with majority of the samples having immature kerogen, with low kerogen conversion potential (Figure 2.21).
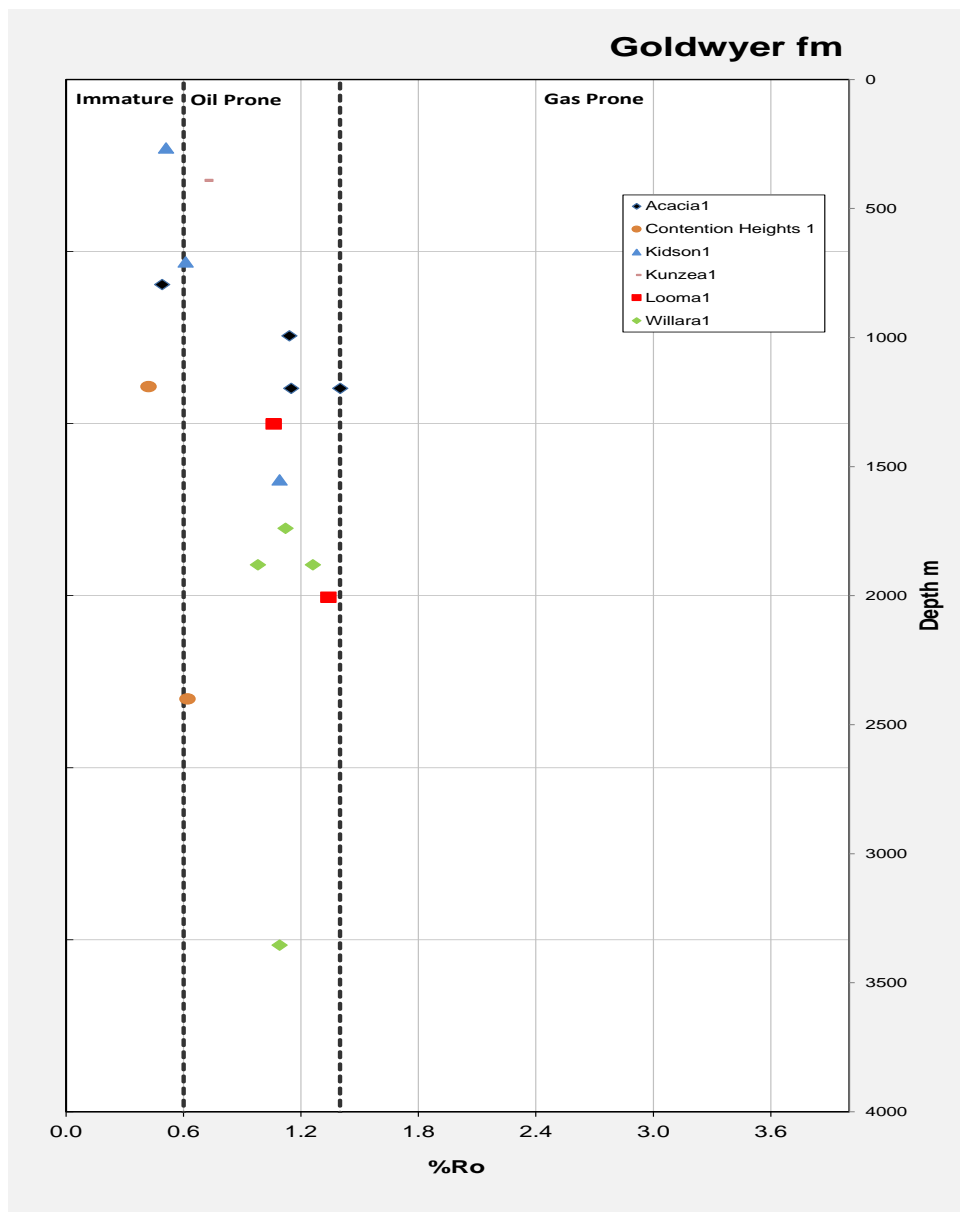
Figure 2.17 Plot of Vitrinite Reflectance (Ro) versus the depth of the Goldwyer Formation in the Canning Basin.
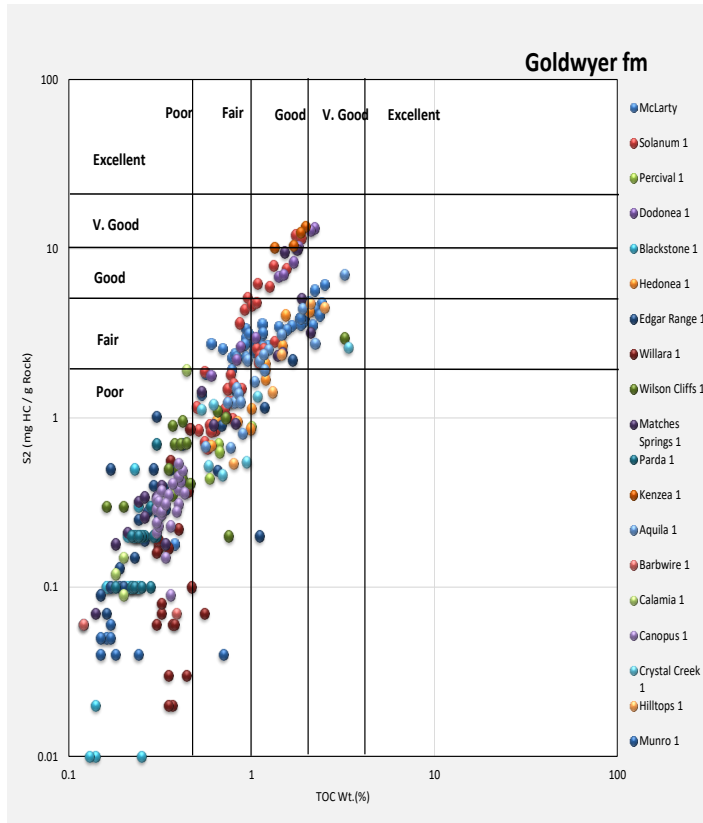
Figure 2.18 Log-log across plot of Rock-Eval Pyrolysis, S2 vs TOC, for the Goldwyer Shales in the Canning Basin.
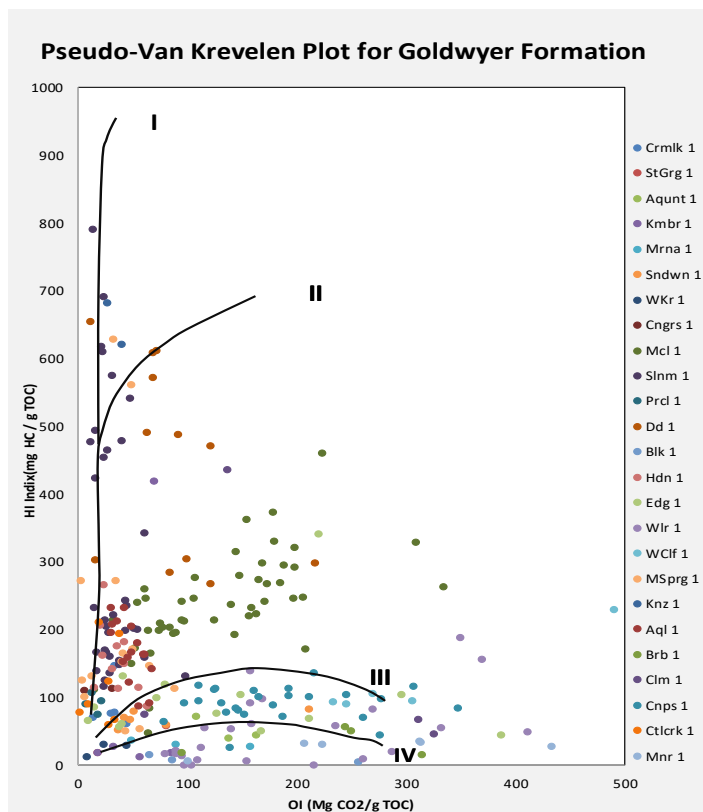
Figure 2.19 Pseudo Van-Krevelen plot of OI vs HI of the Goldwyer shales in the Canning Basin.

64
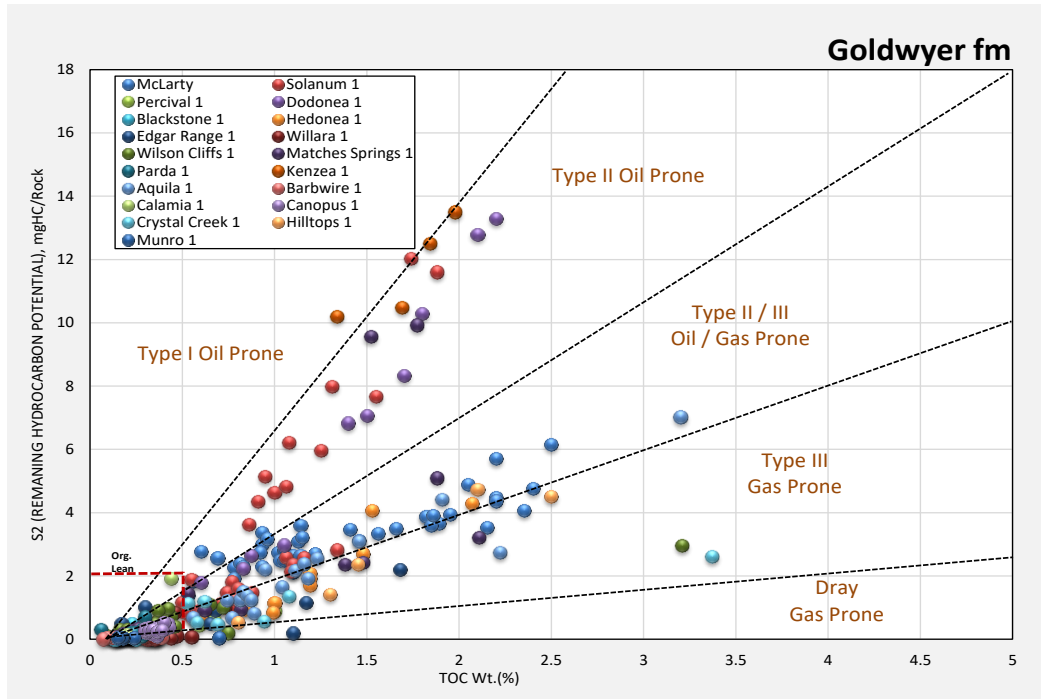
Figure 2.20 Linear cross plot of Rock-Eval Pyrolysis, S2 vs TOC, for the Goldwyer Shales in the Canning Basin.
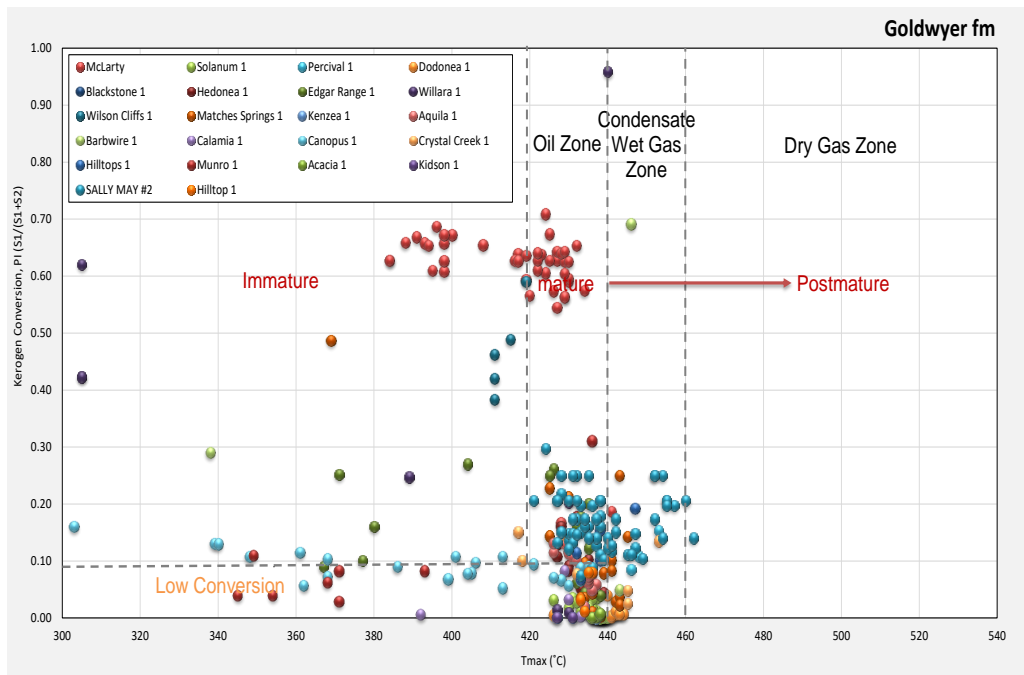
Figure 2.21 Linear cross plot of production index (PI) vs Tmax for the Goldwyer Shales in the Canning Basin.

As inferred from the Rock Eval Pyrolysis data from fifteen wells in the Broome Platform, it shows that 80% of the studied shale samples have average TOCs between 0.5 - 2.5 wt%, suggestive of moderate to very good organic richness (Figure 2.22). A higher TOC content is observed along the Central Broome Platform trending SE-NW (Figure 2.26A, max TOC map). The plots of S2 against TOC show that these shales are mostly Type II and Type II/ III oil and oil/gas-prone kerogen respectively (Figures 2.23 and 2.26B). In this sub-basin, the Production Index and Thermal maturity data suggest that the samples from the Hilltop#1, Aquila#1, Hedonea#1 and Mclarty#1 wells are in the ideal maturity for oil generation, with most of the sample points having moderate to high conversion potential (Figure 2.25). It is further observed from the 2D maps in Figures 2.26 D and E that the maturation levels increase towards the deeper parts in the south-eastern regions of the sub-basin close to the Kidson Sub-basin. The burial depth of the Goldwyer Formation in the Broome Platform ranges from 1000 meters in the northern parts of the sub-basin to between 1400 and 2000 meters in the southern edge of the platform, which has its corresponding response on maturation levels. The Pseudo Van-Krevelen plot of OI and HI data in Figure 2.24 shows that the Goldwyer shale has mostly Type II oil-prone kerogen along the Central Broome Platform, and Type II/III oil and gas prone kerogen around the margins, especially on the north-western margins attached to the Mowla Terrace and south-eastern margins with the Kidson Sub-basin.
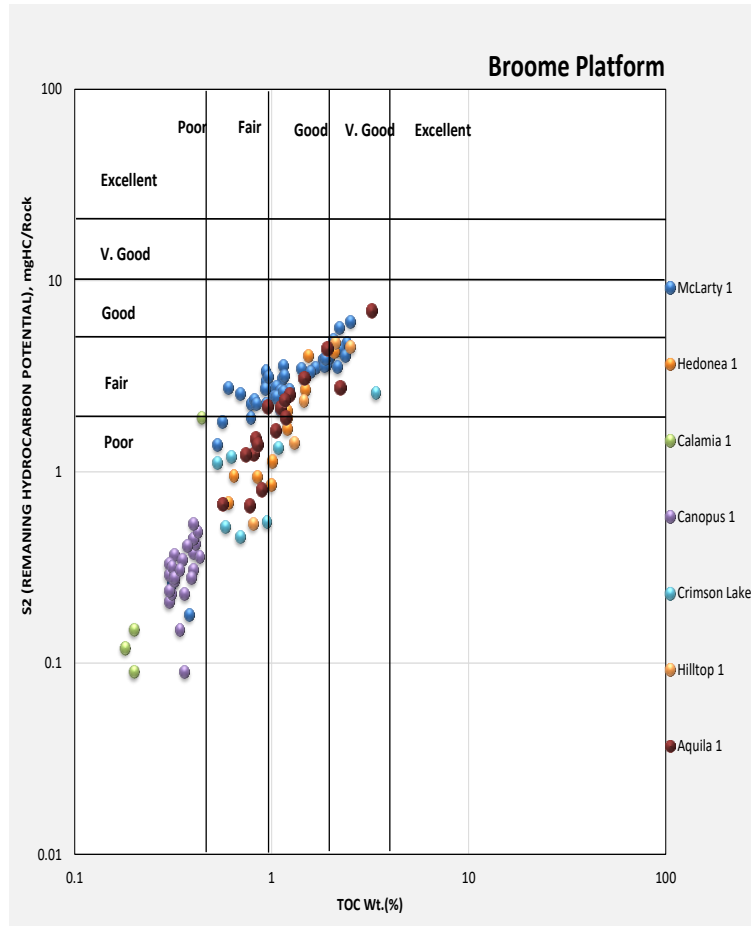
Figure 2.22 Log-log across plot of Rock-Eval Pyrolysis, S2 vs TOC, for the Goldwyer Shales in the Broome Platform.
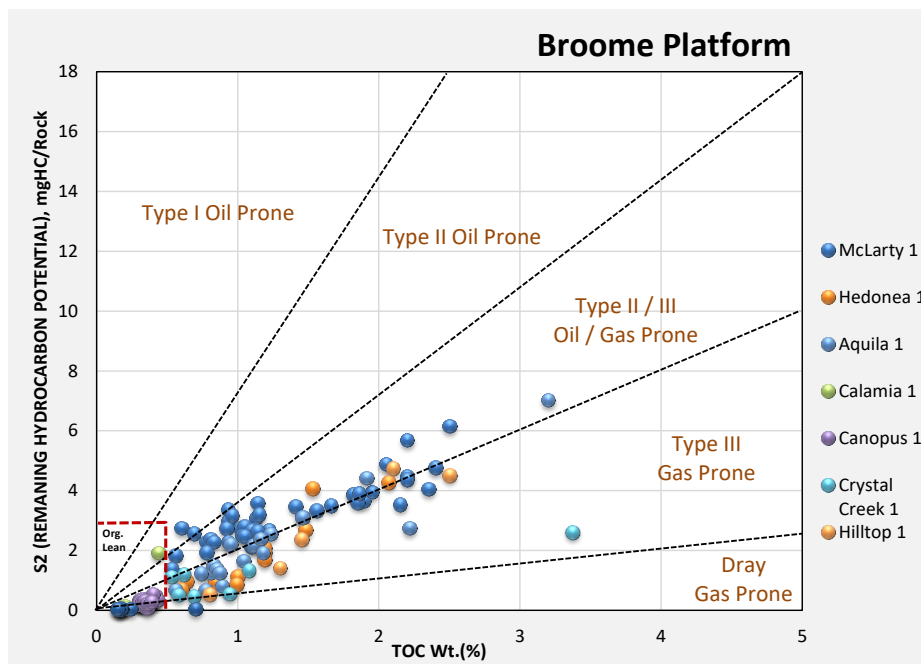
Figure 2.23 Linear cross plot of Rock-Eval Pyrolysis, S2 vs TOC, for the Goldwyer Shales in the Broome Platform.
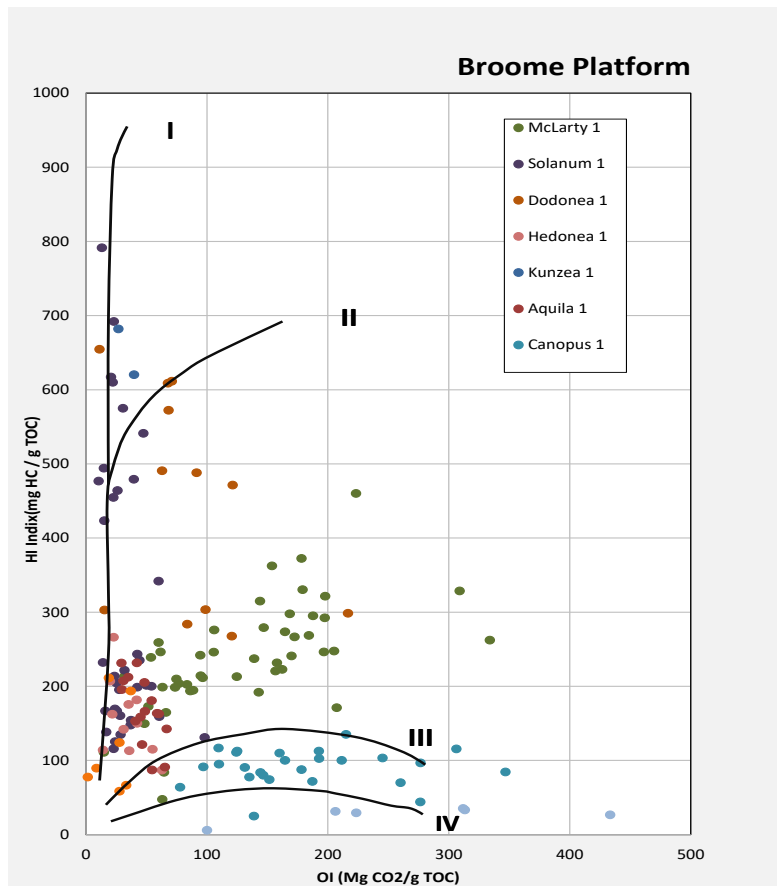
Figure 2.24 Pseudo Van-Krevelen plot of OI vs HI of the Goldwyer shales in the Broome Platform.
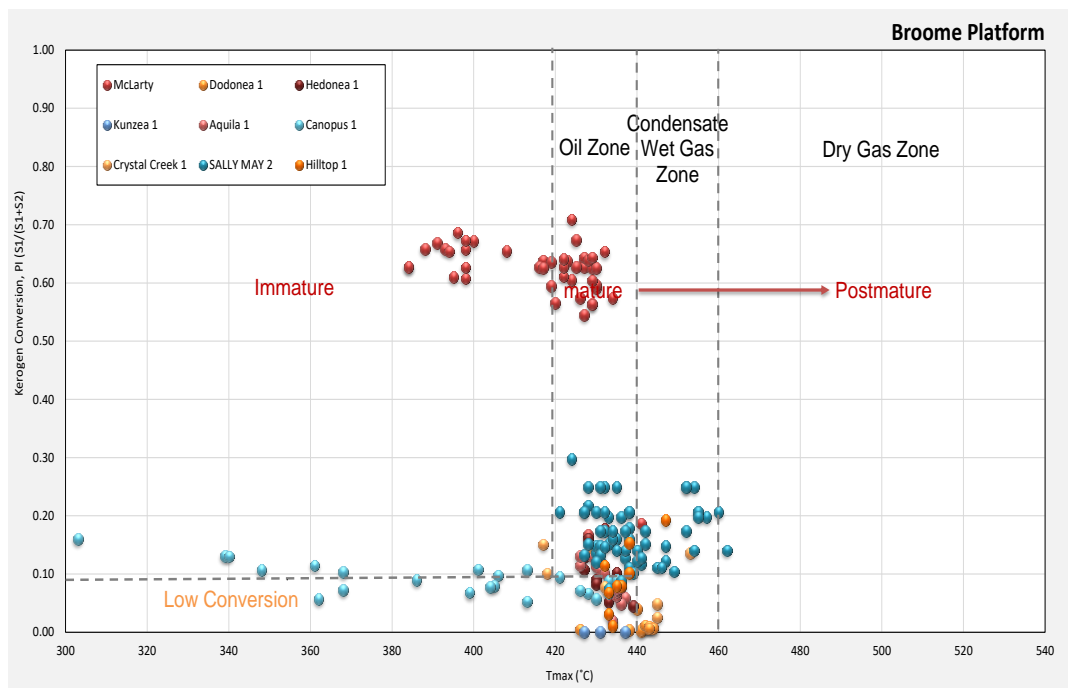
Figure 2.25 Linear cross plot of the Production Index (PI) vs Tmax for the Goldwyer Shales in the Broome Platform.
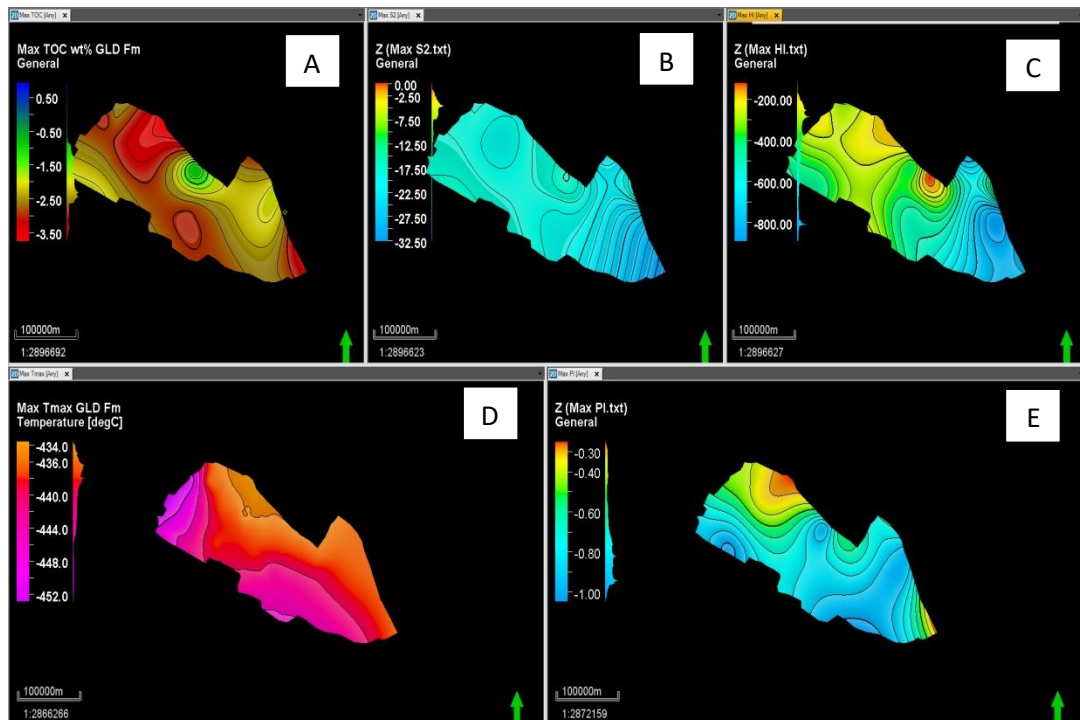
Figure 2.26 The 2D maps show a comparison of various geochemical properties of the Goldwyer shales in the Broome Platform using the petrel software. A: maximum TOC content in wt%, B: maximum S2 mg HC/g rock, C: maximum HI mg HC/g TOC, D: maximum Tmax °C and E: maximum PI in the Broome Platform.

2.3.2.2 Barbwire Terrace

In the Barbwire Terrace, the organic content of the Ordovician Goldwyer shale is generally between 0.6 and 2.2 wt% TOC in the studied wells, which is indicative of moderate to good organic richness (Figure 2.27). A higher organic content was noticed in the upper shale section of the formation in the Dodonea#1 well. The 2D map shows more rich-organic content in the northern part of the terrace as well. However, data availability is scarce in the southern parts due to the limited number of drilled wells (Figure 2.31A). The linear correlation of Rock-Eval Pyrolysis data in figure 2.28 depicted by S2 vs TOC depicts the dominant type II kerogen of the Goldwyer shale in the Barbwire Terrace. The Pseudo Van Krevelen plot in Figure 2.29 shows mainly Type II oil-prone kerogen with HI values over 100 mgHC/g TOC. The thermal maturity of the shales from the Tmax data is between 430 and 445^{0}C, corresponding to the early mature oil window. Here, most of the sampled shales are oil-prone to wet gas; however, about 20% of the samples are Type II/III oil and gas-prone kerogen (Figures 2.30 and 2.31D). With the average PI values of 0.5, the shales probably have low kerogen conversion potential in this sub-basin (Figures 2.30 and 2.31E).
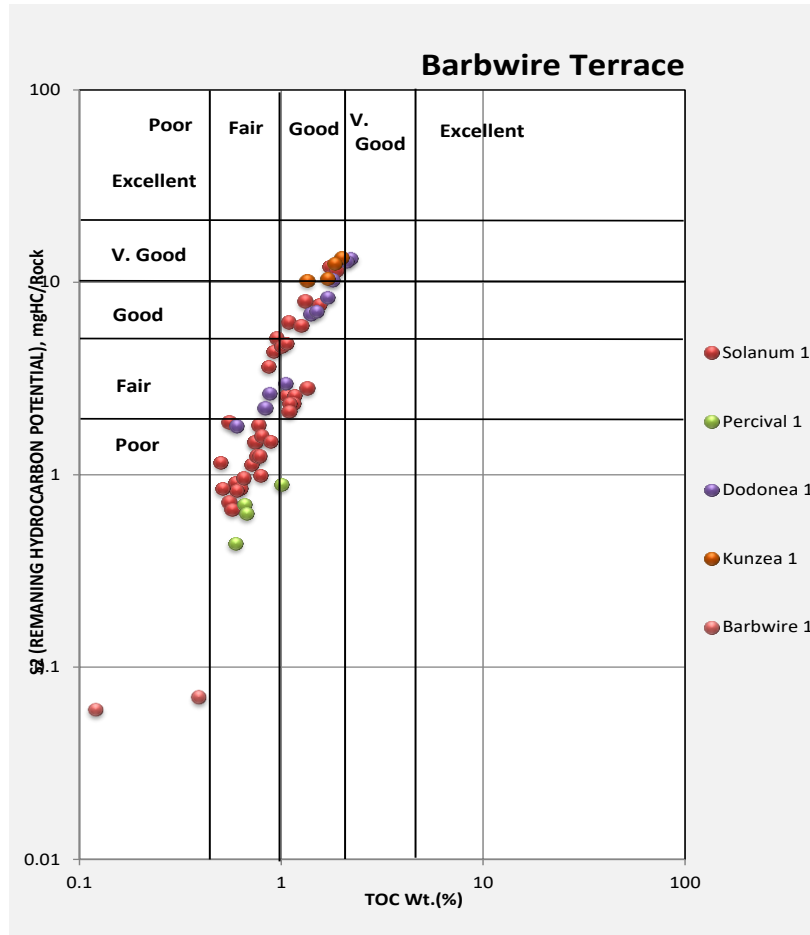
69

Figure 2.27 Log-log across plot of Rock-Eval Pyrolysis, S2 vs TOC, for the Goldwyer Shales in the Barbwire Terrace.
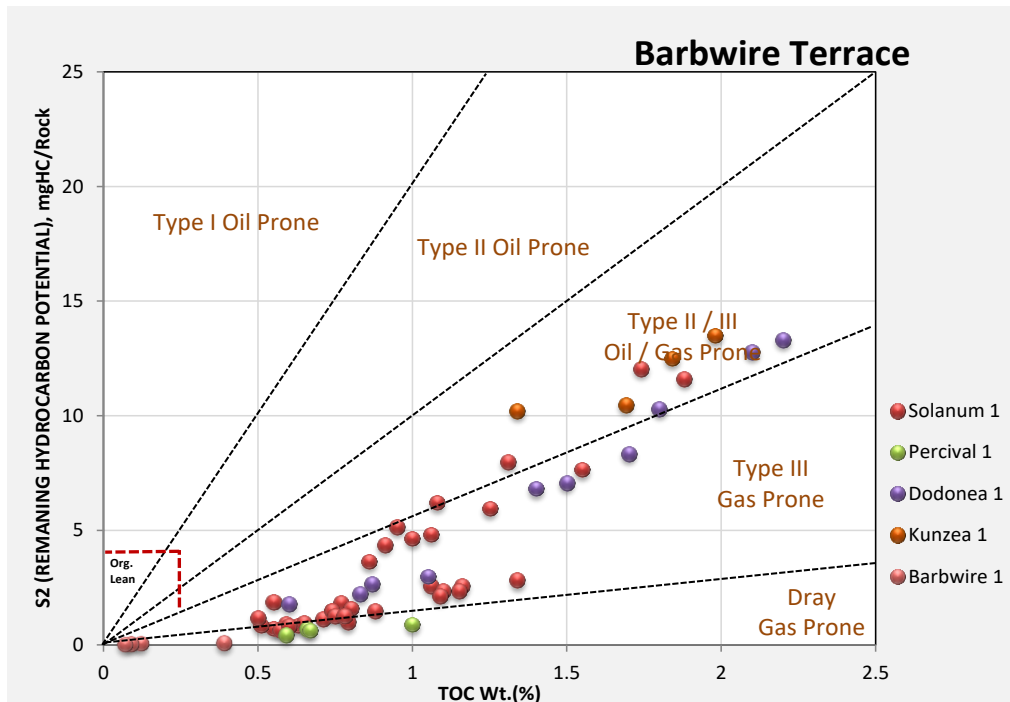
Figure 2.28 Linear cross plot of Rock-Eval Pyrolysis, S2 vs TOC, for the Goldwyer Shales in the Barbwire Terrace.

70
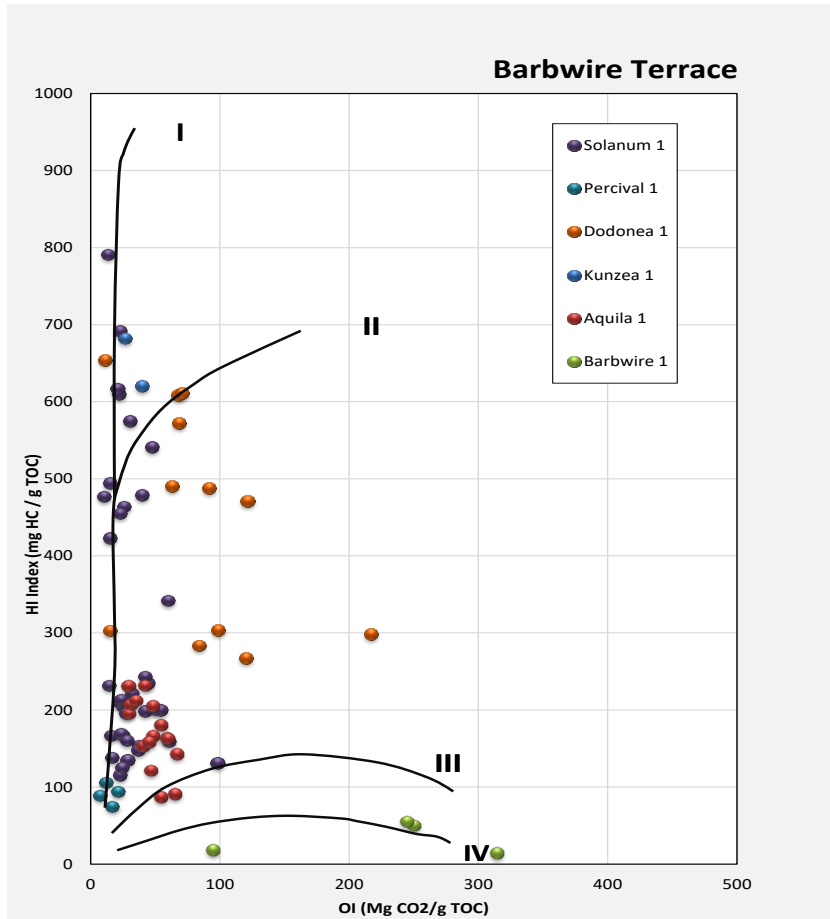
Figure 2.29 Pseudo Van-Krevelen plot of OI vs HI of the Goldwyer shales in the Barbwire Terrace.
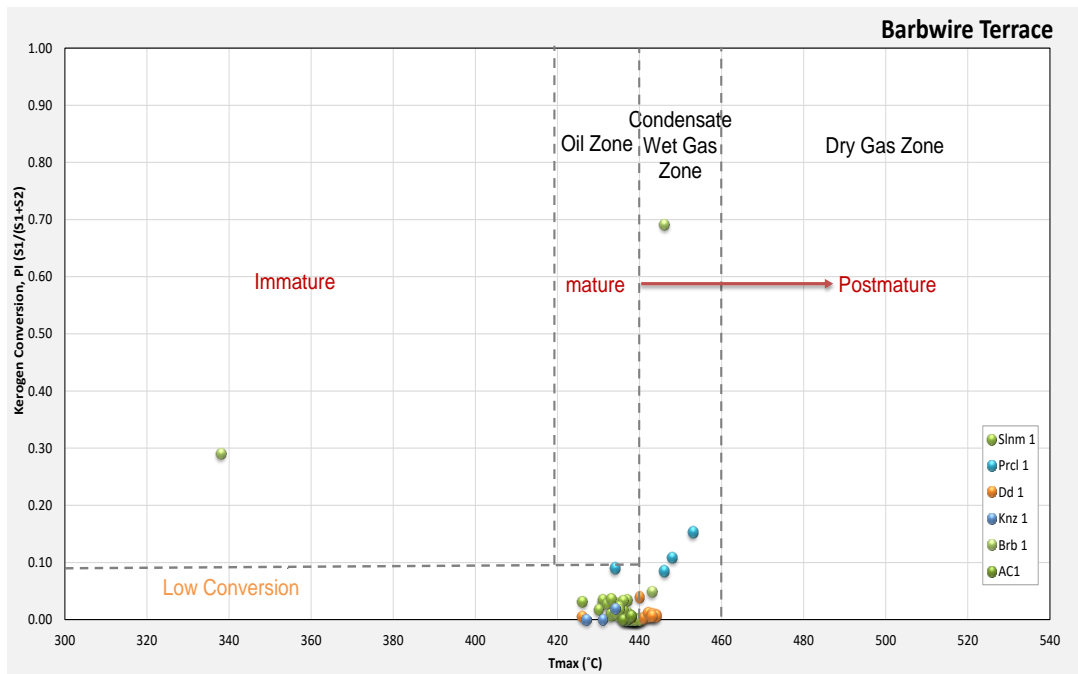
Figure 2.30 Linear cross Plot of the Production Index (PI) vs Tmax for the Goldwyer Shales in the Barbwire Terrace.

71
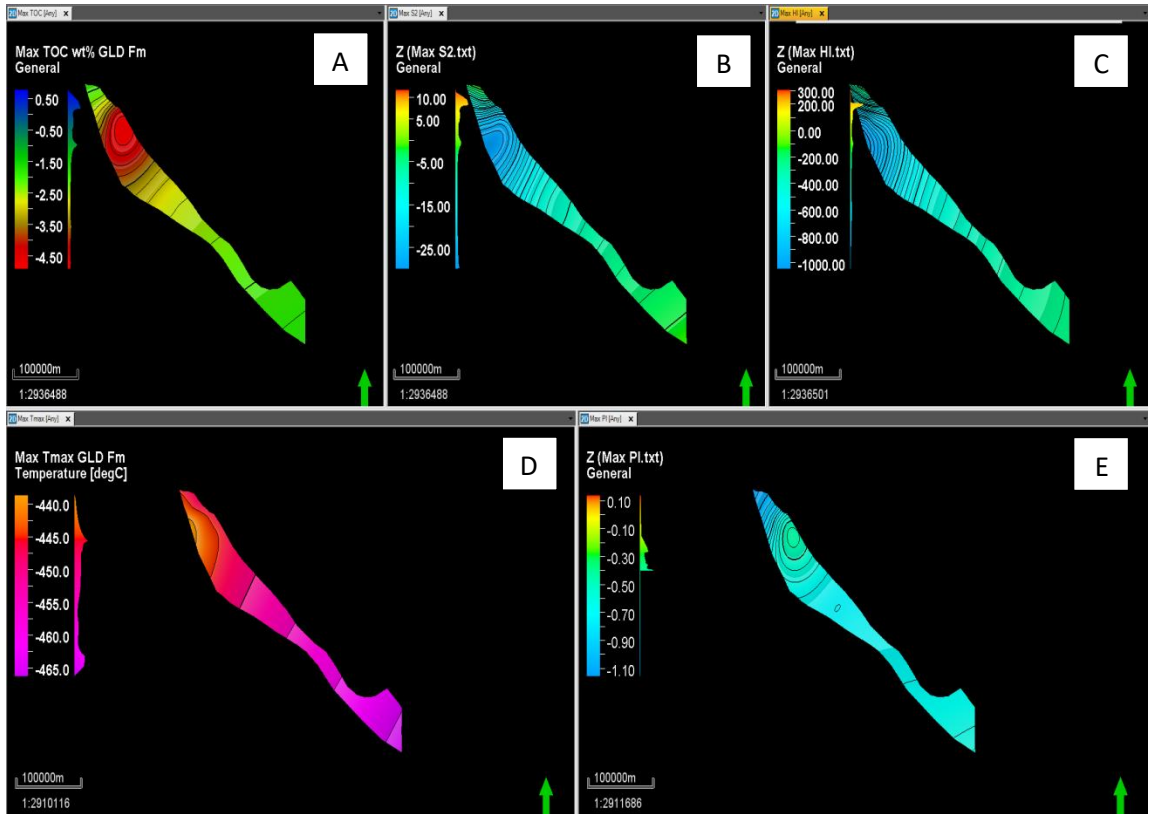
Figure 2.31 The 2D maps show a comparison of various geochemical properties of the Goldwyer shales in the Broome Platform using the petrel software. A: maximum TOC content in wt%, B: maximum S2 mg HC/g rock, C: maximum HI, D: maximum Tmax °C and E: maximum PI in the Barbwire Terrace.

3. Chapter 3: The Effect of Total Organic Carbon Content and Clay Types on Shales Gas Adsorption Potential

3.1 Introduction

Natural gases that consist primarily of methane are stored as free gas inside pore spaces, as well as adsorbed gas on the surface of organic matter and clay minerals in shales (Figure 3.1).
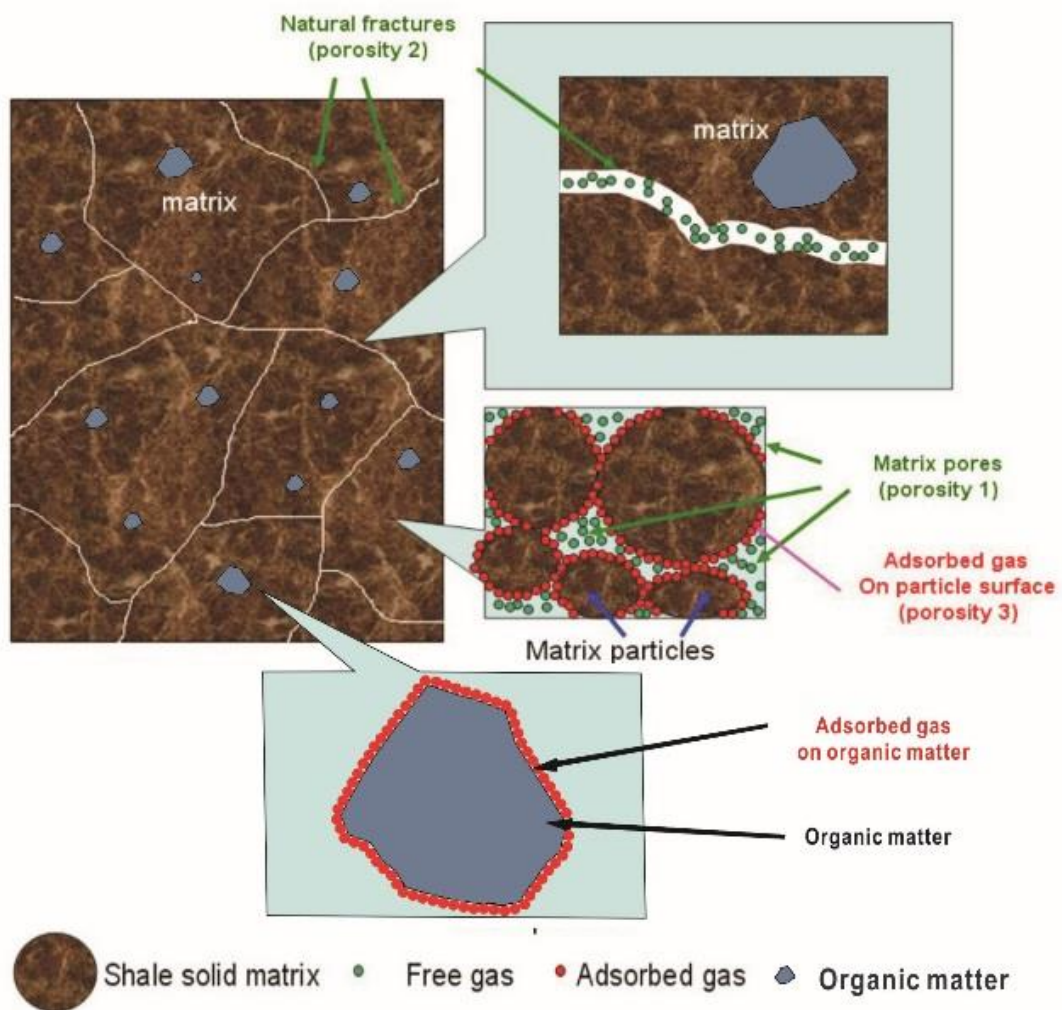
Figure 3.1 The adsorption mechanisms of shale gas (after, Song et al., 2011).

Adsorption is a physical bond of gas molecules onto the solid surface of the pore volume (Gregg and Sing 1995). The process of adsorption is divided into physical and chemical adsorption. Mostly, gases are stored by the process of physical adsorption. Table 3.1 compares physical and chemical sorptions. Natural gas can be adsorbed on the organic matter in shales and in some cases on particular clay

minerals (Das 2012). The forces of the intermolecular attraction between the clay particles and natural gas are the results of van der Waals adsorption or physical adsorption. Das (2012) further claimed that the gas will condense on the surface of the solid when the intermolecular attractive forces between the natural gas and clay atoms are greater than those between the gas molecules themselves, which is what happens between the shale and natural gas. If the partial pressure of the adsorbed gas is equivalent to the contacting gas phase, the adsorbed gas will stay attached on the surface of the solid. Significant amounts of gas are stored in the sorbed state in shale rocks and are self-sourced. However, other studies claimed that the gas might also be migrated from other sources (Bustin 2005; Bustin et al. 2008). Differences in fluid flow, adsorption capacity and the mechanical properties of fine-grained shales will markedly rely on lithology, which is directly related to the sedimentary environment and diagenetic alteration.

Table 3.1 A comparison of physical and chemical sorptions (Ruthven 1984).

Physical Adsorption	Chemical Adsorption
Involves in Van Der Waals forces (Dispersion-Repulsion)	Force of attraction are Chemical Bond forces
Reversible process. Decrease of pressure causes desorption mechanism.	Irreversible process. Decrease of pressure does not cause desorption
Occurs at low temperature and decreases with increasing temperature	Occurs at high temperature
Multi-molecular or mono-molecular layers	Mono-molecular layers only
It does not require any activation energy, rapid process	It requires high activation energy, slow process

More specifically, the potential of sorbed gas of the shale depends on the pressure, temperature, sorption affinity and surface area of the material presented. Also, it is highly dependent on the microporous kerogen quantity, quality and type (Ramos 2004); (Chalmers and Bustin 2007a).

Lu et al. (1995a) and Schettler and Parmoly (1990) claimed that for organic shales, illite is a potential driver of high gas adsorption rather than the TOC content. However, many others claimed a linear relationship between the gas storage capacity and TOC content (Lu et al. 1995a; Manger et al. 1991; Ramos 2004).

Experimentally, calculating the free space during gas adsorption measurement involves expanding a known amount of helium (contained within reference cell) into an unknown sample volume. Continually, the non-adsorptive nature of helium and its smaller molecular size (in comparison to methane and other gases) enhances its use in measuring free-void volumes during adsorption experiments. However, correction is needed if other types of gases are used due to the resultant miscalculation of total adsorbed volume, especially for low organic content samples. Moreover, the molecular size of the adsorbate also controls the transmission of gases within the pore throats of the adsorbent. Cui et al. (2004) pointed out that carbon dioxide diffusion throughout the micro-pores is higher than that of nitrogen and methane because of the larger kinetic parameters of those gases mentioned. Additionally, in silt-like porous materials (such as coal), access to the pores is a function of both the pore diameter and its geometry.

The maximum gas potential of shale plays is determined by integrating the free (total porosity) and sorbed gas capacity in the reservoir. Total porosity and pore size distribution are the functions of lithology. Additionally, increased porosity from aluminosilication (from clays) still plays an essential role (Ross and Bustin 2007). Consequently, clay content is another contributor to the total porosity of mud-rocks. Schettler Jr and Parmely (1991) proposed that clay minerals play an important role in their study of methane adsorption capacity on low TOC shale samples from the Appalachian basin. Similarly, Lu et al. (1995b) measured the adsorption capacity of several Devonian shale samples and pure illite. They concluded that while TOC played the first role in the adsorption capacity of their samples, clay minerals were also responsible for significant gas storage, particularly for those of low TOC content. Moreover, a comparison of adsorbed gas potential for clay and quartz grains in the Devonian shale was also conducted. The average composition of the Devonian shale is 33% quartz, 47% illite and 3% chlorite, with the remaining 17% being other minerals such as pyrite and albite (Schettler Jr and Parmely 1991). On the other hand, a negative correlation was found between the total porosity and carbonate content of fine-grained reservoirs. Ross and Bustin (2007) claimed that the inability of Mercury (Hg) to enter the micropores, due to the carbonate richness of the Gordondale member samples, might have resulted from pore cementation caused by the early precipitation of calcite cement. They further stated that pore reduction may also be caused by the compaction during the thermal maturity of the shale. In

addition, another comparison between different shales revealed that higher clay content causes higher porosity and permeability. On the other hand, increased biogenic silica and carbonate content results in lower porosity and permeability (Bustin et al. 2008). Also, a higher amount of detrital quartz leads to higher porosity and permeability. Furthermore, Lu et al. (1995a) argued that Devonian shale gas has significant sorption capacity due to high internal surface area of the clay minerals. However, carbonate (mainly calcite) and quartz represent the lowest internal surface areas that produce lower sorption capacity (Venaruzzo et al. 2002; Volzone et al. 2002). Moreover, micro-porosity, of 1 to 2 nm radius in mudrocks and shales might also be associated with the kaolinite, illite and montmorillonite clay minerals. For illite and kaolinite, it is mainly attributed to the size of the crystals, whereas for montmorillonite, it is highly dependent on the cation exchange concentration (Aringhieri 2004; Aylmore and Quirk 1967). Ross (2004) highlighted the different moisture capacities of different clay minerals. Mineral-rich coals show higher moisture capacity than organic-rich coals (McCutcheon and Barton 1999). McCutcheon and Barton (1999) also suggested that montmorillonite-rich coal has almost double the moisture capacity than the kaolinite-rich.

Remarkably, organic content enhances adsorption energy due to meso and/or micro-pores formation in coals and organic-rich rocks (Ross and Bustin 2007). Lean organic shales have very low sorption capacity; especially at high reservoir temperature, which brings out limitations to the sorption experiments. Chareonsuppanimit et al. (2012) claimed that the adsorption capacity of shales is much lower than those for coals, which can be related to the lower organic content of shale. Additionally, an error in the calculated adsorption isotherm of the mud-rocks usually comes from low TOC content and moisture effect. This would cause a miscalculation of free space due to the larger access of smaller helium molecules (larger free void volume) as compared to methane (adsorbed volume). The intensity of the error is preliminarily controlled by the pore-size range and distribution. Organic-rich or clay samples would overcome the error because of the high adsorption capacity. Indeed, inaccurate calculations of sorption capacity will cause significant miscalculations of total gas in place of shale gas plays (Ross and Bustin 2007). For such reasons, it is important to analyze the organic matter and clay type effect on the gas adsorption capacity of the fine-grained rocks.

Thermal maturity has a significant effect on the adsorption capacity of shale rocks. Ramos (2004) reported 66 scf/ton sorption capacity from Type I and II kerogens. However, he reversibly concluded that Type III kerogen showed only up to 25 scf/ton sorption capacity. Comparably, poor correlations were found between the organic content and sorption capacity due to some mineralogical differences. Moreover, moisture content decreases with increased thermal maturity, which causes microspores increase and increased sorption capacity of the samples with higher thermal maturity (Ramos 2004). Supportively, Bustin and Clarkson (1998) proved an increase of methane adsorption by increased thermal maturity. However, Ross and Bustin (2007) suggested that there is no direct relationship between the sorption capacity and thermal maturity, represented by Tmax°C of their examined samples under similar moisture and TOC conditions. On the other hand, they stated that the higher sorption capacity of the samples with high thermal maturity is likely related to the organic matter's structural transformation. In addition, organic matter pore surface heterogeneity accompanied with an increase of thermal maturity is caused by the increased aromatic of high-rank coal, this will allow for the coverage of gas molecules on more internal surfaces (Laxminarayana and Crosdale 1999).

Bustin et al. (2008) claimed that in some shale gas adsorption experiments, an overestimation of void volume might occur. On the other hand, an underestimation of adsorbed methane and/or other gases due to the pore system structure may cause the shale matrix to work as a molecular sieve. Therefore, negative sorption is created due to the free space exceeding the absorptive capacity. A proposed solution for this is milling the sample into a very fine powder till very low or no porosity is presented, so only grains are available for all gases. A major disadvantage of this is creating an extra artificial surface area (equivalent to almost 2.0% organic matter when the sample is milled to about 4 um) that depends on the particle size and organic content. Bustin et al. (2008) also proved that during fine-grained shale adsorption analysis, if the shale sample is crushed to a very fine grain size, helium and/or other gases if used, will have access to almost all possible pores minimizing the calculation errors. However, unlike the smaller kinetic diameter (0.26 nm) of helium, methane has a relatively larger kinetic diameter (0.38 nm) that would obstruct the access to smaller pores during conventional adsorption analysis. Another reason to use the crushed sample is to overcome the effect of compressibility caused by pressure. Theoretically, it is difficult to calculate porosity from an extremely low

gas flow rate through the shale grains. Thus, compressibility correction is needed if the plug sample is used to bring the results to reservoir conditions.

The procedures for determining adsorption are normally divided into the category of either mass-based or volumetric-based methods. Mass-based methods occupy the use of a microbalance to directly measure the change in the sample mass associated with adsorption. The advantage of mass-based approaches is its high accuracy. However, given the heterogeneity of the rocks, the oil and gas industry has preferred the volumetric method because it allows for the use of larger sample volumes as mass-based methods. Having said that, most experiments use an extremely small sample which will ignore the heterogeneity of the rocks (Heller and Zoback 2014). Moreover, desorption can be achieved by lowering the pressure of the gas phase or by increasing the temperature of the adsorbed gas (Das 2012). Chemical adsorption can be neglected in the gas adsorption mechanism because the adhesive force between the gas and adsorbed gas are normally much higher than that which is studied in physical adsorption. The chemically adsorbed gas is not possible to be produced. This is because, during the desorption process, the original substance goes through a chemical change (Das 2012).

The aim of this section is to further assess gas adsorption potential for different clay types and for samples with varying TOC content. Therefore, the adsorption potential of pure clay minerals (such as illite, kaolinite and montmorillonite), samples with different amount of TOC and real shale samples were examined.

3.2 Methodology

The high-pressure adsorption measurement was performed using a High-Pressure Volumetric Analyser (HPVA100) instrument. The results of the experiments are sorption isotherms, which represent the volume of adsorbed and desorbed methane at pre-selected pressure intervals. Subsequently, the volumetric isotherms, which fit best with the Langmuir Model isotherm, are constructed to define the maximum adsorption capacity of the studied samples.

3.2.1 Samples description

A total of sixteen different samples were used in this study (Table 3.2). Samples 1 to 4 are real shale samples collected from the Laurel Formation in the Canning Basin. Samples 5 to 9 are synthetic samples that are made from different pure clay minerals. Sample 10 is a mixture of 50% TOC and 50% montmorillonite. Finally, the last six

samples (Samples 11 to 16) are made from different organic (TOC) and clay contents. Table 3.2 illustrates the names and detailed compositions of each sample. For the first four real shale samples, Rock-eval and XRD experiments were performed to get the composition and TOC content.

Table 3.2 Shale, clay and organic-rich samples details.

Sample	Composition
1	40%Quartz, 14%Carbonate and 46%Clay
2	23%Quartz, 39%Carbonate and 38%Clay
3	48%Quartz, 16%Carbonate and 36%Clay
4	65%Quartz, 02%Carbonate and 33%Clay
5	Illite
6	Montmorillonite
7	Na-rich Montmorillonite
8	Kaolinite
9	Organic rich sample compsed of mixture of vitrinite (71%) and semi-fusinite (13%) as well as some other minor components
10	Organic content TOC (%50) and Montmorillonite (%50)
11	(00%) Organic content & (100%) Clay
12	(10%) Organic content & (90%) Clay
13	(20%) Organic content & (80%) Clay
14	(50%) Organic content & (50%) Clay
15	(80%) Organic content & (20%) Clay
16	(100%) Organic content & (00%) Clay

3.2.2   Experiment Setup

High-pressure methane sorption isotherms were collected using the HPVA100 analyser that was designed by a particulate system (the schematic diagram of the HPVA100 instrument can be seen in Figure 3.2) and employing the static volumetric method. This method involves applying a known amount of gas (adsorbent) into the sample cell to be examined. When the sample reaches an equilibrium state with the adsorbent, the final equilibrium pressure is recorded. These data are then used to measure the amount of gas adsorbed by the sample. This process is repeated at given pressure intervals until the maximum pre-selected pressure is achieved. It is worth mentioning that all the experiments were run at a constant temperature of 30°C and pressure increments started from 145 to 870 psi. All the results of the adsorbed gas

volume and equilibrium pressure were then plotted using the Langmuir isotherm equation to find out the maximum adsorbed gas (Langmuir volume, V_L).

The HPVA system consists of a gauge and vacuum pump, a reference cell maintained at constant temperature (generally 30°C) with 2 pressure transducers, a sample compartment surrounded by a thermostat bath and a degassing compartment that is surrounded by a furnace with controllers to adjust the degassing temperature, as well as a temperature control vessel connected to a very constant thermo-bath and a sample holder with a manual isolator.
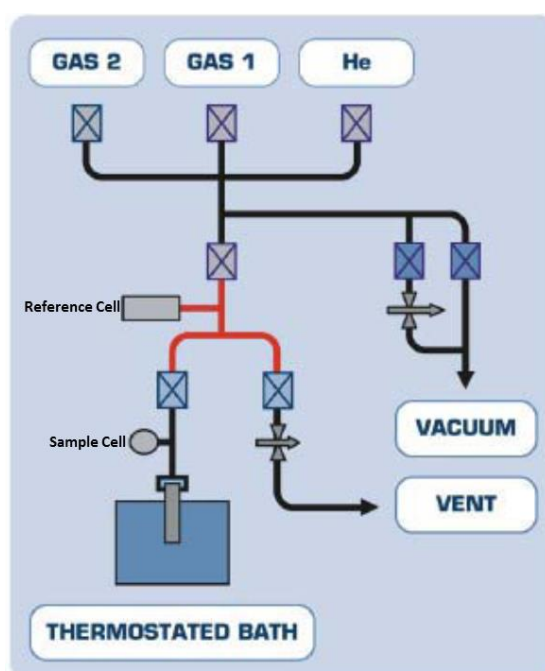
Figure 3.2 Schematic diagram of the HPVA analyser (2011).

3.2.2.1 Preparing the sample

The sample holder was first rinsed and washed thoroughly using tap water and the Alconox detergent. It was then dried using compressed air and methanol. Afterwards, the sample was left in a preheated oven on 110 °C for 2 hours. The holder was next filled with approximately 3 grams of the sample powder. A very accurate balance was used to obtain the optimum weight measurement. After the sample was prepared, the sample holder containing the absorbent was connected to the degassing port and left on 80°C furnace temperature, till the gauge read 0.00. This will ensure the evacuation of the absorbent and the removal of any moisture or contaminants prior to carrying out the experiment. The sample cell (with remaining closed isolator) is then attached to the analysis port.

The purging of the system is done by injecting and releasing the helium into a closed manifold system, until a full vacuum is reached. This step is repeated 3 times to ensure an accurate achievement.

3.2.2.3 Running the experiment

The experiment is a fully automatically run system. The run is first started by calculating the free void inside the sample and the sample cell by applying Boyle's law on a totally free-connected manifold and absorbent. Based on the above-mentioned mechanism, the calculated free space is then used to calculate the amount of sorbet gas in the sample. During isotherm analysis, 6 pressure points are collected at 10 bars increment up to a maximum of 60 bars. Desorption isotherms are also collected for most of the studied samples at the same criteria.

At every pressure increment, methane gas is first injected into the reference cell, then kept on hold until the determined equilibrium pressure, based on preselected equilibrium criteria of 0.01 bars per 1 minute, is reached. The system then allows the methane to freely flow into the sample cell. This is kept on hold for 10 minutes or till an equilibrium is reached. The system will record the pressures, temperatures and volumes of gas inside the reference and sample cells before and after each step for every pressure increment.

The total amount of gas injected into the sample cell is then calculated. Also, the total volume of gas residing in the void volume is measured. The total amount of gas injected to the sample cell minus the volume of gas residing in the void volume will be the volume of gas adsorbed by the sample.

3.2.3 Methane Adsorption Measurement Using Langmuir Theory

The high-pressure volumetric method is used in order to estimate the amount of adsorbed gas for the samples studied. Adsorption occurs when an adsorbent (gas) comes in contact with the adsorbate (sample). When the adsorbent and adsorbate reach an equilibrium state, which is called "the adsorption equilibrium", the data is represented by isotherms. An isotherm is commonly used to present adsorption equilibrium. At a constant temperature, a plot of adsorption capacity versus adsorption equilibrium pressure represents adsorption (Do 1998). There are 5 types of isotherms that could possibly be produced from the adsorption experiment.

Generally, the methane adsorption isotherm fits the Langmuir model (Ross and Bustin 2009). The maximum adsorption capacity will be mostly calculated using the Langmuir equation. Additionally, specific surface areas of the micro-pore of materials also affect the methane adsorption capacity, and this is calculated using low-pressure nitrogen adsorption based on the Brunauer-Emmet-Teller (BET) Theory (Diamond and Kinter 1958). A sample with a high specific surface area (S_{BET}) hypothetically has a higher adsorption capacity due to the existence of greater space for the adsorbed gas to be adsorbed into the micro-pore of the samples.

The Langmuir Isotherm (Type I) is a simplified isotherm for monolayer gas adsorption. Lu et al. (1995b) introduced that the Langmuir Isotherm has 3 basic assumptions:

- Gases are adsorbed at a certain number of localised sites and each site adsorbs one molecule;

- All adsorption sites are homogeneously adsorbent (energetically equivalent);

- There are no intermolecular forces between the gas molecules on adjacent sites.

The Langmuir Isotherm model explains adsorption as the condensation of gas molecules on a solid surface. Afterwards, desorption is claimed to be the evaporation of gas molecules (Matott and Rabideau 2008). Matott and Rabideau (2008) also clarified that the solid surface involves a specific number of adsorption sites (S_{BET} =S), sites occupied by the molecules (Sa) and free sites (Sf). Thus, considering the relation of condensation to the gas pressure (P) at the equilibrium state:

$$k_a S_a = k_f P S_f = k_f P(S - S_a) \quad Eq.\,3.1$$

Where ka is the equilibrium constant at adsorption, kf is the equilibrium constant at desorption.

The fraction of molecules that occupies the surface to the number of adsorption sites:

$$\Phi = \frac{S_a}{S} = \frac{bP}{1 + bP}, \quad Eq.\,3.2, \quad where\ b = \frac{k_f}{k_a}$$

In the monolayer adsorption model, the adsorbed amount of gas (n) in mol/g is directly proportional to the porosity. Hence, the equation of the Langmuir monolayer model can be written as (Siemons and Busch 2007):

$$n = \frac{n_L P}{P + P_L} \quad Eq.\,3.3$$

Where n_L is defined as the maximum adsorption amount and P_L is the Langmuir pressure in which half of the Langmuir volume gas can be adsorbed. According to the monolayer model, the amount of adsorption is directly proportional to the low gas pressure. At high-pressures, the maximum adsorbed amount will be acquired. Song et al. (2011) defined the expression of the Langmuir model to be based on the adsorption volume:

$$V = \frac{V_L P}{P_L + P} \quad Eq.\,3.4$$

Where V_L is defined as the maximum adsorption gas volume in scf/ton and V is the adsorbed volume by a rock (Figure 3.3).
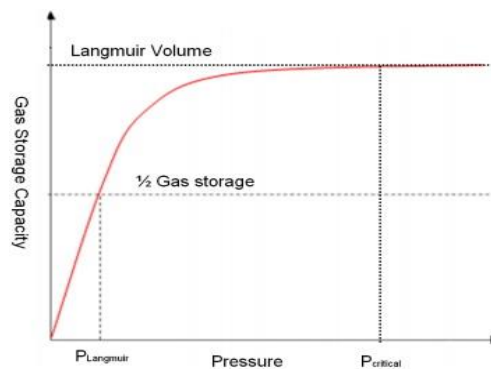
Figure 3.3 The Langmuir Isotherm model (Gregg et al. 1967).

The absorbed gas can be found using the Gibbs excess approach (Gibbs 1957):

$$n_{sorbed} = n_{total} - c_{gas} V_{void} \quad Eq.\,3.5$$

Another way to present the amount of adsorbed gas with the Gibbs excess approach is as follow:

$$n_{sorbed} = n_{total} - n_{unads} \qquad Eq.\,3.6$$

Where n_{total} is the total volume of gas in the system and n_{unads} is the amount of free gas in the sample. $c_{gas}V_{void}$ is the void volume occupied by the gas calculated from the molar concentration in the gas phase. The c_{gas} depends on the appropriate equation of state (EOS) of the gas at a different pressure and temperature condition (Berberan-Santos et al. 2008). The void volume involves the free space and porosity within the sample without any adsorbates (Dąbrowski 2001). To determine the void volume, V_{void}, the helium pycnometry method is applied.

The example of the isotherm generated can be seen in Figure 3.4. The HPVA instrument is expected to produce such an isotherm which can be fitted with the Langmuir Isotherm theory. Therefore, the calculation of maximum adsorption capacity can be carried out from the Langmuir equation (Eq. 3.4).
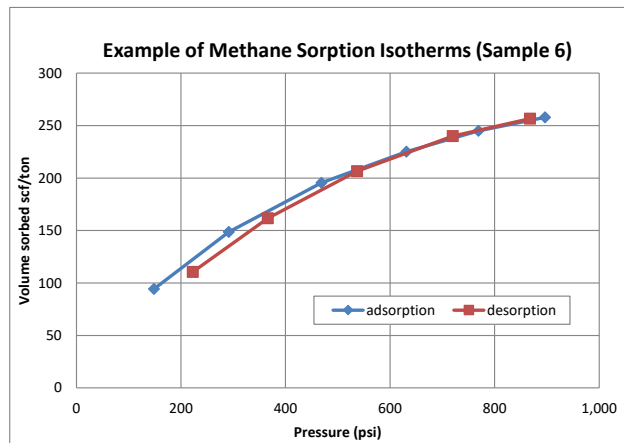
Figure 3.4 Methane adsorption Isotherm example.

The V_L (Langmuir volume) represents the maximum amount of methane that can be adsorbed by the adsorbate. It is believed that the higher the V_L, the better the sample adsorption potential. The Langmuir volume can be calculated from the P/V_{ads} vs. Pressure curve, which can be plotted using the V_{ads} vs. Pressure graph. The linear equation can be achieved from the P/V_{ads} vs. Pressure graph, as seen in Figure 3.5. By re-arranging the Langmuir Equation into P/V_{ads} (Clarkson and Bustin 1999), the relation between the linear equation of the graph with the Langmuir equation can be found. As such, it can be used to determine the V_L and P_L of each sample. The re-arranged Langmuir equation can be expressed as follows:

$$\frac{P}{V_{ads}} = \frac{1}{V_L} P + \frac{V_L}{P_L} \qquad Eq.\,3.7$$

For this example, the linear equation of P/V_{ads} vs. Pressure graph is $y = 0.0022x + 1.1014$. Therefore, $1/V_L$ equals to the slope and can be calculated as follows:

$$\frac{1}{V_L} = 0.0025 \ \rightarrow \ V_L = (0.0025)^{-1}$$

$$V_L = 400 \ \text{Scf/ton}$$

The last part of the equation represents the intercept $\frac{P_L}{V_L}$.

Thus, P_L can be calculated as follows:

$$\frac{P_L}{V_L} = 1.21 \ \rightarrow \ P_L = 400 * 1.21$$

$$P_L = 484 \ psi$$

This can be translated as the pressure at which one-half of the Langmuir volume is absorbed.
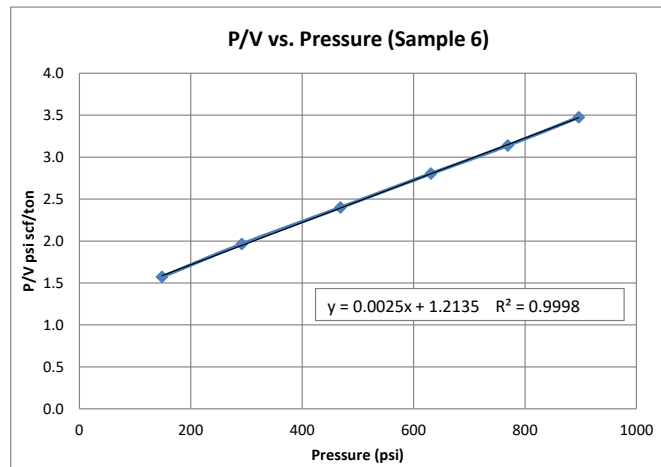
Figure 3.5 Langmuir Theory p/v vs. Pressure example.

3.3 Experimental Results

3.3.1   Canning Basin Shale Samples

Methane sorption experiments were conducted on about 4 grams of four different shale samples from the Laurel Formation in the Canning Basin. All shale samples were grounded to powder, and X-ray diffraction and Rock-Eval results were also acquired for each of the samples. The adsorption isotherms of Samples 1, 2, 3 and 4 were successfully fitted on the Langmuir Isotherm, as seen in Figure 3.6. Sample 1 represents the Blina#1 well, Sample 2 the Curringa#1, Sample 3 the Yullero#1 and Sample 4 the Yarrada#1well. The calculated Langmuir volume (V_L) of Sample 1 was 188.7 scf/ton, TOC was 0.4 wt.% and the total clay amount was 46%. Sample 2

showed a less V_L of 128.2 scf/ton, higher TOC content of 2.89 wt.% and 38% of total clay. Similar to Sample 1, Sample 3 showed a high V_L value of 188.7 scf/ton. However, the TOC was much higher at 3.23 wt.% and the total clay amount was only 36%.
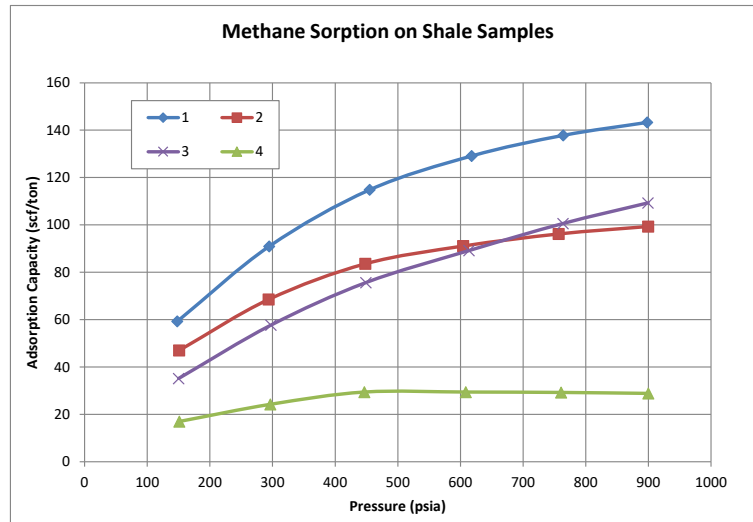
Figure 3.6 Methane Adsorption Isotherms of different shale samples.

Finally, Sample 4 represented the lowest V_L value of 33.4 scf/ton, TOC was 0.57 wt.% and the total clay was 33%. The average Tmax of Samples 1, 2 and 4 was 430°C. However, Sample 3 showed a much higher Tmax value of 450°C, indicating a higher level of thermal maturity. Table 3.3 provides the overall data regarding the adsorption potential, rock eval and mineralogy of the shale samples.

Table 3.3 Shale samples adsorption, Rock-eval and XRD results.

SAMPLE	WEIGHT (GM)	V_L (SCF/TON)	P_L (PSI)	TMAX (°C)	TOC (WT.%)	QUARTZ %	CARBONATES %	TOTAL CLAYS %
1	3.9	188.7	303.6	430	0.41	40	14	46
2	3.7	128.2	252.8	430	2.89	23	39	38
3	4.5	188.7	669.7	450	3.23	48	16	36
4	4.3	33.4	109.7	432	0.57	65	03	33

3.3.2 Organic-rich and Clay Samples

All the samples were run using about 3 grams or more. The weights of all the samples were varied based on the availability. Continually, the weights of the clay samples 5, 6, 7 and 8 were 3.5, 2.9, 3.6 and 3.0 grams respectively. The organic-rich sample (Sample 9) was also run using 3 grams of the sample. On the other hand, Sample 10 was first run using only 1.8 grams, but was then repeated using 3.9 grams of the sample (Sample 10A) (Table 3.4).
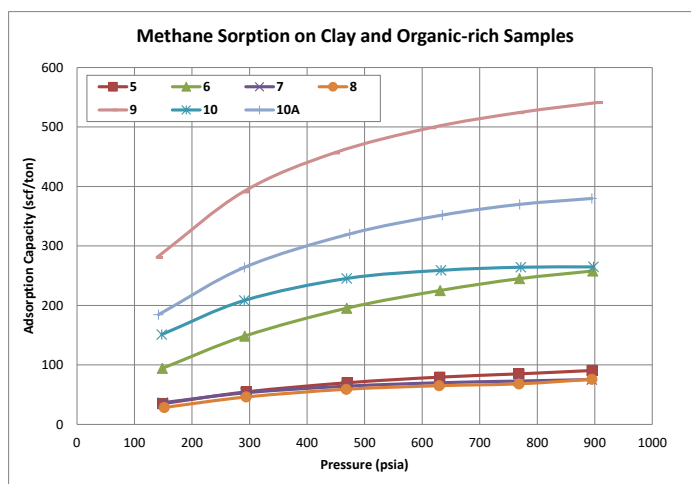
Figure 3.7 Methane sorption of clay and coal samples.

In Figure 3.7, the organic-rich, Sample 9, showed the highest adsorption isotherm compared to the other clay samples, with a calculated Langmuir volume V_L of 666.7 scf/ton. Table 3.4 provides the overall data regarding the adsorption potential of the organic-rich and clay samples.

Table 3.4 Coal and clay samples' results.

Sample	Weight (gm)	V_L (scf/ton)	P_L (psi)
5	3.5	131.6	414.5
6	2.9	400.0	485.4
7	3.6	95.2	233.7
8	3.0	108.7	28.7
9	3.0	666.7	2293.3
10	1.8	312.5	144.2
10A	3.9	476.2	230.0

The adsorption volumes of Samples 5, 7 and 8 are the lowest amongst the clay and organic-rich samples. The calculated Langmuir volume V_L of those samples are relatively low, namely 131.6, 95.2 and 108.7 scf/ton respectively. However, unlike the other clay samples, Sample 6 has a higher adsorption potential with V_L =400 scf/ton. This was expected as the Montmorillonite type of clay has a larger surface area than illite, which resulted in higher adsorption sites available for methane to occupy. Furthermore, Sample 10 was made in the lab from the organic content and Montmorillonite mixture (by mixing 50% of Samples 6 and 9 using 1 gram each). This was done to study the relation between Samples 6 and 9 as they both have high

87

Langmuir volumes compared to the others, and also to see the effect of the organic content on the adsorption potential of clay minerals. Usually, higher organic content or kerogen samples have higher adsorption capacity than non-organic samples. However, the calculated V_L of Sample 10 was only 312.5 scf/ton, which is less than Sample 9. Theoretically, an increased organic content of the clay sample should lead to a higher adsorption potential of the sample. However, this is not the case here with the addition of Sample 9 to 6. Therefore, Sample 10A was created using a higher amount of the sample at the same percent, but double the weight (mixing of 50% using 2 grams each). The results were as expected, as the isotherm and Langmuir volume were almost at the middle for the equally mixed samples. The calculated Langmuir volume V_L of Sample 10A is 476.2 scf/ton. The experiments were successful as all the isotherms can be fitted on the Langmuir Isotherm.

3.3.3 The effect of organic content (TOC) on Clay samples methane sorption

The measurement of the sorption capacity of the clay samples with different TOC compositions was conducted with a constant sample weight set to 3 grams. Six synthetic samples (11 to 16) were made up of Kaolinite clay and the TOC content mixture was increased from 0.00 to 100%. Table 3.5 illustrates the weight in grams and percentages of TOC and clay in each of the mixtures. It also shows the Langmuir volume and pressure for every sample.

Table 3.5 Clay with different TOC composition results.

Sample	Mass of TOC (g)	Mass of Clay (g)	V_L (scf/ton)	P_L (psi)
11	0 (0%)	3 (100%)	108.7	411.4
12	0.3 (10%)	2.7 (90%)	166.7	279.8
13	0.6 (20%)	2.4 (80%)	181.8	192.6
14	1.5 (50%)	1.5 (50%)	333.3	166.0
15	2.4 (80%)	0.6 (20%)	555.6	197.9
16	3 (100%)	0 (0%)	666.7	193.8

Sample 11 is pure kaolinite with no TOC content. The calculated Langmuir volume V_L of this sample was only 108.7 scf/ton. Sample 12 which is made up of 10% TOC and 90% clay showed a higher V_L value of 166.7 scf/ton. Gradually, Sample 13 which has 20% of TOC and 80% clay had V_L of 181.8 scf/ton. Sample 14 which has

an even higher amount of TOC (50%) showed a higher V_L value (333.3 scf/ton). Increasingly, Samples 15 and 16 which have 80% and 100% TOC expressed higher V_L values of 555.6 and 666.7 scf/ton respectively. Figure 3.8 shows the sorption (adsorption and desorption) isotherms of the TOC and clay mixture samples.
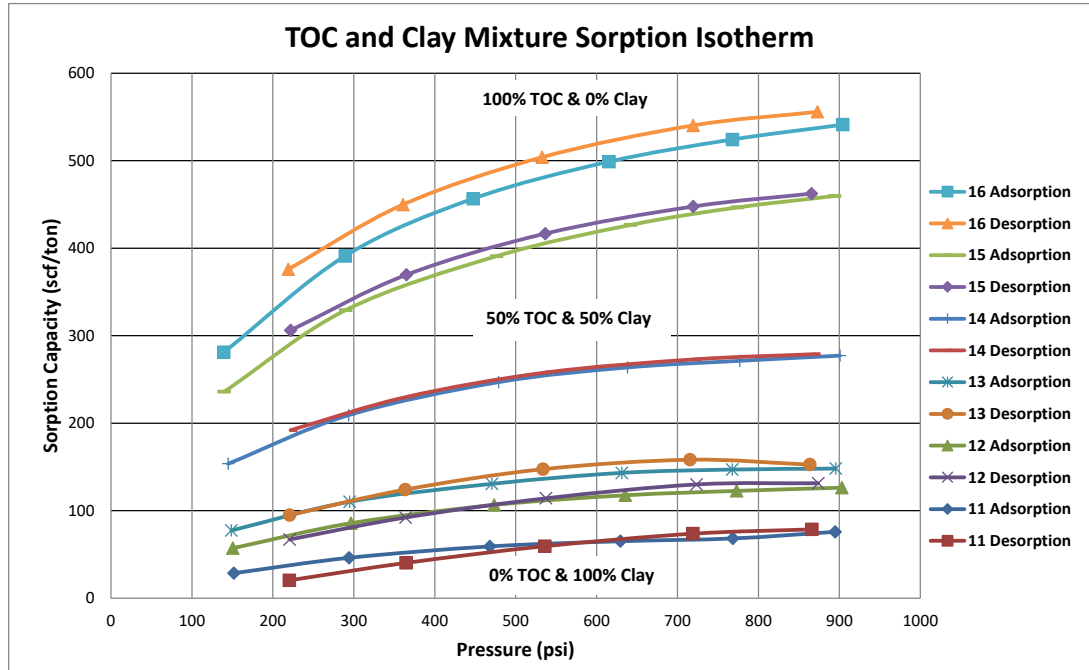
Figure 3.8 Methane Sorption Isotherms of clay samples with different TOC compositions.

3.3.4   Sensitivity Analysis of the HPVA Analyser

3.3.4.1 Shale sample

Unexpectedly, the results of the YLR1-A sample showed a decrease in the adsorption volume with pressure increases (Figure 3.9). According to the Langmuir Theory, the volume of adsorption will increase at higher pressures. Thus, further experiments were conducted for the YLR1 sample by continually increasing the sample weight and the measurement of methane sorption isotherm results were achieved with a different mass.

Initially, the experiment was run with 1.85 grams of YLR1 shale and it was noted as the YLR1-A sample. Additional experiments were run by increasing the weight of the sample by adding around 1 gram of the sample for each increment. The sample weights were 3.22, 4.45 and 5.42 grams for the YLR1-B, YLR1-C and YLR1-D samples respectively (Table 3.6).

Table 3.6 YLR1 Sample data and results.

Sample type	Weight (gm)	V_L (scf/ton)	P_L (psi)
YLR1-A	1.85	41.3	66.5

YLR1-B	3.22	67.6	149.5
YLR1-C	4.45	61.0	137.8
YLR1-D	5.42	67.6	197.0

In most cases, the adsorption isotherm could be fitted on the Langmuir model (Figure 3.9). However, a drop of the adsorbed volume can be seen at higher pressures in most of the cases, especially for the low weighted samples. For the YLR1- A, the sample weight was too low that the isotherm failed to fit the Langmuir model and the calculated Langmuir volume V_L was only 41.3 scf/ton. On the other hand, for the YLR1-B, YLR1-C and YLR1-D samples, the calculated Langmuir volume was quite similar, presenting 67.6, 61.0 and 67.6 scf/ton respectively, and the adsorption isotherm could be fitted onto the Langmuir model.
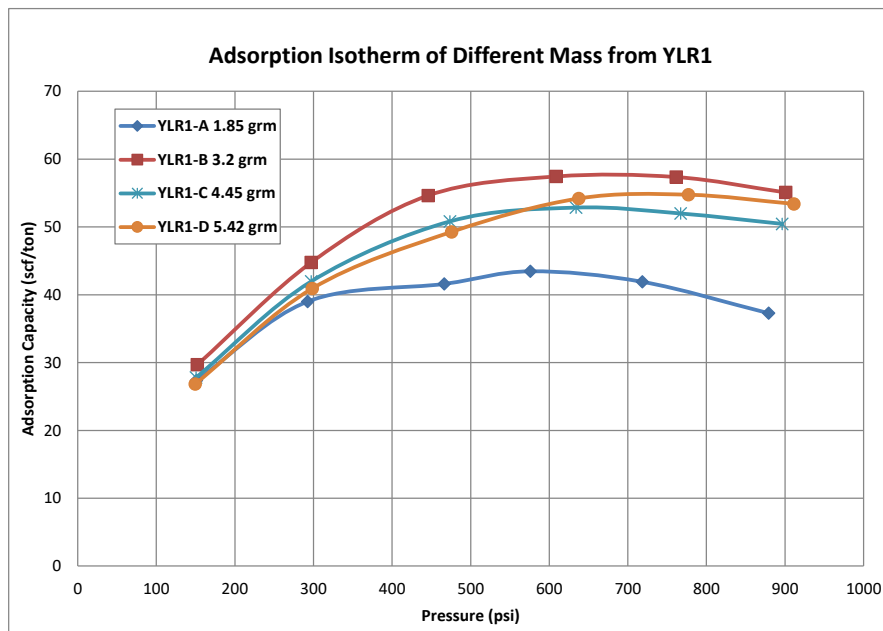
Figure 3.9 Adsorption Isotherm of different mass on YLR1 shale sample.

3.3.4.2 Clay and Organic-rich samples

Similarly, a comparison was made using the kaolinite and organic-rich samples. It is worth noting that a constant powder weight of 4.5 grams was used for all the samples for this time. The experiment was repeated several times for each, at exactly the same conditions of temperature (30°C) and pressure increments. Notably, the kaolinite sample failed to achieve the same results for the repeated tests. Also, the adsorption isotherms could not achieve the same magnitude (Figure 3.10). The calculated Langmuir volumes were different for the repeated tests, namely 128.2, 93.5, 119.0, 169.5 and 86.2 scf/ton for KAO1 to KAO5 respectively (Table 3.7). On the other hand, the organic-rich sample was successful to present the same adsorbed

isotherm at each of the repeated tests (Figure 3.11). Very similar Langmuir volumes for the four repeated tests were achieved for the C1 and C2 samples, as well as the C3 and C4 samples, at 666.7 scf/ton and 625.0 respectively (Table 3.8). Moreover, a comparison between Figures 3.9, 3.10 and 3.11 showed that the volume of the adsorption isotherm of the organic-rich samples is much higher than those for the shale and clay samples; where it ranges between 250 and 650 scf/ton for the former and only between 20 to 80 scf/ton for the latter.
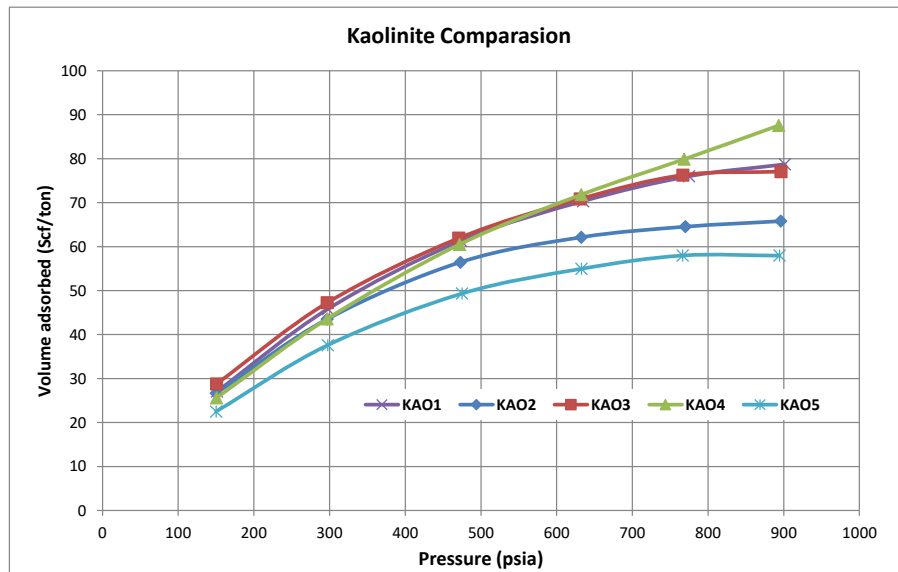
Figure 3.10 The repeated adsorption isotherms of the pure kaolinite clay sample.

Table 3.6 KAO sample data and results.

SAMPLE	WEIGHT (GM)	V_L (SCF/TON)	P_L (PSI)
KAO1	4.4	128.2	540.9
KAO2	4.4	93.5	344.1
KAO3	4.5	119.0	451.7
KAO4	4.4	169.5	854.1
KAO5	4.4	86.2	86.2
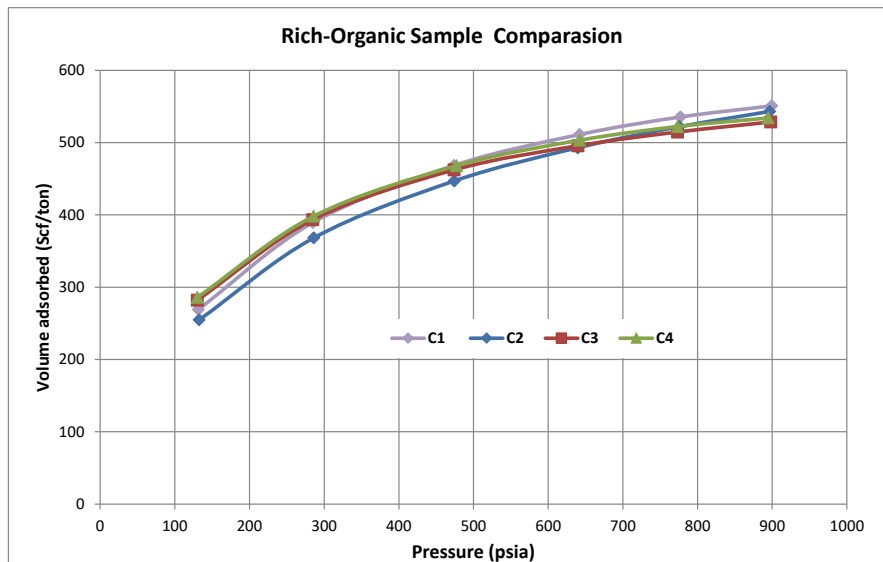
Figure 3.11 Repeated adsorption isotherms of the organic-rich sample.

Table 3.7 Organic-rich sample data and results.

Sample	Weight (gm)	V_L (scf/ton)	P_L (psi)
C1	4.5	666.7	201.7
C2	4.4	666.7	230.4
C3	4.5	625.0	162.4
C4	4.5	625.0	160.6

3.4 Discussion

3.4.1 Effect of Adsorbate's Mass on Methane Adsorption Isotherms for Shale (YLR1) Sample

In general, the adsorption capacity, V_{ADS}, will increase from lower to higher pressures until eventually, it hits the maximum adsorption capacity, which can be found using the Langmuir Isotherm method by calculating the V_L (Langmuir Volume). V_L is the maximum adsorption capacity and V_{ADS} is the amount of methane adsorbed, which is recorded at a constant temperature and different pressure settings. If the V_{ADS} decreases at higher pressures, it indicates negative adsorption which is not a reasonable result for the experiment (Ross and Bustin 2007). The negative adsorption can be affected by many factors and there is no unique solution that can explain such a phenomenon. The adsorption isotherm of the YLR1-A sample, as seen in Figure 3.12, shows a decrease of V_{ADS} from pressures 575 to 879 psi. The V_{ADS} reduces from 43.46 to 37.28 scf/ton.
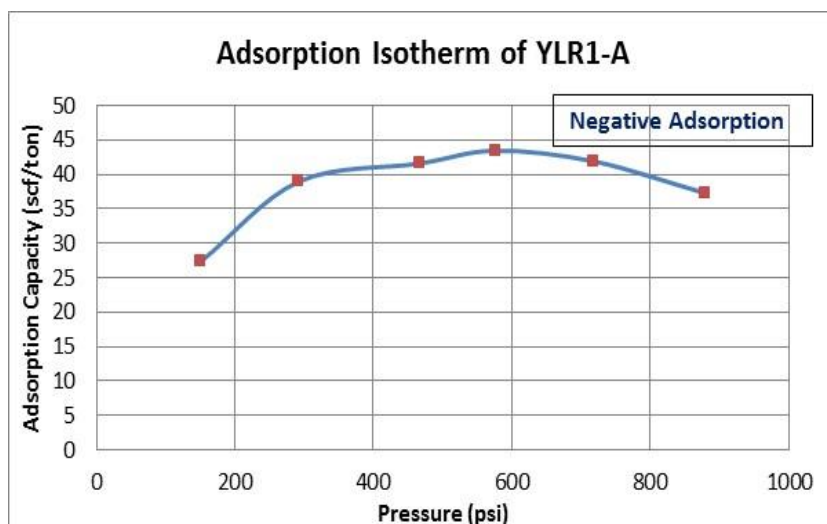
Figure 3.12 Adsorbate mass effect on adsorption isotherm, YLR1-A sample.

In spite of this, several experiments were conducted with the change of the YLR1 adsorbate's mass in order to see the influence on the adsorption isotherm. As can be seen in the results section of Table 3.6, 4 experiments were conducted using the same YLR1 sample. The mass of the adsorbate was gradually increased from 1.85 to 5.42 grams at separate runs. Eventually, at 3.22 grams of the YLR1-B sample, the experiment produced a good adsorption isotherm that can be fitted with the Langmuir Isotherm (Figure 3.9). It appears that if the mass of the adsorbate used is adequate while running the experiment, the adsorption isotherms will tend to be fitted with the Langmuir Isotherm. However, a small quantity of adsorbate would have a smaller surface area to adsorb the adsorbent, resulting in unsatisfactory results, like in the case of YLR1-A.

Additionally, the HPVA uses a static volumetric method to calculate the adsorption capacity. Thus, it is important for the adsorbate to provide enough surface area to adsorb the methane at the equilibrium state. This can be achieved by increasing the sample weight for the low adsorption capacity samples. Moreover, the pore structure of some shales may cause the matrix to work as a sieve, thus preventing gas from entering smaller pores especially at the higher pressures, as can be seen in Figure 3.9 (Ross and Bustin 2007). This might be overcome by pulverizing the sample into the finest particle size (which was already done), in which the overall surface area of the sample can be increased. However, crushing the sample to a very fine grain size will destroy any porosity, if present, thus creating an extra artificial surface area equivalent to the effect of almost 2.0% organic content. When a sample is milled to

93

about 4 um, which in a natural case, if found, will depend on the particle size and organic content.

3.4.2 Effect of Adsorbate's Mass on Maximum Adsorption Capacity on Clay and Organic-rich Samples

The methane adsorption experiment of Sample 6 has a very high maximum adsorption capacity of 400 scf/ton, as mentioned earlier. This is normal for the Montmorillonite clay. However, the V_L of the sample can be compared to the mixture sample 10 which has a lesser V_L value of 312.5 scf/ton. Generally, an increased organic content will lead to a higher adsorption capacity. Sample 10 was produced in order to observe the methane adsorption potential from mixing both samples (clay 6 and organic-rich 9), but the results could not be achieved due to the low sample weight. Initially, Sample 10 only weighed 1.8 grams, but it was later increased to 3.9 grams in Sample 10A (Table 3.4). The mixed sample then had higher V_{ADS} from the different equilibrium pressure conditions. The adsorption isotherm can be seen in Figure 3.13.

Notably, while running the experiment, if the mass of the adsorbate is near to the threshold, the accurate adsorption isotherm can be obtained. From the comparison of the YLR1 samples in section 3.4.1, the threshold of the mass adsorbate appears to be above 3.0 grams. Hence, the investigation into Sample 10 was repeated using a higher mass of 4 grams in total at 50% each sample, resulting in Sample 10A. As it was expected, the results were right in the middle between the two components of the mixture (Figure 3.7).
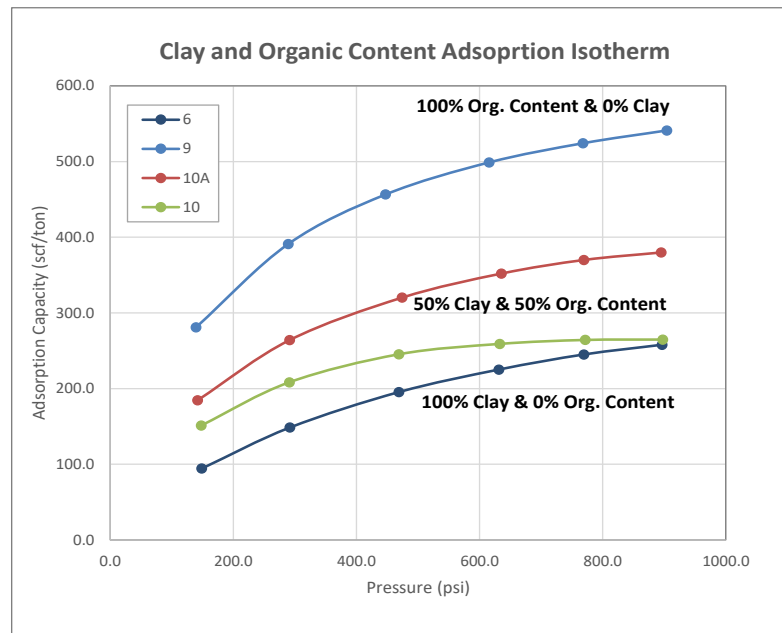
Figure 3.13 A comparison of the clay and coal mixture sorption isotherms.

The achievement proved that when the mass of organic-rich shale, clay and mixed samples are in the range of the calculated threshold, the correct result of V_L for each sample can be achieved. Therefore, for the series of clay experiments conducted with different TOC compositions, the sample weight was set to be 3 grams as it was the most suitable mass for the experiment and sorption isotherms that can be found in Figure 3.8. Thus, it is concluded that Lengmuir isotherm is highly dependent on mass of the sample.

3.4.2.1 Comparison of Methane Adsorption Potential on Organic-rich, Clay, and Shale Samples

There is no doubt that the high TOC sample will yield the highest adsorption potential. It is believed that the high TOC sample could increase the adsorption process, as the organic matter alters the wettability of the shale gas so the gas can be adsorbed and stay still within the pores and surface area of the matrix. Additionally, the thermal degradation of kerogen will produce higher additional fractures and a higher surface area to the matrix. Also, organic matters are sources of gas. It was noted that despite the lower clay and higher quartz content, shale sample 3, which has a higher organic content (TOC) and slightly higher thermal maturity, showed high adsorption capacity. However, some types of clay minerals also have an adequate adsorption potential such as the Montmorillonite type of clay, Sample 6. The adsorption isotherm of all samples can be seen in Figure 3.14. The methane

95

adsorption potential of the lean organic shale (Sample 4) is very low, as compared to the clay and organic-rich samples. However, an increase in the total clay and organic content will significantly increase the adsorption capacity of the shale (Samples 1 and 3). Although the adsorption isotherm seems to be in low values, the maximum adsorption capacity of some samples is still high, which means higher adsorption potentials.

According to our results, the main factors affecting the adsorption capacity of shale are mineral composition and total organic content. Also, from the analysis of Sample 3, it is believed that thermal maturity plays a second role in deriving the potential of the adsorbed gas of the shale. The origin of the shale samples was the Laurel Formation in the Canning Basin, Western Australia. Elkhalgi and Rezaee (2014) carried out the geological framework of the Laurel Formation which shows the mineral abundance of the shale samples (Figure 3.15). Sample 4 has the lowest V_L because it is dominated by quartz and feldspar content, as well as very low TOC and Tmax values.
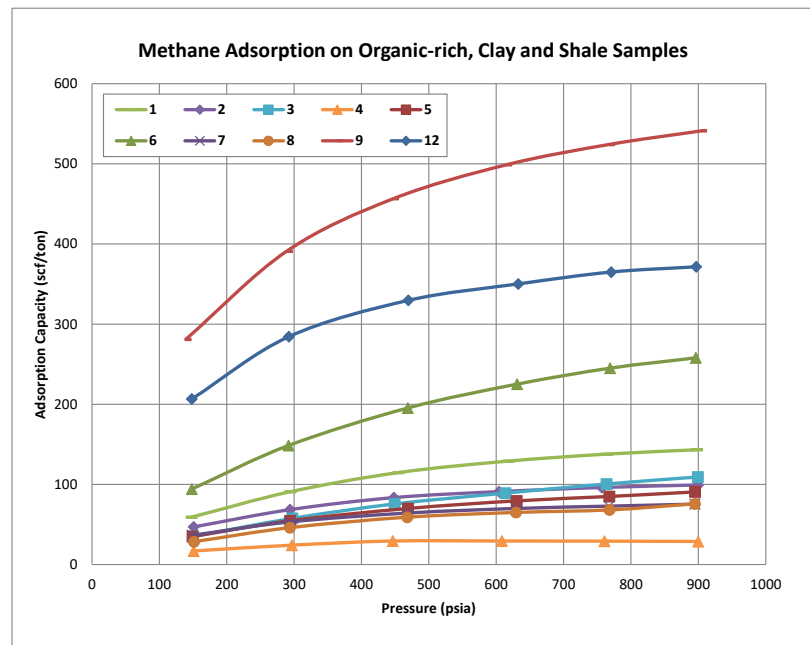
Figure 3.14 Overall adsorption isotherm for the studied samples.

Both minerals are commonly known for their low adsorption potential due to the very low specific surface areas based on the BET experiment (Ji et al. 2010). However, there are many parameters that can affect the methane adsorption capacity of the shale such as TOC, clay content, pore characteristics and many others. The composition itself cannot provide a very accurate result, but it can give a basic idea on how the

composition of shale affects the adsorption potential of the sample. Also, it is believed that the clay content in the shale affects the V_L of the shale. Based on studies done by (Ji et al. 2010), they found that Kaolinite and Illite types of clay have a moderate gas adsorption potential, which are quite pervasive in the shale samples (Figure 3.15). The findings can be correlated with the results of Sample 1 as it has a higher adsorption capacity compared to the other samples.
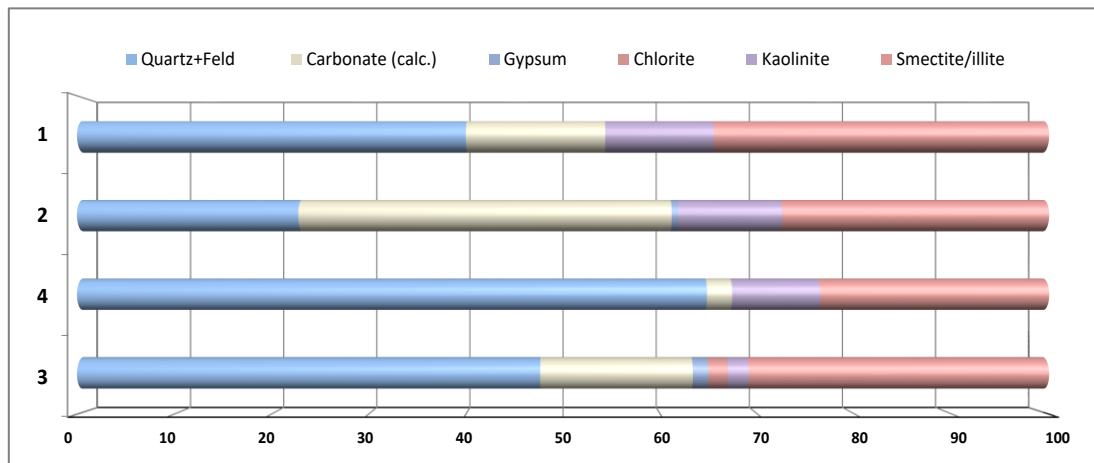
Figure 3.15 Mineral composition of the studied shale samples (Elkhalgi and Rezaee, 2014).

Finally, an organic-rich sample will mostly have the highest adsorption potential due to its organic-rich matter (many research studies consider high-grade coal to be 100% kerogen) that helps the adsorption process. However, some types of clay with larger pore space volumes and surface areas, such as the studied Montmorillonite and sodium-rich Montmorillonite samples will also have reasonable amounts of gas adsorption due to their larger adsorption sites. An adsorption site is the area which the adsorbed gas is trapped and stuck on. Basically, the Montmorillonite type of clay has the highest adsorption site, as compared to illite/ smectite and kaolinite. Also, the minerals, quartz and feldspar, will mostly have a smaller adsorption site which in turn leads to a low adsorption potential (Figure 3.14).

The results of the sensitivity analysis experiments on clay and organic-rich samples showed that the repeatability of the test could not be exactly achieved for the Kaolinite type of clay. Although the test was repeated 5 times using the same sample at a fixed mass and temperature, the isotherms failed to overlay each other and thus the adsorption capacities were different (Figure 3.10 and Table 3.7). However, the repeatability of the rich-organic sample tests was successful (Figure 3.11 and Table 3.8) as all factors were held constant. It can be safely claimed that the HPVA Analyser is sensitive to the organic content of the sample, regardless of its lower

sample weight, in comparison to those used for the clay samples. Therefore, it is recommended for further experiments, the need to examine the sensitivity of the analyser to the clay content, and to achieve the correct adsorbate mass that supports the repeatability of the test.

3.4.2.2 Relation between TOC and Langmuir volume

The Langmuir volume for the TOC and clay mixture is shown in Table 3.5. The definition of the Langmuir volume is the maximum amount of gas that can be adsorbed in an equilibrium state and infinite pressure. In other words, it can also be said to be the maximum amount of methane gas that can be adsorbed in the sample.

According to Table 3.5, Sample 16 (100% TOC) shows the highest Langmuir volume. On the other hand, Sample 11 (100% Kaolinite, 0.0% TOC) shows the lowest Langmuir volume. It can also clearly be seen from Figure 3.8 that the direct increase of the sorption isotherms is according to the increased percentage of the organic matter within the sample. This can be explained as kerogen is the main factor to adsorb the methane gas in the rock. Equally, a high TOC rock would show the high Langmuir volume due to the high organic matter. This was made clear by plotting the Langmuir volumes versus the TOC graph for each sample. Figure 3.16 shows the correlation and correlation co-efficient of the Langmuir volume and TOC for the mixed TOC and clay content samples 11 - 16.
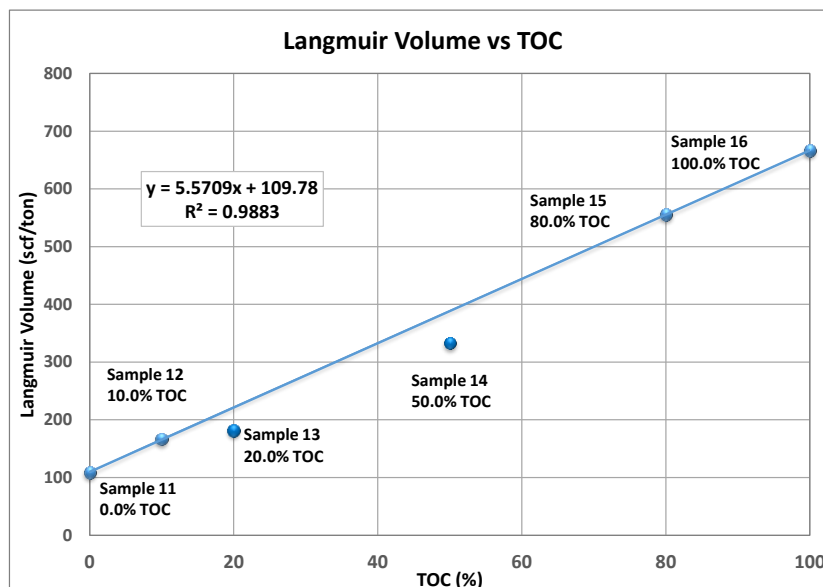
Figure 3.16 Langmuir volume vs TOC.

Note that with known clay and organic matter compositions, the Langmuir volume can be predicted using the following equation:

$$V_L = 5.5709 * TOC + 109.78$$

Where the temperature is 30℃ and all other factors affecting the sorption capacity are considered constant.

3.4.2.3 Relation between clay content and Langmuir volume

It is clear that the adsorption capacity of clay-rich rocks is usually lower than those rich in TOC. According to Table 3.5, the 100% clay content, sample 16, shows the lowest Langmuir volume. Thus, it can be claimed that the pure clay sample has the lowest sorption capacity when compared to the other samples (Figure 3.8). By plotting the Langmuir volume versus the clay content (Figure 3.17), the correlation of the Langmuir volume and clay content can be obtained. The correlation proved that increasing the amount of low adsorption potential clay (Kaolinite) will yield a decrease in the adsorption capacity for the organic-rich rocks.
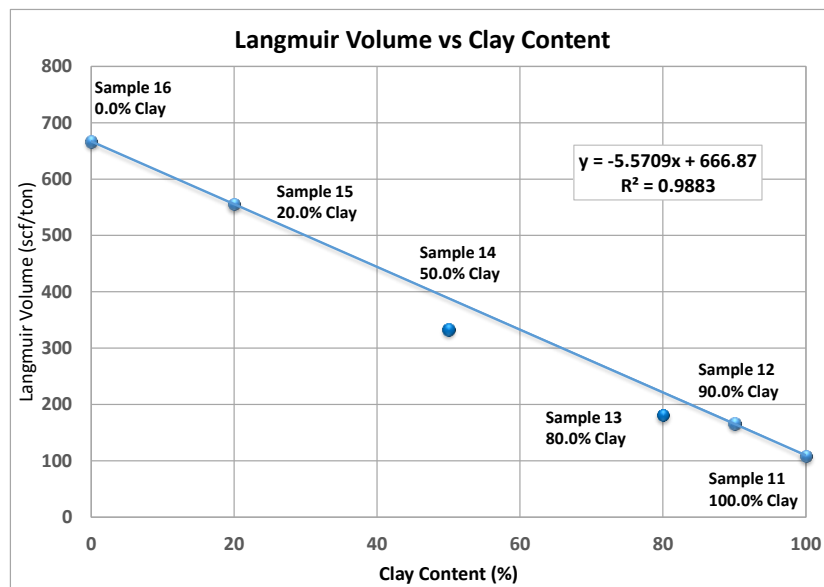
Figure 3.17 Langmuir volume vs clay content

Note that with known clay and organic matter compositions, the Langmuir volume can be predicted using the following equation:

$$V_L = -5.5709 * (clay\ content) + 666.9$$

Where the temperature is 30℃ and all other factors affecting the sorption capacity are considered to be constant.

4. Chapter 4: Petrophysics of Shale Gas

4.1 Overview

Total Organic Carbon (TOC) is important for characterizing the generating potential of a source rock. TOC analysis is usually the first screening process done to assess the potential for hydrocarbon generation. An issue of TOC is that it is not measured with typical wireline tools. Customarily, TOC would be measured via laboratory analysis of sidewall cores, conventional cores and/or cuttings (Passey, Q. R. et al 1990). TOC has been calculated in the past using wireline data by empirical equations such as Schmoker and Passey's equations (Cluff 2011). Well log response was first used in 1984 by Meyer and B. L. Meyer (1984) to evaluate organic-rich source rocks. Their technique was only limited to the use of porosity/resistivity x-plots to differentiate organic-rich from non-organic intervals. High resistivity responds with low density, which responds with the high transit time, which is an indication of good source rock and vice versa. In addition, the use of well log data to evaluate rich organic-rich shales has been widely recognised (Amaefule et al. 1993). They were first used to discriminate potential from non-source rocks. Moreover, in their physical model, (Mendelzon and Toksoz 1985) characterized the properties of source rocks using well log response. They used organic content as a function to calculate the response of the well logs. Organic matter was treated as a rock constituent and its physical properties were detected by calculating the response of neutron, sonic and density logs. Moreover, Meissner (1984) has qualitatively evaluated the thermal maturity of source rocks from the resistivity log response but he did not directly calculate the amount of organic matter.

An estimation of total organic carbon using Passey (1990) technique is based on two main assumptions. First of all, there is a significant amount of organic matter contained within shale and/or lime mud source rocks. Secondly, non-source rocks may also contain organic matter, but are in insufficient amounts (usually less than 1 wt.%). Fluids filling the pore spaces, in additional to the rock matrix and solid organic matter, are the three components of a organic-rich source rock (Nixon 1973). Formation water filling the pore spaces is the fluid type for immature source rocks. An increased thermal maturity of these rocks will cause the solid organic proportion to be gradually transformed into hydrocarbons, thereby replacing the formation water.

In this chapter, well log data is used for TOC and brittleness estimation, as well as porosity and water saturation estimation of the Goldwyer Formation. As shown later, a direct correlation with the core measurements proves the accuracy of the results obtained from the logs.

4.2 TOC Estimation using logs

4.2.1 Passey Method Implementation on Goldwyer and Laurel Shales

The Passey (1990) method implements the effect of increased hydrocarbon (oil and gas) content within the pore spaces of the source rock (shale rock) on the resistivity and porosity logs. The higher the hydrocarbon content, the higher the resistivity and thereafter, the sonic transit time. The presence of TOC is marked as a higher overlain curves' separation on an appropriately plotted resistivity porosity curves on the same log track. On the other hand, lower organic content will be seen as partial or total curves overlap.
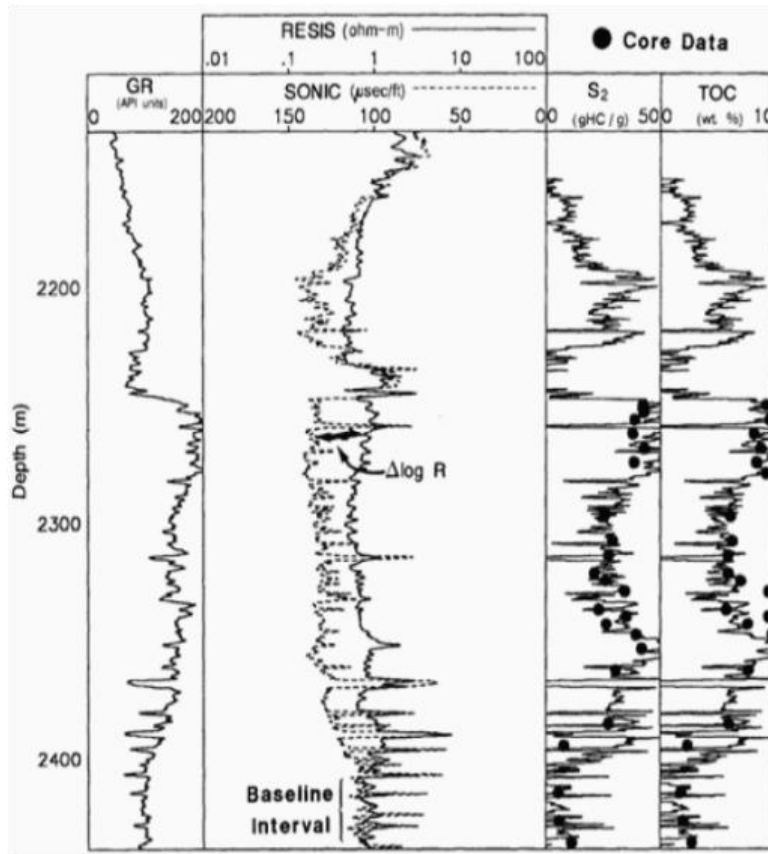
Figure 4.1a Sonic resistivity curves overlaying and the influence of LOM on TOC and Δ log R (Passey 1990).
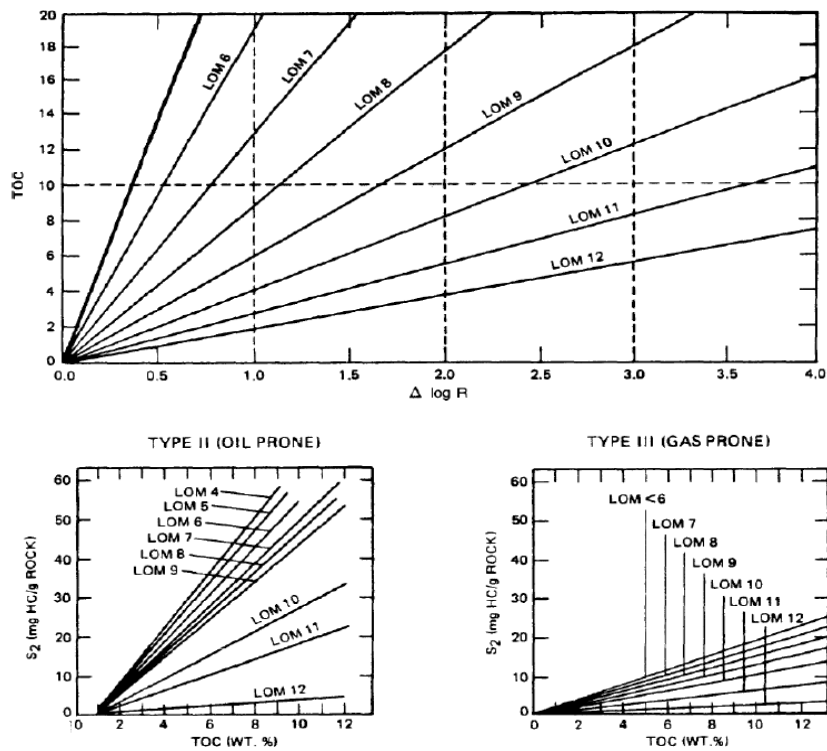
Figure 4.1b LOM estimation from TOC and S2 correlation (Passey 1990).

102

A proper rock classification is needed to eliminate reservoir intervals from organic-rich source rocks. The presence of low velocity and density kerogen will cause porosity log separation from the high resistivity curves responding to the formation fluids. In-place generation of hydrocarbons from mature organic matter will increase the separation intensity. However, the luck of generated hydrocarbons in immature rich-organic rocks curves' separation is preliminary linked to the respond of the porosity log. Therefore, Δlog R techniques prove to be accurate in the calculation of TOC using well log data at a given lithology and thermal maturity.

Passey's Equation is also known as the Δ log R technique. TOC has a linear relationship with Δ log R, where the gradient is influenced by the level of thermal maturity (LOM). LOM can be estimated using the graphs in Figure 4.1b or using Jarvie's Equation of vitrinite reflectance and Tmax (Passey 1990) (section 4.2.1.1.2). Thus, the important equations are:

$$\Delta \log R = \log_{10} \frac{R}{R_{bl}} - 2.50(\rho_b - \rho_{bl}) \quad \text{Eq. 4.1}$$

$$\Delta \log R = \log_{10} \frac{R}{R_{bl}} - 0.02 \ (DT - DT_{bl}) \quad \text{Eq. 4.2}$$

$$TOC = (\Delta \log R) \times 10^{2.297 - 0.1688 \times LOM} \quad \text{Eq. 4.3}$$

Where:

$\Delta \log R$ is the separation of deep resistivity and porosity log

R is the deep resistivity value in ohm.m

R_{bl} is the baseline resistivity value in ohm.m

DT is the sonic transit time in us/f

DT_b is the is the baseline sonic transit time in us/f

ρ_b is the bulk density in g/cc

ρ_{bl} is the baseline bulk density in g/cc

TOC is the total organic carbon in wt%

LOM is the level of maturity

The base line technique is defined as the detection of the well interval where the two resistivity and porosity curves are parallel or overlap each other over a distinct depth range of the fine-grained reservoir rock. This section of overlaying parallelism is known as the organic-lean zone, and it is where the TOC is low (Passey et al. 2010). The non-parallel curves interval is defined as the organic-rich well section. This is called "ΔLogR", which is marked by the inhomogeneous separation between the two

curves varied upon the organic content of the rock at each depth increment through the well section (Figure 4.1a). ΔLogR is TOC dependant, as a function of thermal maturity (Passey 1990). Using Passey's plot in Figure 4.1b, ΔLogR can be converted to TOC if maturity is known.

4.2.1.1 Results

4.2.1.1.1 Lithology discrimination

For each given well, the lithology needs to be discriminated. The gamma ray log, as well as the neutron density overlay log are sufficient for this process. The high gamma ray values are indicative of shale, and where the neutron and density logs are together, it is indicative of limestone. Figure 4.2 shows the lithology discrimination in the Solanum 1 of the Goldwyer Formation in the Barbwire Terrace. The log on the right is calculated using the gamma ray log to find the volume of shale, where the base line values are 200 GAPI and 10 GAPI for shale and limestone respectively. Since shale gamma ranges from about 80 to 200 API, and reaches values as high as 300 GAPI in highly radioactive clays (Rider 1996), the minimum percentage for shale is considered to be 36.8 %.

$$Minimum\ \%\ for\ Shale: Vsh_{min} = \frac{80 - 10}{200 - 10} = 36.8\%, GR\ Index\ Equasion\ I_{GR}$$
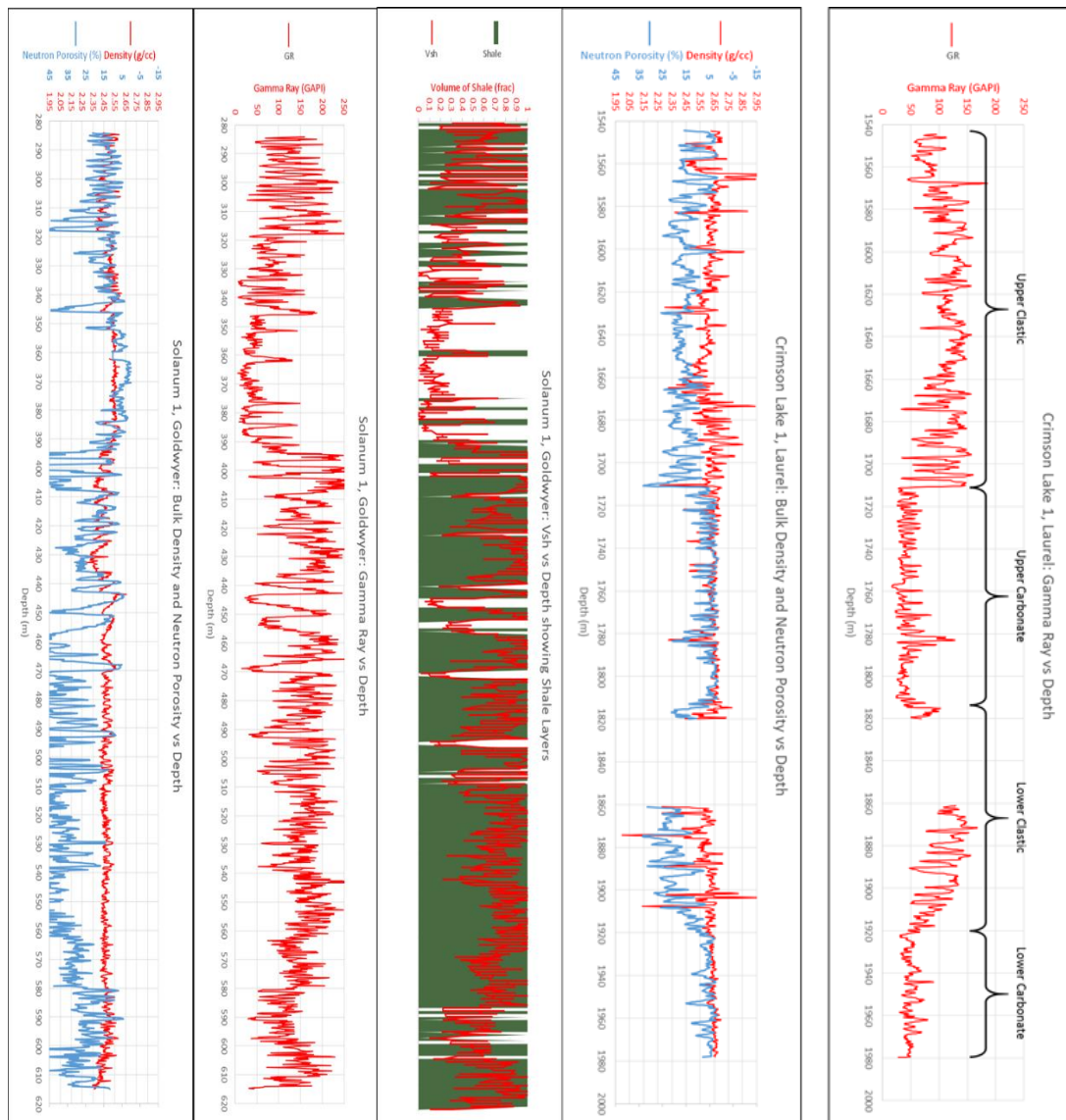
Figure 4.2 Right: Lithology of the Goldwyer Formation in Solanum 1; Left: Lithology of the Laurel Formation in the Crimson Lake#1

As for the Crimson Lake 1 intersecting the Laurel Formation, the formation can be sorted into 4 sub-layers: Upper Clastic, Upper Carbonate, Lower Clastic and Lower Carbonate. The clean layers are the carbonate layers, as seen in Figure 4.2, where there are low values of gamma ray radiation. The shale layers have a high porosity reading from the neutron log due to the clay bound water (Rider 1996).

4.2.1.1.2   Level of thermal maturity

To find the TOC through Passey's equation, the resistivity and porosity logs' base line values, as well as the level of thermal maturity are needed. The level of thermal maturity (LOM) or organic metamorphism measures the maturity of the organic matter contained in the source rock (Hood et al. 1975). Vitrinite reflectance Ro (thermal alteration index) and Tmax are the two main indicators of thermal maturity.

Figure 4.3 and Table 3.1 show the linear correlation of the level of thermal maturity of the Lower Goldwyer shale with depth. The results showed increased LOM with the depth of burial. Due to limited Ro data in the Ordovician shales of the Goldwyer Formation, Ro was calculated from Tmax using Jarvie's Equation 4.4. The results follow the hypothesis and the correlation was obtained. Equation 4.4, proposed by (Jarvie et al. 2007), is used in this study to calculated the LOM from vitrinite reflectance (Ro) (Equation 4.5).
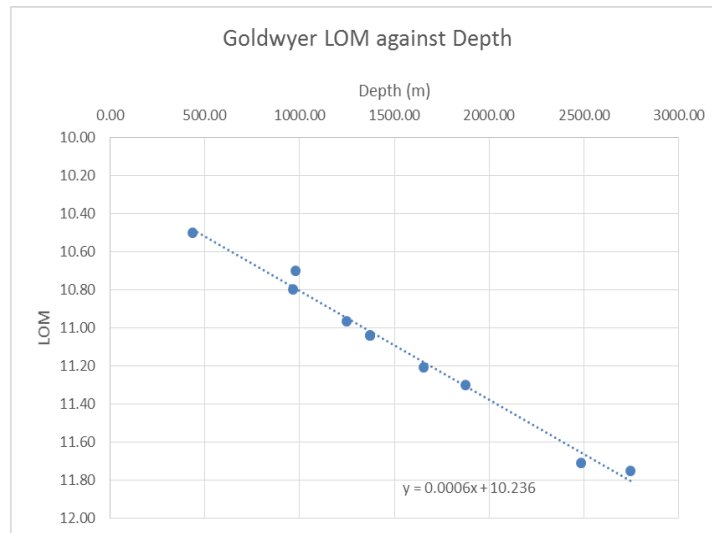
Figure 4.3 Cross plot of the level of Thermal Maturity vs depth of the Lower Goldwyer Shale in the Central Canning Basin.

Table 4.1 Estimated TOC and LOM of the Lower Goldwyer Formation in the Central Canning Basin.

Well Name	Top	Bottom	Depth	Thick	LOM	TOC
Solanum 1	284.00	615.00	436.63	331.00	10.50	1.22
Hedonia 1	915.50	1049.50	976.78	134.00	10.70	0.44
Wilson Cliff	2532.88	2847.44	2745.14	321.69	11.75	0.32
Fruitcake 1	1168.00	1577.00	1372.50	409.00	11.04	0.70
Kanak 1	842.00	1086.00	964.00	244.00	10.80	0.61
Looma 1	1371.00	1934.00	1652.50	563.00	11.21	1.21
Missing 1	1057.00	1440.00	1248.50	383.00	10.97	0.18
Patience 2	2337.00	2629.00	2483.00	292.00	11.71	1.68
Robert 1	1231.00	1826.00	1371.00	595.00	11.04	1.55

This section shows the two methods to calculate the LOM. One way is to use Passey's graphs of TOC against S2 (Figure 4.1b). Another is to use Jarvie et al. (2001) equation of vitrinite reflectance against Tmax:

$$Ro \% = 0.0180 \times Tmax\text{-}7.16 \quad \text{Eq. 4.4 (Jarvie et al. 2001)}$$

Then, calculate the LOM by using its near linear relation with vitrinite reflectance (Figure 4.4):

LOM= 3.9282(%Ro) + 5.866 Eq. 4.5 (Passey et al. 2010).
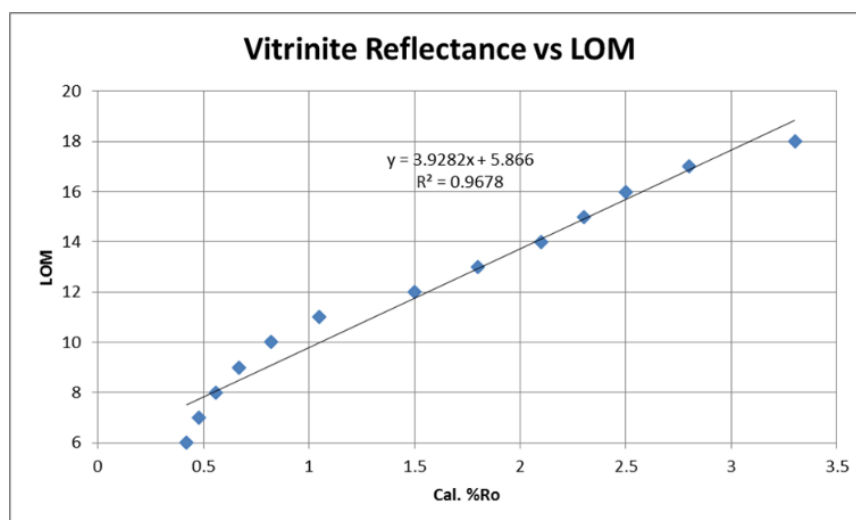
Figure 4.4 Linear cross plot illustrates the relationship of the LOM with Vitrinite Reflectance

4.2.1.1.3 TOC Estimation from Sonic-Resistivity logs

Due to the limited measured TOC data in the Canning Basin (especially as most of the wells that were drilled targeted only conventional oil resources), geochemical study has become limited and uncertainty of the results is significant. Therefore, resistivity-sonic log based ΔlogR technique proposed by Passey (1990) was used to enhance the database used in this research. The results were found to be reliable for the Goldwyer Formation and the estimated TOC was almost the same as the measured TOC. Figure 4.1a shows the resistivity sonic overlain and the plotting of measured TOC versus estimated TOC using the ΔlogR technique from Passey (1990). Similarly, the base line values were obtained for the Goldwyer shale section in the McLarty#1 well, specifically for the organic lean interval (Figure 4.5). The plot was made using the IP software. The gamma ray (GR) log was plotted using green curve in the first track. The depth is showed in the second track, while the interval transit time (DT) and deep log resistivity curves were plotted using pink and black respectively in the same third track. In the second track, the black dots are the measured TOC from core and cutting samples, while the blue curve is log TOC, estimated using Passey's method by applying both Equations 4.2 and 4.3, both in wt.% units.

For this example, the value for the R base line is 2.3 ohm-m. The DT base line is 69 us/ft in the lean organic section at an average depth of 2030 metres. LOM is calculated from rock-eval Tmax data across the Lower Goldwyer shale facies using Equations 4.4 and 4.5 and was found to be 9.7. The average deep resistivity in the

organic-rich section is 20 - 25 ohm-m and DT is 72 us/ft. For the Goldwyer Formation, average log TOC was found to range from 0.5 wt% in the Parda#1 well to 2 wt% in the Aquila#1. The Lower Goldwyer Shale has as high as 4.0 wt% maximum TOC value in the Hedonea#1 well. Moreover, the Upper Goldwyer Shale showed about the same value at the Hilltop#1 well. These values are located in the Broome Platform.
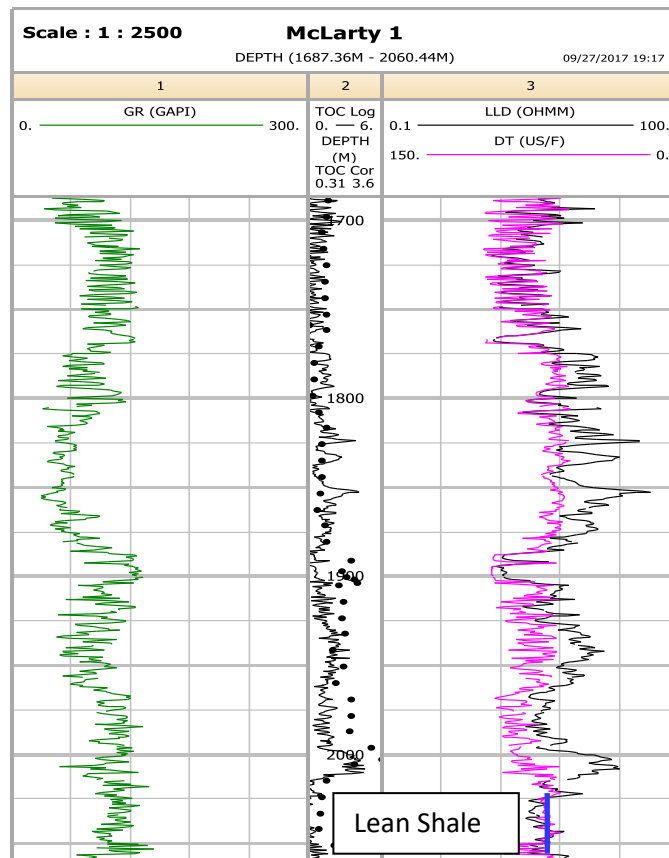
Figure 4.5 Sonic resistivity curves overlaying from the Mclarty#1 well from the Broome Platform in the Canning Basin.

4.2.1.1.4   TOC Estimation from Density-Resistivity logs

To find the base line values, an overlay of resistivity and density is plotted and the scales are adjusted until a significant section of overlaid parallelism is found. A baseline value is needed for each shale layer. $R_{baseline}$ and $RHOB_{baseline}$ are independently obtained for both the Upper and Lower Goldwyer shales (Figure 4.6). For this well example in particular, the $R_{baseline} = 100$ ohm.m and $RHOB_{baseline}$ is 2.48 gm/cc. The average estimated TOC using the Passey method is found to be 1.69 wt.%. Figure 4.7 shows the vertical correlation of the predicted TOC using the resistivity-density approach (green dots) and measured TOC from the core samples in wt.% (red dots). The correlation seems to be valid in the lower shale section,

where the TOC values from both methods are almost overlaying each other. However, the Upper Goldwyer shale section seems to have poor correlation as the data is scattered and far from consistent that could be related to the higher carbonate content.
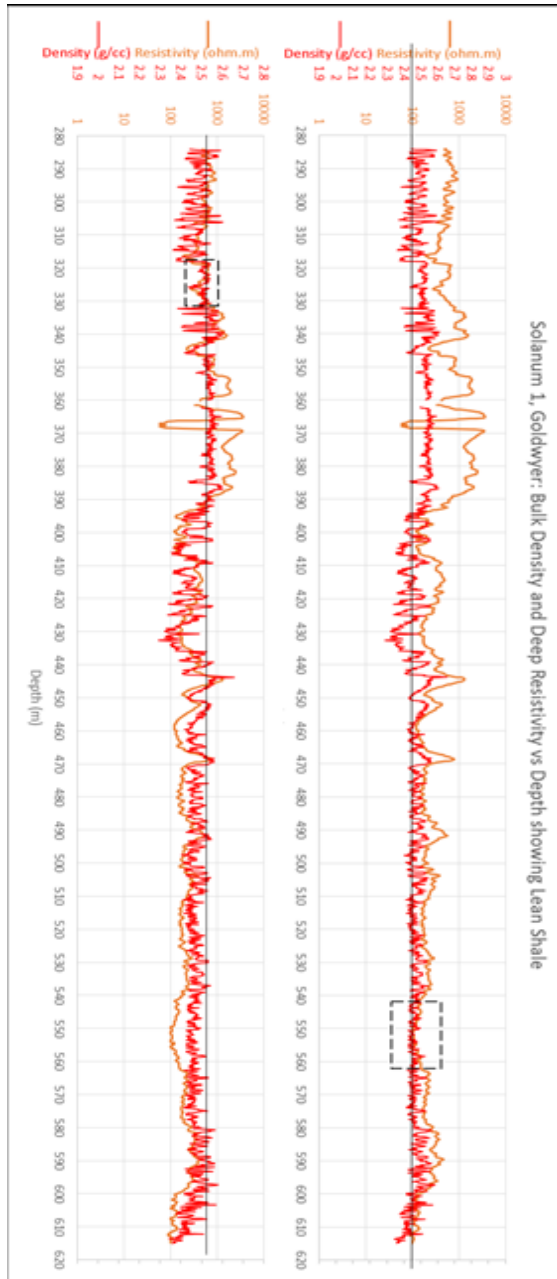
Figure 4.6 The well section shows the density-resistivity overlaying and base line value depiction of the Upper and Lower Goldwyer shales from the Solanum#1 well in the Barbwire Terrace.
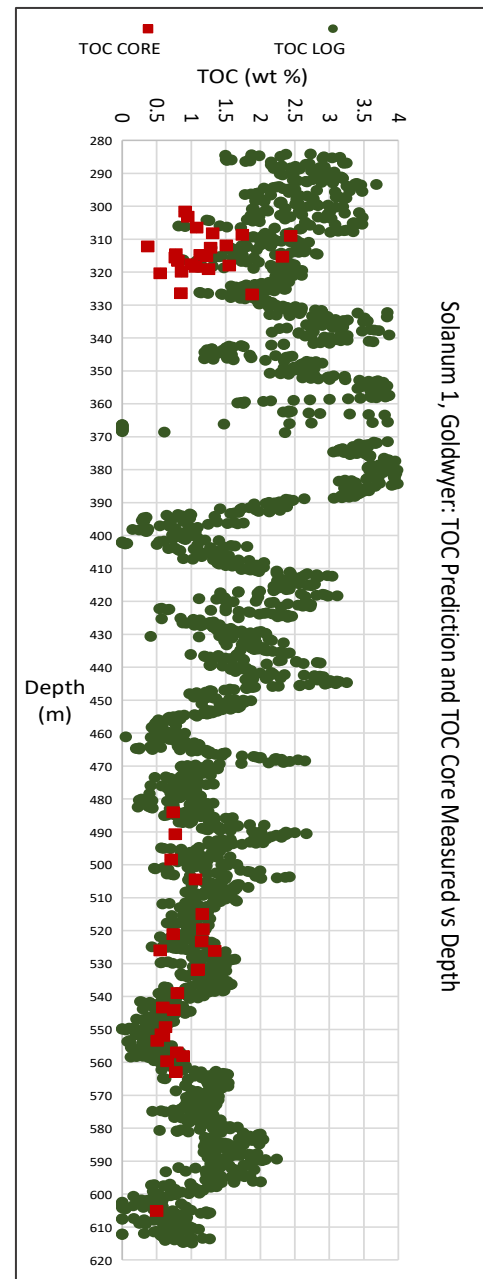
Figure 4.7 The Goldwyer shale from the Solanum#1 well in the Barbwire Terrace.

4.2.1.2 Highlights of shale gas Plays

4.2.1.2.1 Resistivity sonic correlation

One of the most useful applications of the resistivity sonic cross plot is to identify the variation of the TOC content in different zones through the shale section. As

shown in Figures 4.8 (orange circle) and 4.9 (orange data cubes), the organic-rich shale zone can be easily defined - where higher resistivity and sonic transit time values are encountered. Thus, this technique is also very useful in identifying shale gas sweet spots. In the carbonate unit in Figure 4.8 (blue rectangle), where it is believed that generated hydrocarbons have been accumulated, a sudden increase of the resistivity log and low sonic transit time values are clear in Figure 4.9 (blue data points on x-plot). The lithology and fluid contents for this section are confirmed from the well report at this interval. The gamma-ray reading on Figure 4.8 also indicates the lithology variations across the formation, which can be matched with Figure 4.9 that is inferred from the resistivity and DT x-plot. In the organic-rich interval, an increase of the interval transit time is consistent with increases in resistivity values. This results from the low density kerogen proportion in the formation (red data points on x-plot in Figure 4.9). In the lean shale section however, sonic transit time values are high and resistivity values are low (yellow clustered data in Figure 4.9).
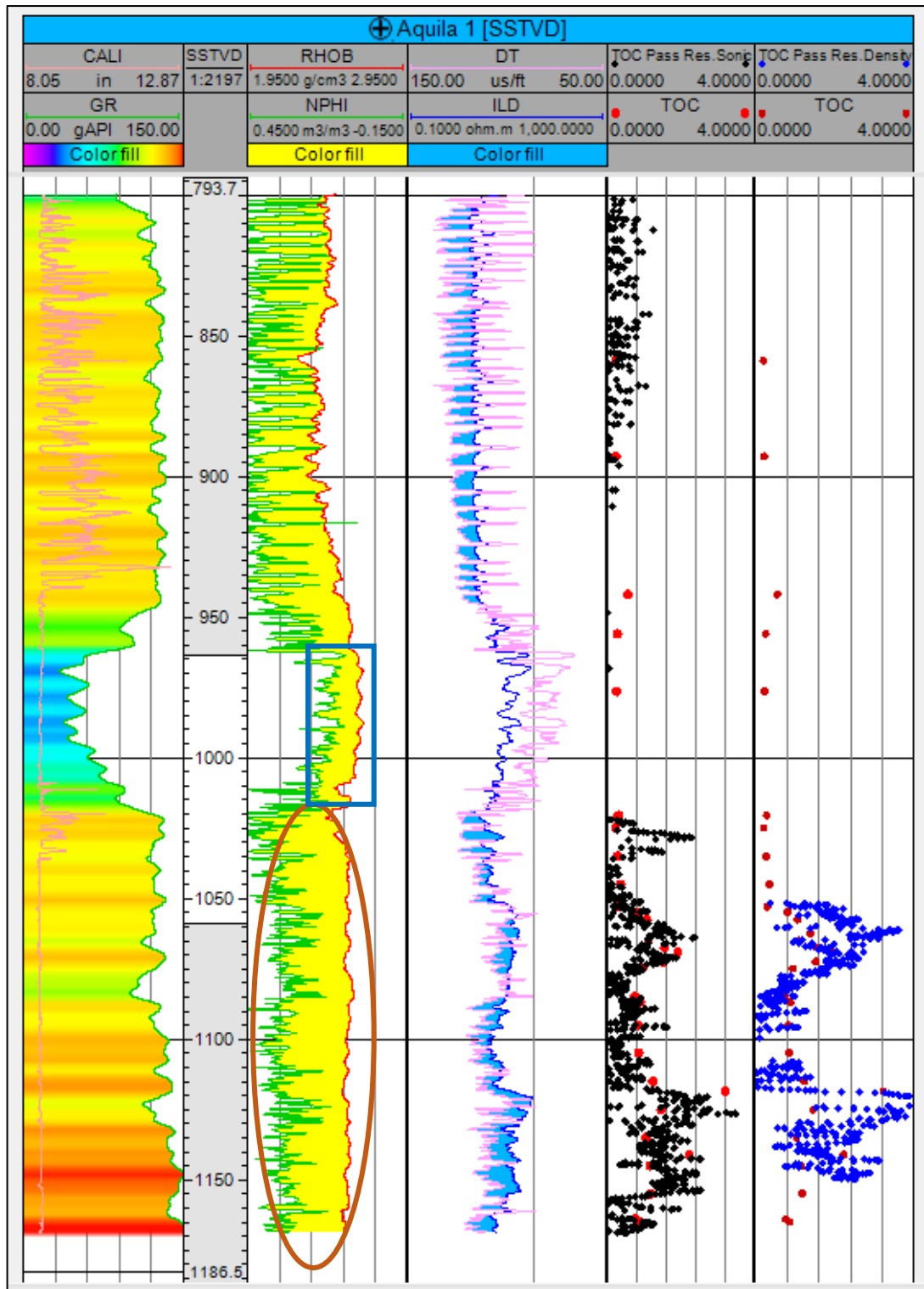
Figure 4.8 Plot of the composite well log of the Aquila#1 well in the Broome Platform using the Petrel software.
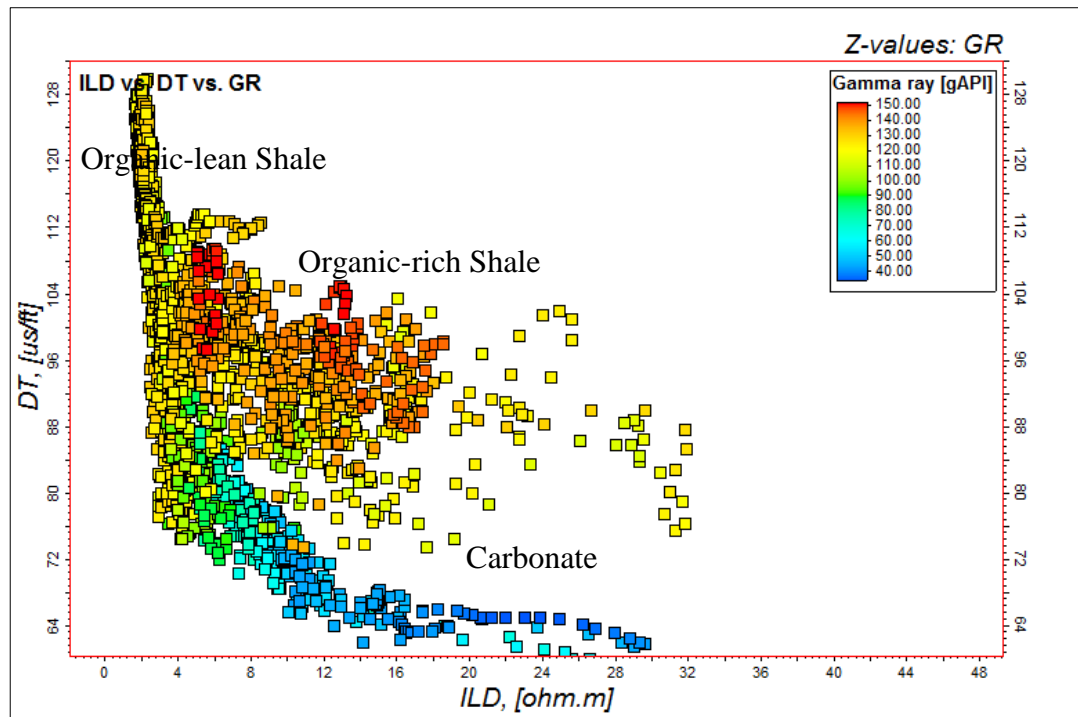
Figure 4.9 Resistivity-sonic x-plot used to differentiate lithology and organic richness of shale gas formations.

4.2.1.2.2   RHOB Correlation

The log density (RHOB), Total Organic Carbon (TOC wt.%) and Thermal maturity indicator (T_{max} °C) data were gathered from 9 wells located in different locations in the Central Canning Basin, mainly in the Barbwire Terrace and Broome Platform. A linear correlation was obtained between the log density and TOC, and Tmax respectively (Figures 4.10 and 4.11). The presence of low density organic matter has a notable effect on the formation density of the Goldwyer Formation. The higher the organic content, the lower the formation density. The correlation coefficient is 0.76 (Figure 4.10), in which the extractable Equation 4.6 can be used to estimate the TOC content of the Goldwyer shale, if other parameters are considered constant. Although the resultant TOC from this equation might be overestimated due to the effect of the lithology on the density log, it can still be used to give an overall idea of the organic content, where there is a lack of geochemical data. It can also be seen from Figure 4.10 that the average log density is between 2.4 to 2.7 gm/cc, which indicates a wide range of lithology that already had its effect on the correlation. Also, TOC values range from 0.5 to 2.5 wt% and the Tmax range is from 430 to 450^{0}C. On the other hand, increased thermal maturity means an increase of organic matter expulsion to hydrocarbons. This will produce a higher porosity and reduce the total organic content of the rock, which will result in higher formation density. Figure 4.11 shows

an increase in the density of the Goldwyer Formation due to the increase of thermal maturity, which could be linked to the increase of pressure due to the increase of depth of burial. This needs to be further investigated to approve the effect of pressure on density in thermal maturity of the Goldwyer Fornmation.
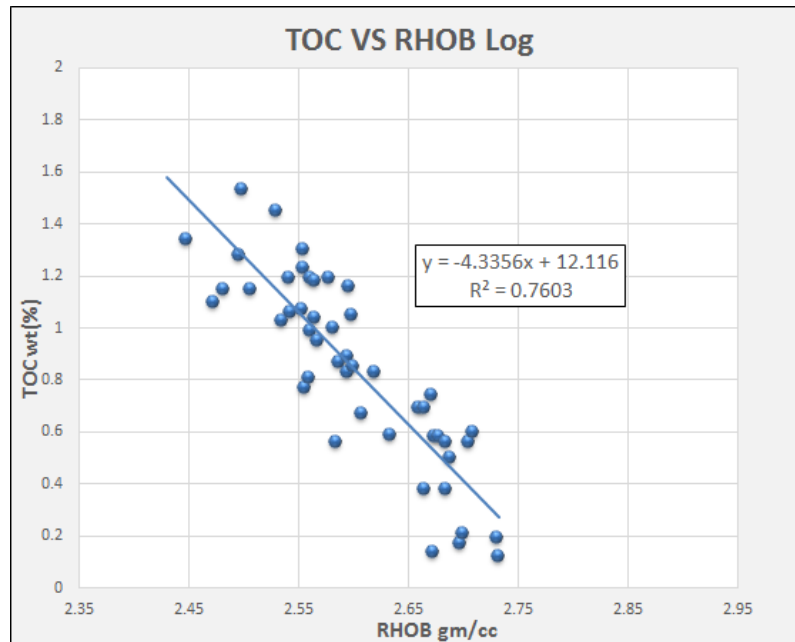
Figure 4.10 Linear correlation of TOC vs. RHOB for the Goldwyer Formation in the Canning Basin.
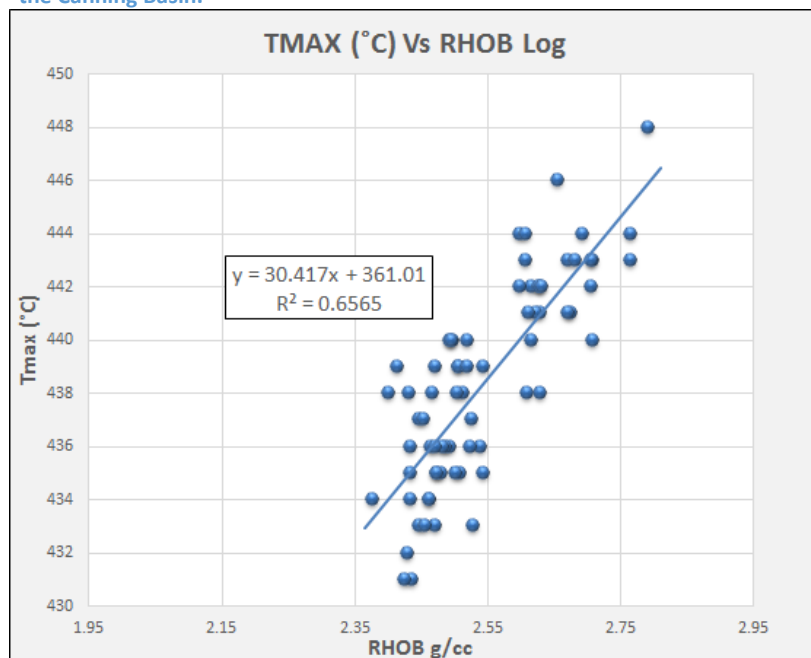
Figure 4.11 Linear correlation of Tmax vs. RHOB for the Goldwyer Formation in the Canning Basin.

TOC = -4.356 * ρ_b + 12.116 wt.% Eq. 4.6

113

The 3D structure model and simple grid of top, middle and lower zones were created using the software. A total number of 1006943 of grid sells was generated in the model.   Stratigraphic surfaces of the formation were generated using input data from well tops acquired from well reports and well correlation based on minimum curvature algorithm with gridding increment of 100x100 for each surface. The lower Goldwyer formation was divided into 6 layers in this model. As it will be explained in detail later in the chapter the petrophysical properties of the Goldwyer shale were estimated externally using well log and core data and imported to the Petrel software. Each property was upscaled and 3D modelled and the corresponding 2D average maps were created. The number of wells involved in the calculation allowed for the building of a 3D property model for the estimated TOC from the well log data. It was decided to use TOC results estimated using the Sonic-Resistivity logs technique in section "3.2.1.1.3" to build the model as they were found to be the most accurate for the Goldwyer Shale. Figure 4.12 is a 2D view of the resultant model, and figure 4.13 is the average 2D map created for this model. TOC values seem to be higher along the south-eastern to north-western trend through the central area of the Broome Platform. It ranges from 2 to 5 wt.% in this area and drops as low as 0.5 wt.% towards some marginal areas, which could be related to the lack of input data. In the Barbwire Terrace, the average TOC calculated from logs using the Passey method was found to be around 1 to 1.5wt.%. This is mainly in the northern part of the terrace. Figure 4.14 presents the 2D view of the built TOC property model in the Barbwire Terrace, and figure 4.15 is the average 2D map created from this model. The red area of the model (orange on the map) has poor input data and is thus not considered in this 3D study.
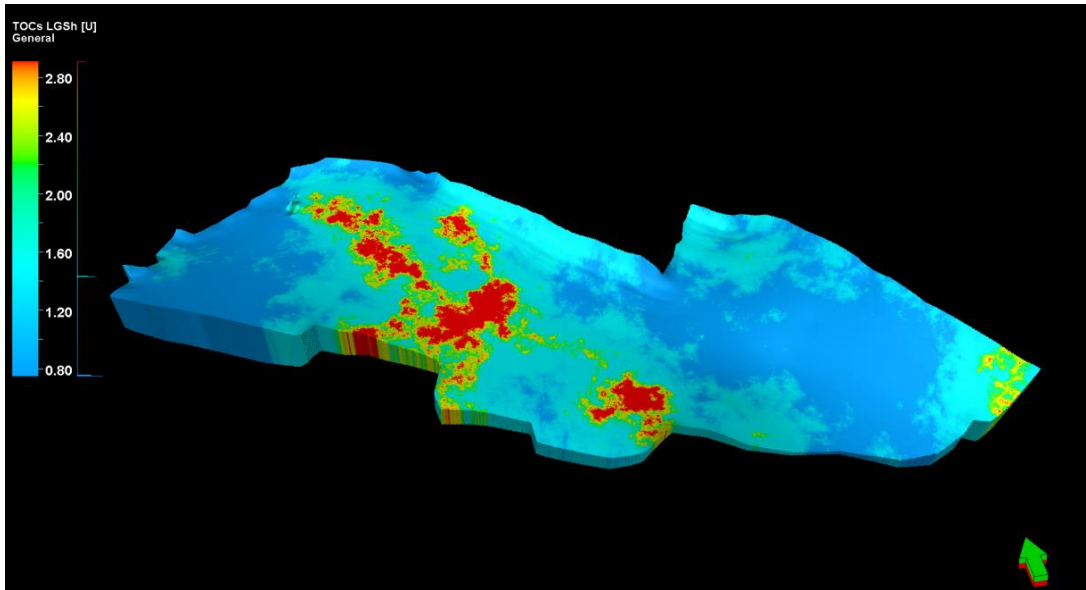
Figure 4.12 3D model of TOC property estimated from the well log data in the Broome Platform.
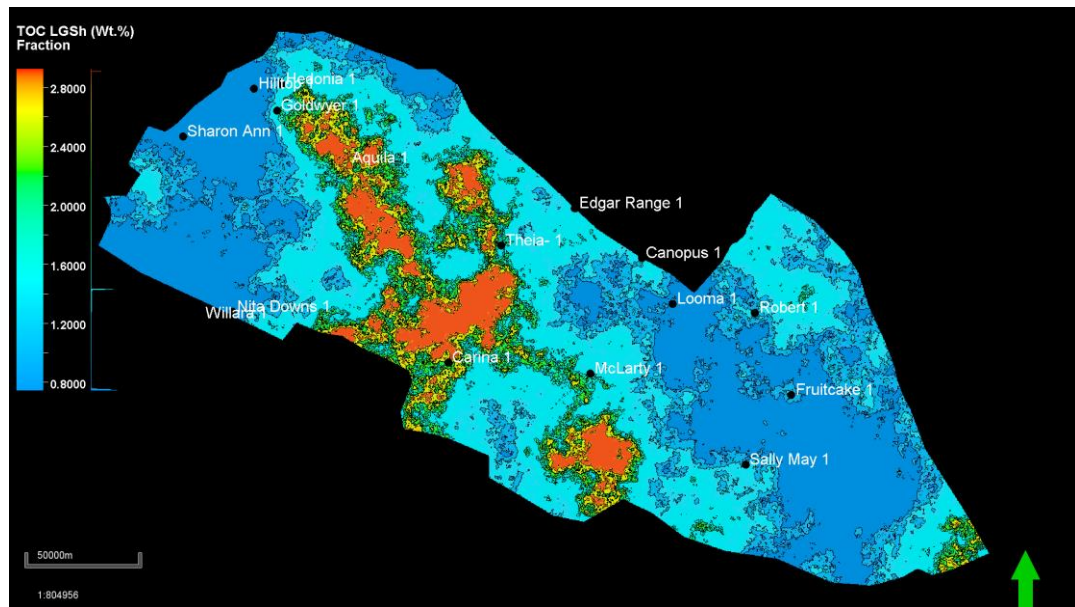
Figure 4.13 Average 2D map of TOC property estimated from the well log data in the Broome Platform.
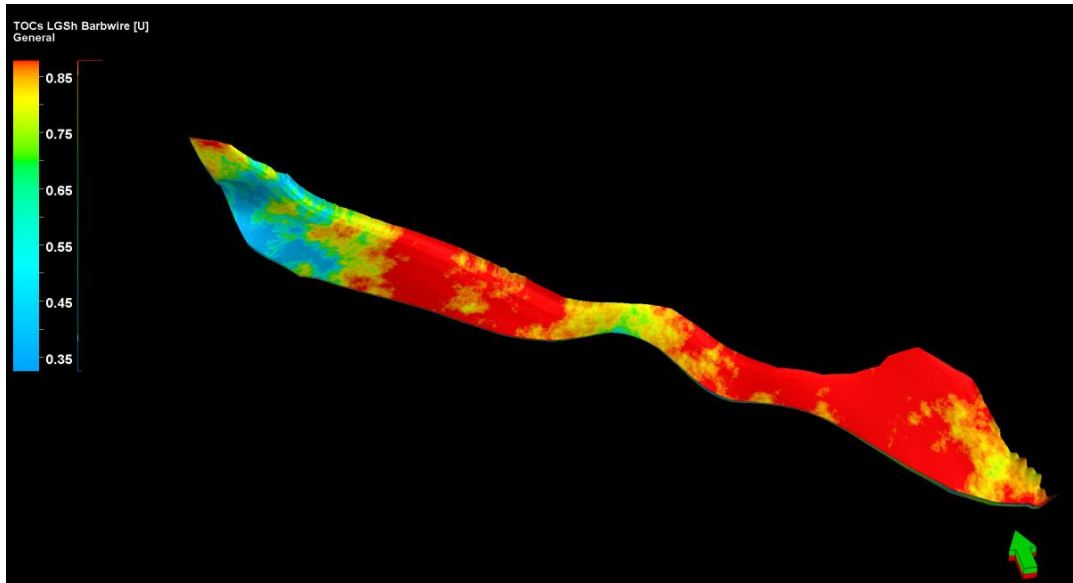
Figure 4.14 3D model of TOC property estimated from the well log data in the Barbwire Terrace.
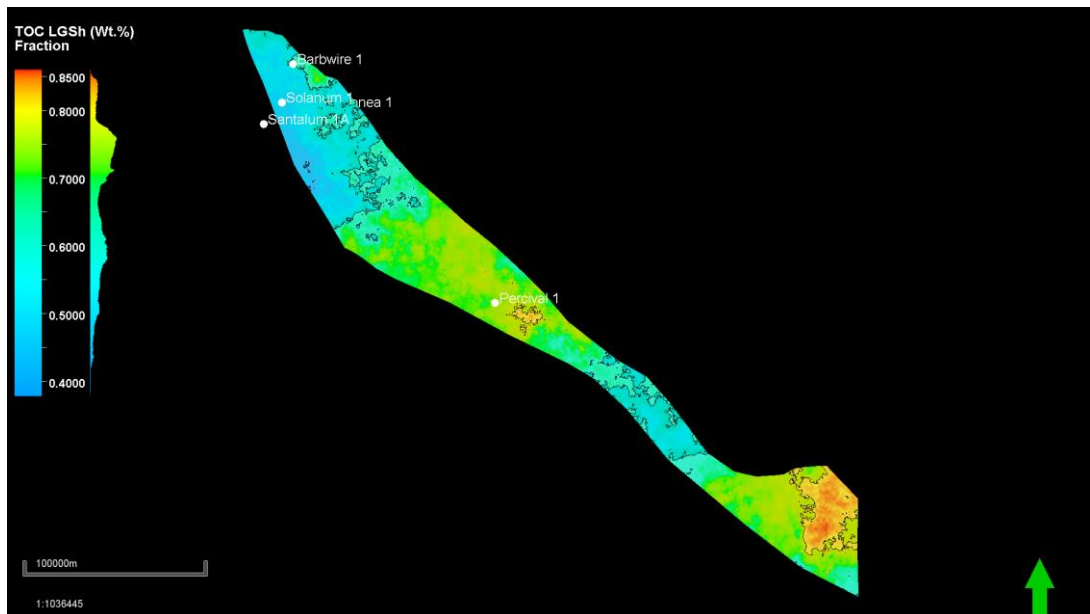
Figure 4.15 Average 2D map of TOC property estimated from the well log data in the Barbwire Terrace.

Similar calculations were done for 19 cored and un-cored wells in the Goldwyer Formation for each of the Upper and Lower Goldwyer shales. Calculations of log TOC were also done for the Laurel Formation in the Lennard Shelf and Fitzroy Trough. Average TOC values were found to be between 0.20 and 3.4 wt.%, with the maximum reaching 5.0 wt.% from the Yulleroo#1 well in the Fitzroy Trough.

4.3 Shale Gas Fracability Index

Mineralogy has a direct effect on brittleness. Increased quartz content will produce a higher brittleness of the rock. Clays however, are more ductile components and thus cause brittleness to reduce significantly (Saneifar et al. 2013). Therefore, a

116

successful fracturing development of shale gas reservoirs relies on proper rock classification. Where organic-rich shale is the reservoir, a comprehensive evaluation of the compositional and petrophysical properties is a necessity. Very high heterogeneity within shale successions has made similar types of studies challenging and very restricted using conventional cores. According to (Amaefule et al. 1993; Leverett 1941; Lucia et al. 2003; Pittman 1992), it is essential to take well log data into account. A comparison between well log and core data shows the accurate use of well logs in brittleness calculations (Saneifar et al. 2013). Moreover, the optimum fracturing design is important for the potential connection of shales' pathways. It enhances fluid flows through the reservoir to the well bore. Having high organic content and gas in place are significant factors for potential shale gas play. However, the production is directly related to hydraulic fracturing, especially if natural fracturing is lacking (Gupta et al. 2012). Natural fractures need to be connected by artificial fractures (King 2010). The significance of brittle shale reservoir is that they have the capacity to uphold fractures (whether natural or hydraulic). According to Rickman et al. (2008), the potentiality of brittle rock is determined by Young's modulus and Poisson's Ratio. The maintenance of the rock fractures is determined by Young's modulus. The higher the value, the better maintained are the open fractures. On the other hand, Poisson's Ratio determines the possibility of initiated fractures. The lower the values, the higher the initiation possibility.

4.3.1 Calculation of Brittleness Index from X-ray Diffraction Data.

Quantitative X-ray diffraction analyses provided precise mineralogy for seven Goldwyer Formation core samples obtained from six wells and five more samples from the Laurel Formation in four other wells in various sub-basins across the Canning Basin (Tables 4.2 and 4.3). The Brittleness Index was calculated for each sample using the Equation 4.7 to elaborate on the effect of mineralogy on the most prospective shale gas targets of the Canning Basin.

Brittleness index (BI) = (Qtz+Carb)/ (Qtz+Carb+Cly+ TOC) Eq. 4.7

Where:

Qtz= Quartz Content, Carb= Carbonate Content, Cly= Total Clay Content

117

BI values are directly affected by mineralogy. The higher the brittle minerals such as quartz, feldspar and carbonates, the higher the brittleness of the shale rock (ex. Willara#1 0.71BI, Goldwyer#1 0.56BI and Dodonea#1 0.84BI samples). Both clastic and carbonate content are high in these samples, compared to the others from the Goldwyer Formation. On the other hand, an increase in clay content of the Mclarty#1 and Solanum#1 samples resulted in a significant drop of BI values (0.49 and 0.51 BI respectively). Comparably, the Laurel Formation has high brittleness content due to higher clastic over carbonate minerals in the Yulleroo#1 and Yarrada#1 samples from the Fitzroy Trough (Table 3.3).

Table 4.2 Brittleness Index from XRD mineralogy for seven core samples of the Goldwyer Formation in the Canning Basin.

Well Name	Depth (m)	Qtz+Feld. %	Carb. %	Clay. %	TOC wt.%	BI
Willara#1	2376.83-2379.88	20.6	42.7	25.8	0.17	0.71
Goldwyer#1	981.1512-983.59	21.4	29.4	39	0.96	0.56
McLarty#1	2008.33	34.2	6.1	41.7	2.89	0.47
Percival#1	2065.50-2065.65	35.4	2.2	54	0.47	0.41
Solanum#1	360.0-360.10	32.6	13.6	45.2	0.97	0.5
Dodonea#1a	1542.37-1542.47	42.7	7.6	42	0.96	0.54
Dodonea#1b	1548.42-1548.51	20.2	52	13	1.45	0.83

Additional XRD data was obtained from the Western Australia Department of Mines open file records. The ternary diagram was created for the three main matrix components of each sample (Quartz and Feldspar, Carbonate and Clay minerals). Figure 4.16 shows the plot of the Goldwyer samples on the diagram. Majority of the samples are plotted on the line trending between Quartz + Feldspar and clay, with more fallen towards the clay end, which means moderate to low fracability. These

118

samples mostly come from the northern and central Broome Platform. A higher clastic and carbonate content matrix of the samples coming from the Southern Broome Platform and Northern Barbwire Terrace causes higher friability, where they are plotted near the Quartz + Feldspar and Carbonate ends (ex. SLMY1'1, SLMY1'2, DD1'1 and SLNM1 samples).
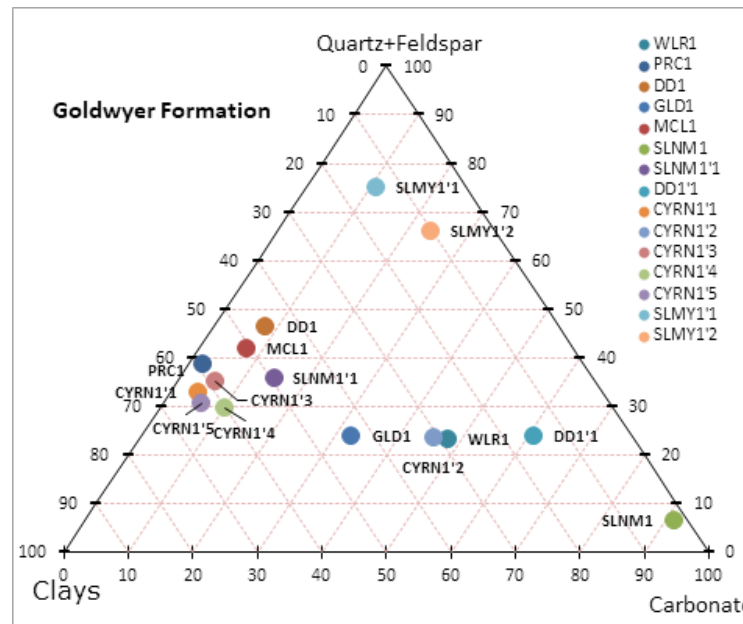
Figure 4.16 The ternary diagram shows the identification of shale gas fracability from XRD mineralogy for the Goldwyer Formation.

In comparison, majority of the samples, especially from the Yulleroo#1 well are plotted closer to the Quartz and Feldspar end in the ternary diagram (Figure 4.17). This would result in a higher fracability of the samples. The samples of the Laurel Formation come mainly from clay rich intervals, where the carbonate content is very limited or negligible.

Table 4.3 Brittleness Index using XRD mineralogy for the seven core samples of the Goldwyer Formation in the Canning Basin.

Well Name	Depth (m)	Qtz+Feld. %	Carb. %	Clay. %	TOC wt.%	BI
Blina#1	1114.3	25.5	1.6	49	0.55	0.36
Blina#1a	1118.5	29	10.4	33.1	0.41	0.54
Curringa#1	1869	16.6	28	27.8	2.89	0.62

119

| Yarrada#1 | 1825.8 | 49.9 | 2 | 25.1 | 0.57 | 0.67 |
| Yulleroo#1 | 3660.4 | 35.5 | 11.7 | 24.6 | 3.23 | 0.66 |
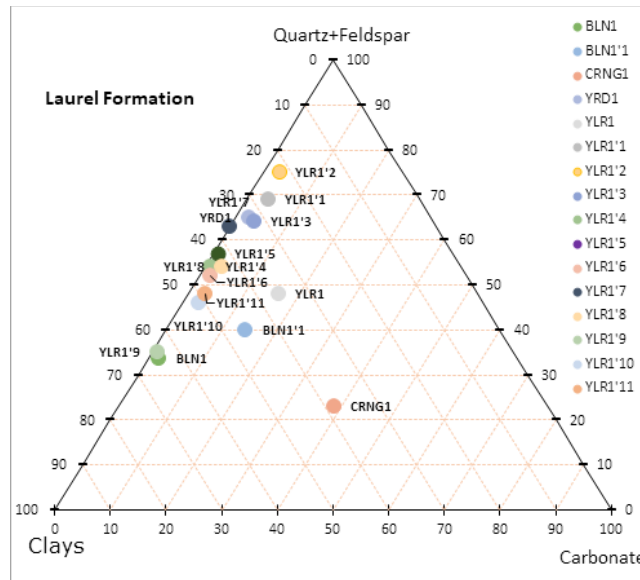
Figure 4.17 The ternary diagram shows the identification of shale gas fracability from XRD mineralogy for the Laurel Formation.

4.3.2 Estimation of Brittleness Index (BI) From Well Log Data

Because of data limitation in the Canning Basin and especially for the prospective Goldwyer Formation, an equation was obtained from the linear correlation between the compressional (DTp) and shear (DTs) sonic transit times obtained from the measured well log data. This will allow for higher resolution modelling of the Brittleness Index of the formation across a larger area of the basin.

Defining the brittleness of shale reservoirs helps to achieve desirable fracturing results. Young's modulus and Poisson's ratio are the two elastic properties used to determine the fracibility behaviour of the rock matrix. They can be directly calculated from sonic compressional, shear slowness and density logs. To obtain these two dynamic values for the Goldwyer Formation, sonic well log data was analysed from twenty wells in the Canning Basin. Two of which had both compressional and shear sonic transit times (DTp and DTs respectively) measured. Correlations were made between Vp (compressional velocity) and Vs (Shear velocity) calculated from DTp and DTs respectively for the Looma#1 and Robert#1 wells (Figure 4.18). A good correlation was obtained and the correlation coefficient

of R^2 is 0.72. The resultant new equation $Vs = 0.55 * Vp - 47.54$ was then used to estimate Vs from the Vp in the remaining wells used in the study.
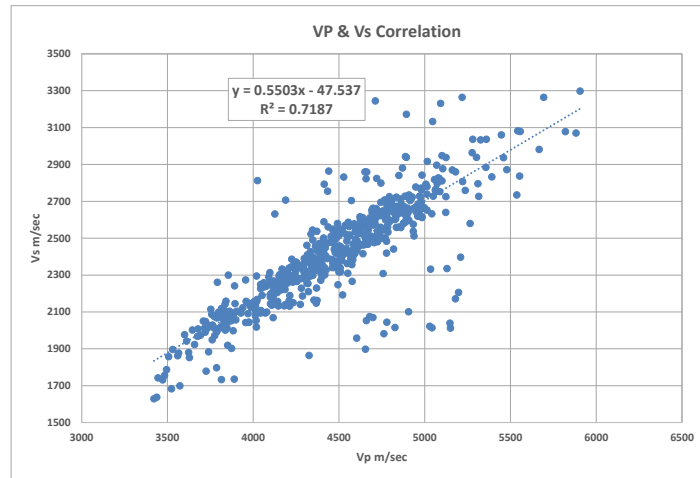
Figure 4.18 Cross-plot of Vp vs Vs from the Goldwyer shale in the Robert#1 well in the Central Canning Basin.

Krief et al. (1990) and Castagna et al. (1985) proposed two separate equations (Equations 4.8 and 4.9) to calculate shear wave velocity from compressional wave velocity. Both equations are Vp dependant and widely used amongst rock physics researchers. These equations were tested on the Goldwyer shale in the Robert#1 well. The resulted Vs was then compared with the real and estimated Vs, using the newly obtained equation from the aforementioned sonic logs correlation (Equation 4.10) (Figure 4.19). AS can be seen in the figure there is a good correlation between Vs calculated from the newly developed equation and measured Vs.
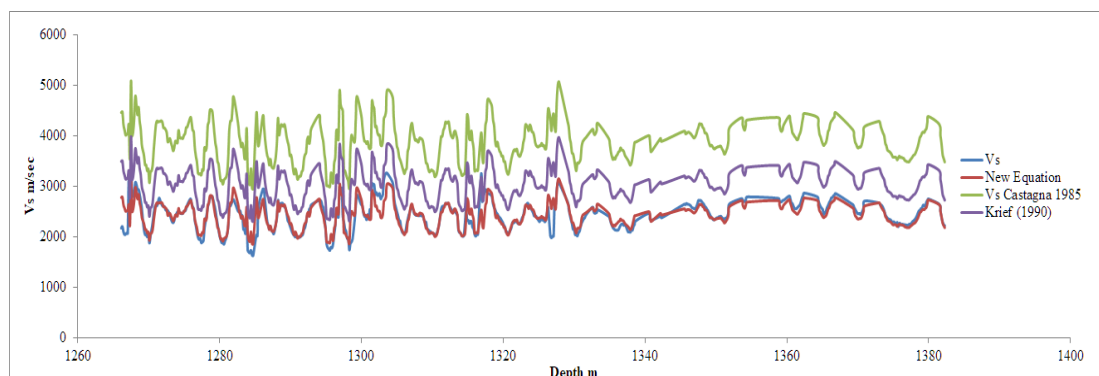
Figure 4.19 Comparison of Vs estimation using different inputs, an example from the Robert#1 well.

$$Vs = \sqrt{(0.452 * Vp^2) - 1.743} \quad \text{(Krief et al. 1990) Eq 4.8}$$

$$Vs = \frac{Vp - 1360}{1.16} \quad \text{(Castagna et al. 1985) Eq 4.9}$$

$$Vs = 0.55 * Vp - 47.54 \quad Sonic\ Velocity\ \text{Eq 4.10}$$

121

The dynamic Young's modulus and Poisson's ratio were calculated throughout the Goldwyer section in each well used in the study using Equations 4.11 and 4.12. A normalisation of the results was necessary to obtain the Brittleness Index (BI %). Young's Modulus values range from 1.6 to 4.5 psi and Poisson's ratio range from 0.25 to 0.35. Figure 4.21 shows the cross plot depicting the brittleness range of the Goldwyer Formation from Cyrene#1 in the Northern Broome Platform in the Canning Basin. The Z axis of GR on the plot highlights the increase of ductile content, such as TOC and clay minerals, which cause a reduction in the brittleness of the rock. The blue shaded area in the lower section of the composite log in Figure 4.18 corresponds to the high GR data on Figure 4.20. Both Figures 4.19 and 4.20 were created using the Interactive Petro-physics "IP" software.
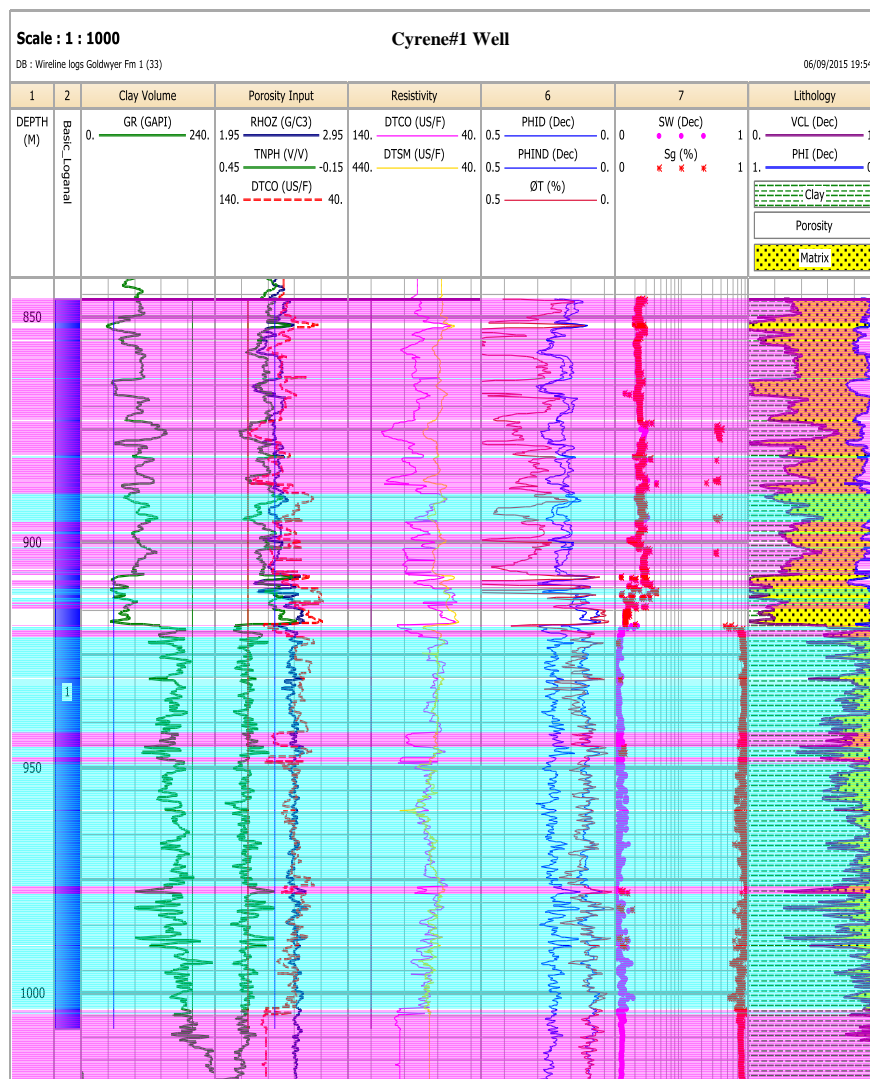
Figure 4.20 The composite well log of the Cyrene#1 well in the Northern Broome Platform.
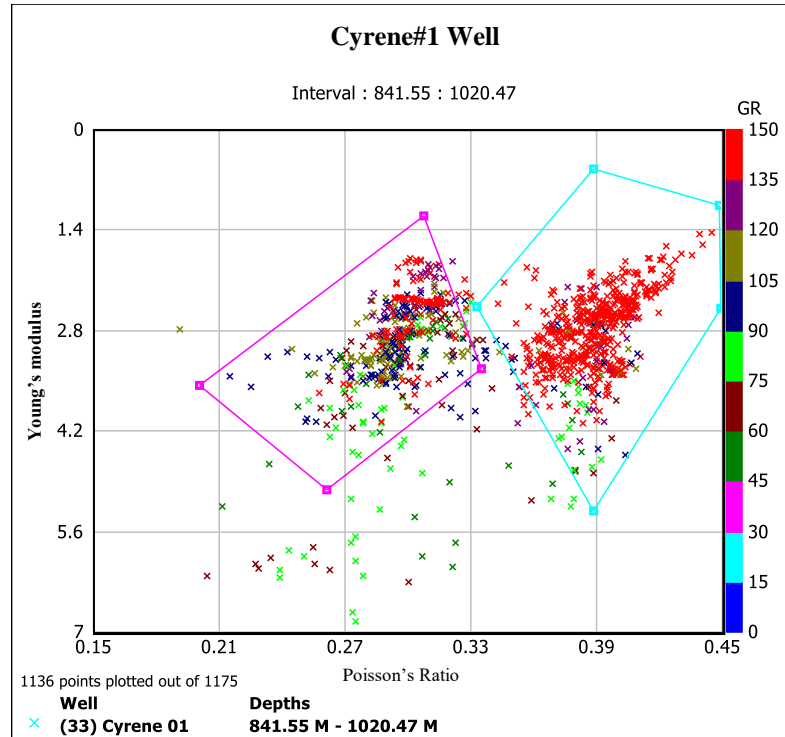
Figure 4.21 The left Cross-plot of Young's modulus and Poisson's ratio showing the brittleness average of the Goldwyer Formation from the Cyrene#1 well. The Z axis is that of Gamma-rays in API.

$$E = \frac{\rho Vp^2(3Vp^2 - 4Vs^2)}{Vp^2 - Vs^2} \text{ Eq. 4.11}$$

$$\mu = \frac{Vp^2 - 2Vs^2}{2(Vp^2 - Vs^2)} \text{ Eq. 4.12}$$

$$E_{brittle} = \frac{E - E_{min}}{E_{max} - Emin}$$

$$E_{brittle} = \frac{\mu_{min} - \mu}{\mu_{min} - \mu_{max}}$$

$$BI\% = \frac{E_{brittle}E + E_{brittle}\mu}{2} * 100 \text{ Eq. 4.13}$$

The Brittleness Index was estimated in 19 wells in the Central Canning basin. The lower shale section of the Goldwyer Formation was solely focused on, as it was considered to be the most prospective part. Using the Petrel software, the 3D property model, as shown in Figures 4.22 and 4.24 were created. Simultaneously, average 2D maps were created from these models in as shown in figures 4.23 and 4.25. Higher BIs were observed in the southern and northern regions of the Broome Platform (yellowish regions). The histogram of the model on the left-hand side of Figure 4.22 illustrates the data range between 35 - 65%. Well log data was used from six wells to calculate the Brittleness Index in the Barbwire Terrace. However, most of these wells are located in the northern part of the sub-basin. The average BI was

123

found to be 40 - 70% in most of this area. The central part of the terrace showed lower average BI of about only 40%. On the other hand, the southern part of the Barbwire Terrace has a lack of data due to the non-presence of wells (Figure 4.22 & 4.25).
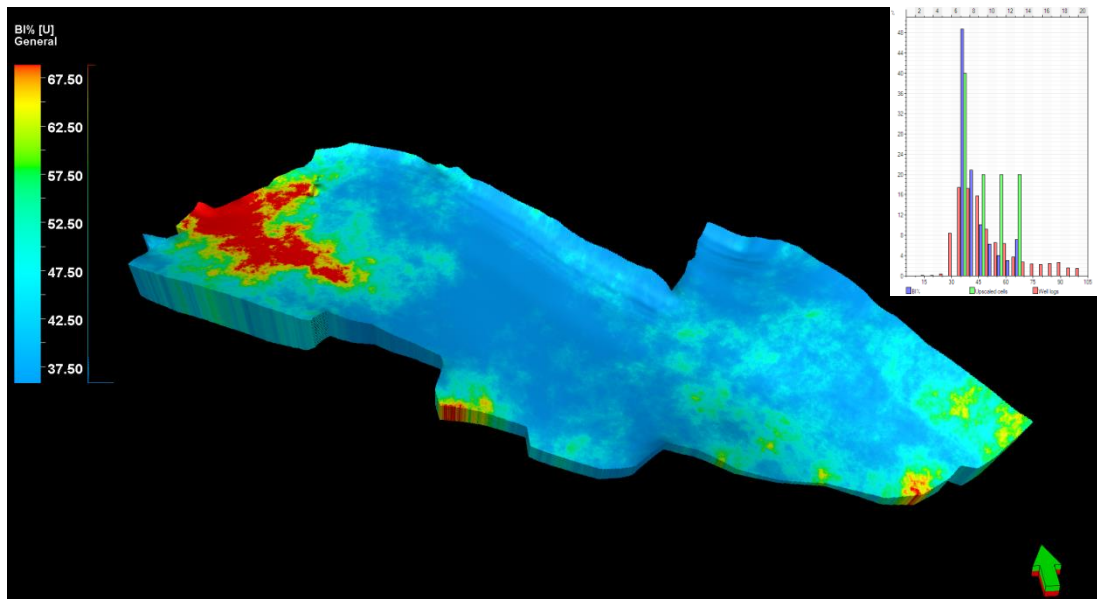
Figure 4.22 3D property model of log estimated Brittleness Index (BI) of the Lower Goldwyer shale in the Broome Platform, using the Petrel software.
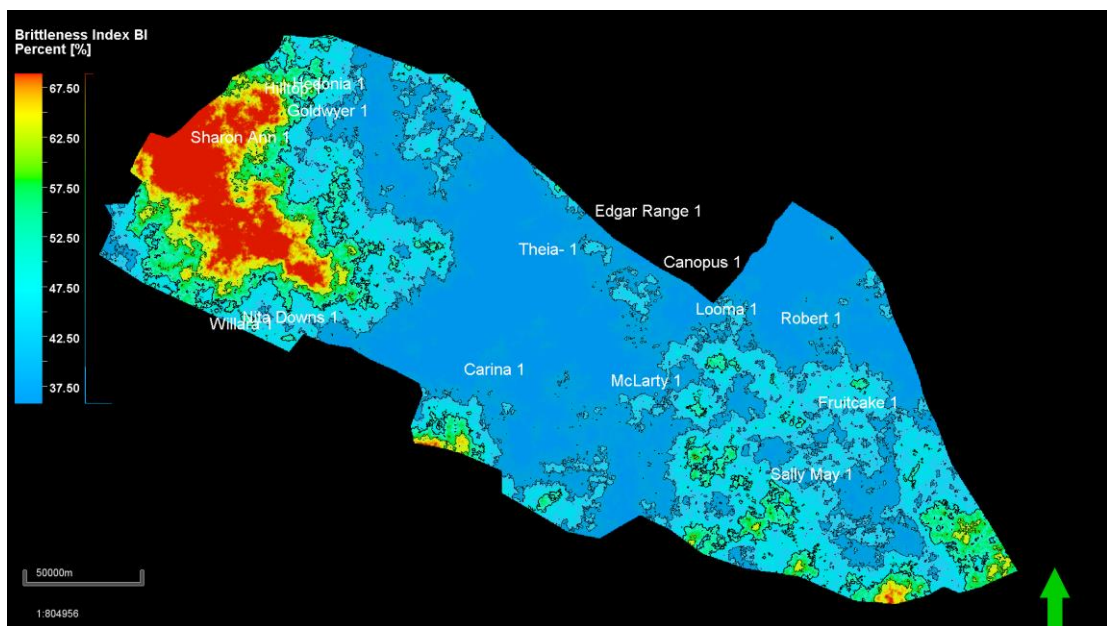
Figure 4.23 Average 2D map of estimated Brittleness Index (BI) of the Lower Goldwyer shale in the Broome Platform, using the Petrel software.
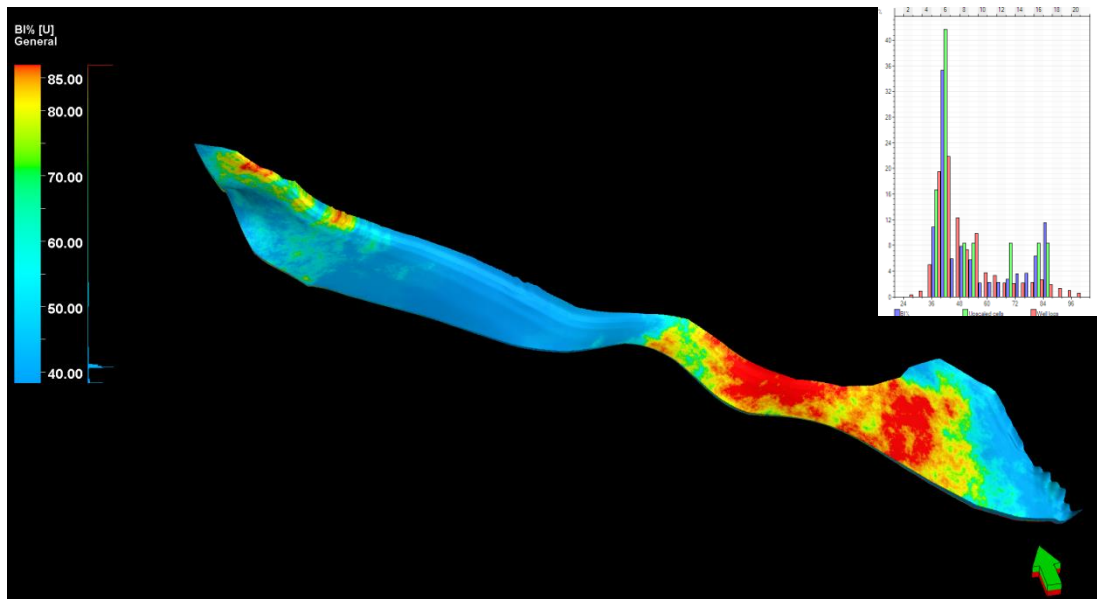
Figure 4.24 3D property model of log estimated Brittleness Index (BI) of the Lower Goldwyer shale in the Barbwire Terrace, using the Petrel software.
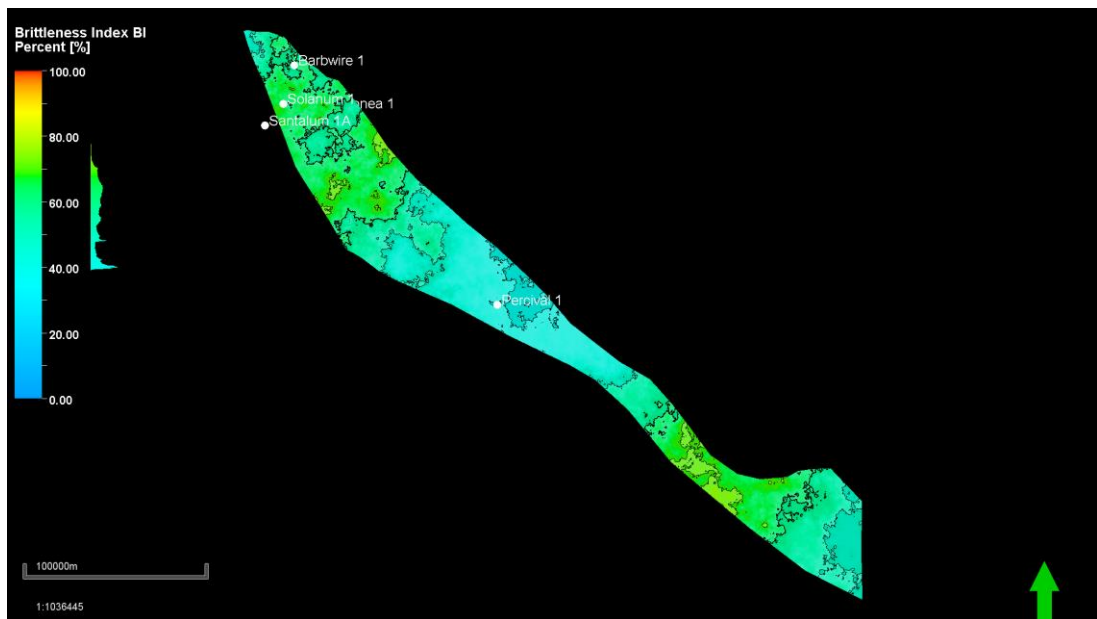
Figure 4.25 Average 2D map of log estimated Brittleness Index (BI) of the Lower Goldwyer shale in the Barbwire Terrace, using the Petrel software.

4.3.2.1   Estimation and Modelling of Total Porosity from Well Logs Data

According to (Sondergeld et al. 2010), the total porosity of shale gas reservoirs is highly dependent on the rock matrix and organic content. The presence of low density components such as organic matter impose the necessity of a special approach to evaluate the volumetrics of such a resource. Therefore, Sondergeld et al. (2010) proposed the following equations to calculate total porosity from the density log involving the total organic content and water saturation of the shale gas play:

126

$$\emptyset_{T} = \frac{\rho_{m} - \rho_{b}\left(\rho_{m}\frac{W_{TOC}}{\rho_{TOC}} - W_{TOC} + 1\right)}{\rho_{m} - \rho_{fl}}$$ (Sondergeld et al. 2010) Eq. 4.14

Where:

$\emptyset_{T}$ is the total porosity

ρ_{b} is the bulk density in g/cc

ρ_{m} is the matrix density in g/cc

ρ_{fl} is the fluid density (gas) in g/cc

ρ_{TOC} is the density of organic matter in g/cc

W_{TOC} is the organic content in wt.%

Assuming that the type of fluid is gas, and considering the variable gas density in shale gas formations, which is affected by fluid densities (either gas or water) in the formation and pressure, ρ_{fl} has to be obtained from the following equation:

$$\rho_{fl} = \rho_{g}\left(1 - S_{wT}\right) + \rho_{w}S_{w}$$

Where:

ρ_{g} is the density of gas in g/cc

ρ_{w} is the density of formatuion water in g/cc

S_{w} is the water saturation calculated from Archie's equation $S_{W_{archie}} = \sqrt{\frac{a}{\emptyset^{m}}\frac{R_{w}}{R_{t}}}$

R_{w} is formation water saturation, assuming 100% water saturation in the lean organic section

and when $S_{w} = 1$, Archie's equation can be rearranged to $R_{w} = R_{t-waterzone} * \emptyset^{m}$, where $m = 1.8$ for the shale matrix.

Due to the uncommon availability of both sonic and density logs for the same wells in the study area, TOC was estimated using the new Equation 4.6 that was obtained from the linear correlation of TOC and log density of the Goldwyer Formation in the Canning Basin. Consequently, the total organic porosity was estimated using porosity logs by applying equation 4.14 and. Step-by-step calculations were implied on each well in the study area. Specifically for this calculation, the following values are defined as:

$\rho_m = 2.65$ gm/cc, $\rho_{TOC} = 1.35$ gm/cc, $\rho_g = 0.09$ gm/cc, and $\rho_w = 1.05$ gm/cc,

Figure 4.22 shows the composite well log of the Dodonea#1 well. The total porosity range of the Goldwyer shale was found to be from 0.02 to 0.14 in the carbonate intervals. In the lower shale section of the Goldwyer formation, it was at an average of 0.05. Other porosity logs such as neutron porosity and density are plotted in the same track, the green and red curves respectively. The fifth track shows sonic (light blue colour) and deep resistivity logs (dark blue) overlaying each other. As explained above, the separation between the two curves highlights the variably of the organic content through the section, as well as gives an indication of the lithology variations that will have a direct significance on the porosity values.

The effect of organic content and lithology on the brittleness and porosity of the lower shale section of the Goldwyer Formation can be observed in Figure 4.26. The higher TOC content in the lower half of the shale section is correlated with lower BI and higher log porosity, despite the higher clay content. Core data observations confirmed the higher clay content in the lower section of the bottom Goldwyer shale, yet the porosity is high, which could be related to higher organic porosity. High GR readings in the first track also indicate more organic and fine-grained matrix. Chapter 5 has a more detailed lithofacies classification of the Goldwyer Formation.
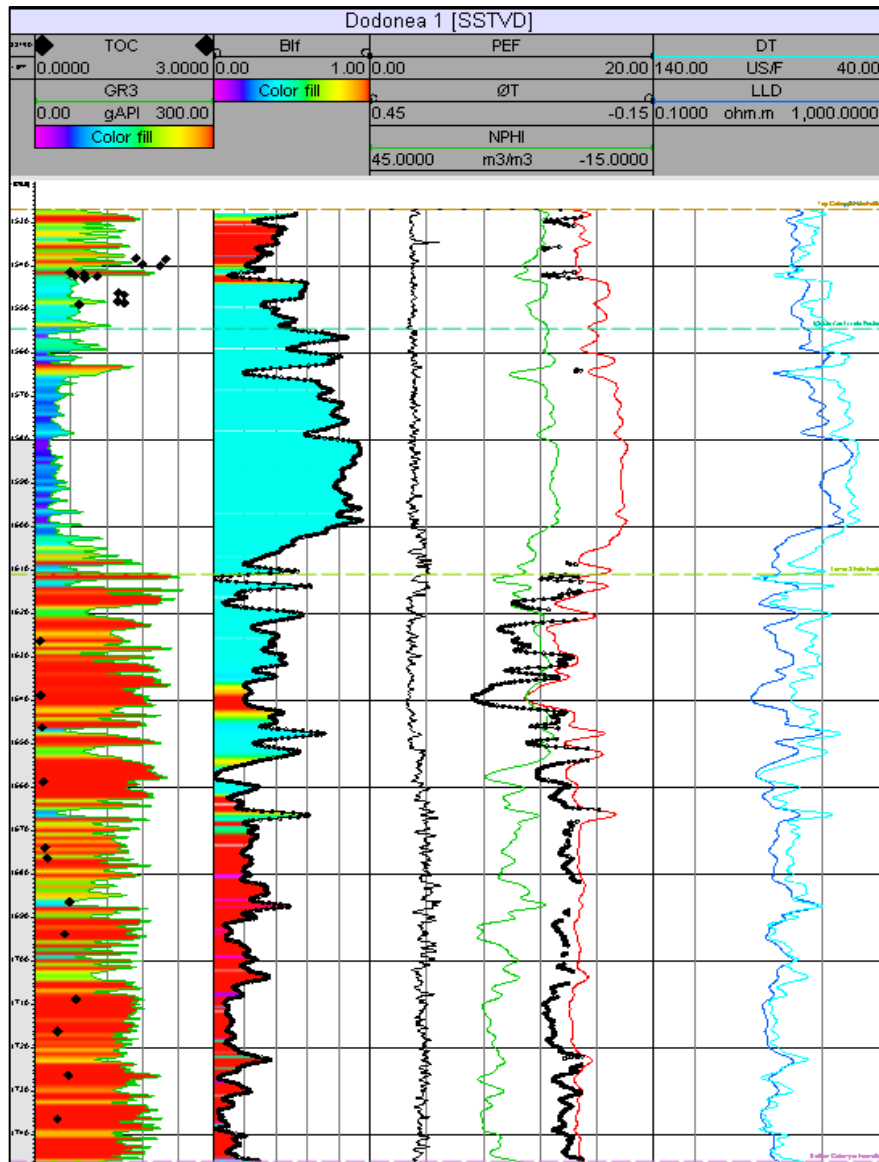
Figure 4.26 **The composite well log from the Dodonea#1 of the Goldwyer Formation in the Barbwire Terrace. The first left-hand track measures depth in meters. The second track measures Total Organic Content (TOC) in wt.% and gamma ray in the API logs. The third track shows the Brittleness Index (BI) calculated from the log data using the procedure explained earlier in this chapter. The black dotted curve in the fourth track is the estimated total porosity, estimated from Equation 3.14 in this section.**

Following the sweet spots identification objective of this research, as well as the use of well log data to increase the resolution of the results and to create a 3D model and average 2D map of the prospective shale gas Goldwyer Formation, 3D property models were created for the estimated total porosity in the Broome Platform and Barbwire Terrace across the Central Canning Basin. Average 2D maps were also created from these models. The distribution of the total porosity in the Broome Platform can be depicted in Figure 4.27 and 4.28. Higher porosity values are seen

towards the central and northern parts of the platform, and to the far end of the south-eastern margins (yellow and red portions); however, well data is limited in the southern parts of the area, which may raise some concerns on the credibility of the results. Generally, the average porosity in the modelled area is around 6% (light blue regions). In the Barbwire Terrace (Figure 4.29 & 4.30), the average porosity is about 5.5%, with significant increases toward the far end of the terrace, where it reaches about 14%. This could be related to the higher carbonate content in the Barbwire Terrace, as compared to the Broome Platform.
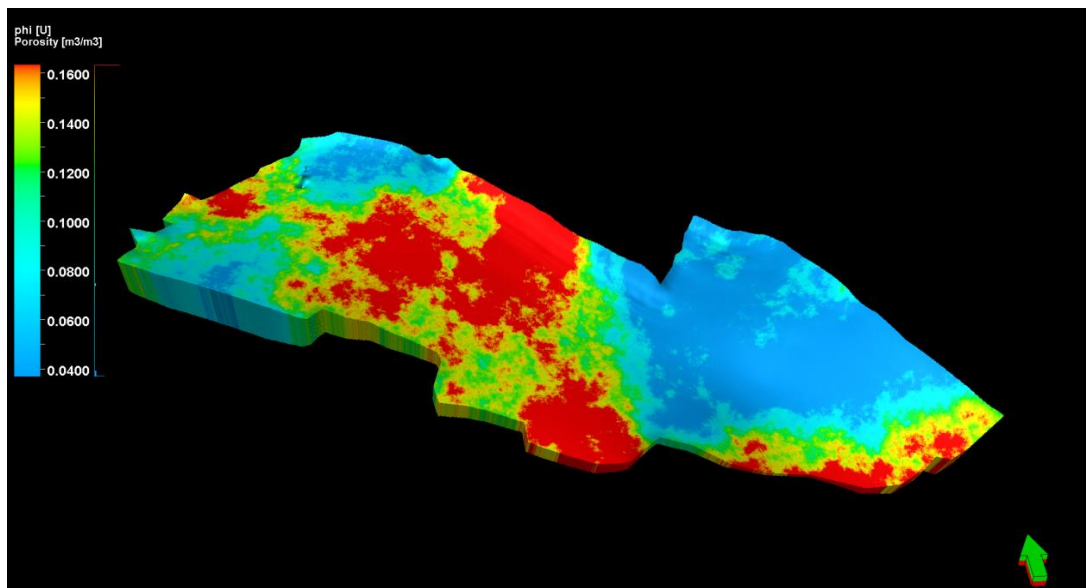
Figure 4.27 3D property model of log estimated total porosity of the Lower Goldwyer shale in the Broome Platform, using the Petrel software.
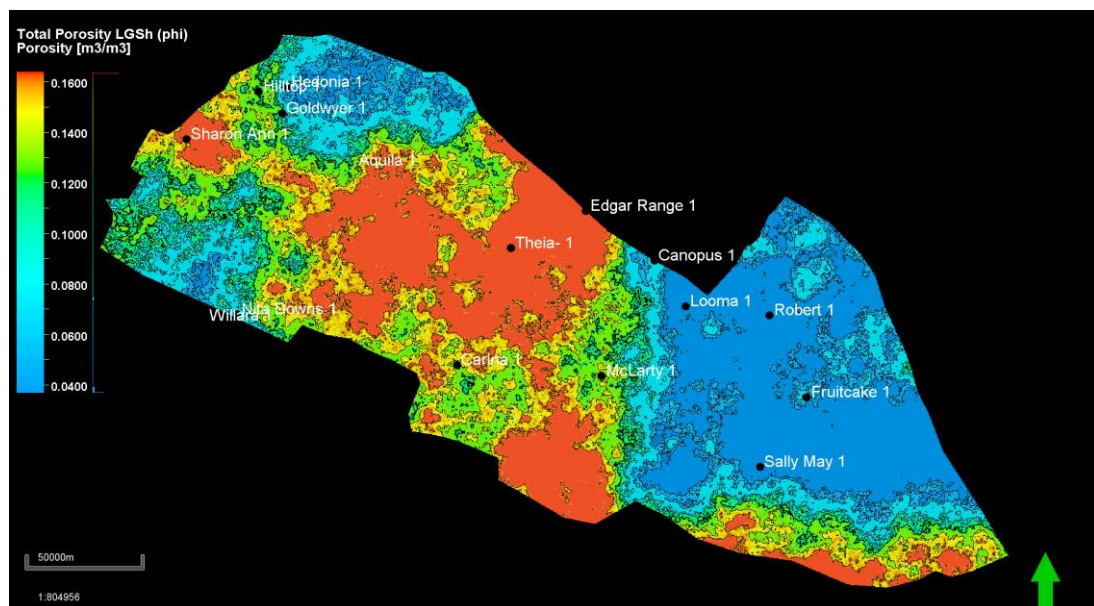
Figure 4.28 Average 2D map of log estimated total porosity of the Lower Goldwyer shale in the Broome Platform, using the Petrel software.
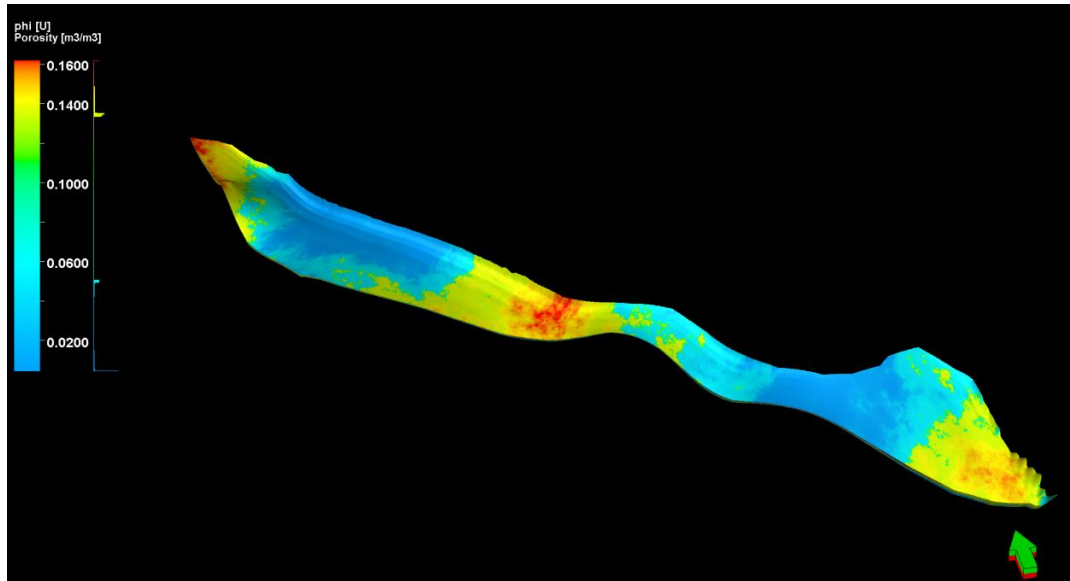
Figure 4.29 3D property model of log estimated total porosity of the Lower Goldwyer shale in the Barbwire Terrace, using the Petrel software.
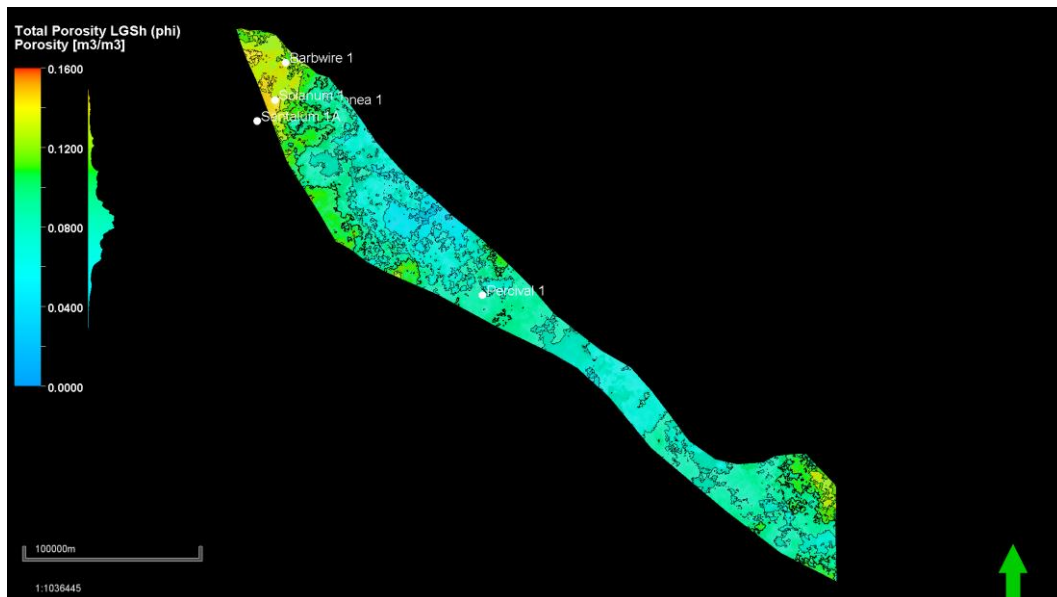
Figure 4.30 Average 2D map of log estimated total porosity of the Lower Goldwyer shale in the Barbwire Terrace, using the Petrel software.

5. Chapter 5: Lithofacies Analysis and Sequence Stratigraphy of the Goldwyer Formation

5.1 Background

Shale composition heterogeneity is the result of different formation processes in the sedimentary environment. Depositional drivers include reworking and wave base, turbidity flows and oceanic slop deposits, etc (Myrow et al. 2010). Vertical and lateral grain size dissimilarity is one of these characteristics. However, the

shale presents some common features, such as cross and planner bedding and lamination, living borrows, increasing and/or decreasing upward grain sizes and stacking patterns. The accumulation of thick mud deposits can be found in both shallow and deep marine conditions (Slatt and Abousleiman 2011). Shale deposits can be divided into two main components: organic and inorganic. Plant and/or algae remains, spores and biogenic quartz such as spicules and Paleozoic planktonic are the constituents of the organic portion in shales. On the other hand, detrital quartz, feldspar minerals, calcite apatite and clay minerals form the inorganic portion. The compaction and dissolution of silt or mud size grains is caused by burial. This will introduce minerals such as spherite, siderite, quartz and autogenic clays. The geomechanical properties of shale are highly affected by texture and composition. The platy structure of the shale rocks, which is the result of the depositional process, is the usual cause of the fracibility of the rock. During the deposition and compaction of shale, strata boundaries (which forms weakness planes throughout the rock's matrix) between laminae and/or layers are created. A significant amount of shale porosity is contributed by organic porosity; however, it is only recognized under high resolution SEM images (Slatt and Abousleiman (2011)). A wide range of lithofacies is present in gas shales. A diversity of mineral composition can be seen over the systematic stacking patterns of the gamma ray log. Gamma ray parasequences can be used as a brittleness indicator for shale successions. The increased upward GR values indicate an increased organic, phosphatic and clay rich content, which means an upward increase of ductile composition. On the other hand, a decreased upward GR refers to the increased upward calcite and quartz rich content, which means an upward increase of brittle content.

A detailed lithofacies study gives a proper identification of the sedimentary environment and depositional conditions of the rock (Abouelresh and Slatt 2012). An identification of the sequence stratigraphic framework is highly dependent on the interpretation of the depositional stacking patterns, as well as the sequence and parasequence boundaries created by the deposition and erosion of the rocks in the basin. The use of the radioactive gamma ray log was highly recommended by Abouelresh and Slatt (2012) to study the lithofacies and sequence stratigraphy of fine-grained shale rocks. The major components of the sequence stratigraphy are

system tracts, sequence and parasequence components and bed-sets. The condensed section (CS) of the stratigraphic sequence is usually characterised by high organic and phosphate content. This will create a high gamma ray response that can be easily distinguished from the other facies on the log. The gamma ray log counts the presence of radioactive minerals (K, Th and U) within the shale (Hampson et al. 2005), which can be used to identify the source, as well as the depositional and diagenetic processes that occurred to the rock. For instance, rich potassium and thorium mud deposits indicate fast sedimentation rates and the terrestrial origin of the inhabited minerals (Paxton et al. 2007). On the other hand, low sedimentation rates in anoxic conditions will produce mud deposits rich in uranium. Organic deposits, phosphates and uranium bearing minerals are examples of such sediments. However, a high mobility of uranium needs to be considered during the interpretation to avoid errors. According to Slatt and Rodriguez (2010), the limitation of biostratigraphic data in Paleozoic sedimentary rocks is the main cause of the insufficient recognition of the stratigraphic framework in these rocks. Thus, it was necessary to rely on lithofacies interpretation and stacking patterns (Schwalbach and Bohacs 1992). Singh (2008) made use of the gamma ray stacking pattern in his study of fine-grained sedimentary rocks (Figure 5.1). They classified three types of gamma ray patterns according to the vertical changes of the gamma ray log responses. They used the term, "Upward-increasing GRP", where rich organic deposits gradually replaced more carbonate or shaly deposits in a relative rise of sea level or retrogradational deposition of the shoreline. The second term used in their classification was the "Upward-decreasing GRP". It describes the gradual replacement of rich organic deposits by more shaly or carbonate deposits, during a drop of relative sea level or progradational deposition of the shoreline. In some cases, the relative sea level is constant, where no distinct change can be seen on the gamma ray log of the depositional environment. The term, "constant GRP", is used in this case, indicating a similar lithology across the facies.
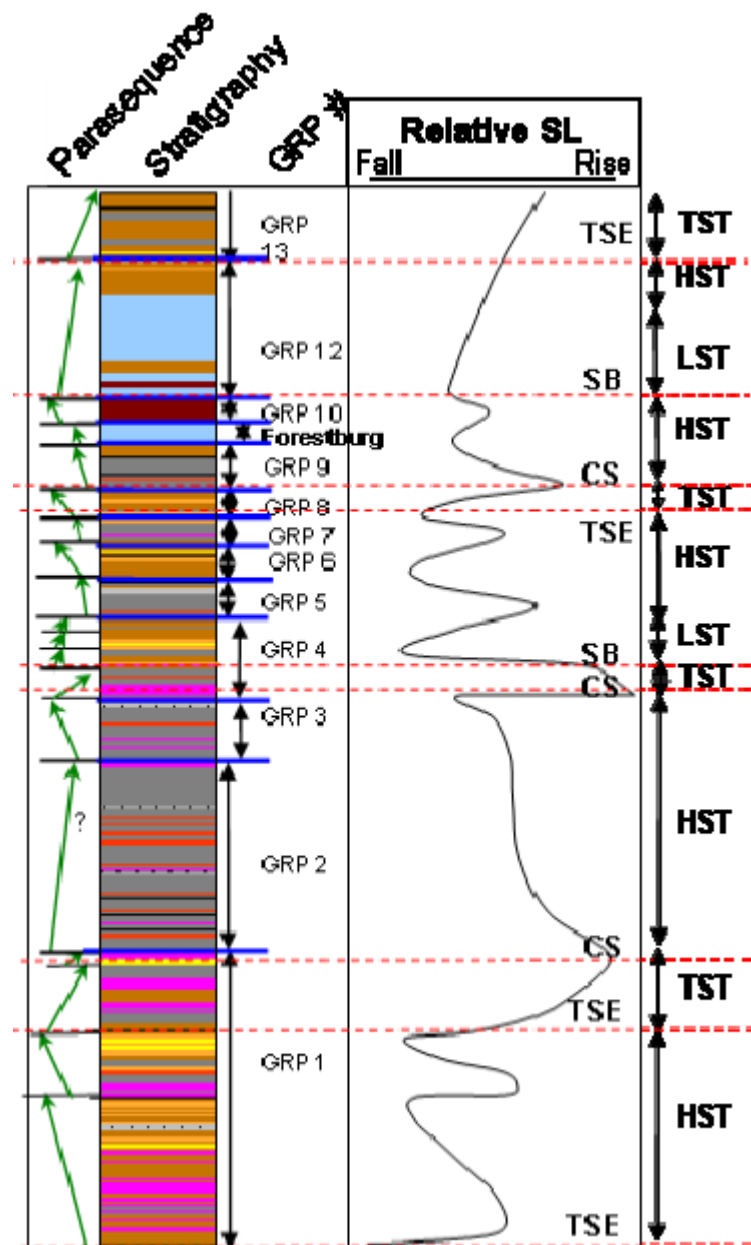
Figure 5.1 Gamma-ray parasequences and sequence stratigraphy interpretation in shale successions (Singh 2008).

5.1.1 Elements of sequence stratigraphy

Sequence stratigraphy describes the distribution of strata in a given space and time lapse. It is highly dependent on the interplay between the sediment supply and accommodation space, which can be obtained from the architecture of different depositional facies in the basin. This relationship results from the relative interaction between eustasy, climate and tectonics. The amount of sediments that can be precipitated in a basin is controlled by the accommodation space. The formation and destruction of accommodation is controlled by tectonism (Emery

134

and Myers 2009). Two forms of tectonism are present: extensional subsidence or lithospheric flexure. High frequency sea level changes are created by syn- and post-rift megasequences in the marine basins. A deficiency of high resolution biostratigraphy in Palaeozoic shale sediments makes it more difficult to develop higher order stratigraphic sequence. This will produce more complex stratigraphy of low frequency cycles that have been superimposed by higher frequency cycles of the Mesozoic sediments (Slatt and Rodriguez 2012). The thickness trends and resolutions of these facies are of great importance for shale gas evaluation and modelling. As a factor of oxygen conditions, the relative hydrocarbon potential index (RHP) can be used as a sea level indicator. A coupling of the sequence stratigraphy model with seismic data will provide a privilege model for organic facies' modelling and correlation.

The old known sequence stratigraphy term is now applied directly to shale gas reservoirs. It involves the use of analysis and principles of the depositional cycles in a relative manner. The relative rise and fall of the sea level records in the stratigraphic strata is interpreted. For example, the "High-Stand System Tract" term (also known as "Transgressive System Tract") is used, where a slow sea level rise leaves rich organic fine deposits at the top of the succession. This usually overlies the Transgressive System Tract deposits that result from a rapid rise of the sea level. At the bottom of the succession however, there are usually coarser deposits of the "Low-Stand System Tract" (also known as "Regressive System Tract") present and these were accumulated due to the falling and turnaround of the sea level at the earlier stages of deposition (Figure 5.2).

Specific Sequence stratigraphic units are correlated using the discipline of Sequence stratigraphy. They are marked by either changes in sea level or sedimentary supply or both. Each unit of sequence in sequence stratigraphy is bounded by unconformity or its correlative conformity.
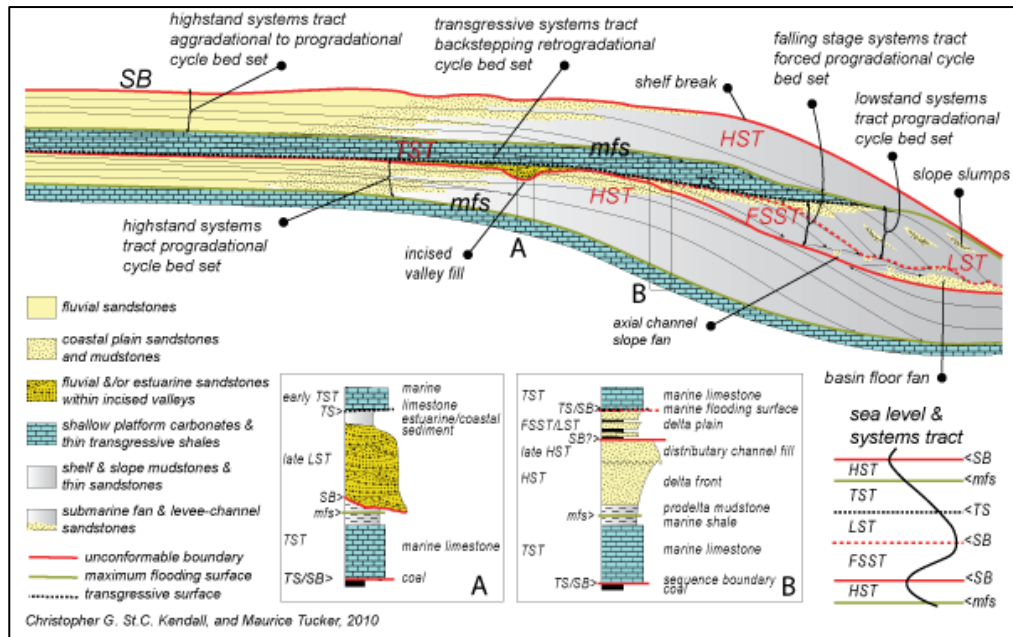
Figure 5.2 Lithofacies and sequence stratigraphy as a result of interaction between the relative sea level and sedimentary environment (Christopher et al. 2010).

5.1.2 Concept of sequence stratigraphy

A detailed observation of different data types such as petrographic, sedimentological, and geochemical analysis provides a high resolution sequence model, by looking into the smallest possible depositional cycles of the column. Originally, only large-scale sequence stratigraphy was defined where the lateral distribution and chronological order of the stratigraphic unit are only defined at large scales on the super-group level. This large-scale observation avoided the use of sequence stratigraphy in petroleum exploration at the time. However, the development of the sequence concept in the 1970s (which was then defined as "a relatively conformable succession of genetically related strata bounded by unconformities or their correlative conformities") allowed for the interpretation of smaller scale cycles, which was effectively applied in petroleum exploration. Thereafter, higher resolution data sets such as well logs and core data were also used in sequence stratigraphy. This extended the use of sequence stratigraphy to production and fluid flow technology. Different data sets will produce different types of sequence study and yet lead into different approaches. Those types were proposed by a variety of researchers. For example, (Hunt and Tucker 1995; Mitchum Jr 1977) proposed the transgressive regressive (TeR) sequences stratigraphy, while the genetic sequence stratigraphy was proposed by (Frazier 1974; Galloway 1989).

136

Because of common stratigraphic frameworks, the aforementioned types of sequences studies may temporally or spatially overlap at any scale. This elevated the need for a new definition of sequence stratigraphy that will accommodate all variations. The definition, "a cycle of change in accommodation or sediment supply defined by the recurrence of the same types of sequence stratigraphic surfaces through geologic time", by (Catuneanu and Zecchin 2013) is then used to overcome the overlap of the various definitions. The concept of sequence stratigraphy was then classified into the first, second, third and fourth order scales. The classification is based on the accuracy and resolution of observation that was developed in accordance to the sequence concept through time. Consequently, the evolution of the sequence concept indicates that sequence stratigraphy can be applied at different scales of observation, which corresponds to different hierarchical levels. Following this classification, sequence stratigraphy from the 40s to 60s of the 20th century is considered second order. These are regional lithostratigraphic sequences that cover a large scale of transgression-regression marine cycles (Sloss 1963). Contentiously, a low rank or third scale sequence now refers to the seismic stratigraphy of the 70s era. This has recently been developed into the sub-seismic scale that is referred to as the fourth order sequence. A high resolution sequence is defined as high-frequency sequence stratigraphy. The parasequence letter is then used to highlight the fourth order sequence stratigraphy of the seismic scale (Duval et al. 1998; Schlager 2010; Van Wagoner et al. 1990). It also includes low rank cycles that are termed "parasequences". The complexity comes from using a single term to define such various scales of observation.

In the hierarchy of sequence stratigraphy, all lower ranks (higher resolution sequences) come under the first order sequence (Catuneanu 2006). Therefore, similar features can be observed throughout the different scales. A similarity is usually linked to the sediment supply and tectonics. Moreover, the shoreline direction and type of shift is one of the main controllers of the sequence boundaries.

5.1.2.1 Allocyclic controls on sequence development

Einsele et al. (1991) defined "allocyclicity" as those external factors such as climate, eustasy and tectonic that have an external control upon the depositional system of a sedimentary basin. They directly affect the architecture of the sedimentary basin as they influence the sea level, depositional rate and/or sediment

supply, energy and sequence boundaries at a larger scale. An evidence of both eustasy and tectonic controls on sequence stratigraphy have been recognized since 1988 (Cloetingh 1988; Posamentier et al. 1988; Vail 1991).

In some cases, depositional cycles might be created by fault-related subsidence rather than global eustasy (Dorsey et al. 1997). Episodic fault-controlled subsidence was also considered (Cloetingh 1988). Syn-depostional tectonics was found to have a direct effect on sequence architecture produced by changes of eustasy. It is usually associated with normal faults, folds and in some cases, with active uplift (Catuneanu and Zecchin 2013). An interplay between the sediment supply and tectonics controls the movement of the shoreline. The deposits of transgression and/or regression surfaces and the resulted depositional trends can be directly related to these movements. On the other hand, the ongoing structure type and distribution controls the lateral changes of sequence architecture. Sediment supply and composition are highly influenced by climate changes, which can be observed from sequence stratigraphy and depositional trends. This enhances the use of sequence stratigraphy to identify the paleo-environment of the sedimentary basins (Cecil 1990; Feldman et al. 2005; Leeder et al. 1998). An example might be carbonate productivity and decreased fluvial run-off deposits in the Mediterranean Sea.

5.1.2.2 Autocyclic controls on sequence development

Sediments progradation and retrogradation are the result of internal depositional factors that are unrelated to changes of climate and sea levels (Einsele et al. 1991). The term used is "autocyclic" depositional factors. Although internal depositional factors play a role within the depositional system itself, such as river mouth diversion causing delta lobe switching, their extent may create a shoreline shift. This shift in the surrounding depositional system may produce related system tracts of sequence stratigraphy.

A continued sea level rise may cause landward shoreline progradation, which is called "autotreat". This is the result of the increased size of the depositional system due to the constant sediment supply and creation of accommodation space (Muto and Steel 1992). Progradation is created when the accommodation space growth is faster than the sediment supply. Bounded surfaces of sequence stratigraphy are created by an interplay of accommodation space and sediment supply that produces system tracts. The transgression system tracts are usually followed by regression

system tracts made by shoreline reorganisation. A quantification of the relative contribution of accommodation space and/or sediment supply is unattainable because of the constant relationship between the internal and external depositional factors in the same environment. Regardless the process type, be it allogenic or authogenic, sea-level movement plays a substantial role in forming the architecture of the sedimentary basin, where all depositional factors may play a role in creating sequence stratigraphy. The interplay between the sediment supply and accommodation space draws the architecture of the sequence surfaces. Moving seawards, erosion and forced marine regression and the formed relative conformities are produced by only relative changes of the sea level (Zecchin and Catuneanu, 2012). Moreover, the allogenic sequence controls are superior in most sequence stratigraphic mechanisms. Sediment supply-related surfaces might also be created by autogenic controls. In some cases, sedimentary environments affected by the autogenic mechanism may exceed those of allogenic effects (Muto et al. 2007). This may extend to cover hundreds of square kilometres.

5.2   Lithofacies and Visual Core Observation

The Goldwyer formation was studied in details on a 407.5 meters fully recovered core from the Theia#1 well that is stored in the Perth Core Library. Full access to the visual and digital core data was provided by Finder Exploration and the Department of Mines and Petroleum of Western Australia. A high frequency centimeter scale of observation was followed throughout the section. The criteria of facies changes such as color variations, lithology, organic content, and sedimentary structure and texture was used to classify the different lithofacies and stratigraphic intervals of the formation. The resulted classification is as follows:

5.2.1   Silty mudstone (Concretionary)

This is the main facies of the Lower Goldwyer shale. It consists of dark grey to black silty mudstone, rich organic, pyritic in place to rich pyritic, and has gradational to sharp contacts (Figure 5.3A). It is also composed of light grey calcareous concretion, nodular to lenticular that forms clusters of semi cyclic intervals ranging from a few centimetres to about half a metre thick. These intervals are interbedded with the silty mudstone. The sedimentary structure is dominated by massive to thin bedding. The average clay content of this facies is 60%. Carbonate content is present and there is concretion in various quantities across the facies. The average pyrite is 3%, while the

average organic content is 4.0 wt.% TOC, which reflects the anoxic depositional conditions: rich in trilobites and graptolites usually full with some broken shells.

5.2.2 Calcareous silty mudstone

This facies is present throughout the Lower Goldwyer shale. The stripy to thinly laminated sedimentary structure is common in this facies due to the rich calcareous and silty content. Calcareous intervals presents as a low angle cross lamination that occasionally develops to become lenses (Figure 5.3B). They also create weak planes across the facies. Calcareous concretion is very rare to absent here (light grey to grey). Also, poor to low bioturbation may affect the preservation of organic matter in this facies (low to high organic content of 0.5 - 3.0 wt.%). The low TOC and calcareous content of this facies is related to the oxic conditions and shallower depth of the water.

5.2.3 Heterolithic lenticular wackestone–packstone & silty mudstone

This facies is characterised by the alternative lamination of wackestone-packstone and silty mudstone. This way of lamination indicates the fluctuation of the sea level in the marginal basin area: partly to well-bioturbated, lenticular bedding and ripple cross-lamination sedimentary structure. There is the compaction and disturbance of sediments around the nautiloids, due to the sediments load in place. Occasional carbonate concretion is contained within this facies. The reworking in the relatively shallower water produced the bioturbation and lenticular bedding of the wackestone-packstone beds. It has low to moderate organic content. Low current and storm base waves are also well-preserved (Figure 5.3 C & D).

5.2.4 Bioclastic/intraclastic grainstone and silty mudstone

It is a poorly sorted facies consisting of nodular limestone interbedded with dark grey to black silty mudstone, light grey grainstone, grain-supported and fossiliferous. It is moderate to well bioturbated (Figure 5.3 E), has a shallow marine environment of high energy deposits and low to moderate TOC (0.5 to 2.06 wt.% in black mudstone). The facies is mainly found in the base of the Goldwyer Formation in sharp contact with the top underlying Willara Formation (Figure 5.3F). It represents a high energy condition created by the wave currents.

5.2.5 Bioturbated wackestone–packstone

There are well to heavily bioturbated, 10-30 cm thick beds of wackestone to packstone facies. They are light grey to yellowish, having sharp to slightly gradational contacts, massive and variegated, as well as poorly sorted. They are associated with silty mudstone facies and lenticular bedded of heterolithics mudstone, as well as vertical and horizontal burrowing. There is a shallow depositional environment and medium energy, where bioturbation is active. Also, there is a presence of low organic content due to higher oxidation and borrowing activities (Figure 5.3G).
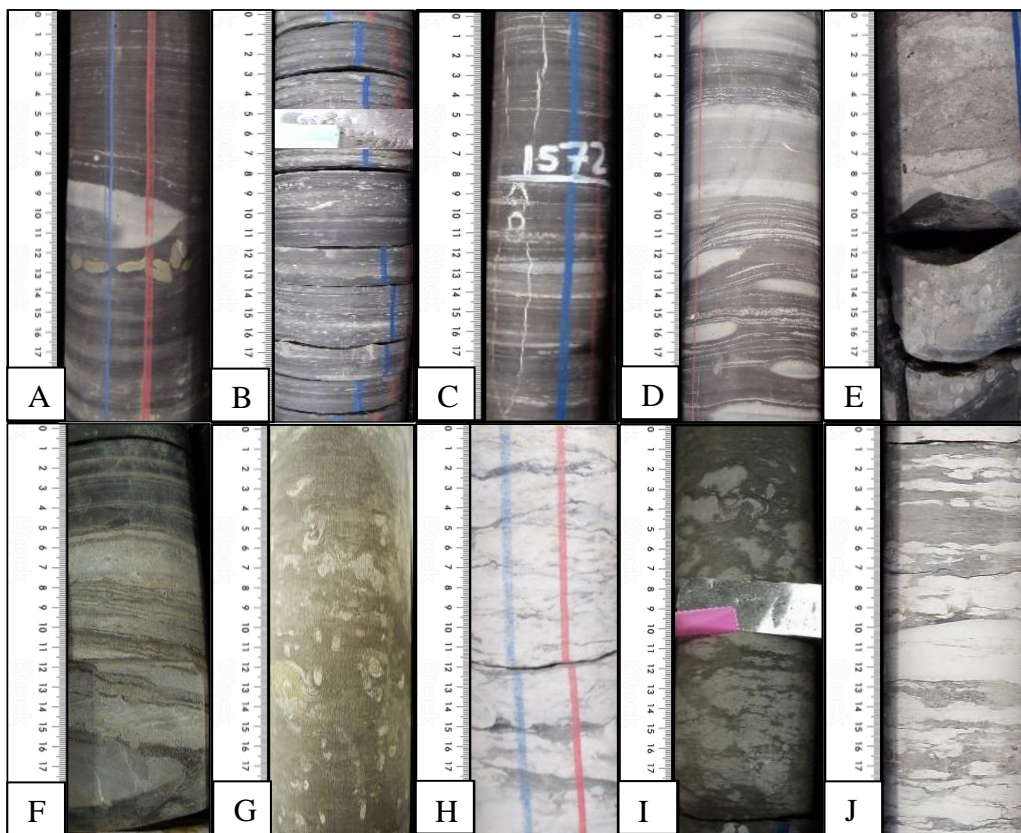
Figure 5.3 Core photos of various lithofacies of the Goldwyer formation showing: A. Calcareous concretion and nodular pyrite within rich-organic silty-mudstone; B. Planner lamination and bioturbation of calcareous silty mudstone; C. vertical fractures and silty and calcareous interlamination of silty mudstone; D. lenticular bedding and ripple cross-lamination of silty mudstone facies; E. Heavily bioturbation; F. Reworked wave base deposits (SB at the base of the Goldwyer Formation); G. Heavily bioturbated wackestone to packstone facies; H & I. Nodular limestone mixed with rich organic mud; J. Lenticular bedded light grey mudstone.

5.2.6 Nodular packstone–grainstone–rudstone

This facies is common through the Lower Goldwyer shale and middle carbonate unit of the Goldwyer Formation. It is composed of nodular limestone (packstone–grainstone–rudstone) and is sometimes slightly mixed with black silty mudstone, which has high TOC, and is light grey to yellow. The facies ranges from 10cm to

over 1.5m thickness in various intervals of the section. There is massive bedding, with some horizontal weakness points and bioclastic reworked debris in place. Also, there is a medium to high depositional environment, with medium to high energy and low TOCs (Figures 5.3 H & I).

5.2.7   Well Bioturbated Lenticular bedded Silty Mudstone

This facies is manly present in the Upper Goldwyer shale section. It is made of well-bioturbated lenticular bedded mudstone. Mudstone is dark greenish grey to black and the limestone nodules are light yellowish. The ripple marks the sedimentary structure with rich bioturbation and calcareous nodules. There is about equal proportion of lime to mud content, with sharp contacts with the overlain and underlying. Also, there is moderate to low energy, so thereafter, expected medium to low TOC. The average thickness ranges between 1.5 to 4 metres (Figure 5.3J).

5.3 Sequence stratigraphic framework of the Goldwyer Formation

To obtain a reliable stratigraphic model, it is important to use as much data as possible. The integration of geological, geophysical, geochemical and petrophysical data sets will enrich the stratigraphic interpretation. The approach itself is a conceptual depositional model that relays on genetic data (Catuneanu and Zecchin 2013). Within the last thirty years, sequence stratigraphy modelling process has shifted from genetic analysis to the field criteria process. This involves the use of interpretation of system tracts, stratal stacking patterns and environmental controls that create these features; which are the key factors that sequence stratigraphy is built upon. Therefore, many authors rely on sequence boundaries and stratal features, rather than the origin of those strata to build their sequence stratigraphic model. The interaction between those controls could make the interpretation very challenging because of the non-definite limit of one dominant identified factor upon others (Catuneanu and Zecchin 2013).

5.4.1   Stratigraphic Intervals

In this section Theia#1 (Figure 5.4) has been used as an example to show stratigraphic intervals used for Glodwyer sequence stratigraphic analysis.

5.4.1.1 1588.9-1595 m Interbedded Grainstone–Rudstone & Concretionary Silty Mudstone

This is a light-dark grey, sometimes black calcareous silty mudstone facies interbedded with the nodular to layered carbonate concessions. The mud layers are tilted around the concession where some fractures had developed (Figure 5.3F).

142

Carbonate concretion tends to form 20cm beds in some cases and carbonate lenses in others. The calcite cement fills the pore spaces which react with diluted hydrochloric acid. The facies in an overall progradational interval shows a decreasing upward gamma ray response (GRP1) (Figure 5.4). The TOC content of this facies is variable from medium to low, due to the fluctuation of the sea level; hence the presence of calcite and concretion. Thus, the sedimentary environment is characterised by medium to low energy and regarded to be relatively shallow, where occasional oxic conditions may occur (Figure 5.5).

5.4.1.2 1569.25-1588.9m Interbedded Calcareous Silty Mudstone and Concretionary & Heterolithic Mudstone

Dark grey silty mudstone is the dominant lithology of this facies. Thin layers of very fine sandstone and silty content driven by the shallow marine sedimentary environment create the ripple sedimentary structure in between the mud layers. The facies is characterised by occasional limestone concretions increasing upwards in abundance and less silty lamination towards the top of the interval. The sedimentary structures include ripple marks, striped, sometimes massive and with a calcite cemented texture (Figure 5.3 C&D). The TOC content is generally low, except for some black shale beds increased towards the top of the facies, due to relative sea level rise and increased anoxic conditions (Figure 5.5 TSL1 and RHP curve). Although there is an overall aggradational parasequence, these thin layers can be seen on the gamma ray curve as high API peaks (Figure 5.4 GRP2). The facies well represents the Lower Goldwyer shale with medium to low energy as it has sharp contacts with the underlying and gradational with overlain facies.

The cyclicity of calcareous silty mudstone, concretionary & heterolithic mudstone and thinner heavily beds of bioturbated heterolithic lenticular wackstone-packstone is well present. The wackstone–backstone facies is light grey, hard, pyritic and fossiliferous. The sedimentary structures also include lenticular carbonates concretion and vertical to sub-vertical fractures mainly at 1571.90 - 1572.10m. The top most contact of the facies is graptolite rich.

5.4.1.3 1527.57-1569.25 m Rich Organic Black Concretionary Silty Mudstone.

This is the most common facies across the Lower Goldwyer shale. It is made of dark grey to black silty mudstone. It becomes darker to the top, pyritic in places and sometimes rich (Figure 5.3 A). The presence of pyritic flakes, that in some

occasions develop to become thin beds of 3 – 5 cm thick, is an indication of the highly reduced sedimentary environment. The high concretionary silty mudstone is the dominant lithology of this interval. The concretion is light coloured, nodular to lenticular that forms clusters of semi cyclic intervals ranging from a few centimetres to about half a metre thick. These intervals are interbedded with silty mudstone. Less carbonate concretion is present from 1528.62 - 1540.05 m (mainly mudstone). There is also a high gamma ray response of alternative progradational and retrogradational depositional cycles (Figure 5.4 GRP3-6). GRP4 and GRP6 represent an upward increase of gamma ray parasequence due to the increased clay and organic content. GRP3 and GRP5 represent an upward increase of gamma ray parasequence due to the increased calcareous and quartz content. This facies is rich in trilobite, graptolites and broken shells. The broken shells may indicate transport from a nearby environment. They are usually related to siliceous mudstones.

The facies contains frequent 3 - 7 cm thick, dark brown, highly oxidized thin fissile layers of mudstone. The sedimentary structure is dominated by tilted mud layers around the carbonate concretions that may indicate the development of carbonate concretion during mud deposition and a compacted facies. The dissolution of some lenses of concretions provides secondary carbonate porosity within the mudstone layers. The interval is highly fractured from 1547.8 - 1544.20m, dominated by closed vertical to sub-vertical fractures filled with calcite cement. It is deposited in a possible deep marine sedimentary environment revealed by low energy and rich organic content, which is usually related to high sea levels (Figure 5.5 TSL2, 3&4).

5.4.1.4 1504.2-1527.57 m Sandy to Silty and Concretionary Mudstone
This is similar to the aforementioned interval (1569.25 - 1588.9m), but with less thickness of units and organic content. This can be seen on the depositional parasequences in Figure 5.4 (GRP7, GRP8 and GRP9), where a higher fluctuation of sea level is also present (Figure 5.5 TSL3 and RSL 2). Unlike the previous facies, the abundance of concretion decreases upward and the less silty lamination may indicate a reversible sea level trend. The facies becomes black shale, rich organic and more anoxic above 1518.7m (more anoxic conditions on the RHP curve), which confirms the deepening of the marine and low energy environment.

This lithofacies is composed of dark grey to black interlaminated calcareous silty mudstone with some inter-bedding of concretionary silty mudstone. It becomes less calcareous and striped towards the top of the facies. The concretionary silty mudstone is light grey carbonate lenses and nodules (Grainstone & Rudstone) and distributed within the silty mudstones. It is slightly bioturbated and occasionally pyrite rich. The concretion forms thin layers about 10cm thick. There is a low organic content below 1498.8m and thus a shallower environment that has higher energy conditions (Figure 5.5 TSL4 and increased RHP). The facies becomes cyclic heterolithics, concretions and bioturbated wackestone–packstone and silty mudstone from 1498.8 - 1474.21m. It contains repeated storm bed deposit intervals of about 20 - 50 cm thick. These are nodular packstones, grainstones and radstones, buff to light grey, nodular and highly bioturbated. The sedimentary structures include some ripple marks, calcite cement and stripy silty interbeds, laminated to banded and very low-angle cross-lamination. This interval is rich in trilobites pieces and full of graptolites and rare nautiloids. There is also sharp contact with the overlain and gradational with the underlying facies. However, the contact between the cycles is gradational. The top of this facies marks one of the highest gamma ray reading (GRP10, Figure 5.4) that reflects the maximum flooding surface (see the following section for more details). It is mainly an aggradational parasequence of black mudstone facies.

A black calcareous silty mudstone is present, becomes silty mudstone in place. This is followed by pyritic light yellowish stylolithic nodular limestone units with dark-grey to black packstone. The common pyrite along the bedding plains then becomes thick laminae. It shows very low angled to fade lamination (calcite filled) but is quite angled around the concretions. Very low to no lamination, with occasional ripple lamination, which consists of fossiliferous of trilobites, graptolites and broken fossil shells. There is also the presence of medium to high energy and moderate to low sea levels (Figure 5.5 RSL4). As seen in GRP11 (progradational), it depicts a significant increase of carbonate and silty content. There is very limited available geochemical data, as only a few data points show variable organic content

of up to 3.91 wt. % at 1472.10m. The contacts are graditional, with overlain and underlying facies. The facies is rich in trilobites, as pieces and fully preserved graptolites and rare nautiloids. The base of this facies is believed to be the boundary between the high stand system tract (HST) and the low stand system tract (LST), where a maximum flooding (MSF) surface has resulted. It is followed by a significant sea level fall that produced the middle carbonate facies of the Goldwyer Formation.

5.4.1.7 1427.5-1452.34 m Limestone

This facies was deposited in a continuous marine regression with some cycles of upwelling. The gamma ray parasequence is characterised by constant upward GRP (Figure 5.4 GRP12 and GRP14; Figure 5.5 ASL1). The base of the middle carbonate facies is mainly dark grey silty mudstone, rich in siltstone, light grey stylolite and limestone nodules decreased to nodular mudstone upwards. It becomes more of stylolithic limestone to the top of the facies. The heavily bioturbated dark grey to black mudstone is interbedded with bioturbated limestone, which is in massive units yellowish colour, moderate to thick bedding and are very finely grained. The facies is rarely stylolithic, with some silty mudstone inter-bedding. Also, there is low organic content and relatively high oxic conditions (Figure 5.5, decreased upward RHP).

5.4.1.8 1397.08-1427.5 m Interbedded Stylolithic limestone and silty mudstone (Bioturbated)

Light grey stylolite and limestone nodules decreased to become nodular mudstone upwards. Not only does it become mainly stylolithic limestone to the top, it is also more compacted at the top, slightly fossiliferous and sometimes with some bioturbation. The contact is gradational, with the overlain and underlying limestone facies. The shallow sedimentary environment is represented by the shelf deposits. High sea level fluctuation caused the deposition of various lithologies through this facies. Rich organic black silty mudstone (common reservoir facies) resulted from the sudden increase of sea level and increased water depth (Figure 5.4 GRP15). It represents lenses of pyrite caused by reduced depositional conditions (Figure 5.5, increased upward RHP). The lower 5 cm of each mudstone unit is black, but it becomes lighter coloured upwards. The highest TOC values of the Goldwyer shale is recorded in these units (up to 5.91 wt.%TOC). Mudstone is massive, hard, with very low to no lamination, and occasional ripple lamination. The interval has a

sharp contact with the overlain and underlying facies. The sea level is expected to be very high (TSL5 and TSL6), with rich organic content from 1422 - 1427.5 m and 1397.08 - 1416.25 m.

5.4.1.9 1367.4- 1397.08 m Interbedded Stylolithic- Nodular Silty Mudstoen and Concretionary Silty Mudstone

This is the top interval of the Middle Goldwyer carbonate. It consists of cyclic interbedded silty mudstone and limestone facies. The mudstone is dark grey to black calcareous that becomes silty mudstone sometimes. It is fossiliferous, has very low angle to fade and no lamination with pyritic lenses. The lower 10 cm is black but it becomes lighter coloured upwards. The grey to dark grey mudstone is interbedded with bioturbated limestone and calcareous mudstone. This causes the increasing upward GRP and overall retrogradational cycle (Figure 5.4, GRP17). A period of sea level fall however occurred at the base of this facies, causing the decreased upward GRP16. The sedimentary structures include stripy calcite lamination and some concretion. The interval has a gradual contact with the overlain and sharp contract with the underlying facies.

5.4.1.10 1297- 1367.4 m Interbedded Calcareous Silty Mudstone and Silty Stylolithic Limestone

This specific facies implies the cyclicity of thick intervals of calcareous silty mudstone (4 - 5 m thick) and silty stylolithic limestone (1 – 2 m thick), with some rich organic black silty mudstone beds. The overall depositional cycle is aggradational of generally high GR reading. The calcareous silty mudstone is grey to light grey, thinly laminated to slightly pyritic and is rich in bioturbation in parts. It is a relatively massive bedding, hard with no obvious fractures. There is sharp contact with the overlain and underlying facies. It is very low to non-organic, probably due to the interplay of the sea level that may have caused the activeness of scavengers. The interbedding limestone is yellowish light grey, which was formed due to the wave storm action (wave ripples) in the shallow marine shelf. The base of this facies would be a sequence boundary with the underlying carbonate facies, where a new sea level rise cycle has begun. It is fossiliferous and biturbated in parts and silty in others with a nodular structure, which becomes compacted at the top of each cycle. It has sharp contact with the overlain and underlying cycles. TOC is believed to be high in the black shale with the stylolithic structure, although geochemical data is limited.

5.4.1.11 1198.19-1297 m Cyclic Mudstone, Partly Bioturbated Lenticular Ripple Silty Mudstone and Bioturbated Grainstone-Packstone

Three depositional cycles are well and repeatedly developed in this facies: the well-bioturbated lenticular silty mudstone, silty stylolithic limestone and calcareous mudstone. Cyclicity is also clear on the GRPS (GRP20, 21, and 22 in Figure 5.4). The silty mudstone is dark greenish grey to black, with lenticular yellowish limestone interlayering. The sedimentary structures include ripple marks, bioturbation and nodular silty layers. The mudstone is loose and sticky, which may indicate the richness of the clay swallowing clay type. There is sharp contact with the underlying and gradational with the overlain unit. The silty stylolithic limestone is composed of brownish stylolithic limestone that is produced as storm deposits. The limestone is bioturbated to highly biturbated and fossiliferous in place. There is gradational contact with the underlying, while the contact with the overlain unit is sharp. The moderate to low sea level starts with high and then falls gradually towards the top of the facies (Figure 5.5 TSL9 and RSL9). The significant fluctuation of the sea level has resulted in the high diversity of this facies. The calcareous silty mudstone is grey with thinly laminated silty layering. It is slightly pyritic and becomes bioturbated in parts. It increases darker grey upwards. Calcite is cemented through the thin detrital laminae. The massive bedding is hard with obvious fractures. Although no geochemical data is available, the Upper Goldwyer shale in this well is expected to be organic rich with less maturation levels.

5.4.1.12 1188-1198.19 m Interbedded to Interlaminated Mudstone and Silty To Sandy Limestone

Here, there is interbedded to interlaminated mudstone and silty to sandy limestone. The well-bioturbated lenticular bedded silty mudstone is interbedded with massive limestone units. The high fluctuation of the sea level is well-signed in this facies by the upward increase of the calcareous content. Also, there is the retrogradational depositional cycle at the top of the Goldwyer Formation (GRP23).
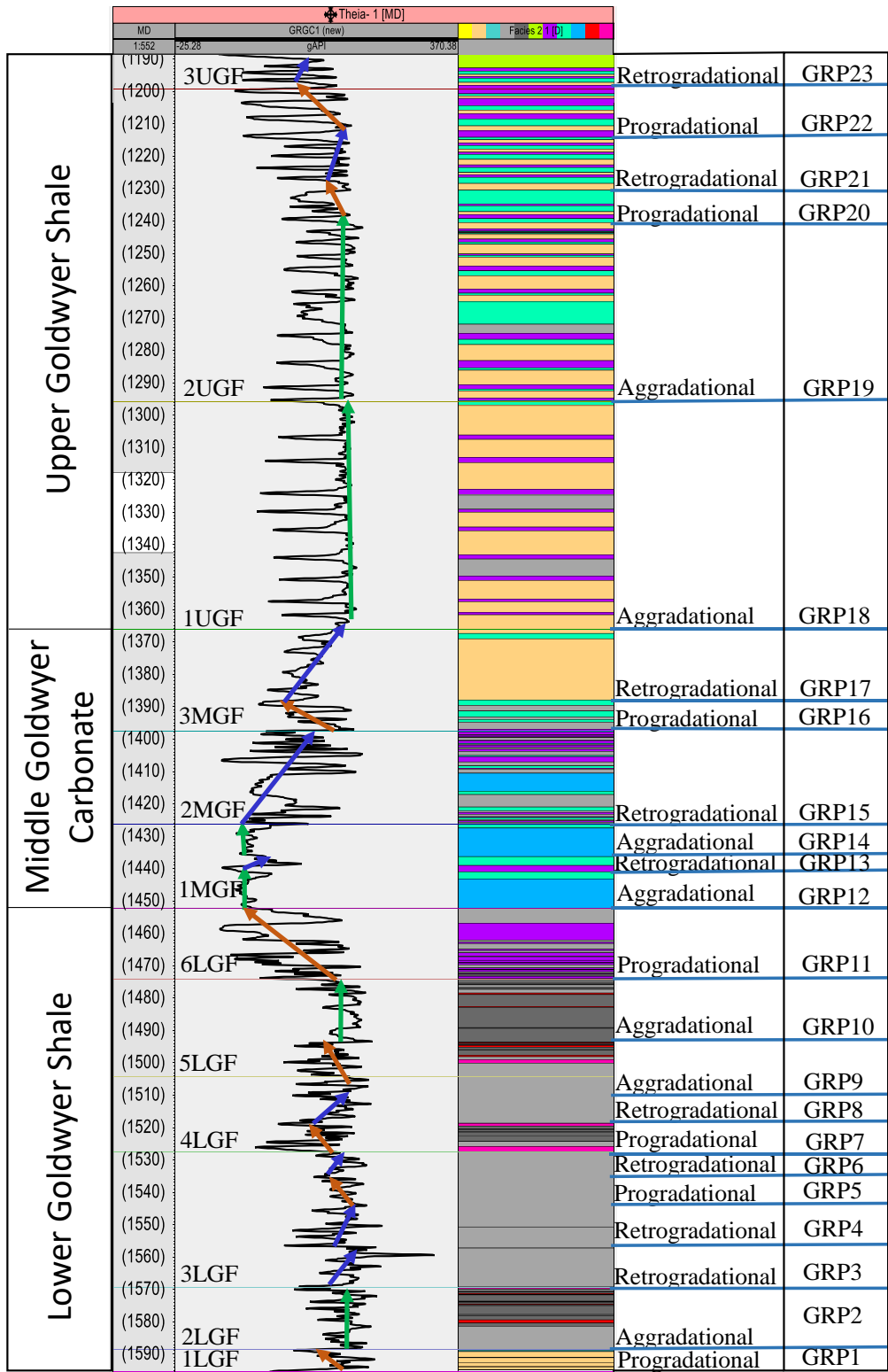
Figure 55.4 shows gamma ray stacking patterns (GRP) and depositional cycles of the Goldwyer Formation from the Theia#1 well in the Central Canning Basin. An upward decreased GRP results from an upward inncreased of calcareous content produced by progradational depositional cycle cused by relative sea level fall. An upward decreased GRP results from an upward increeadsed clay and organinc content produced by retrograditional depositional cycle caused by relative sea level rise. Constant sea level movement and later sedimentation build up will produce a comogenouse composition of the aggradational depositional cycle.

5.4.2 Sequence stratigraphy of the Goldwyer Formation

Based on the criteria of transgressive surfaces of erosion and maximum flooding surfaces, the sequence stratigraphic events of a stratigraphic succession are established. The deposition of sediments caused by the sea level rise generates a transgressive surface of erosion (TST) or sequence boundary (SB). The thickness variations of the stratigraphic intervals within the same sequence indicate different sources of sedimentary supply (Abouelresh and Slatt 2012).

The possible fluctuation of relative sea levels and stratigraphic stacking patterns of the Goldwyer Formation have been interpreted and correlated from the GR response and detailed core study in the Theia 1 well. The changes of the upward patterns of the residual hydrocarbon potential index (RHP) were also used to support the interpretation of the change of the organic facies. 72 data points were gathered for the Theia 1 well.

In the overall presentation, the Goldwyer Formation can be subdivided into three main stages of relative sea level, namely a high relative sea level during the deposition of the Lower Goldwyer shale, a low relative sea level during the deposition of the Middle Goldwyer carbonate (which gradually rises towards the top of the section) and the second high relative sea level stage during the deposition of the Upper Goldwyer shale that gradually falls towards the highest end of the section. Moreover, five upward increased RHP cycles found in the Goldwyer Formation indicate an overall change of the organic facies characteristics, from oxic to anoxic conditions. Each of these cycles was notably followed by an upward decrease of the RHP pattern, which indicates a change from anoxic to oxic characteristics of the organic facies. This will help to identify key shale gas intervals of the Goldwyer shale section.

The Goldwyer Formation sets on a sequence boundary (SB) created by an erosional surface on top of the underlying Willara Formation. This was notably identified from the sharp increase of GR response and reworked base deposits of the core at the base of the 1LGF facies (Figure 5.3F and Figure 5.5). The Lower Goldwyer shale is dominated by dark grey to black silty mudstone, which in most cases, is slightly calcareous to non-calcareous. The well-developed and thick mud rock units of this section, along with the rich organic content and anoxic water conditions,

reflect the calm and deep sedimentary environment. The favourable deposition of the rich-organic facies is maximised during a low stand system tract development (LST) of the Lower Goldwyer shale. Three condensed sections (CSs) or maximum flooding surfaces (MFS) were identified at the top of each major transgression cycle within this section (Figure 5.5 Top of TSL1, TSL 4 and TSL8). These sections are characterised by the highest GR response (Figure 5.4 GRP4, GRP10 and GRP 18-19), TOC and RHP content in the formation (4.4 wt.% TOC @ 1498 metres and 4.5 wt.% TOC @ 1552 metres and 5.91 wt.% TOC @ 1271.0 metres) of these 5 - 10 metre units. Moreover, GR, TOC and RHP curves were used to define the high frequency changes of the relative sea level. The increased clay and decreased calcareous and quartz content is marked by an upward increase of the gamma ray patterns. These have resulted from a relative sea level rise or relative transgression of sea level (TSL). Also, the upward increased TOC content and RHP indicate an upward increase of organic content and anoxic basin conditions (blue arrows on GR and RHP curves). On the other hand, a relative fall of sea level or relative regression of sea level (RSL) results in an upward decrease of gamma ray patterns caused by the increased calcareous and quartz, as well as decreased clay content. It can be similarly linked to the decreased upward TOC and RHP content (orange arrows on GR and RHP curves).

The Middle Goldwyer carbonate consists of limestone dominated with some rich organic intervals (ex. 1MGF). It is characterised by overall upward increased GR response and a high relative sea level RSL. The high energy process produced an oxic basin condition and low TOC content in this facies. The upper stratigraphic interval (3MGF) of this section is however, interbedded stylolithic limestone and silty mudstone. A flooding surface has also occurred in 3MGF, leading to the deposition of a rich organic flooding surface (fs) (5.6 wt.% TOC @1397 m in depth) (Figure 5.5).

The Upper Goldwyer shale however, has higher carbonate and silt content than the Lower Goldwyer shale. The continued cyclicity of the clay and carbonate intervals throughout this section is due to the constant repeated fluctuations of the relative sea level (Figure 5.5). Thicker intervals of low GR response are present in the 2UGF compared to the 1UFG facies (Figure 5.5 and 5.6), because of the higher carbonate content and longer periods of the shallow depositional cycles. This was

also confirmed from the detailed core study. The average thickness of each unit is 2 - 3 m in 2UGF and less than 1 m thick in the 1UFG. The Upper Goldwyer shale starts with a low stand system tracts (LST) deposit in the lower section (1UGF), capped by the richest organic interval of the condensed section and maximum flooding surface (5.9 wt. % TOC @ 1271.0 metres in depth). The overall increase of the relative sea level till reached the top of TSL8 cycle caused the possible deposition of the Palaeozoic G-presca, which is the worldwide well-known rich-organic source unit. Comparably, the generally higher calcareous content and lower organic richness of the Upper Goldwyer shale are related to the shallower water conditions than those of the Lower Goldwyer shale. After the deposition of the maximum flooding surface, a relative sea level fall began and the cycle high stand system tract (HST) was developed (including the deposition of the 2UGF and 3UGF stratigraphic intervals). Lighter grey and expected lean organic facies were deposited. The sequence boundaries (SB) bounding the Upper Goldwyer shale are the remarks of the deposition of the end of the Middle Goldwyer carbonate and beginning of the Upper Goldwyer section at the base, and end of the Goldwyer Formation and the start of the Anderson Formation at the top.

Moreover, although it is not common in the Goldwyer Formation, a few constant stacking of similar types of sediments occurred as the result of aggradational relative sea level (ASL) change, where the GR log has a generally constant upward stacking pattern (Figure 5.5).
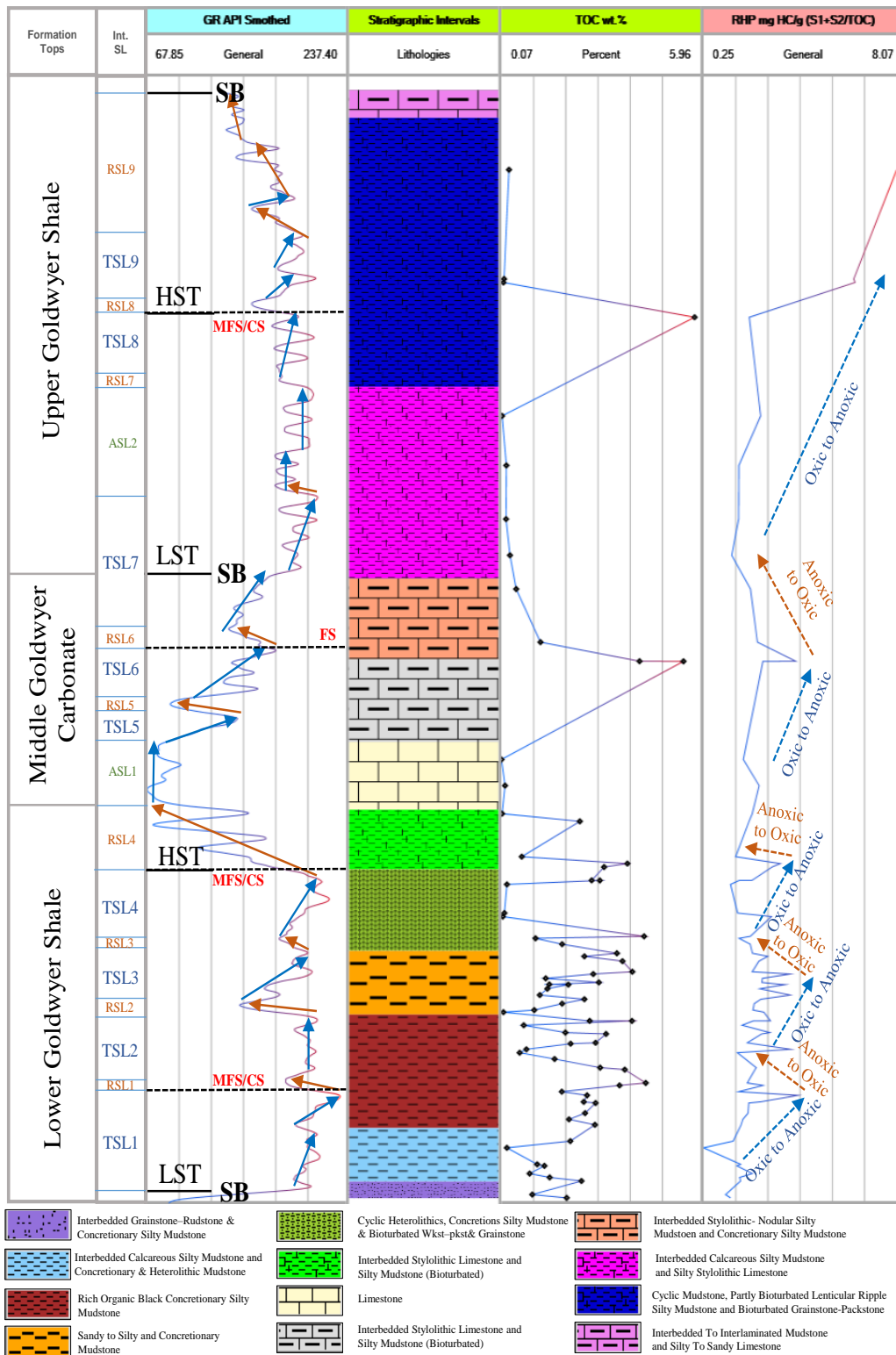
Figure 5.5 The correlation chart of defined stratigraphic interval of the Goldwyer Formation from the Theia#1 well, Formation tops, interpreted relative sea level, gamma-ray log GR, stratigraphic intervals, TOC curve and relative hydrocarbon potential curve. (TSL= transgresssion of relative sea level , RSL= reggresssion of relative sea level, LST= low stand system tract, HST= high stand system tract, MFS= maximum flooding surface, FS= flooding event, CS= condensed section, and SB= sequence boundary).

5.4.3 Thickness Trends and Lateral Distribution of the Stratigraphic Intervals

5.4.3.1 Cross-section A

The SE-NW cross section in Figure 5.6 demonstrates the vertical and lateral variations of the Goldwyer lithofacies across the Central and Northern Broome Platform. Based on the previously discussed lithofacies and sequence stratigraphy framework, the Goldwyer Formation is found to have six dominant stratigraphic intervals in the lower shale section and 3 intervals in each of the middle carbonate and upper shale sections. The stratigraphic intervals of the Lower Goldwyer shale are well presented in homogenous thickness throughout most of the studied wells in this cross section. More specifically, the Goldwyer Formation represents a moderate range of depth to the top of the formation in the Northern Broome Platform at about 800 - 1000 metres, as in Sharon Ann#1, Hilltop#1, Goldwyer#1, Aquila#1, Kanak#1 and Theia#1 wells. On the other hand, a significant increase of depth was noted in the Looma#1 and Mclarty#1 wells. This could be related to the Dampier fault zone (extensional NW trending south dipping faulting in the Central Canning Basin), which created half grabens during the Ordovician time (Romine et al. 1994). Moreover, the significant thinning of the Upper Goldwyer shale in the northern parts of the Broome Platform could be linked to the uplift and erosion of the area during the late Ordovician to the early Silurian.

Furthermore, similar well log responses present in all of the wells with higher gamma ray readings (located in the wells of the central and southern parts of the platform) correspond to the higher organic content and deeper anoxic environment. The measured TOC values are notably higher in the Lower Goldwyer shale sections in these areas compared to the northern regions.

Considering the effect of the complex tectonics and depositional settings of the Central Canning Basin, it was necessary to use seismic data to re-evaluate the geological settings and tectonism that affected the Goldwyer Formation in the area. This will provide a better interpretation of the following cross section in the central parts of the basin.

Figure 5.6 Cross section A through the Broome Platform to correlate the identified stratigraphic intervals of the Goldwyer Formation. The gamma-ray log GR is plotted for each well (created using the Petrel software).

This section was designed to establish a seismic interpretation along the selected seismic survey in the Central Canning Basin. The study area covers about 11000 km^2 within the onshore Central Canning Basin. 2D seismic and petroleum well logs data were used in the investigated area to improve and update the geological information and tectonic history of the Goldwyer Formation. This is mainly in order to interpret the top and base of the Goldwyer Formation in the Central Canning Basin, as well as to generate a new fault model to investigate the main structures in the area and their influence on the sedimentary packages. The interpreted data helped to identify the thickness trends and spatial distribution of the Goldwyer section. This was achieved by interpreting 36 2D seismic lines and relevant well data from 5 wells loaded into the Petrel Software. The seismic data was acquired during 1998 and are of generally good quality (Figure 5.7).
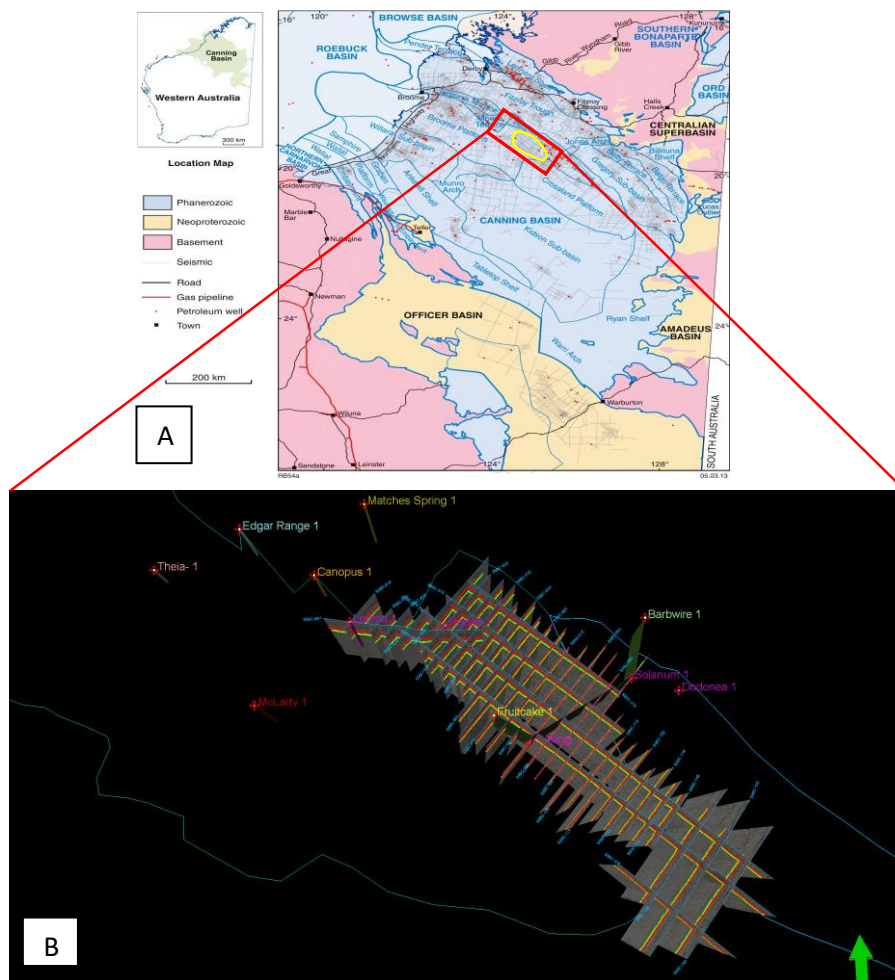
Figure 5.7 (A) Shows location map of the seismic survey study area in the onshore central Canning Basing WA, (B) The 2D seismic base map onshore within the Central Canning Basin.

5.4.3.2.1 Horizon Picking

The procedures used to pick the horizons commenced with the examination of the seismic sections that intersected with the drilled wells. Based on the formation tops, the reflectors were picked and tracked along the seismic sections. The reflectors' clarity and data resolution at the top of the seismic sections is better than that of the bottom of the section. Thus, a top-to-bottom approach was applied, which is based on interpreting the reflectors at the top of the seismic sections and working towards the bottom.

Goldwyer shales horizon was interpreted across the entire data set in order to map the formation's thickness and distribution (Figures 5.8, 5.9 and 5.10). The top and base of the Goldwyer Formation were accurately picked along most of the seismic sections, showing quite a homogenous thickness distribution across the area. This might indicate that the formation has not been impacted by structural and tectonic activities during the deposition. Figure 5.13 and 5.14 shows 2D interpretation maps of the Top and Base Goldwyer formation in the Central Canning Basin. The white dash lines on the maps illustrate the location of the stratigraphic cross section B generated from well log data. The study area displays the main elements of hydrocarbon systems and contains evidence of extensive extensional tectonic and possible compressional activities. The Goldwyer Formation exists all over the studied area, with apparent thickness of about 300 – 350 m.

5.4.3.2.2 Faults

A part of this study was to generate a fault model in the basin. Therefore, faults have received great attention and were picked along most of the seismic sections. The majority of the interpreted faults are vertical to sub-vertical normal faults, with few reverse faults. Most of these faults are rooted to the basement. Faults have noticeably influenced the Goldwyer Formation, thereby creating faulted structural traps within the formation.

The normal faults are a result of extensional settings that have affected the basin during the Ordovician time. These extensional events might be a result of the rifting system that occurred during this era. Many structural traps are generated by thick-skinned normal faults, common with high dips and low heaves. The general structure in the onshore Central Canning basin is dominated by NW-SE trending normal fault blocks facing to the SW and NE (Figures 5.8, 5.9, 5.10 and 5.11).
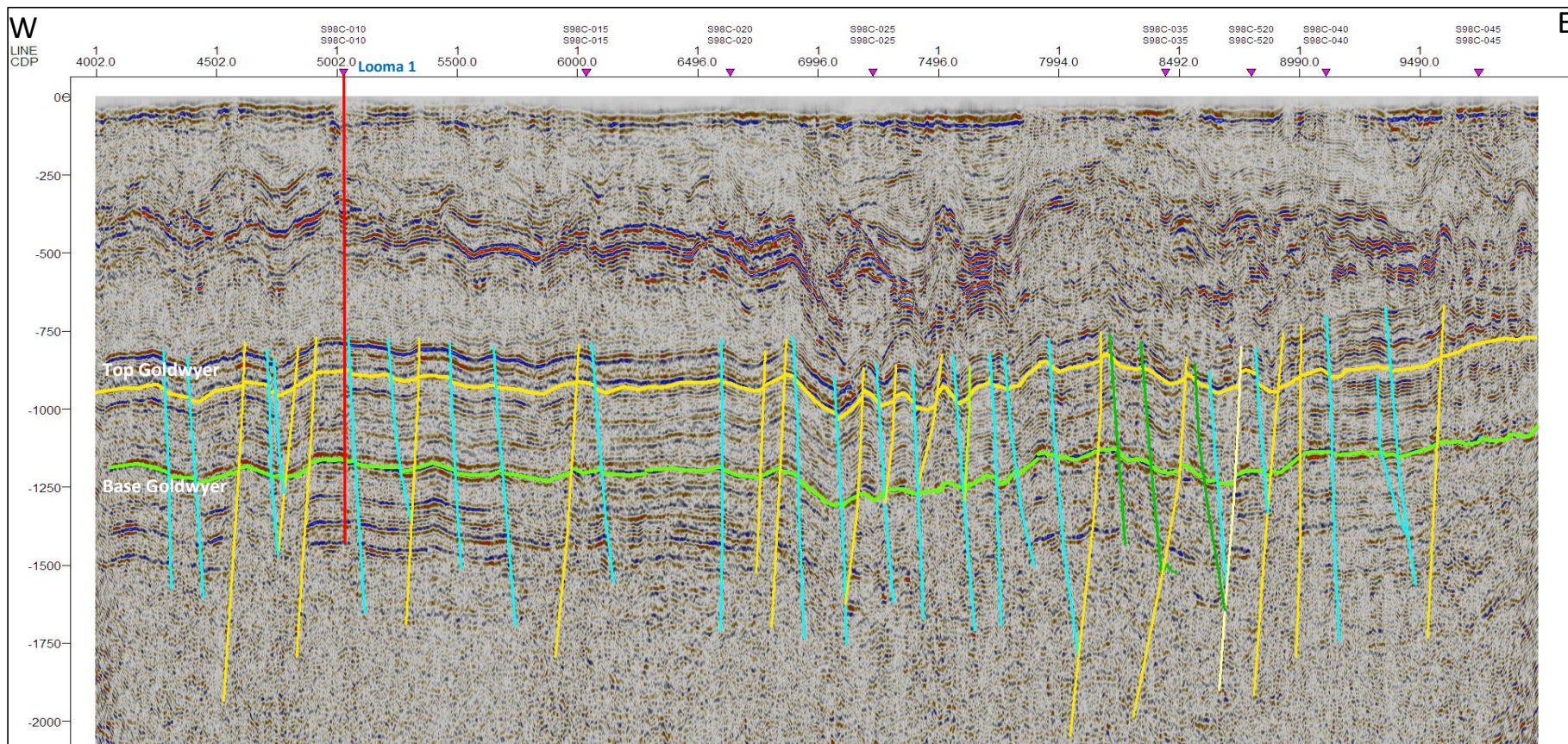
Figure 5.8 The interpreted seismic line oriented E-W onshore within the Central Canning Basin.
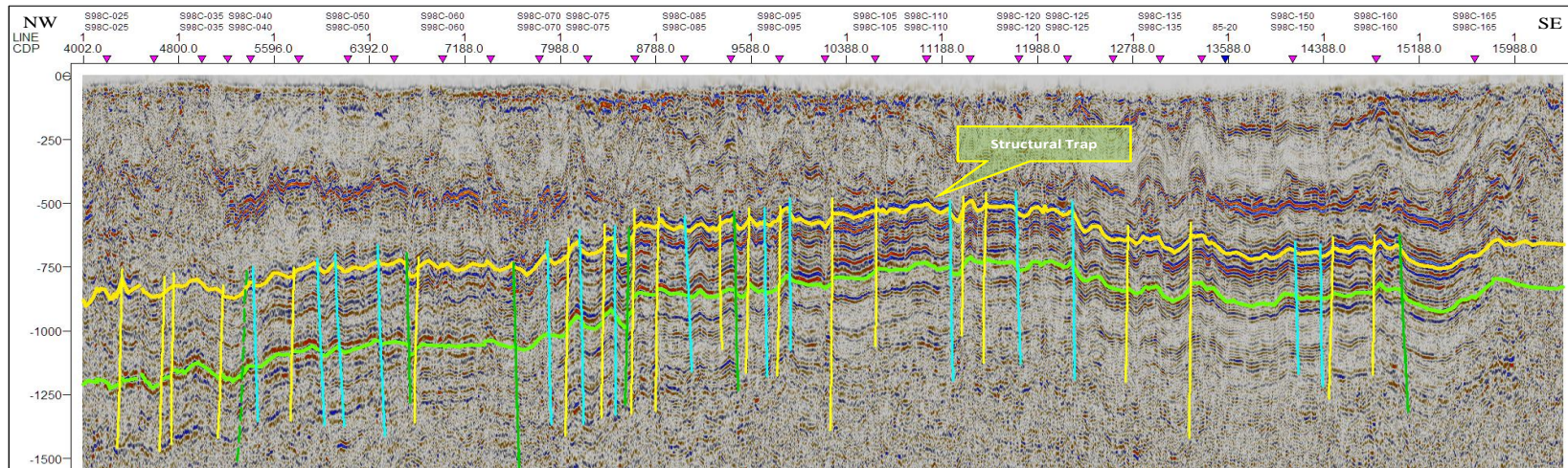
Figure 5.9 The interpreted seismic line oriented NW-SE onshore within the Central Canning Basin showing: 1. Vertical to sub-vertical normal fault; 2. Faulted structural trap within the Goldwyer Formation; 3. Most of the faults are rooted to the basement (thick-skinned nature).
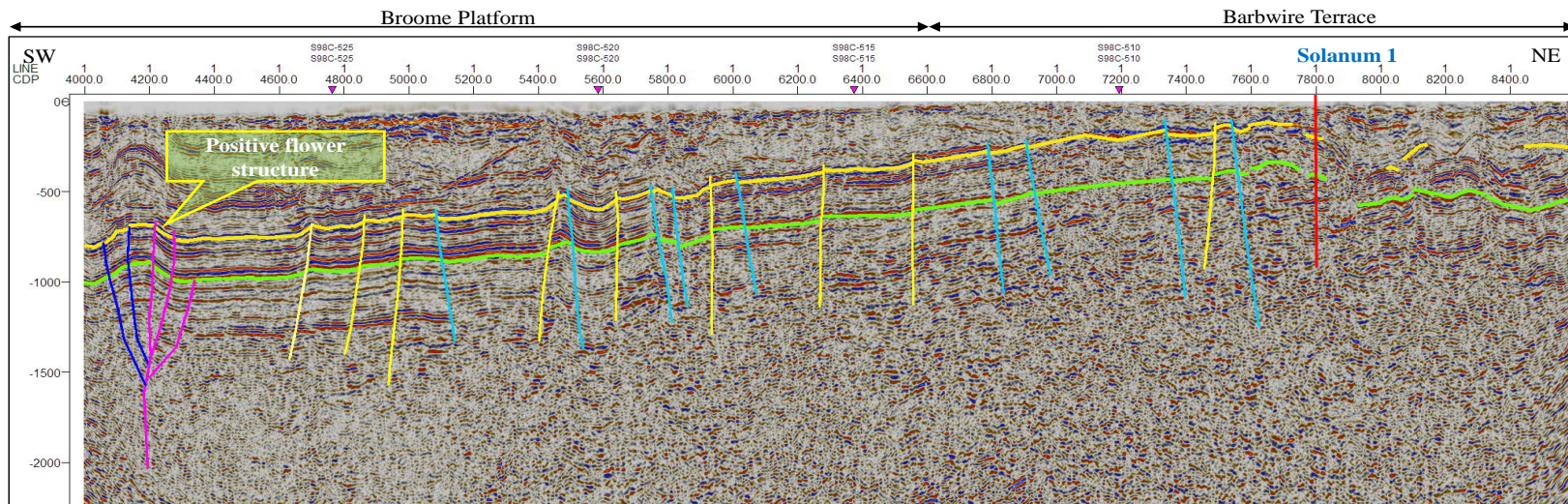
Figure 5.10 The interpreted seismic line oriented NE-SW onshore within the Central Canning Basin show an increased depth of the Goldwyer Formation in the Broome Platform at the basin boundaries.
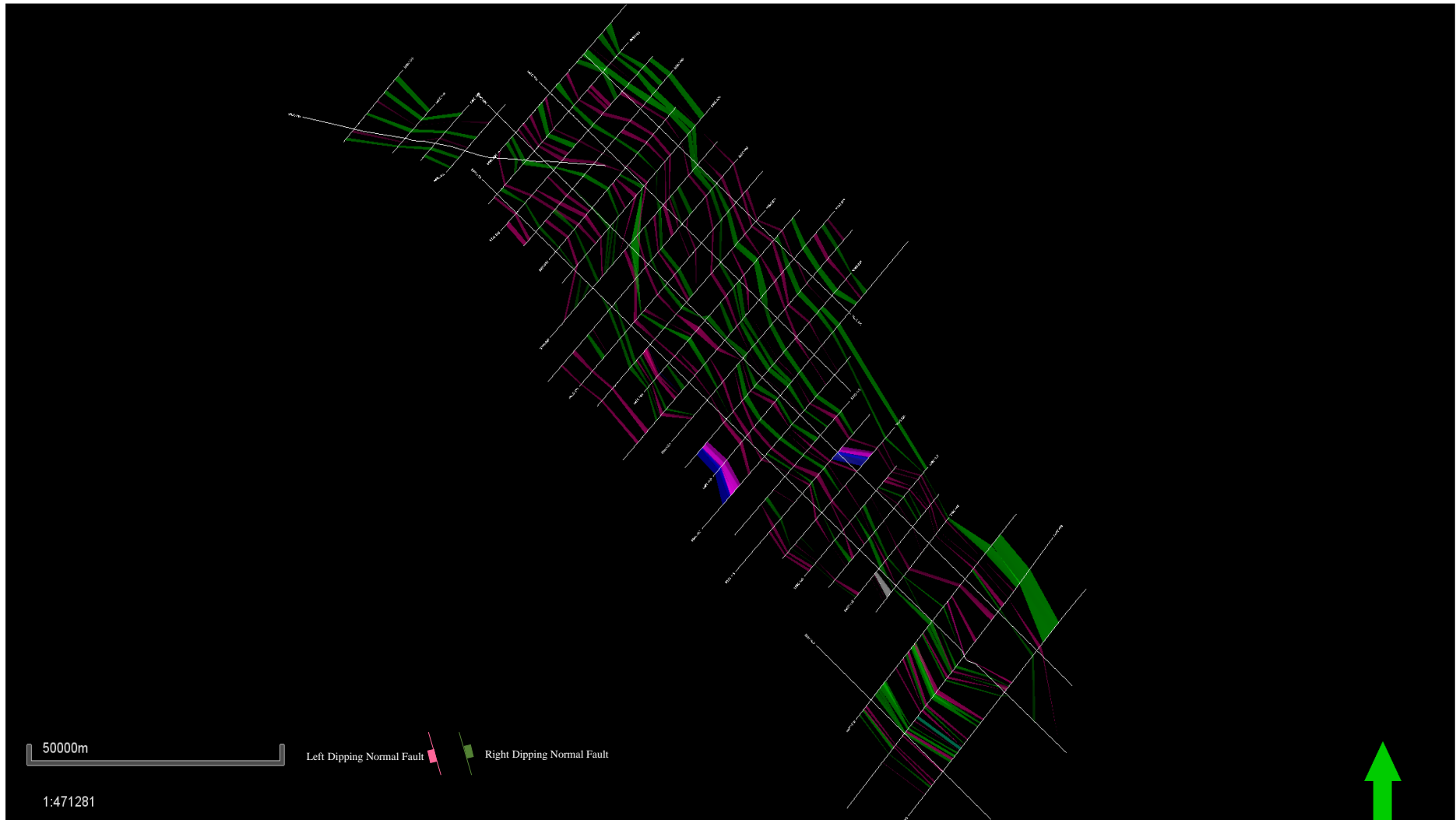
Figure 5.11 The tectonic map of the top Goldwyer Formation onshore within the Central Canning Basin showing: NW-SE trending faults.

160

5.4.3.3 Cross-section B

Normal faulting and subsidence that occurred in the boundaries between the Broome Platform and Barbwire Terrace resulted in a great depth shift of the Goldwyer Formation (Figure 5.12). The higher calcareous content of the Goldwyer lithofacies in the Barbwire Terrace has caused the lower GR readings and less organic content in the Solanum#1, Dodonea#1 and Barbwire, compared to the McLarty#1 and Theia#1 wells. The depth to the top of the Goldwyer Formation is only 280 metres in the Solanum#1 and 780 metres in the Barbwire#1 wells. This would explain the lower maturity levels of the Goldwyer shales in the Barbwire Terrace, compared to the Southern Broome Platform. Therefore, the depositional basin margins are expected to be the Barbwire Terrace and the deeper basin is towards the Broome Platform. The 2D seismic interpretation maps of the top and base of the Goldwyer formation show similar depth trends in the cross-section areas (Figure 5.13 and 5.14).

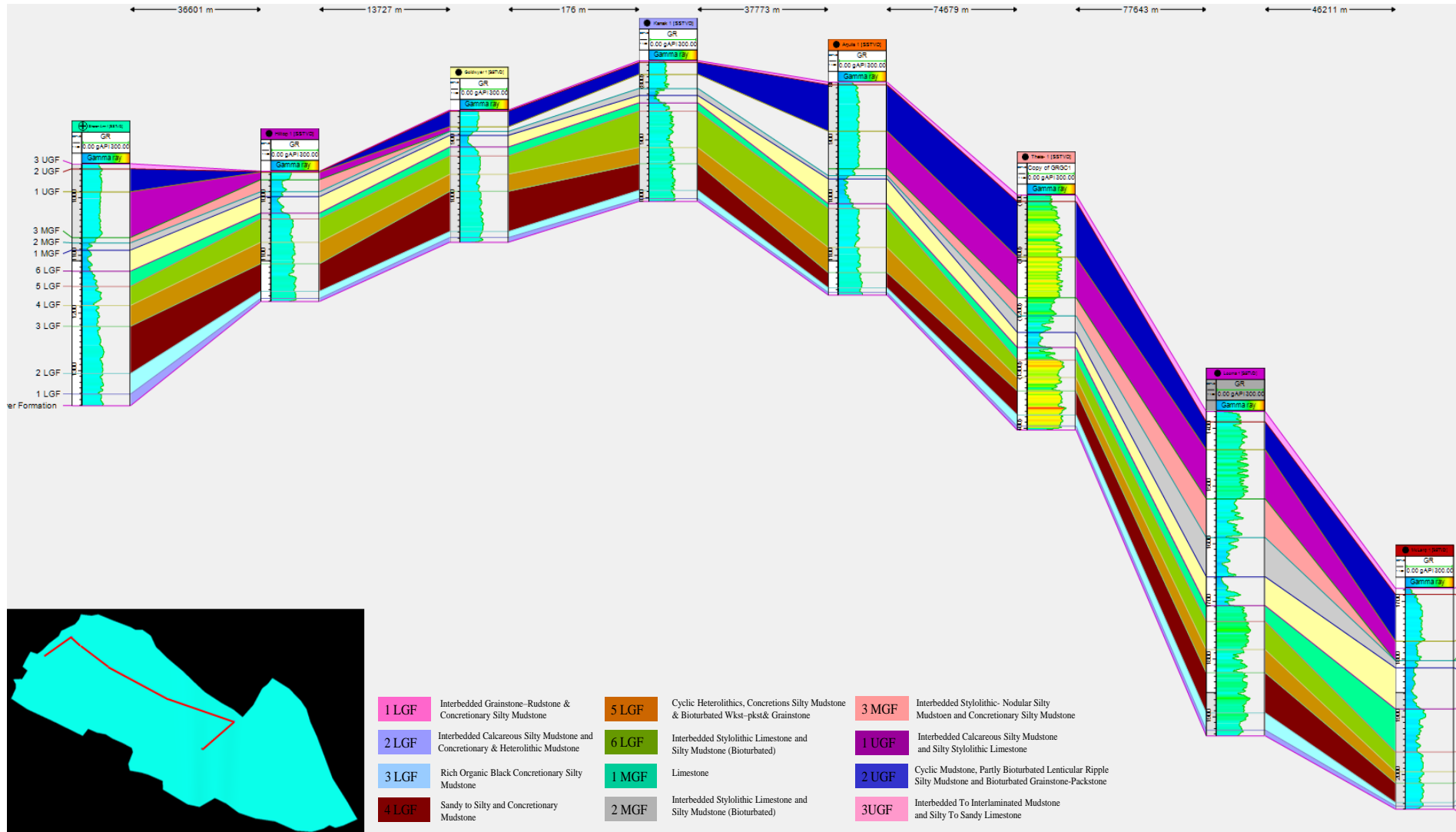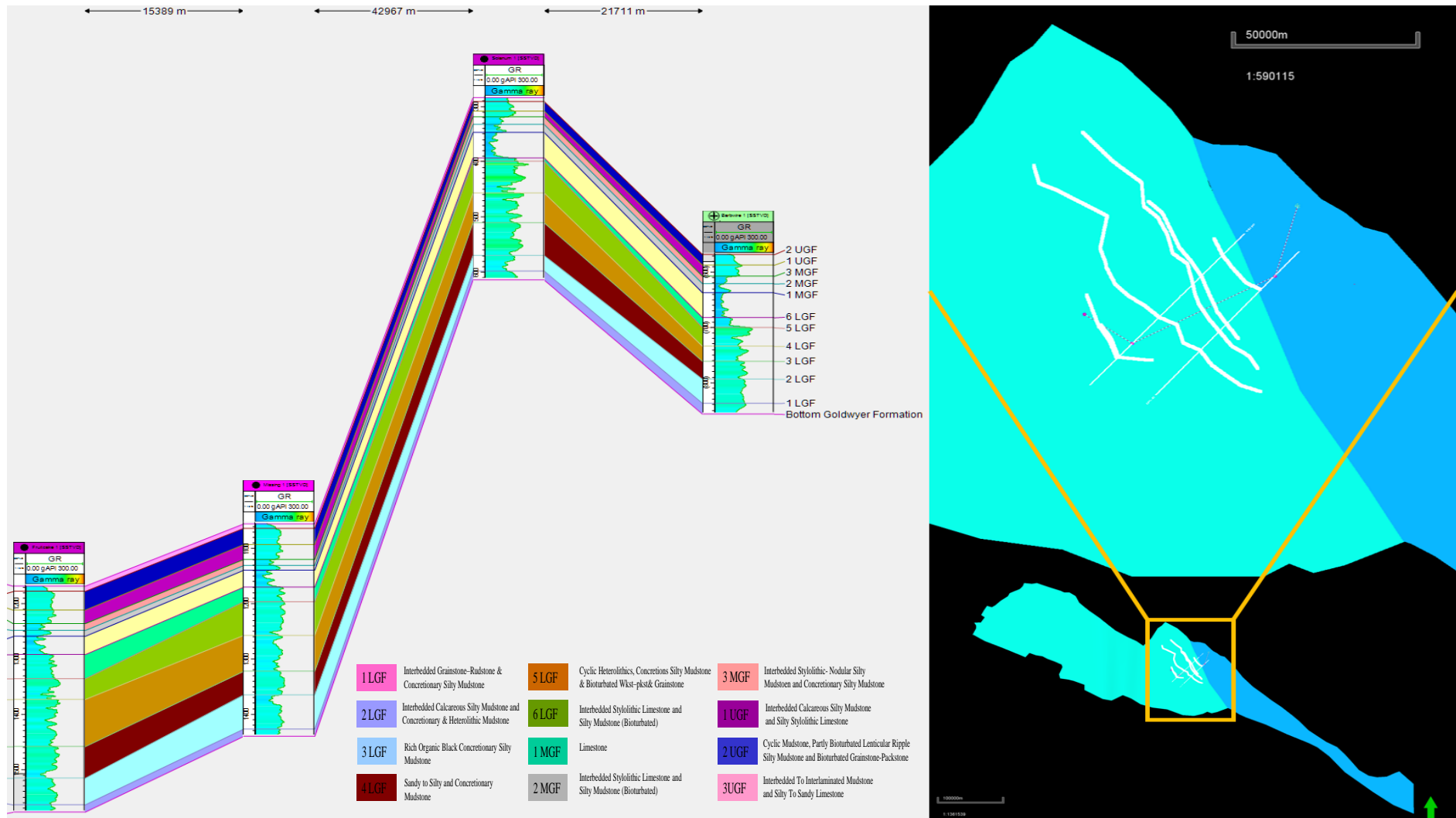**Figure 5.12 The cross section B through the Broome Platform to correlate the identified stratigraphic intervals of the Goldwyer Formation. The gamma-ray log GR is plotted for each well (created using the Petrel software).**
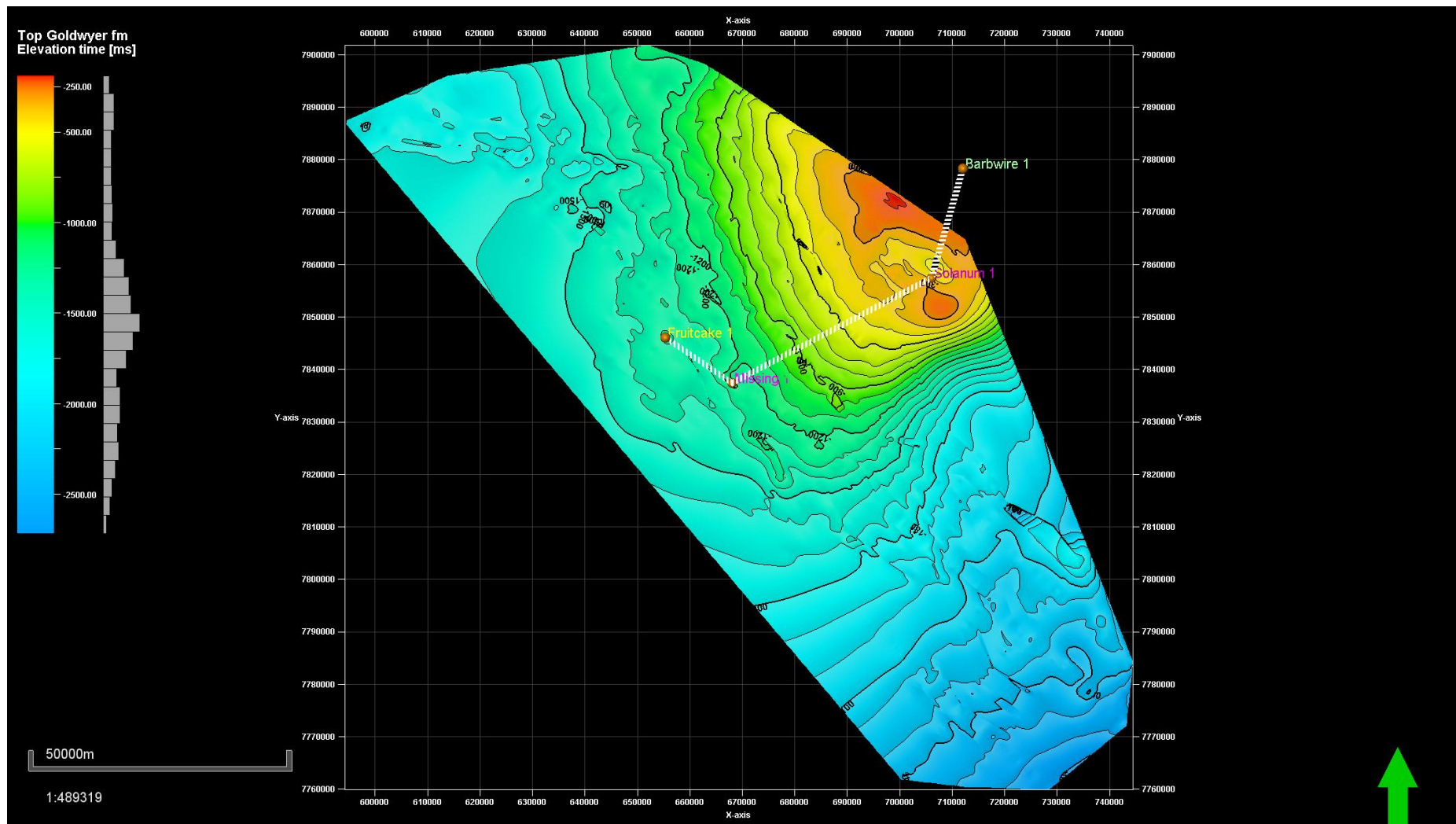
Figure 5.13 2D seismic interpretation map of the Top Goldwyer formation in the central Canning Basin. White dashed line on the map illustrates the location of the cross-section in figure 5.12.
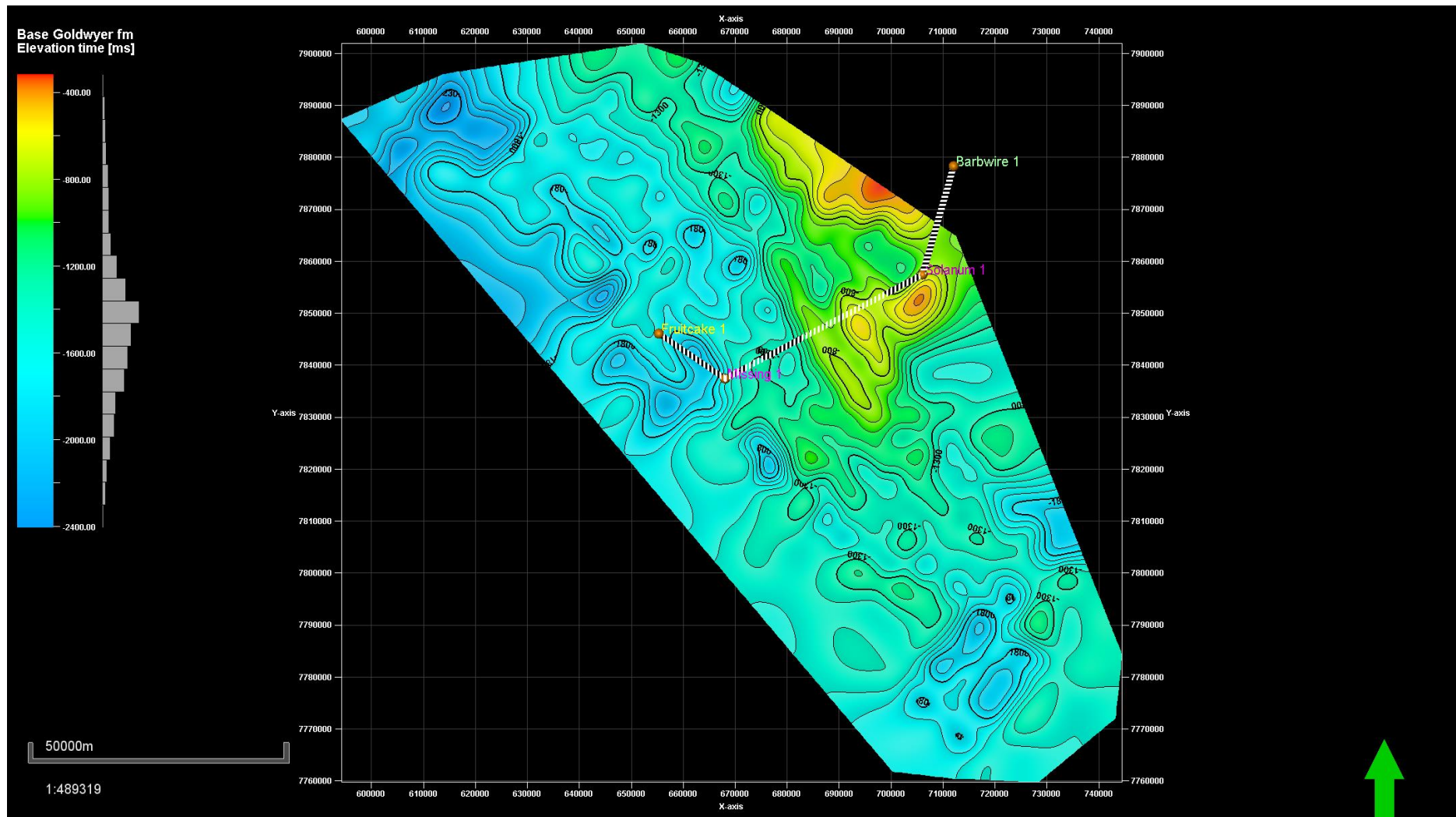
Figure 5.14 2D seismic interpretation map of the Base Goldwyer formation in the central Canning Basin. White dashed line on the map illustrates the location of the cross-section in figure 5.12.

6. Chapter 6: Discussion and Conclusions

6.1.1 Geochemical Evaluation

The Carboniferous Laurel Formation generally has a variant TOC content, indicating fair to excellent organic richness. However, most of the S2 data indicated poor hydrocarbon generation potential. Furthermore, Type II/ III kerogen is dominant in the Lennard Shelf and Type III oil/gas-prone and gas-prone kerogens are both available in the Fitzroy Trough. The Laurel shale is mostly thermally immature to mature oil-prone in the Lennard Shelf and mature to over mature in the Central Fitzroy Trough. The lack of data distribution across the sub-basins caused significant uncertainty in some of the studied areas. The Ordovician Goldwyer Formation is found to be in the oil generation window showing Ro values over 0.7% in the Northern Broome Platform and the Barbwire Terrace. The analysed data shows higher Tmax values in the Eastern Broome Platform and the Northern Barbwire Terrace (reaching 460ºC), which indicates the peak mature oil generating window with condensate gas. The Goldwyer Formation is believed to be overmature in the Kidson sub-basin, where the depth of burial is significantly high. The total organic content in the Goldwyer Formation varies between 0.2 - 3.5 wt.%, reaching a maximum of 5.90 in the Theia#1 and 4.8 wt.% in the Kunzea#1 well. The Pseudo VanKrevelen plot shows that the Goldwyer shale has mostly Type II oil-prone and Type II/ III oil and gas-prone kerogen. The logarithm plot of TOC vs S2 shows that the Goldwyer shale has a fair to good hydrocarbon generation potential.

6.1.1 Total Organic Content Estimation and Modelling

The estimation of total organic content of the Goldwyer Formation using various well-log techniques has been examined. A comparison of the results against the measured TOC values has led to the identification of the best available method. The sonic-resistivity logs separation, density-resistivity logs separation and core-log density comparison techniques were used. The sonic-resistivity logs separation technique was found to have the most accurate results and best match with the measured TOC data for the Goldwyer shales. The organic facies identification and lithology separation was also successfully obtained using the

resistivity sonic cross plot. Therefore, it was mainly used for property model generation and interpretation.

6.1.2   Fracability Index

A comprehensive understanding of the rock's mechanical properties is very important for shale gas evaluation. The Brittleness Index (BI) of the Goldwyer shale was calculated using the mineralogy data obtained from the quantitative XRD analysis.   The higher organic and clay content of the Goldwyer shales caused low to moderate brittleness levels. The shear sonic transit time was calculated for most of the studied wells in the Canning Basin using the new equation obtained from the linear correlation between the measured compressional (DTp) and shear (DTs) sonic transit times. The 3D property model that was built using the estimated BI revealed a higher brittleness content in the southern and northern regions of the Broome Platform, with values ranging between 35 - 65%. Moreover, the range of the average BI in the Northern Barbwire Terrace is between 40 - 70%, which can be related to the higher calcareous content (Figure 4.22 & 4.23 and Figure 4.24 & 4.25 respectively).

6.1.3   Total Porosity Estimation and Modelling

Unlike conventional reservoirs, the porosity estimation of shale gas reservoirs relies on the organic content and density of the matrix and gas components. Therefore, the total porosity of the Goldwyer Formation was estimated using well logs and density data. The created 3D property model revealed an average porosity of around 6% for the Lower Goldwyer shale in the northern and southern parts of the Broome Platform, and around 10% in the central regions, which could be related to the lower organic content. Moreover, the total porosity of the Goldwyer shale was found to be directly related to the total organic content, in spite of the higher clay content.

6.1.4   Shale Gas Adsorption

A comparative study was conducted on the adsorbed methane potential of the organic-rich, clay and shale sample. The focus was more on the organic content and pure clay minerals which have a significant relation with the shale gas composition. Nonetheless, real shale samples were also included in the study. Notably, the montmorillonite type of clay yielded the highest methane adsorption capacity, as compared to the other pure clays (Kaolinite, Illite and Na-

montmorillonite). The quartz-rich sample had the lowest methane adsorption potential from all of the studied samples. Moreover, the clay fraction affects the gas storage capacity of the shale gas. The results from the experiment showed that clay-rich shales have a reasonably high adsorption capacity and can be compared with TOC-rich shales. A higher TOC content of the rock causes a higher adsorption potential, which explains the importance of the TOC content in methane adsorption enhancement.

6.1.5 Sweet Spots

The geological, geochemical and petrophysical study of the Goldwyer shales has led to the identification of the sweet spots areas in the Central and Northern Canning Basin. 3D models and 2D maps of the key parameters highlight the most favourable areas for shale gas exploration and development. For example, maps A of the Goldwyer shale in figure 2.26 & 2.27 shows rich to very rich organic content in Central and Northern Broom platform and North Barbwire Terrace. Higher thermal maturity levels (exceeding 460°C) were also depicted from the maps in the Central Broome Platform and Norther Barbwire Terrace indicating late oil generation window to condensate and dry gas. Moreover, the 3D property model of the estimated TOC shown in figure 4.12& 4.14 and the maps in figure 4.13& 4.15 confirm a very similar distribution of the organic content in the Broome Platform and Barbwire Terrace. The southern and northern regions of the Broome Platform have shown more favourable brittleness levels on the created model and map in figure 4.22 and 4.23, and in the Northern Barbwire Terrace (Figure 4.24 & 4.25). The estimated total porosity of the Lower Goldwyer shale ranges from 4.0 to 16.0% with higher trend in the Central and to the North-western regions of the Broome Platform (figure 4.27& 4.28). The average porosity of the Lower Goldwyer shale in the Barbwire Terrace is 5.0 to 10.0% mainly in the North-Western end of the sub-basin (Figure 4.29& 4.30).

6.1.6 Lithofacies

A detailed study has been conducted on 415 metres of the fully recovered core of the Goldwyer Formation from the Theia#1 well. A visual core observation and petrographic analysis have revealed seven main lithofacies in the Goldwyer Formation. These include: 1) Concretionary silty mudstone, 2) Calcareous silty mudstone, 3) Heterolithic lenticular wackestone–packstone and silty mudstone, 4)

Bioclastic/intraclastic grainstone and silty mudstone, 5) Bioturbated wackestone–packstone, 6) Nodular packstone–grainstone–rudstone and 7) Well Bioturbated lenticular bedded limestone and silty mudstone. Depositional environment and different water settings were observed from the depositional variations and sedimentary structures of these fancies.

The Goldwyer Formation can be divided into two deep depositional settings: one that produced the low energy in the lower and upper shale sections and the other, a relatively shallow depositional setting that produced the medium energy carbonate deposits of the middle carbonate unit. The depositional environment of the lower Goldwyer shale is therefore considered to be the deep restricted marine environment, where calcareous and concretionary silty mudstones are thick and dominant. The total organic content and residual hydrocarbon potential (RHP) analysis revealed that the concretionary silty mudstone and calcareous silty mudstone facies are the richest organic facies of the Goldwyer Formation (characterised by deep anoxic water conditions and high pyrite content). It also has a distinctive gamma ray reading that results from the high clay and organic content. The Upper Goldwyer shale is, however, regarded to be created in relatively shallower depositional conditions, which is characterised by the interbedded and interlamination of the carbonate layers in lighter mudstone facies. These layers created low GR peaks throughout the section.

6.1.7   Parasequence Variations and Gamma ray Patterns

The use of the gamma ray log allowed for the interpretation of the parasequence stacking patterns of the Goldwyer Formation. The formation expressed three known gamma-ray stacking patterns: the upward increased gamma ray parasequence (which is the thickest and most common in the formation), the upward decreased gamma rays parasequence and the constant gamma ray parasequence. The lower Goldwyer shale has eleven gamma ray parasequences, while the middle Goldwyer carbonate and upper Goldwyer shale have six gamma ray parasequences throughout their different lithofacies (Figure 5.4). A larger scaled observation was followed due to the thick section and repeatability of similar responses. The boundaries between these parasequences were tied to the lithofacies and sequence stratigraphic boundaries that were laterally correlated through the cross sections.

6.1.8 Sequence stratigraphic Framework

An integrated of lithofacies classification, gamma ray parasequence, organic facies distribution and residual hydrocarbon potential index has led to the interpretation of the relative sea level changes and the resulted sequence boundaries of the Goldwyer Formation. The lower Goldwyer shale is mostly found to have an overall high gamma ray response resulting from rich clay and organic silty mudstone facies deposited by a low energy environment of a lowstand system tract event. It is bounded by a sequence boundary at the base and has a condensed section near its top boundary. The Middle Goldwyer carbonate is composed of highstand system tract deposits consisting of mainly constant GRP at the lower half, caused by siliclastic deposits, followed by a gradual increase of the water depth to the top of the unit. A short flooding period created a high TOC and GR kick layer within the section. The Lower Goldwyer shale, on the other hand, expressed a lowstand system tract of relatively low energy deposits, followed by shallower interbedded carbonate and mudstone deposits of the high stand system tract, separated by rich organic and high GR of the maximum flooding surface deposits (Figure 5.5).

6.1.9 Thickness Trends and Lateral Distribution

The systematic variations of thickness trends, lateral distribution and depth of the Goldwyer stratigraphic intervals were identified in the Central Canning Basin. The two selected cross-sections across the Broome Platform (X-section A) and the Barbwire Terrace (X-section B) revealed the significant architecture of the Goldwyer Formation. The depth and thickness of the Upper Goldwyer shale increases towards the southern regions of the Broome Platform and to the southern margins of the NW parts as well. However, some of its lithofacies are absent in the northern regions of the NW parts of the platform. However, the Lower Goldwyer shale shows a homogenous thickness trends across most of the Broome Platform with a significant depth increase to the eastern and south-eastern parts of the platform. This could be related to the extensional fault tectonism and subsidence that occurred in the Central Canning Basin. Higher gamma ray readings (250 - 300 API) of the darker and more anoxic rich organic facies were also noted in these deepening areas. The thermal maturity level is also higher due to the increased depth of burial. Therefore, this area would be highly considered for future gas shale development. The calcareous lithology of the

Goldwyer Formation is significantly increased in the Barbwire Terrace. Cross section B, between the Broome Platform and the Barbwire Terrace, shows the major depth variation of the whole Goldwyer section. Seismic interpretation and fault modelling confirmed the effect of the intensive structure and tectonism on the depositional settings and thickness trends of the Goldwyer formation at the basin margins.

6.1.10 Seismic Interpretation of the Goldwyer Formation

2D seismic data was interpreted to update the geological information and the tectonic history of the Goldwyer Formation in the Central Canning Basin. The top and base horizons of the Goldwyer Formation were accurately picked, as well as the fault model generation and main structures investigation in the area, in order to have an influence on the sedimentary package. Also, the interpreted data helped to identify the thickness trends and spatial distribution of the Goldwyer section. The study area displays the main elements of the hydrocarbon systems and contains evidence of extensive extensional tectonic and possible compressional activities. The Goldwyer Formation exists all over the studied area with apparent thickness of about 300 - 350 m in the Barbwire Terrace and increases towards the Broome Platform. This can provide more knowledge about shale gas prospectivity in the onshore Central Canning Basin. Many structural traps are generated by thick-skinned normal faults, commonly with high dips and low heaves. The general structure in the onshore Central Canning Basin is dominated by NW-SE trending normal fault blocks facing to the SW and NE.

7. Reference

2011. HPVA User Guide World Wide Web Address: http://www.particulate systems.com/Repository/Files/HPVA_Operator_Manual.pdf.

Abouelresh, M.O. & Slatt, R.M. 2012. Lithofacies and sequence stratigraphy of the Barnett Shale in east-central Fort Worth Basin, Texas. *AAPG bulletin*, 96, 1-22.

Administration, U.S.E.I. & Kuuskraa, V. 2011. World shale gas resources: an initial assessment of 14 regions outside the United States. US Department of Energy.

Amaefule, J.O., Altunbay, M., Tiab, D., Kersey, D.G. & Keelan, D.K. 1993. Enhanced reservoir description: using core and log data to identify hydraulic (flow) units and predict permeability in uncored intervals/wells. *SPE annual technical conference and exhibition*. Society of Petroleum Engineers.

Ambrose, R.J., Hartman, R.C., Diaz Campos, M., Akkutlu, I.Y. & Sondergeld, C. 2010. New pore-scale considerations for shale gas in place calculations. *SPE Unconventional Gas Conference*. Society of Petroleum Engineers.

Aringhieri, R. 2004. Nanoporosity characteristics of some natural clay minerals and soils. *Clays and clay minerals*, 52, 700-704.

Aylmore, L. & Quirk, J. 1967. The micropore size distributions of clay mineral systems. *Journal of Soil Science*, 18, 1-17.

Berberan-Santos, M.N., Bodunov, E.N. & Pogliani, L. 2008. The van der Waals equation: analytical and approximate solutions. *Journal of Mathematical Chemistry*, 43, 1437-1457.

Bessereau, G., Guillocheau, F. & Huc, A.-Y. 1995. Source rock occurrence in a sequence stratigraphic framework: the example of the Lias of the Paris Basin.

Best, M. & Katsube, T. 1995. Shale permeability and its significance in hydrocarbon exploration. *The Leading Edge*, 14, 165-170.

Bissada, K. 1982. Geochemical constraints on petroleum generation and migration-a review. *Proceedings ASCOPE*, 81, 69-87.

Boehlert, G.W. & Genin, A. 1987. A review of the effects of seamounts on biological processes. *Seamounts, islands, and atolls*, 319-334.

Bohacs, K. 1998. Contrasting expressions of depositional sequences in mudrocks from marine to non marine environs.

Bohacs, K.M. 1993. Source quality variations tied to sequence development in the Monterey and associated formations, southwestern California. *Petroleum Source Rocks in a Sequence-Stratigraphic Framework: AAPG Studies in Geology*, 7, 177-204.

Bohacs, K.M. 2000. Keys to Exploration: Lake-Basin Type, Source Potential, and Hydrocarbon Character within an Integrated Sequence-Stratigraphic/Geochemical Framework.

Bohacs, K.M., Grabowski Jr, G.J., Carroll, A.R., Mankiewicz, P.J., Miskell-Gerhardt, K.J., Schwalbach, J.R., Wegner, M.B. & Simo, J.T. 2005. Production, destruction, and dilution—the many paths to source-rock development.

Brown, S., Boserio, I., Jackson, K. & Spence, K. 1984. The geological evolution of the Canning Basin—implications for petroleum exploration. *The Canning Basin, WA: Proceedings of the Geological Society of Australia and Petroleum Exploration Society of Australia Symposium, Perth*, 85-96.

Burchette, T.P. 1993. Mishrif Formation (Cenomanian-Turonian), Southern Arabian Gulf: Carbonate Platform Growth Along a Cratonic Basin Margin: Chapter 16.

Bustin, R. & Clarkson, C. 1998. Geological controls on coalbed methane reservoir capacity and gas content. *International Journal of Coal Geology*, 38, 3-26.

Bustin, R., Link, C. & Goodarzi, F. 1989. Optical properties and chemistry of graptolite periderm following laboratory simulated maturation. *Organic Geochemistry*, 14, 355-364.

Bustin, R.M. 2005. Gas shale tapped for big pay. *AAPG explorer*, 26, 5-7.

Bustin, R.M., Bustin, A.M., Cui, A., Ross, D. & Pathi, V.M. 2008. Impact of shale properties on pore structure and storage characteristics. *SPE shale gas production conference*. Society of Petroleum Engineers.

Cadman, S., Pain, L., Vuckovic, V. & Le Poidevin, S. 1993. Canning Basin. *WA Bureau of Resource Sciences, Australian Petroleum Accumulations Report*, 9, 81.

Caineng, Z., Dazhong, D., Yuman, W., Xinjing, L., HUANG, J., Shufang, W., Quanzhong, G., ZHANG, C., Hongyan, W. & Honglin, L. 2015. Shale gas in China: Characteristics, challenges and prospects (I). *Petroleum exploration and development*, 42, 753-767.

Carey, S. 1976. The expanding earth (Developments of geotectonics, vol. 10). Amsterdam: Elsevier.

Carlsen, G. & Ghori, K.A.R. 2005. Canning Basin and Global Palaeozoic Petroleum Systems—A Review. *The APPEA Journal*, 45, 349-364.

Carr, A. & Williamson, J. 1990. The relationship between aromaticity, vitrinite reflectance and maceral composition of coals: implications for the use of vitrinite reflectance as a maturation parameter. *Organic Geochemistry*, 16, 313-323.

Castagna, J.P., Batzle, M.L. & Eastwood, R.L. 1985. Relationships between compressional-wave and shear-wave velocities in clastic silicate rocks. *Geophysics*, 50, 571-581.

Catuneanu, O. 2006. Principles of sequence stratigraphy. Elsevier.

Catuneanu, O. & Zecchin, M. 2013. High-resolution sequence stratigraphy of clastic shelves II: controls on sequence development. *Marine and Petroleum Geology*, 39, 26-38.

Cecil, C.B. 1990. Paleoclimate controls on stratigraphic repetition of chemical and siliciclastic rocks. *Geology*, 18, 533-536.

Chalmers, G.R. & Bustin, R.M. 2007a. On the effects of petrographic composition on coalbed methane sorption. *International Journal of Coal Geology*, 69, 288-304.

Chalmers, G.R. & Bustin, R.M. 2007b. The organic matter distribution and methane capacity of the Lower Cretaceous strata of Northeastern British Columbia, Canada. *International Journal of Coal Geology*, 70, 223-239.

Chareonsuppanimit, P., Mohammad, S.A., Robinson Jr, R.L. & Gasem, K.A.M. 2012. High-pressure adsorption of gases on shales: Measurements and modeling. *International Journal of Coal Geology*, 95, 34-46, doi: http://dx.doi.org/10.1016/j.coal.2012.02.005.

Christopher, s., c kendall & 2010, a.m.T. 2010.

Clarkson, C. & Bustin, R. 1999. The effect of pore structure and gas pressure upon the transport properties of coal: a laboratory and modeling study. 1. Isotherms and pore volume distributions. *Fuel*, 78, 1333-1344.

Cloetingh, S. 1988. Intraplate stresses: a tectonic cause for third-order cycles in apparent sea level.

Cluff, R. 2011. Practical use of core data for shale petrophysics–a petrophysicist's perspective. *SPWLA 2011 Annual Symposium, Short Course*.

Crowe, R., Towner, R. & Gibson, D. 1978. Permian and Mesozoic Geology of the Derby and Mount Anderson 1: 250,000 Sheet Areas, Western Australia. Department of National Development, Bureau of Mineral Resources, Geology and Geophysics.

Cui, X., Bustin, R.M. & Dipple, G. 2004. Selective transport of CO 2, CH 4, and N 2 in coals: insights from modeling of experimental gas adsorption data. *Fuel*, 83, 293-303.

Curtis, J.B. 2002. Fractured shale-gas systems. *AAPG bulletin*, 86, 1921-1938.

Dąbrowski, A. 2001. Adsorption—from theory to practice. *Advances in colloid and interface science*, 93, 135-224.

Dalrymple, R.W., Zaitlin, B.A. & Boyd, R. 1992. Estuarine facies models: conceptual basis and stratigraphic implications: perspective. *Journal of Sedimentary Research*, 62.

Das, J. 2012. Extracting Natural Gas Through Desorption in Shale Reservoirs. *The Way Ahead*, 8, 11-13.

Dean, W.E., Arthur, M.A. & Stow, D. 1984. Origin and geochemistry of Cretaceous deep-sea black shales and multi-colored claystones, with emphasis on Deep Sea Drilling Project site 530, Southern Angola Basin. *Initial Reports of the DSDP*, 75, 819-844.

Degens, E., Emeis, K.-C., Mycke, B. & Wiesner, M. 1986. Turbidites, the principal mechanism yielding black shales in the early deep Atlantic Ocean. *Geological Society, London, Special Publications*, 21, 361-376.

Demaison, G. 1991. Anoxia vs. Productivity: What Controls the Formation of Organic-Carbon-Rich Sediments and Sedimentary Rocks?: Discussion (1). *AAPG bulletin*, 75, 499-499.

Dewhurst, D.N., Aplin, A.C., Sarda, J.P. & Yang, Y. 1998. Compaction-driven evolution of porosity and permeability in natural mudstones: An experimental study. *Journal of Geophysical Research: Solid Earth (1978–2012)*, 103, 651-661.

Diamond, S. & Kinter, E.B. 1958. Surface areas of clay minerals as derived from measurements of glycerol retention. *Clays and clay minerals*, 5, 334-347.

Do, D.D. 1998. Adsorption analysis: equilibria and kinetics. Imperial College Press.

Dorsey, R.J., Umhoefer, P.J. & Falk, P.D. 1997. Earthquake clustering inferred from Pliocene Gilbert-type fan deltas in the Loreto basin, Baja California Sur, Mexico. *Geology*, 25, 679-682.

Droste, H. 1990. Depositional cycles and source rock development in an epeiric intra-platform basin: the Hanifa Formation of the Arabian peninsula. *Sedimentary Geology*, 69, 281-296.

Druce, E.C. & Radke, B. 1979. The geology of the Fairfield Group, Canning Basin, Western Australia. Australian Government Pub. Service.

Duval, B.C., Cramez, C. & Vail, P.R. 1998. Stratigraphic cycles and major marine source rocks.

Edwards, D., Summons, R., Kennard, J., Nicoll, R., Bradshaw, J., Bradshaw, M., Foster, C., O'Brien, G. & Zumberge, J. 1997. Geochemical characteristics of Palaeozoic petroleum systems in northwestern Australia. *The APPEA Journal*, 37, 351-379.

Einsele, G., Ricken, W. & Seilacher, A. 1991. Cycles and events in stratigraphy.

Eisma, D. 1986. Flocculation and de-flocculation of suspended matter in estuaries. *Netherlands Journal of Sea Research*, 20, 183-199.

Elkhalgi, M. & Rezaee, R. 2014. Geologic Framework of the Laurel Formation, Canning Basin. *International Petroleum Technology Conference*. International Petroleum Technology Conference.

Emery, D. & Myers, K. 2009. Sequence stratigraphy. John Wiley & Sons.

Erik, N.Y., Özçelik, O. & Altunsoy, M. 2006. Interpreting Rock–Eval pyrolysis data using graphs of S 2 vs. TOC: Middle Triassic–Lower Jurassic units, eastern part of SE Turkey. *Journal of Petroleum Science and Engineering*, 53, 34-46.

Espitalie, J., Deroo, G. & Marquis, F. 1985. Rock-Eval pyrolysis and its applications. *Revue De L Institut Francais Du Petrole*, 40, 563-579.

Feldman, H.R., Franseen, E.K., Joeckel, R. & Heckel, P.H. 2005. Impact of longer-term modest climate shifts on architecture of high-frequency sequences (cyclothems), Pennsylvanian of Midcontinent USA. *Journal of Sedimentary Research*, 75, 350-368.

Forgotson, J. 2007. Distribution and Properties of Shale Gas in the Arkoma Basin.

Forman, D.J., Wales, D.W. & Burne, R.V. 1981. Geological evolution of the Canning Basin, Western Australia. Australian Government Pub. Service.

Foster, C., O'Brien, G. & Watson, S. 1986. Hydrocarbon source potential of the Goldwyer Formation, Barbwire Terrace, Canning Basin, Western Australia. *The APPEA Journal*, 26, 142-155.

Frazier, D.E. 1974. Depositional episode: their relationship to the Quaternary stratigraphic framework in the northwestern portion of the Gulf basin. *The University of Texas at Austin, Bureau of Economic Geology, Geological Circular*, 74, 28.

Galloway, W.E. 1989. Genetic stratigraphic sequences in basin analysis I: architecture and genesis of flooding-surface bounded depositional units. *AAPG bulletin*, 73, 125-142.

Ghadeer, S.G. & Macquaker, J.H. 2012. The role of event beds in the preservation of organic carbon in fine-grained sediments: analyses of the sedimentological processes operating during deposition of the Whitby Mudstone Formation (Toarcian, Lower Jurassic) preserved in northeast England. *Marine and Petroleum Geology*, 35, 309-320.

Ghori, A. 2004. PS Western Australia's Geothermal Resources.

Ghori, K.A.R. 2013. Emerging unconventional shale plays in Western Australia. *The APPEA Journal*, 53, 313-336.

Gibbs, J.W. 1957. The collected works of J. Willard Gibbs. Yale University Press.

Gipson, M. 1966. A study of the relations of depth, porosity and clay mineral orientation in Pennsylvanian shales. *Journal of Sedimentary Research*, 36, 888-903.

Glorioso, J.C. & Rattia, A. 2012. Unconventional reservoirs: Basic petrophysical concepts for shale gas. *SPE/EAGE European Unconventional Resources Conference & Exhibition-From Potential to Production*.

Goodarzi, F. & Norford, B. 1987. Optical properties of graptolite epiderm—a review. *Bull. Geol. Soc. Den*, 35, 141-147.

Gregg, S.J. & Sing, K.S. 1995. Adsorption, surface area and porosity. Academic Press, London [u.a.

Gupta, N., Rai, C.S. & Sondergeld, C.H. 2012. Integrated petrophysical characterization of the Woodford shale in Oklahoma. *SPWLA 53rd Annual Logging Symposium*. Society of Petrophysicists and Well-Log Analysts.

Guthrie, J.M. & Bohacs, K.M. 2009. Spatial variability of source rocks: A critical element for defining the petroleum system of Pennsylvanian carbonate reservoirs of the Paradox Basin, SE Utah.

Haines, P. 2004. Depositional facies and regional correlations of the Ordovician Goldwyer and Nita Formations, Canning Basin, Western Australia, with implications for petroleum exploration. *Geological Survey of Western Australia, Record*, 7.

Haines, P. 2012. Geology and petroleum prospectivity of state acreage release areas 112-3, 112-4 and 112-5, officer basin, western australia.

Haines, P. & Ghori, K. 2006. Rich oil-prone Ordovician source beds, Bongabinni Formation, onshore Canning Basin, Western Australia: AAPG 2006 International Conference and Exhibition, Perth, Western Australia, 5–8 November, 2006. *Extended Abstracts, 4p*.

Hampson, G.J., Davies, W., Davies, S.J., Howell, J.A. & Adamson, K.R. 2005. Use of spectral gamma-ray data to refine subsurface fluvial stratigraphy: late Cretaceous strata in the Book Cliffs, Utah, USA. *Journal of the Geological Society*, 162, 603-621.

Heller, R. & Zoback, M. 2014. Adsorption of methane and carbon dioxide on gas shale and pure mineral samples. *Journal of Unconventional Oil and Gas Resources*, 8, 14-24.

Hildenbrand, A. & Urai, J. 2003. Investigation of the morphology of pore space in mudstones—first results. *Marine and Petroleum Geology*, 20, 1185-1200.

Hood, A., Gutjahr, C. & Heacock, R. 1975. Organic metamorphism and the generation of petroleum. *AAPG bulletin*, 59, 986-996.

Horsfield, B., Curry, D., Bohacs, K., Littke, R., Rullkötter, J., Schenk, H., Radke, M., Schaefer, R., Carroll, A. & Isaksen, G. 1994. Organic geochemistry of

freshwater and alkaline lacustrine sediments in the Green River Formation of the Washakie Basin, Wyoming, USA. *Organic Geochemistry*, 22, 415-440.

Hunt, D. & Tucker, M.E. 1995. Stranded parasequences and the forced regressive wedge systems tract: deposition during base-level fall—reply. *Sedimentary Geology*, 95, 147-160.

Jarvie, D., Claxton, B., Henk, B. & Breyer, J. 2001. Oil and shale gas from Barnett shale, Ft. Worth Basin, TX. *Poster presented at the AAPG National Convention, Denver, CO*.

Jarvie, D.M. 1991. Total organic carbon (TOC) analysis: Chapter 11: geochemical methods and exploration.

Jarvie, D.M. 2012. Shale resource systems for oil and gas: Part 2—Shale-oil resource systems.

Jarvie, D.M., Hill, R.J., Ruble, T.E. & Pollastro, R.M. 2007. Unconventional shale-gas systems: The Mississippian Barnett Shale of north-central Texas as one model for thermogenic shale-gas assessment. *AAPG bulletin*, 91, 475-499, doi: 10.1306/12190606068.

Ji, L., Chen, W., Bi, J., Zheng, S., Xu, Z., Zhu, D. & Alvarez, P.J. 2010. Adsorption of tetracycline on single-walled and multi-walled carbon nanotubes as affected by aqueous solution chemistry. *Environmental Toxicology and Chemistry*, 29, 2713-2719.

Jinchuan, Z., Zhijun, J. & Mingsheng, Y. 2004. Reservoiring mechanism of shale gas and its distribution. *Natural Gas Industry*, 24, 15-18.

Johnson & Baldwin. 1996. Shallow clastic seas. *Oxford: Blackwell Publishing*, 232–280.

Jonasson, K.E. 2001. Western Australia atlas of petroleum fields onshore Canning Basin. *Petroleum Division*, 2.

Kadkhodaie, A. & Rezaee, R. 2017. Estimation of vitrinite reflectance from well log data. *Journal of Petroleum Science and Engineering*, 148, 94-102.

Kennard, J. 1994. Canning Basin Project Stage II-Geohistory Modelling. Australian Geological Survey Organisation.

King, G.E. 2010. Thirty years of gas shale fracturing: What have we learned? *SPE Annual Technical Conference and Exhibition*. Society of Petroleum Engineers.

Krief, M., Garat, J., Stellingwerff, J. & Ventre, J. 1990. A petrophysical interpretation using the velocities of P and S waves (full-waveform sonic): The Log Analyst, 31, 355–369. *Google Scholar*.

Krushin, J.T. 1997. AAPG Memoir 67: Seals, Traps, and the Petroleum System. Chapter 3: Seal Capacity of Nonsmectite Shale.

Lakatos, I.J. & Lakatos-Szabo, J. 2009. Role of conventional and unconventional hydrocarbons in the 21st century: comparison of resources, reserves, recovery factors and technologies. *EUROPEC/EAGE Conference and Exhibition*. Society of Petroleum Engineers.

Laxminarayana, C. & Crosdale, P.J. 1999. Role of coal type and rank on methane sorption characteristics of Bowen Basin, Australia coals. *International Journal of Coal Geology*, 40, 309-325.

Leeder, M.R., Harris, T. & Kirkby, M.J. 1998. Sediment supply and climate change: implications for basin stratigraphy. *Basin Research*, 10, 7-18.

Leverett, M. 1941. Capillary behavior in porous solids. *Transactions of the AIME*, 142, 152-169.

Lobza, V. & Schieber, J. 1999. Biogenic sedimentary structures produced by worms in soupy, soft muds: observations from the Chattanooga Shale (Upper Devonian) and experiments. *Journal of Sedimentary Research*, 69.

Loucks, R.G. & Ruppel, S.C. 2007. Mississippian Barnett Shale: Lithofacies and depositional setting of a deep-water shale-gas succession in the Fort Worth Basin, Texas. *AAPG bulletin*, 91, 579-601.

Lu, X.-C., Li, F.-C. & Watson, A.T. 1995a. Adsorption measurements in Devonian shales. *Fuel*, 74, 599-603.

Lu, X.-C., Li, F.-C. & Watson, A.T. 1995b. Adsorption studies of natural gas storage in Devonian Shales. *SPE Formation evaluation*, 10, 109-113.

Lucia, F.J., Kerans, C. & Jennings Jr, J.W. 2003. Carbonate reservoir characterization. *Journal of Petroleum Technology*, 55, 70-72.

Macquaker, J., Gawthorpe, R., Taylor, K. & Oates, M. 1998. Heterogeneity, stacking patterns and sequence stratigraphic interpretation in distal mudstone successions: examples from the Kimmeridge Clay Formation, UK.

Macquaker, J.H., Taylor, K.G. & Gawthorpe, R.L. 2007. High-resolution facies analyses of mudstones: implications for paleoenvironmental and sequence

stratigraphic interpretations of offshore ancient mud-dominated successions. *Journal of Sedimentary Research*, 77, 324-339.

Manger, K., Oliver, S., Curtis, J. & Scheper, R. 1991. Geologic influences on the location and production of Antrim shale gas, Michigan Basin. *Low Permeability Reservoirs Symposium*. Society of Petroleum Engineers.

Marshall, J. 1998. The recognition of multiple hydrocarbon generation episodes: an example from Devonian lacustrine sedimentary rocks in the Inner Moray Firth, Scotland. *Journal of the Geological Society*, 155, 335-352.

Martineau, D.F. 2007. History of the Newark East field and the Barnett Shale as a gas reservoir. *AAPG bulletin*, 91, 399-403.

Matott, L.S. & Rabideau, A.J. 2008. ISOFIT–a program for fitting sorption isotherms to experimental data. *Environmental Modelling & Software*, 23, 670-676.

McCutcheon, A. & Barton, W. 1999. Contribution of mineral matter to water associated with bituminous coals. *Energy & fuels*, 13, 160-165.

Meissner, F.F. 1984. Petroleum Geology of the Bakken Formation Williston Basin, North Dakota and Montana.

Mendelzon, J. & Toksoz, M.N. 1985. Source rock characterization using multivariate analysis of log data. *SPWLA 26th Annual Logging Symposium*. Society of Petrophysicists and Well-Log Analysts.

Meyer, B.L. & B. L. Meyer, M.H.N. 1984. Identification of source rocks on wireline logs by density/resistivity and sonic transit time/resistivity crossplots. *AAPG bulletin*, 68, 121.

Mitchum Jr, R.M. 1977. Seismic stratigraphy and global changes of sea level: Part 11. Glossary of terms used in seismic stratigraphy: Section 2. Application of seismic reflection configuration to stratigraphic interpretation.

Muto, T. & Steel, R.J. 1992. Retreat of the front in a prograding delta. *Geology*, 20, 967-970.

Muto, T., Steel, R.J. & Swenson, J.B. 2007. Autostratigraphy: a framework norm for genetic stratigraphy. *Journal of Sedimentary Research*, 77, 2-12.

Myrow, P.M., Lamb, M., Lukens, C., Houck, K., Kluth, C. & Parsons, J. 2010. Hyperpycnal wave-modified turbidites of the Pennsylvanian Minturn

Formation, north-central Colorado. *Minturn Fieldtrip Material. Department of Geology, The Colorado College*.

Newell, R.I. 1988. Ecological changes in Chesapeake Bay: are they the result of overharvesting the American oyster, Crassostrea virginica. *Understanding the estuary: advances in Chesapeake Bay research*, 129, 536-546.

Nicoll, R.S. 1993. Ordovician conodont distribution in selected petroleum exploration wells, Canning Basin, Western Australia. Australian Government Publishing Service.

Nicoll, R.S. & Gorter, J.D. 1984. Interpretation of additional conodont colour alteration data and the thermal maturation and geothermal history of the Canning Basin, Western Australia.

Nixon, R. 1973. Oil source beds in Cretaceous Mowry Shale of northwestern interior United States. *AAPG bulletin*, 57, 136-161.

O'Brien, N.R. 1996. Shale lamination and sedimentary processes. *Geological Society, London, Special Publications*, 116, 23-36.

Passey, Q.R., Bohacs, K., Esch, W.L., Klimentidis, R. & Sinha, S. 2010. From Oil-Prone Source Rock to Gas-Producing Shale Reservoir â" Geologic and Petrophysical Characterization of Unconventional Shale-Gas Reservoirs. *International Oil and Gas Conference and Exhibition in China*. Society of Petroleum Engineers, Beijing, China.

Passey, S.C., J. B. Kulla, F. J. Moretti, and J. D. Stroud. 1990. A Practical Model for Organic Richness from Porosity and Resistivity Logs. *The American Association of Petroleum Geologists Bulletin* 74, 1777-1794.

Passmore, V. 1991. Promising hydrocarbon potential seen in Canning Basin off Australia. *Oil and Gas Journal;(United States)*, 89.

Paxton, S.T., Aufill, M., Cruse, A.M., Puckette, J.O., Hurst, D.D. & Samson, T. 2007. Use of spectral gamma ray profiles for discriminating depositional and stratigraphic successions in Upper Devonian-Lower Mississippian gas shale intervals, North America. *2007 GSA Denver Annual Meeting*.

Pepper, A.S. 1991. Estimating the petroleum expulsion behaviour of source rocks: a novel quantitative approach. *Geological Society, London, Special Publications*, 59, 9-31.

Pittman, E.D. 1992. Relationship of porosity and permeability to various parameters derived from mercury injection-capillary pressure curves for sandstone (1). *AAPG bulletin*, 76, 191-198.

Pool, W., Geluk, M., Abels, J., Tiley, G., Idiz, E. & Leenaarts, E. 2012. Assessment of an unusual European shale gas play: the Cambro-Ordovician alum shale, southern Sweden. *SPE/EAGE European Unconventional Resources Conference & Exhibition-From Potential to Production*.

Posamentier, H., Jervey, M. & Vail, P. 1988. Eustatic controls on clastic deposition I—conceptual framework.

Potter, P.E., Maynard, J.B. & Depetris, P.J. 2005. Mud and mudstones: Introduction and overview. Springer Science & Business Media.

Powell, D. 1976. The geological evolution of the continental margin off northwest Australia. *APEA J*, 16, 13-23.

Pryor, W.A. 1975. Biogenic sedimentation and alteration of argillaceous sediments in shallow marine environments. *Geological Society of America Bulletin*, 86, 1244-1254.

Ramos, S. 2004. The effect of shale composition on the gas sorption potential of organic-rich mudrocks in the Western Canadian sedimentary basin.

Rezaee, R. 2015. Fundamentals of gas shale reservoirs. John Wiley & Sons.

Rice, D.D. 1993. Composition and origins of coalbed gas. *Hydrocarbons from coal: AAPG Studies in Geology*, 38, 159-184.

Rickman, R., Mullen, M.J., Petre, J.E., Grieser, W.V. & Kundert, D. 2008. A practical use of shale petrophysics for stimulation design optimization: All shale plays are not clones of the Barnett Shale. *SPE Annual Technical Conference and Exhibition*. Society of Petroleum Engineers.

Rider, M. 1996. The geological interpretation of wireline logs. *Whittles, Caithness*.

Romine, K., Southgate, P., Kennard, J. & Jackson, M. 1994. The Ordovician to Silurian phase of the Canning Basin WA: structure and sequence evolution. *The sedimentary basins of Western Australia*, 677-696.

Ross, D.J. & Bustin, R.M. 2007. Impact of mass balance calculations on adsorption capacities in microporous shale gas reservoirs. *Fuel*, 86, 2696-2706.

Ross, D.J. & Bustin, R.M. 2009. The importance of shale composition and pore structure upon gas storage potential of shale gas reservoirs. *Marine and Petroleum Geology*, 26, 916-927.

Ross, D.J.K. 2004. Sedimentology, geochemistry and gas shale potential of the Early Jurassic Nordegg Member, northeastern British Columbia.

Russell, M.J. 1998. EP 353 Canning Basin charge modelling. *In SRK Consulting, 1998*, Canning Basin Project, 104-112.

Saneifar, M., Aranibar, A. & Heidari, Z. 2013. Rock Classification in the Haynesville Shale-Gas Formation Based on Petrophysical and Elastic Rock Properties Estimated from Well Logs. *SPE Annual Technical Conference and Exhibition*. Society of Petroleum Engineers.

Savrda, C.E., Bottjer, D.J. & Gorsline, D.S. 1984. Development of a comprehensive oxygen-deficient marine biofacies model: evidence from Santa Monica, San Pedro, and Santa Barbara Basins, California Continental Borderland. *AAPG bulletin*, 68, 1179-1192.

Schettler Jr, P. & Parmely, C. 1991. Contributions to total storage capacity in Devonian shales. *SPE Eastern Regional Meeting*. Society of Petroleum Engineers.

Schettler, P. & Parmoly, C. 1990. The measurement of gas desorption isotherms for Devonian shale. *GRI Devonian Gas Shale Technology Review*, 7, 4-9.

Schieber, J. 1994. Evidence for high-energy events and shallow-water deposition in the Chattanooga Shale, Devonian, central Tennessee, USA. *Sedimentary Geology*, 93, 193-208.

Schieber, J. & Riciputi, L. 2004. Pyrite ooids in Devonian black shales record intermittent sea-level drop and shallow-water conditions. *Geology*, 32, 305-308.

Schieber, J., Southard, J.B. & Schimmelmann, A. 2010. Lenticular shale fabrics resulting from intermittent erosion of water-rich muds—Interpreting the rock record in the light of recent flume experiments. *Journal of Sedimentary Research*, 80, 119-128.

Schlager, W. 2010. Ordered hierarchy versus scale invariance in sequence stratigraphy. *International Journal of Earth Sciences*, 99, 139-151.

Schleicher, M., Koster, J., Kulke, H. & Weil, W. 1998. Reservoir And Source-Rock Characterisation Of The Early Palaeozoic Interval In The

Peribaltic Syneclise, Northern Poland. *Journal Of Petroleum Geology*, 21, 33-56.

Schwalbach, J.R. & Bohacs, K.M. 1992. Sequence stratigraphy in fine-grained rocks: examples from the monterey formation. Frontmatter and Road Logs.

Selley, R.C. 1985. Elements of petroleum geology.

Shuangfang, L., Huang, W., Fangwen, C., Jijun, L., Min, W., Haitao, X., Weiming, W. & Xiyuan, C. 2012. Classification and evaluation criteria of shale oil and gas resources: Discussion and application. *Petroleum exploration and development*, 39, 268-276.

Siemons, N. & Busch, A. 2007. Measurement and interpretation of supercritical CO_2 sorption on various coals. *International Journal of Coal Geology*, 69, 229-242.

Singh, P. 2008. Lithofacies and sequence stratigraphic framework of the Barnett Shale, northeast Texas.

Slatt, R.M. 2015. Sequence stratigraphy of unconventional resource shales. *Fundamentals of Gas Shale Reservoirs*, 71-88.

Slatt, R.M. & Abousleiman, Y. 2011. Merging sequence stratigraphy and geomechanics for unconventional gas shales. *The Leading Edge*, 30, 274-282.

Slatt, R.M. & Rodriguez, N. 2010. Comparative sequence stratigraphy and organic geochemistry of North American unconventional gas shales: Commonality or coincidence. *Critical assessment of shale resource plays (ex. abs.), AAPG/Society of Economic Geologists/Society of Petroleum Geologists/Society of Petrophysicists and Well-Log Analysis Hedberg Conference, Austin, Texas*.

Slatt, R.M. & Rodriguez, N.D. 2012. Comparative sequence stratigraphy and organic geochemistry of gas shales: Commonality or coincidence? *Journal of Natural Gas Science and Engineering*, 8, 68-84, doi: 10.1016/j.jngse.2012.01.008.

Sloss, L. 1963. Sequences in the cratonic interior of North America. *Geological Society of America Bulletin*, 74, 93-114.

Sondergeld, C.H., Newsham, K.E., Comisky, J.T., Rice, M.C. & Rai, C.S. 2010. Petrophysical considerations in evaluating and producing shale gas

resources. *SPE Unconventional Gas Conference*. Society of Petroleum Engineers.

Song, B., Economides, M.J. & Ehlig-Economides, C.A. 2011. Design of multiple transverse fracture horizontal wells in shale gas reservoirs. *SPE Hydraulic Fracturing Technology Conference*. Society of Petroleum Engineers.

Sorby, H.C. 1908. On the application of quantitative methods to the study of the structure and history of rocks. *Quarterly Journal of the Geological Society*, 64, 171-233.

Staff. 2010. 2025 Unconventional gas outlook, the next wave. *Core Energy Group*, 1.

Stow, D.A. 1985. Fine-grained sediments in deep water: an overview of processes and facies models. *Geo-Marine Letters*, 5, 17-23.

Strapoc, D., Mastalerz, M., Schimmelmann, A., Drobniak, A. & Hasenmueller, N.R. 2010. Geochemical constraints on the origin and volume of gas in the New Albany Shale (Devonian–Mississippian), eastern Illinois Basin. *AAPG bulletin*, 94, 1713-1740.

Suárez-Ruiz, I., Flores, D., Mendonça Filho, J.G. & Hackley, P.C. 2012. Review and update of the applications of organic petrology: Part 1, geological applications. *International Journal of Coal Geology*, 99, 54-112.

Talbot, M. 1988. The origins of lacustrine oil source rocks: evidence from the lakes of tropical Africa. *Geological Society, London, Special Publications*, 40, 29-43.

Tissot, B. 1977. The application of the result of organic geochemical studies in oil and gas exploration. Chapter 2 in: Hobson, GD (ed.) Developments in Petroleum Geology—1. Applied Science Publishers Ltd., London.

Tissot, B. 1984. Recent advances in petroleum geochemistry applied to hydrocarbon exploration. *AAPG Bull*, 68, 545-563.

Tissot, B. & Welte, D. 1978. Petroleum Previous Hit formation Next Hit and occurrence: a new approach to oil and gas exploration. Berlin, Springer-Verlag.

Tourtelot, H.A. 1960. Origin and use of the word "shale". *American Journal of Science*, 258, 335-343.

Trabucho-Alexandre, J. 2015. Organic Matter-Rich Shale Depositional Environments. *Fundamentals of Gas Shale Reservoirs*, 21-45.

Vail, P. 1991. The stratigraphic signatures of tectonics, eustacy and sedimentology-an overview. *Cycles and events in stratigraphy*, 617-659.

Van Wagoner, J.C., Mitchum, R., Campion, K. & Rahmanian, V. 1990. Siliciclastic sequence stratigraphy in well logs, cores, and outcrops: concepts for high-resolution correlation of time and facies.

Venaruzzo, J., Volzone, C., Rueda, M. & Ortiga, J. 2002. Modified bentonitic clay minerals as adsorbents of CO, CO 2 and SO 2 gases. *Microporous and Mesoporous Materials*, 56, 73-80.

Volzone, C., Rinaldi, J. & Ortiga, J. 2002. N2 and CO2 Adsorption by TMA-and HDP-Montmorillonites. *Materials Research*, 5, 475-479.

Waples, D.W. 1983. Reappraisal of anoxia and organic richness, with emphasis on Cretaceous of North Atlantic. *AAPG bulletin*, 67, 963-978.

Wright, V.P. & Burchette, T.P. 1996. Shallow-water carbonate environments. Blackwell Science.

Yeates, A., Gibson, D., Towner, R. & Crowe, R. 1984. Regional geology of the onshore Canning Basin, WA. *The Canning Basin, WA Proceedings of the Geological Society of Australia & Petroleum Exploration Society of Australia Symposium, Perth*, 23-55.

Zhang, T., Ellis, G.S., Ruppel, S.C., Milliken, K. & Yang, R. 2012. Effect of organic-matter type and thermal maturity on methane adsorption in shale-gas systems. *Organic Geochemistry*, 47, 120-131.

Zou, C., Dong, D., Wang, S., Li, J., Li, X., Wang, Y., Li, D. & Cheng, K. 2010. Geological characteristics and resource potential of shale gas in China. *Petroleum exploration and development*, 37, 641-653, doi: 10.1016/s1876-3804(11)60001-3.

Zou, C., Dong, D., Wang, Y., Li, X., Huang, J., Wang, S., Guan, Q., Zhang, C., Wang, H. & Liu, H. 2015. Shale gas in China: Characteristics, challenges and prospects (I). *Petroleum exploration and development*, 42, 689-701.